

KINETICS OF GASIFICATION OF CARBON AND CARBOTHERMIC REDUCTION OF IRON OXIDE

*A Thesis Submitted
In Partial fulfilment of the Requirements
for the Degree of
DOCTOR OF PHILOSOPHY*

by
DEBAJYOTI BANDYOPADHYAY

to the
**DEPARTMENT OF METALLURGICAL ENGINEERING
INDIAN INSTITUTE OF TECHNOLOGY, KANPUR
JULY, 1989**

12 JUL 1990

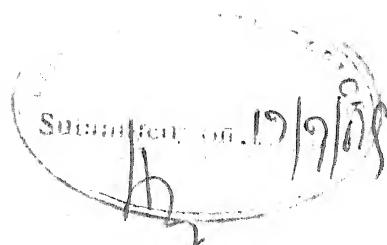
CENTRAL LIBRARY
PT T. KANPUR

Acc. No. **A108433**

Th
669.1
B223 K

ME-1989-D-BAN-KIN

CERTIFICATE



It is certified that this work on "Kinetics of gasification of carbon and carbothermic reduction of iron oxide" by Debajyoti Bandyopadhyay has been carried out under our supervision and that this work has not been submitted elsewhere for a degree.

N. Chakraborti

(N. Chakraborti)
Asst. Professor

A. Ghosh

(A. Ghosh)
Professor

Department of Metallurgical Engineering
Indian Institute of Technology
Kanpur

dedicated

to

my beloved parents

ACKNOWLEDGEMENT

In my journey through a problematic path, the light of right direction and destiny has come from my supervisors Prof.A. Ghosh and Dr.N. Chakraborti. Their valuable suggestions and analytic minds have made it possible for me to sail through all the predicaments. Author's sense of gratitude knows no bound for Prof. Ghosh's patience help throughout this study. Author also thanks his supervisors for suggesting him the problem of the study.

Thanks are also due to all his laboratory mates, specially S.K. Choudhary and P. Tiwari for their help as well as encouragement. The author is also indebted to the metallurgical work shop, glass blowing section of the institute for their help in designing and fabrication of the experimental set-up.

Author wants to thank Mr.T. Roy, S. Bhowmik for taking the trouble of correcting the manuscript.

Author sincerely acknowledges the help of Mr.A. Sharma, D.P. Tripathi, Ram Avatar at various stages of this study.

The good will and support of many of the friends and well wishers whose names have not been included in the list was a great asset to the author in course of the study.

Author is in debt to all his beloved family members for their patience and constant encouragement which has made it possible for him to complete the study.

The nice typing of the manuscript by Mr.B.D. Biswas and the tracing of figures by Mr.V.P. Gupta are sincerely acknowledged.

Very timely help of Mr.Sushil Kumar and Mr.S.N. Singh for printing the thesis is gratefully acknowledged.

The project sponsored by the Steel Authority of India as well as the help and suggestions provided by the Direct Reduction Process Development Division, Research and Development Centre for Iron and Steel, SAIL, Ranchi, have been of considerable value throughout this course of investigation and the author gratefully acknowledges the same.

Debajyoti Bandyopadhyay

LIST OF CONTENTS

	Page
LIST OF TABLES	ix
LIST OF FIGURES	xi
LIST OF SYMBOLS	xvi
SYNOPSIS	xx
CHAPTER	
1 LITERATURE REVIEW	1
1.1 Introduction	1
1.2 Literature Review on Kinetics of Gasification of Carbon by CO ₂	6
1.2.1 Nature of carbon	6
1.2.2 General consideration of kinetics	9
1.2.3 Rate and mechanism of surface reaction	13
1.2.4 Mass and heat transfer limitations on rate	38
1.2.5 Surface area	49
1.2.6 Catalysis of gasification reaction	58
1.2.7 Summary and conclusion on kinetics of reaction of carbon with carbon dioxide	64
1.3 Literature Review on Kinetics of Carbothermic Reduction	67
1.3.1 Direct reduction versus reduction via gaseous medium	67
1.3.2 General features of carbothermic reduction	69
1.3.3 Catalytic effect of freshly produced iron in carbothermic reduction	79
1.3.4 Reaction mechanisms and rate equations	85
1.4 Plan of Work	91
2 APPARATUS	96
2.1 Apparatus for Measurement of Gasification Rate of Graphite in Carbon dioxide	96
2.1.1 Gas train	96
2.1.2 Thermogravimetry set-up	100
2.2 Char Making Apparatus	104
2.2.1 Gas purification train	105
2.2.2 Char making furnace	105
2.3 Apparatus for Carbothermic Reduction Gas Analysis Set-up	105
2.4 Gas Analysis Set-up	112

CHAPTER		Page
3	MATERIAL PREPARATION AND EXPERIMENTAL PROCEDURE	114
3.1	Material Preparation	114
3.1.1	Preparation of graphite powder	114
3.1.2	Preparation of coconut char	115
3.1.3	Preparation of iron oxide	116
3.1.4	Preparation of iron oxide micropellets	116
3.2	Experimental Procedure	117
3.2.1	Reactivity study of graphite in carbon dioxide	118
3.2.2	Reactivity study of coconut char in carbon dioxide	121
3.2.3	Trials for simultaneous measurement of weight loss and product gas analysis in carbothermic reduction	121
3.2.4	Reactivity study of coconut char in carbon dioxide - monoxide gas mixture	123
3.2.5	Weight loss measurement of coconut char and iron oxide powder mixture	124
3.2.6	Weight loss measurement of coconut char powder and iron oxide micropellet mixture	125
3.2.7	Product gas analysis and bed temperature measurement for carbothermic reduction	125
4	RESULTS ON REACTIVITY MEASUREMENTS IN CARBON DIOXIDE AND CARBON DIOXIDE-MONOXIDE MIXTURE	129
4.1	Effect Of Experimental Variables	129
4.1.1	Gas flow rate	134
4.1.2	Particle size	134
4.1.3	Compaction pressure	137
4.1.4	Bed depth	137
4.1.5	Concentration of carbon monoxide in gas	140
4.2	Measurement Errors	140
4.2.1	Errors in temperature measurement	140
4.2.2	Errors in flow measurement	144
4.2.3	Errors in weight loss measurement	144
4.3	Procedure for Rate Calculation	145
5	CALCULATION OF ISOTHERMAL AND NON-ISOTHERMAL EFFECTIVENESS FACTORS FOR GASIFICATION REACTION	162

CHAPTER

Page

7.1.3	Error in temperature measurement	224
7.2	Rate Calculation Procedure	225
7.3	Results Of The Calculation	229
7.4	Calculation Procedure Of Rate Of Carbon Loss From Gasification (w_{cp}) And The Results	229
7.5	Discussion On Results	243
7.6	Comparison With Carbothermic Rate Data Of Abraham et al.	246
8	SUMMARY AND CONCLUSIONS	253
9	SCOPE FOR FUTURE STUDIES	259
REFERENCES		261
APPENDIX		
1	ΔH° and ΔG° values of CO	268
2	ΔH° and ΔG° values of CO ₂	269
3	ΔH° and ΔG° values of Fe ₂ O ₃	270
4	ΔH° and ΔG° values of Fe ₃ O ₄	271
5	ΔH° and ΔG° values of Fe _x O	272
6	Examples of dimensional inconsistencies of the model of Tien et al.(78)	273
7	Program for non-isothermal rate calculation	274
8	Program for instantaneous rate calculation of gasification	282
9	Program for calculation of A and E factors of isothermal mass transfer analysis	286
10	Program for carbothermic rate calculation	288
11	Weight loss versus time data for coconut char in CO ₂ , CO ₂ -Ar mixtures	293
12	Weight loss versus time data for coconut char in CO-CO ₂ mixture	297
13	Weight loss versus time data for carbothermic reduction	301

LIST OF TABLES

Table	Title	Page
1.1	Present status of rotary kiln based direct reduction in India	3
1.2	Comparison of ϕ_{CO} values calculated in two ways	29
1.3	Values of I_2, I_3 and their ratios for different workers at various temperatures	34
1.4	Conditions used by Ghosh et al for effectiveness factor calculation	45
1.5	Surface area values of different types of carbon	51
1.6	Experimental conditions and salient features of carbothermic reduction	71
1.7	Experimental conditions and salient features of carbothermic reduction for powder mixture	74
2.1	Gases used and their functions	98
2.2	Reagents used for purification of inert gas	98
2.3	Scrubbing agents for carbon dioxide purification	99
4.1	Experimental conditions for measurement of gasification rate in CO_2	130
4.2	Experimental conditions for measurement of gasification rate of coconut char in CO_2	131
4.3	Experimental conditions for measurement of gasification rate of coconut char in CO_2 -Ar gas mixture	132
4.4	Experimental conditions for measurement of gasification rate of coconut char in CO - CO_2 gas mixture	133
4.5	Rate of gasification of graphite in CO_2	153
4.6	Rate of gasification of coconut char in CO_2	159
4.7	Rate of gasification of coconut char in CO_2 - Ar, 160 gas mixture	
4.8	Rate of gasification of coconut char in CO_2 - CO 161 gas mixture	
6.1	Values of r_g , η and K_c for graphite in CO_2	190

Table	Title	Page
6.2	Values of r_g , η and K_{CT} for coconut char in CO_2 and CO_2 - Ar gas mixture	191
6.3	Values of r_g , η and K_{CT} for coconut char in CO_2 - CO gas mixture	192
6.4	Non-isothermal effectiveness factor (η_T) and intrinsic rate of gasification (K_{CT}) in CO_2 and CO_2 - Ar gas mixture for coconut char	198
6.5	Non-isothermal effectiveness factor (η_T) and intrinsic rate of gasification in CO_2 - CO gas mixture for coconut char	199
6.6	Comparison of rates obtained by zero bed depth extrapolation (\dot{r}_g) with K_c for graphite	202
6.7	Comparison of rates obtained by zero bed depth extrapolation (\dot{r}_g) with K_{CT} for coconut char	202
6.8	Activation energy (kJ/mol) values of I_1 , I_2 , I_3 for different workers	215
6.9	Activation energy (kJ/mol) values of reversible oxygen steps and gasification step for different workers	217
7.1	Experimental conditions used for carbothermic reduction	221

LIST OF FIGURES

Figure	Title	Page
1.1	Schematic representation of C - CO ₂ reaction	11
1.2	Effect of temperature and gas composition on the rate of oxidation of electrode graphite granules (0.5 mm dia.) in CO ₂ - CO gas mixture	15
1.3	Langmuir - Hinshelwood mechanism for a reaction: A + B ----> product	17
1.4	Alternative Langmuir mechanism for a reaction: A + B ----> product	17
1.5	Equilibrium constant K _e for oxygen exchange reaction as a function of temperature	23
1.6	Constants of the gasification step as a function of temperature	24
1.7	Temperature dependence of the rate parameter θ_1 for oxidation in CO - CO ₂ mixtures	31
1.8	Equilibrium constants K _e for oxygen exchange reaction	35
1.9	Temperature dependence of mass transfer for C - CO ₂ reaction in porous carbon pellet	39
1.10	Effect of particle size on rate of oxidation of coke spheres in CO ₂	42
1.11	Rate of oxidation of electrode graphite as a function of particle diameter in CO ₂	43
1.12	Comparison of effectiveness factors, calculated by two methods (sample dia. = 2.0 cm and thickness = 0.25 cm)	46
1.13	Specific surface area(s) versus fractional conversion(F) curves for different investigators	53
1.14	Rate of gasification per unit surface area versus fractional conversion	56
1.15	Rate per unit surface area versus fractional conversion of coke	57
1.16	Rate of oxidation in CO ₂ at 1100°C related to internal surface area (BET) of unoxidized carbon	59

Figure	Title	Page
1.17	Variation of observed and calculated parameters with fractional reduction of iron oxide and graphite powder mixture	81
1.18	Variation of observed and calculated parameters with fractional reduction of iron oxide micropellet and graphite powder mixture	82
2.1	Schematic representation of the gas train	97
2.2	Thermogravimetry set-up	101
2.3	Charmaking apparatus	106
2.4	Modified TGA set-up	108
2.5	Different parts of the dead volume cutting device	109
2.6	Apparatus for the product gas analysis and bed temperature measurement	113
3.1	Schematic representation of compaction unit	119
3.2	Gas chromatograph calibration curves for CO - CO ₂ mixture at room temperature	128
4.1	Effect of particle size on weight loss of graphite in CO ₂	135
4.2	Effect of particle size on weight loss of coconut char in CO ₂	136
4.3	Effect of compaction pressure on weight loss of graphite in CO ₂	138
4.4	Effect of bed depth on weight loss of graphite in CO ₂	139
4.5	Effect of bed depth on weight loss of coconut char in CO ₂	141
4.6	Effect of CO on weight loss of coconut char	142
4.7	Effect of CO on weight loss of coconut char at 1151 K	143
4.8a	Reproducibility of weight loss data of graphite in CO ₂	146
4.8b	Reproducibility of weight loss data of coconut char in CO ₂	147

Figure	Title	xiii Page
4.9	Polynomial fitting of weight loss in CO ₂	150
4.10	Instantaneous rate versus time for coconut char in CO ₂	152
4.11a	Instantaneous rate versus fractional conversion for graphite in CO ₂	153
4.11b	Instantaneous rate versus fractional conversion for coconut char in CO ₂	154
4.12a	Ratio of rates (r_1/r_g) versus fractional conversion for graphite in CO ₂	156
4.12b	Ratio of rates (r_1/r_g) versus fractional conversion for graphite in CO ₂	157
6.1	Log r_g versus $1/T$ for different investigators	181
6.2	$(p_{CO_2} - p_{CO_2,e})/r_g$ versus p_{CO} for coconut char in CO ₂ - CO	185
6.3	r_g versus p_{CO_2} for coconut char in CO ₂ - Ar	186
6.4	Variation of θ_1 and θ_{CO} with temperature for coconut char in CO ₂ - CO	187
6.5	Variation of θ_1 with temperature for coconut char in CO ₂ and CO ₂ - Ar	188
6.6	Arrhenius plot for graphite and coconut char	197
6.7	r_g versus bed depth for graphite in CO ₂	203
6.8	r_g versus bed depth for coconut char in CO ₂	204
6.9	K_{CT} versus p_{CO_2} for coconut char in CO ₂ , CO ₂ - Ar	205
6.10	K_{CT} versus p_{CO} for coconut char in CO ₂ - CO	206
6.11	Variation of $(K_{CT})_{CO_2-CO} / (K_{CT})_{CO_2}$ with p_{CO} for coconut char	208
6.12	$1/K_{CT}$ versus $1/p_{CO_2}$ for coconut char in CO ₂ , CO ₂ - Ar	210

Figure	Title	Page
6.13	p_{CO_2}/K_{CT} versus p_{CO} for coconut char in $CO_2 - CO$	211
6.14	$\ln I$ versus $1/T$ for coconut char	213
7.1	Sample curves for exit gas composition and rate of carbon loss as function of time	230
7.2	Reproducibility of estimated fractional reduction of iron oxide amongst duplicate sets	231
7.3	Variation of rates, exit gas composition and bed temperature with fractional reduction(f) of iron oxide (Expt.1)	232
7.4	Variation of rates, exit gas composition and bed temperature with fractional reduction(f) of iron oxide (Expt.2)	233
7.5	Variation of rates, exit gas composition and bed temperature with fractional reduction(f) of iron oxide (Expt.3)	234
7.6	Variation of rates, exit gas composition and bed temperature with fractional reduction(f) of iron oxide (Expt.4)	235
7.7	Variation of rates, exit gas composition and bed temperature with fractional reduction(f) of iron oxide (Expt.5)	236
7.8	Variation of rates, exit gas composition and bed temperature with fractional reduction(f) of iron oxide (Expt.6)	237
7.9	Variation of rates, exit gas composition and bed temperature with fractional reduction(f) of iron oxide (Expt.7)	238
7.10	Variation of rates, exit gas composition and bed temperature with fractional reduction(f) of iron oxide (Expt.8)	239
7.11	Experimental (\dot{w}_C) and predicted (\dot{w}_{CP}) rate of carbon loss for iron oxide powder and coconut char powder mixture	241
7.12	Experimental (\dot{w}_C) and predicted (\dot{w}_{CP}) rate of carbon loss for iron oxide micropellet and coconut char powder mixture	242

Figure	Title	xv Page
7.13	Sample result of Abraham et al.(3) for iron oxide pellet and graphite powder mixture	247
7.14	Comparison of experimental reduction rate with rate predicted from gasification	249
7.15	Comparison of $(r_g) \text{ CO-CO}_2 / (r_g) \text{ CO}_2$ observed by Tiwari(141) and calculated from extrapolation formula(32) and calculated from extrapolation formula(32)	251

LIST OF SYMBOLS

a, a^*	=	Dimensionless parameter
d	=	Mean diameter of gas molecule, cm
D, D_b, D_e, D_k	=	Overall, bulk, effective and Knudsen diffusivity respectively, $\text{cm}^2 \text{s}^{-1}$
D_p	=	Average particle diameter, cm
E	=	Dimension less parameter
E_1, E_2, E_3	=	Activation energies of I_1, I_2, I_3 respectively kJ.mol^{-1}
E_{i1}, E_{j1}	=	Activation energy of forward and backward reaction of reversible oxygen exchange step, kJ.mol^{-1}
E_{j3}	=	Activation energy of gasification step, kJ.mol^{-1}
f	=	Fractional reduction of iron oxide in carbothermic reduction
F	=	Fractional gasification of carbon
ΔG°	=	Change in standard free energy, of a reaction, kJ.mol^{-1}
ΔH°	=	Change in standard heat of formation of a reaction, kJ.mol^{-1}
i_2	=	Dimensionless parameter
I_1, I_2, I_3	=	Rate parameters of Langmuir-Hinshelwood rate expression
k_1	=	Rate parameter of gasification of carbon $\text{g.mol}^{-1} \text{cm}^{-3} \text{atm}^{-1} \text{s}^{-1}$
k_2	=	Thermodynamic parameter of adsorption of CO, atm^{-1}
k', k'', K'	=	Rate parameters of equations of Roberts and Shatterfield
K	=	Rate of reaction
K_b	=	Thermal conductivity of bulk, $\text{g.cm.s}^{-3} \text{.k}^{-1}$
K_c	=	Isothermal intrinsic rate of gasification, s^{-1}

K_{CT}	=	Intrinsic rate of gasification after mass and heat transfer correction, s^{-1}
K_e	=	Effective thermal conductivity, $g.cm.s^{-3}.K^{-1}$
K_g	=	Corrected thermal conductivity of gas, $g.cm.s^{-3}.K^{-1}$
K_g^o	=	Thermal conductivity of gas, $g.cm.s^{-3}.K^{-1}$
K_r	=	Thermal conductivity due to radiation after porosity correction, $g.cm.s^{-3}.K^{-1}$
K_r^o	=	Intrinsic thermal conductivity due to radiation, $g.cm.s^{-3}.K^{-1}$
K_s	=	Intrinsic thermal conductivity of solid, $g.cm.s^{-3}.K^{-1}$
K_{LH}	=	Intrinsic rate of gasification by Langmuir-Hinshelwood rate equation, s^{-1}
L_c	=	Effective length of bed, cm.
M	=	Molecular weight
P_b	=	Break away pressure, $kg.cm^{-2}$
PCO, PCO_2	=	Partial pressure of carbon monoxide and carbon dioxide, atm
PCO_2, e	=	Equilibrium partial pressure of carbon dioxide at the reaction condition, atm
\dot{Q}	=	Volumetric flow of gas, $cm^3.s^{-1}$
r_g	=	Rate of gasification of carbon, s^{-1}
r_g^o	=	Rate of gasification at zero bed depth, s^{-1}
r_o	=	Initial radius of iron oxide pellet
R	=	Isothermal rate of gasification, s^{-1}
R_{cp}	=	Non-isothermal rate, s^{-1}
R_d	=	Rate of gasification relative to external geometric surface area, $g.atom-C.cm^{-2}.s^{-1}$
R_l	=	Local rate of oxidation of carbon, s^{-1}
RCO_2	=	Rate of gasification, $g.mol.cm^{-3}.s^{-1}$

v	=	Volume ratio of product to that of an equivalent amount of reactant
v_{β}	=	Ratio of activities of two solid reactants viz. iron oxide and carbon, expressed as the volume ratio
v_v	=	Dimensionless parameter defining relative molar quantities of two solids
\dot{w}	=	Rate of total weight loss, g.s^{-1}
\dot{w}_c, \dot{w}_o	=	Rate of weightloss of oxygen and carbon respectively in carbothermic reduction, g.s^{-1}
\dot{w}_{cp}	=	Rate of carbon loss in carbothermic reduction predicted from gasification rate, g.s^{-1}
Δw	=	Total weight loss in carbothermic reduction at any time $t=t$, g
Δw_c	=	Weight loss of carbon in carbothermic reduction at any time $t=t$, g
Δw_o	=	Weight loss due to oxygen removal from oxide in carbothermic reduction at any time $t=t$, g
x	=	Dimensionless distance
x_{CO}	=	Fraction of carbon monoxide in the product gas of carbothermic reduction
x_{CO_2}	=	Fraction of carbon dioxide in the product gas of carbothermic reduction
y	=	Dimensionless pressure
z	=	Dimensionless temperature

Greek Symbols

β	=	Dimensionless parameter
ϵ	=	Emissivity of solid
η	=	Effectiveness factor
$\bar{\eta}$	=	Effectiveness factor which depend upon the net effect of structure changes on gasification

μ	=	Viscosity of gas, $\text{g.cm}^{-1}.\text{s}^{-1}$
ν	=	Stoichiometric co-efficient
ρ	=	Bulk density, g.cm^{-3}
ϕ	=	Rate parameters of effectiveness factor calculation by method by Alam et al.
ϕ_1, ϕ_2	=	Rate parameter of gasification in presence and absence of CO respectively, $\text{atm}^{-1}.\text{s}^{-1}$
ϕ_M	=	Modified Thiele's modulus
ϕ_w	=	Thermodynamic parameter of adsorption of CO atm
ψ	=	Dimensionless parameter
ϵ	=	Fractional porosity
ω	=	Dimensionless parameter
$\sigma_{\text{CO-CO}_2}$	=	Lenard Jones parameters for CO-CO ₂
$\Omega_{\text{CO-CO}_2}$	=	Collision integral of CO-CO ₂

SYNOPSIS

KINETICS OF GASIFICATION OF CARBON AND CARBOTHERMIC REDUCTION OF IRON OXIDE

A Thesis Submitted
In Partial Fulfilment of the Requirements
for the Degree of
Ph. D

by
DEBAJYOTI BANDYOPADHYAY

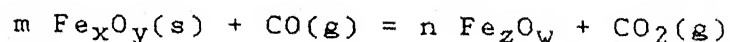
to the
Department of Metallurgical Engineering
Indian Institute of Technology, Kanpur
July, 1989

Blast furnace route is the most important one for production of iron. Both indirect as well as direct reduction of iron oxide take place in the blast furnace. The former is the reduction of oxide by reducing gas and the latter is reduction by solid carbon. Direct reduction is predominant at the lower part of the stack.

Blast furnace technology requires metallurgical grade coking coal which is getting depleted day by day. So alternative routes for ironmaking have come. One of them, i.e. the rotary kiln process, uses non-coking coal for reduction. Here again, direct reduction is important. So understanding of fundamentals of reduction of iron oxide by solid carbon is important. The present thesis is concerned with it.

Investigations on the direct reduction of iron oxide by solid carbon have established that the reduction process takes place via gaseous intermediates. The overall reaction is a combination of the following two reactions :

Gasification of carbon : $C(s) + CO_2(g) = 2CO(g)$ and
reduction of iron oxide :



As gasification is a component reaction and the rate

controlling step for the overall reaction, as reported by many investigators, it becomes an integral part of direct reduction and thus of considerable importance. The reduction of iron oxide by carbon via gaseous intermediates may in general be termed as 'carbothermic reduction'.

A thorough literature survey on kinetics of gasification of carbon and carbothermic reduction of iron oxide reveals that though considerable amount of informations are available on both the topics but still some anomalies and gaps exist. The present thesis is directed to either eliminate or to throw some light on these.

It being a fundamental study, pure iron oxide and carbon were employed as the raw materials for the investigations. Considerable emphasis has been laid on the kinetics of gasification of carbon due to its importance, as already mentioned.

Literature review shows that very few attempts have been made to predict the rate of carbothermic reduction of iron oxide from that of gasification rate and one such effort by Abraham in this laboratory exhibited one order of magnitude difference between the two. A probable reason for the discrepancy may be erroneous value of gasification rate of graphite, as used by them and thus it was decided to redetermine graphite gasification rate. Again many workers have reported that freshly produced iron in carbothermic reduction greatly enhances the gasification rate of carbon, and this is one major problem for quantitative correlation of carbothermic rate with rate predicted from that of gasification reaction. It has been reported in literature that highly reactive form of carbon does not seem to suffer catalytic effect from iron produced during carbothermic reduction, and

thus coconut char was chosen as the solid reductant of iron oxide for correlation purposes. It was, therefore, necessary to have gasification rate data on coconut char under different temperatures and gaseous environments.

A series of experiments were carried out for graphite and coconut char. Graphite of -200 +230 ASTM size was employed here to reproduce experimental condition of Abraham. Two other particle sizes were also used to see the effect of particle size. Other process parameters like bed depth, CO_2 flow rate, compaction pressure etc. were varied during experiments to find their effects on rate. Gasification measurement of graphite could be carried out with only CO_2 gas in the temperature interval of 1222-1283K. Gasification of coconut char was carried out in three CO - CO_2 mixtures, ranging from 20% CO to 80% CO , besides measurements in CO_2 and CO_2 -Ar gas mixtures, in the temperature range of 1081-1283K.

Again heat and mass transfer limitations may have profound effect on the gasification kinetics. So mass transfer analysis for both graphite and coconut char were carried out using the mathematical technique of Tien and Turkdogan to calculate isothermal effectiveness factor. It has been established in this thesis that I_2 and I_3 of Langmuir-Hinshelwood rate equation are not universal in nature, and vary with type of carbon used. As the technique of mass transfer analysis presented by Roberts et al need values of I_2 and I_3 , the same could not be utilised. To calculate the non-isothermal effectiveness factor for gasification rate, the mathematical technique presented by Tien et al was attempted. But it was found to suffer dimensional inconsistency. So a separate model was developed for heat transfer

xxiii
calculation. Due to slow rate of reaction, non-isothermal effect for graphite was unimportant. Calculation of heat and mass transfer limitations on rate called for extensive use of computer and all required programs were developed during the course of the present investigation. The salient findings on gasification rate measurements of graphite and coconut char may be briefly presented as follows :

Instantaneous rate versus fractional conversion plots for graphite and coconut char did not show any steady state value and thus rates at 5% conversion were chosen for further analysis assuming that the bed did not change much from the initial characteristics. The reactivity values thus obtained for graphite and coconut char were found to match quite well with some reported values in the literature. Mass transfer analysis revealed its considerable effect on gasification kinetics of both graphite and coconut char. Coconut char at high temperature suffered significantly, from heat transfer limitations as well. It gradually decreased with decrease of temperature. Carbon monoxide was found to have profound inhibiting effect on the gasification rate of coconut char and the effect was found to be more prominent at high temperature. This is in contrast with what has been reported in literature. Rate values at zero bed depth, which in principle should give intrinsic chemical rate free of heat and mass transfer limitations were obtained by extrapolating the experimentally observed rates at different bed depth to zero bed depth, and these were found to match very satisfactorily with calculated intrinsic rate values for both graphite and coconut char. This served as a cross check for the correctness of both experimental data as well as heat and mass transfer calculations.

The gasification rate data of coconut char did not obey first order rate equation. It was also not possible to conclude with certainty about validity of Langmuir-Hinshelwood rate equation for the present set of data on coconut char. A scan of literature also shows confusion in this regard.

Studies on carbothermic reduction of iron oxide with coconut char as the solid reductant consisted of two types of geometry.

(a) iron oxide (-325 mesh) and coconut char powder (-200 +270 mesh) mixture,

(b) iron oxide micropellet (approx. 2 mm dia) and coconut char powder mixture.

As the weight loss in carbothermic reduction is a combination of weight loss due to gasification of carbon, and weight loss due to removal of oxygen from oxide, it is essential to have knowledge of the variation of actual gas composition with progress of reaction to calculate percentage reduction. An effort was made to simultaneously measure the weight loss and perform gas analysis with the help of a specially designed thermogravimetry apparatus. But due to some unavoidable problems, the two aspects were decoupled. Weight loss measurements for both the abovementioned geometries were carried out in a specially designed reaction chamber in the temperature range of 1078-1284K. Product gas analysis was carried out with the help of a gas chromatograph under identical conditions of weight loss measurements. Temperature history of the bed was registered during carbothermic reduction. The weight loss data and the gas analysis data were processed by a computer for calculation of instantaneous weight of carbon, instantaneous rate of carbon loss, instantaneous rate of

oxygen loss, percentage reduction of iron oxide etc. The important findings of this study may be presented briefly in the following manner.

The gas composition versus fractional conversion plots for both the geometries were found to follow the equilibrium gas composition line for stagewise reduction. This ensured that the reduction of iron oxide by solid carbon took place in a stagewise manner. In case of powder mixture of iron oxide and coconut char, the gas composition was very close to the gas composition at equilibrium with iron oxide system at all the temperatures, at least at the third stage, and thus gasification was exclusively rate controlling. But for iron oxide micropellet and coconut char powder system at highest temperature, the experimental gas composition was found to lie well above the equilibrium line at the third stage indicating that the reduction step was also partly controlling the overall rate. With decrease of temperature, the experimental gas composition started falling closer to the equilibrium line. So at lower temperatures, the rate was exclusively controlled by gasification. This was explained by larger mass transfer resistance for oxide micropellet at high temperature, and large activation energy of gasification reaction.

Rate of carbon loss at the highest temperature, and for both the geometries were found to be significantly enhanced with progress of reduction. This was a clear indication of catalysis of gasification reaction by freshly produced iron. Again at lower temperatures no catalytic effect could be observed. These findings are partly in disagreement with what has been concluded in literature. Catalytic effect at higher temperature has been explained by better contact of

the particles due to sintering, as well as more importance of external surface area of carbon.

Attempt was made to predict the carbothermic reduction rate from the rate of gasification. Some quantitative disagreement was observed in the two rates. The discrepancy could be explained from the difference in mode of calculation of rate.

At the same time recalculation showed very good agreement between predicted and experimental rate of reduction in connection with Abraham's earlier study in this laboratory. This removed another anomaly. Results of the present set of calculation established that the formula reported in literature and used by Abraham for extrapolating the gasification rate data in CO_2 to CO-CO_2 gas mixture was erroneous.

CHAPTER 1

1.1 Introduction

The practised technology for production of liquid iron or hot metal from iron ore is by blast furnace route which even today enjoys the status of most thermally efficient and economic process. Blast furnace route shares around 95 pct. (98 pct. in India)(1) of total hot metal production worldwide. It is well known fact that both indirect and direct reduction of iron oxide takes place in blast furnace. The former is the reduction of oxide by reducing gas like CO and the latter is by carbon. The direct reduction is predominant at the lower part of the stack.

Though blast furnace is the most trusted route for ironmaking but presently it is suffering from a major drawback from raw materials' quality point of view. Blast furnace needs metallurgical grade coking coal for its operation which day-by-day is getting depleted throughout the world. In India there are only localized and limited coking coal deposits (2312 MT approximately). So alternative ironmaking processes outside blast furnace are of importance.

Sponge iron is a highly porous metallic iron produced from iron oxide by suitable reducing agent in solid state. Primarily due to the abovesaid problem for blast furnace ironmaking, sponge iron is gaining its importance throughout the world. There are yet few other reasons for which sponge iron is gathering momentum as a potential substitute for conventional ironmaking. These are as follows.

(i) blast furnace ironmaking requires high quality coking coal as reducing agent whereas sponge iron can be produced using other

types of reductants such as non-coking coal, natural gas

(ii) high capital investment and longer gestation period are necessary for integrated steel plant. On the other hand sponge ironmaking can be taken up in small scale and can depend upon local availability of reducing agent

(iii) sponge iron-electric arc furnace route is cheaper than blast furnace-basic oxygen steelmaking route in small scale

(iv) sponge iron can practically substitute steel scrap in electric arc furnace and this can alleviate periodic scrap shortage in India

(v) sponge iron is much more consistent in composition as compared to steel scrap and is almost free from tramp elements (like Cu, Sn, Pb, As, etc.)

As India was poor in petroleum or natural gas deposits, a process of ironmaking based upon the use of non-coking coal was considered to be the best and is the approach being pursued even now.

Sponge iron can be produced by use of non-coking coal in one of the two following routes.

(i) gasification of coal and reduction of iron oxide by the reducing gas thus generated. This route is not considered economically viable due to the cost involved in separate gasifier

(ii) direct use of solid coal as reducing agent and this is the route chosen.

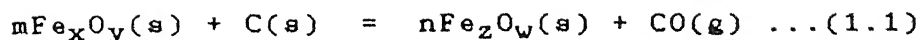
Rotary kiln process is the most widely tried technology for production of sponge iron by coal. Here iron ore lumps, non-coking coal lumps, flux etc. are charged into a rotary kiln. The maximum operating temperature of the kiln is around 1150°C . Reduction of iron

oxide is principally by carbon, and what in text book is known as 'Carbothermic Reduction'. In India, National Metallurgical Laboratory, Jamshedpur took initiative in this in late sixties and early seventies. Some plants have been set-up in the last decade. The present status of direct reduction based on rotary kiln in India is summarized in Table 1.1.

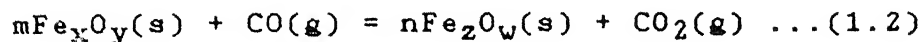
Table 1.1 Present status of rotary kiln based direct reduction in India(2)

Name of the Company -----	Location -----	Installed Capacity(tpa) -----	Remarks -----
Sponge Iron India Limited	Polancha (A.P.)	60,000	One additional unit of 30,000 tpa has been added recently
Orissa Sponge Iron Limited	Palasponga (Orissa)	150,000	Capacity can be doubled
Ipitata Sponge Iron Limited	Joda (Orissa)	90,000	Already in production
Bihar State Indsl. Dev. Corp. Ltd.	Chandil (Bihar)	150,000	Plant under construction
M/s Hope India Limited	Purulia (West Bengal)	-	Under negotiation
M/s Sunflag Limited	Udharbha (Maharashtra)	-	First direct reduction based integrated steel plant in India
M/s Birla Jute Mills	Barbil (Orissa)	-	Under negotiation

Therefore, 'Direct reduction' or 'Carbothermic reduction' i.e. reduction of iron ore by carbon in solid state is of considerable importance in Indian context, since it is the principal reaction in the rotary kiln process of sponge ironmaking. The reaction may be represented as:



This reaction is basically a combination of two gas-solid reactions viz.



The reason for using symbols x, y, z and w is that there are three oxides of iron, viz. Fe_2O_3 , Fe_3O_4 , Fe_xO ($0.87 < x < 0.955$). Use of symbols allows generalization applicable to any oxide. Appendix 1 to Appendix 5 presents the ΔH° and ΔG° values of different oxides of iron and for CO , CO_2 in the experimental temperature range.

Reaction 1.2 is the 'Reduction reaction' and reaction 1.3 is 'Gasification reaction' concerned with gasification of carbon. The objective of the present investigation is to carry out some fundamental studies on kinetics of the above reactions. It has been found by several investigators that gasification reaction controls the overall carbothermic reduction (Eq.1.1). That is why kinetics of gasification also becomes very important. In view of the same considerable emphasis has been laid on the study of kinetics of gasification reaction.

So it is clear from the above discussions that reduction of iron oxide by carbon is a very important reaction so far as either blast furnace or rotary kiln is concerned. Gasification being an integral part and probable rate controlling step of the carbothermic reduction, fundamental aspects of both reduction reaction and gasification reaction are of importance. The present thesis is concerned with it.

Review of the literature, which will be presented in

subsequent sections reveals that even though considerable extent of informations are available on carbothermic reduction, some anomalies still exist both in the field of gasification of carbon as well as reduction of iron oxide. A previous study (123) in this laboratory on carbothermic reduction of iron oxide by graphite shows that there is a significant quantitative disagreement among the experimental carbothermic rate and the rate predicted from gasification of carbon. There is no general agreement on whether gasification reaction undergoes any significant catalytic effect from freshly produced iron during carbothermic reduction and thus is an unresolved question. Catalysis of gasification reaction complicates the interpretation of reduction data of powder mixture of oxide and carbon. Again mass transfer and heat transfer limitations have been found to influence the gasification reaction and thus needs attention to either eliminate them during reaction or evaluate them quantitatively.

So it was decided to reevaluate the gasification rate of graphite in CO_2 to check the correctness of what has been reported by Abraham et al (123) and to correlate it with their carbothermic reduction data.

Again literature evidence shows that catalytic effect of freshly produced iron is less significant on gasification rate of carbons which are inherently fast in reaction with CO_2 . So high reactive form of carbon like coconut char was selected with the intention of either eliminating or minimizing the catalytic effect of reduced metallic iron on rate of gasification reaction. It was decided to eliminate heat and mass transfer resistance on gasification reaction to evaluate intrinsic rate.

The thesis has been divided into eight chapters. Chapter 1 reviews the literature on gasification and carbothermic reduction. It also contains plan of work. Chapter 2 gives the design and fabrication features of the apparatus used for conducting different types of experiments. Chapter 3 contains the types of materials used, their mode of preparation and the experimental procedures. Chapter 4 presents the results on gasification measurement of graphite in CO_2 and coconut char in CO_2 , CO-CO_2 , $\text{CO}_2\text{-Ar}$ mixtures. As quantitative evaluation of both heat and mass transfer resistances are of great significance. Chapter 5 summarizes the salient features and formulations for the same. Chapter 6 discusses the results of gasification measurements and the intrinsic rate of reaction after elimination of heat and mass transfer limitations from experimental rate. Chapter 7 has in it the results and discussions of carbothermic reduction of iron oxide. Chapter 8 contains the conclusions reached from the present investigation. Chapter 9 suggests the scope for future study.

1.2 Literature Review on Kinetics of Gasification of Carbon by CO_2

1.2.1 Nature of carbon

Carbons with intermediate ordering can conveniently be classified into two main groups(4).

(i) carbon formed by gas phase reaction, such as by twining or high temperature cracking of gaseous hydrocarbons (product is carbon black) or liquid hydrocarbons

(ii) carbon formed by dehydration and dehydrogenation of liquid hydrocarbons such as petroleum coke from petroleum or of solid hydrocarbons like wood char from wood or of carbon-hydrogen-oxygen

compounds like coal char from coal. If the starting material is solid then the final product retains some of the shapes of the starting material.

In general, the product of the first group is more or less in powder form whereas the second group produces carbon of more massive form i.e. in lumps. Physical properties of carbon depends upon the starting material and the mode of preparation. If the starting material is solid then the final product retains a good portion of the morphology of the initial hydrocarbon molecules. For example, coal char contains large cellulose molecules originally present in wood.

Carbon is having continuous planar hexagonal stacking of atoms. Graphite has the most ordered structure in terms of sequential arrangement of 'C' atoms. Even then different types of defects are present in graphite structure. A brief account of the types of defects(5) present in carbon structure has been presented below:

(i) Layer-stacking defects: perfect planar networks of hexagons of carbon atoms though present as parallel layers, may be displaced from the ideal hexagonal or rhombohedral sequence, thus leading to disordered stacking sequence. These types of carbons are known as "Tarbostatic". Ordering of the stacking defects needs heating of carbon above 1200°C and as gasification takes place below 1200°C , this defect can not be removed during reaction.

(ii) Carbon - network bond defect: a network of finite size is conventionally referred to as a carbon macromolecule which in case of near ideal graphite is aromatic in nature. The principal types of bond defects are:

(i) Edge defect: whenever the C-C bond can not be formed, for example one carbon macromolecule is out of plane with respect to its immediate neighbours, but the electronic valency is satisfied by some way or the other. This type of defect arises very often because foreign atoms or groups are bonded at the edge defect and significantly alters the chemical behaviour of carbon. Sometimes carbon atoms at the edge defect may form weak spin-pairing bonds with atoms of neighbouring macromolecules and at high temperature such weak spin-pairing bonds would tend to dissociate and couple with foreign atoms or molecules (like CO_2) to give other products.

(ii) Hole or claw defect: this type of defect arises when C-C broken bonds lead to holes or rupture in the network of hexagons of carbon. The space limitation in the structure leads to unpaired electrons for one or more of the atoms at the defect site and trap foreign atoms or groups, thus increases the possibility of reaction. Entrapment of foreign atoms causes considerable bulges or buckles in the network.

(iii) Twinning effect: at the joining of the twinning planes, alternative 4 atom and 8 atom rings form. This gives rise to deformation of the crystal structure.

The defect sites in the crystal structure of carbon, as mentioned are responsible for adsorption of foreign atoms or molecules and oxygen atoms in particular for gasification of carbon by CO_2 . The adsorption capacities of some varieties of carbon may be arranged in the order as shown below.

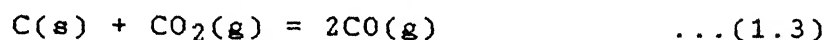
active char > soot > coke or retort graphite > natural graphite

Rate of gasification depends upon the extent of imperfections present in a particular carbon structure. For example as coconut char is structurally more imperfect than graphite, the former exhibits higher reaction rate with CO_2 .

When hydrocarbons are heated(6) above 400°C , dissociation and polymerization begins and is termed as 'Charring'. Upon further heating, condensed ring structures are formed and at very high temperature (2000°C - 3000°C) 'Graphitization' occurs. Thus as graphite is considered to be near-ideal structure of carbon, carbons of other forms are characterized with reference to graphite.

1.2.2 General considerations of kinetics

The reaction of carbon with carbon dioxide, viz.



is a gas-solid reaction. Due to this reaction, a piece of carbon keeps loosing weight with progress of time. The rate of reaction of carbon with an oxidising agent like CO_2 is therefore expressed in terms of rate of loss of carbon from the sample. Various units have been employed, such as g/g. min, g-mole/ cm^3 .s, min^{-1} , Kg/Kg.s etc.

However, the most acceptable expression of rate has been as noted in Eq.1.4, viz.,

$$\text{rate}(r_g) = - \frac{(dW_c/dt)}{W_c} \quad \dots(1.4)$$

where $(-dW_c/dt)$ is the rate of weight loss of carbon and W_c is the instantaneous weight of carbon. The rate expressed by Eq.1.4 gives the rate of gasification per unit mass of carbon and has unit of Time^{-1} .

In industry, a terminology "Reactivity" has been under use to express the rate of reaction of carbon with carbon dioxide. It can

be defined as the ease with which a carbon particle reacts with CO_2 . The rate (r_g) as defined by Eq.1.4 may be used as a measure of reactivity.

A simplified picture of reaction of a carbon particle with carbon dioxide has been presented in Fig.1.1. The kinetic steps are:

(a) transportation of CO_2 from bulk gas to the external surface of carbon particle through boundary layer

(b) diffusion of CO_2 into the interior of the pores of the sample i.e. pore diffusion

(c) adsorption of CO_2 on the pore surface and external surface

(d) surface chemical reaction in the adsorbed layer

(e) desorption of CO i.e. the product of the reaction

(f) outward diffusion of CO from interior to sample surface through pores

(g) transportation of CO from the sample surface to the bulk gas phase through boundary layer.

Amongst the kinetic steps mentioned above, (c), (d) and (e) are chemical steps as some form of chemical reaction is involved in them and rest of the steps are transport steps. Out of the above, one or more than one steps would be controlling the rate.

Many physical variables have profound influence on rate. They may be listed as

(a) Temperature of reaction

(b) Particle size of carbon

(c) Gas composition

(d) Nature of carbon

(e) Impurities associated with carbon and gas

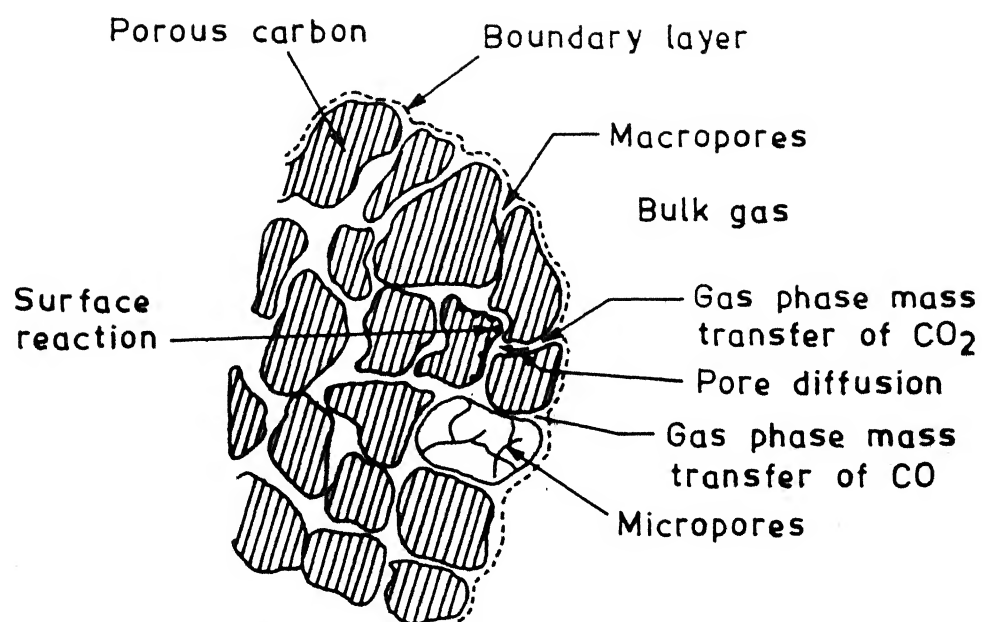


Fig. 1.1. Schematic representation of C-CO₂ reaction.

So far as mass transfer is concerned, it can be broadly classified into the following:

(1) the transfer of CO and CO₂ across the concentration boundary layer around the carbon particle. This may be referred to as external mass transfer

(2) counter diffusion of CO and CO₂ through the pores of carbon, specially macropores. This may be called as internal mass transfer.

Many investigations have been carried out on rates of gasification of various types of carbonaceous material by CO₂. The rates have been found to vary over a wide range by several orders of magnitude. However, it has been mostly characterised by a high activation energy (200 - 350 kJ/mole) indicative of predominance of chemical control ascribed to slow surface chemical reaction step (step c to step e). A further confirmatory proof of chemical control is significant catalytic or inhibition effect of a variety of elements and compounds on the rate of gasification. However, it has also been established that mass transfer tends to contribute significantly to control of reaction rate, depending upon the experimental conditions. This will be elaborated later. It may be noted here that the reaction tends to be exclusively chemically controlled if

- (i) the temperature is low
- (ii) the particle size is small

The reaction 1.3 is endothermic in nature. The value of standard enthalpy of reaction (ΔH°) are 111.590 kJ/mol and 111.520 kJ/mol at 1000K and 1200K respectively. This endothermic nature often causes significant drop of temperature inside the particle while the reaction is in progress. Under such circumstances, the reaction will

be partially controlled by the rate of heat transfer as well.

Another important feature of this reaction is the large retardation of rate by the product gas, viz. carbon monoxide. This effect has been found by several investigators and shall be discussed in details subsequently. However, in order to illustrate the effect Fig.1.2 presents some data on graphite collected by Turkdogan and Vinters(29), who measured rates of gasification of various forms of carbon in CO-CO₂ mixtures of different compositions. Fig.1.2 shows that the rate at 25% CO₂ -75% CO mixture can be as low as two orders of magnitude less than that in pure CO₂. It has been observed by investigators(29,79,89) that the retarding effect of CO is larger at lower temperature.

1.2.3 Rate and mechanism of surface reaction

Due to the importance of gasification reaction of carbon both in the field of metallurgical and chemical industries, numerous investigations (7-50) have been carried out in the last four decades by chemists, chemical engineers and metallurgists. Different forms of carbon under various experimental conditions like varying particle size and geometry, different types of gaseous environments (like pure CO₂, CO-CO₂ mixture, inert gas- CO₂ mixture etc.) have been employed.

Salient kinetic features of gasification of carbon in carbon dioxide containing gases have already been stated in Sec.1.2.2, viz. high activation energy, large variation of rate from worker to worker, strong retarding influence of carbon monoxide resulting the rate to be primarily controlled by the surface reaction step.

In view of the fact that it is either exclusively or

significantly controlled by surface reaction step, the same assumed special importance. Many investigators conducted experiments to find out rate and mechanism of surface reaction. In order to achieve the same, efforts were made in all careful measurements to eliminate mass transfer control by proper selection of experimental conditions. In this brief literature review it is not possible to mention about all these investigations. Neither it is necessary in view of some excellent reviews that have been published from time to time, e.g. Johnson(56), Reif(14), Walker(21), Rao and Jalan(32). Therefore, in this review attempt will be made to elucidate the significant features and developments only. As stated earlier, the surface reaction consists of adsorption of reactant gas on the surface, reaction on the surface and desorption of the product gas. The process of adsorption and desorption are much more likely to be rate controlling step in heterogeneous reaction, since both may involve appreciable energies of activation(51), particularly the desorption step. This concept is in fact the basis of the modern treatment of surface reaction, due to Langmuir(52) and Hinshelwood(53). This treatment involves, first, obtaining an expression for the concentrations of the reactant molecules on the surface and then expressing the rate of formation of gaseous products in terms of these concentrations. The rate is then expressible in terms of the concentrations of the gaseous reactants. The Langmuir and Hinshelwood mechanism for a reaction between A and B may be formulated as in Fig.1.3.

Another type of mechanism for surface reactions was also considered by Langmuir(52). According to this mechanism the reaction occurs between a gas molecule and an adsorbed molecule so that only

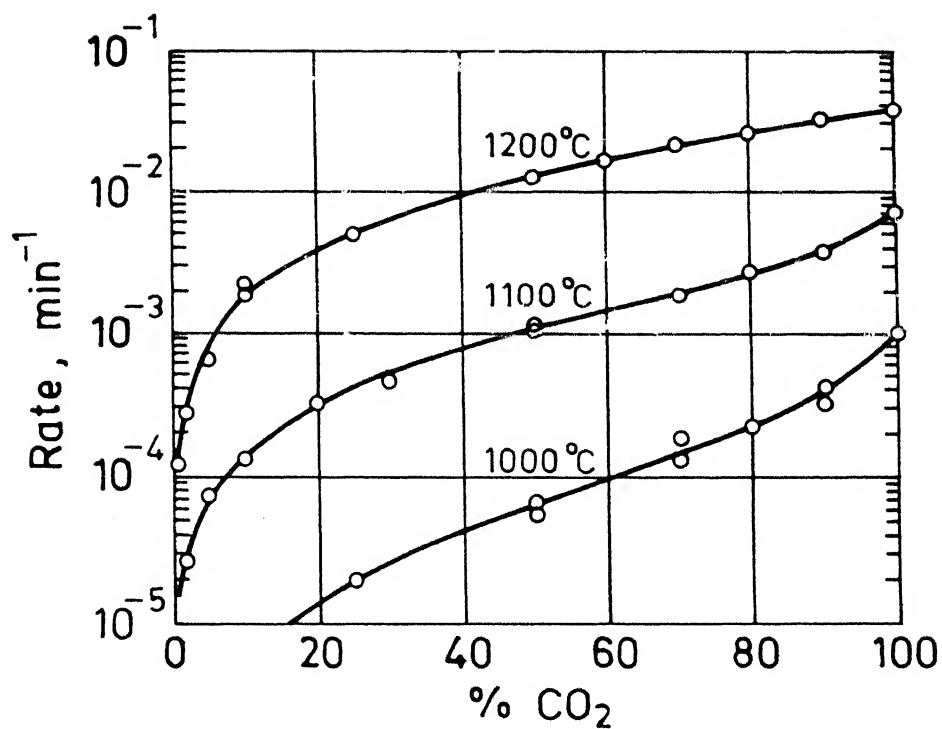


Fig. 1.2. Effects of temperature and gas composition on the rate of oxidation of electrode graphite granules (~0.5 mm dia) in CO₂-CO mixtures. (29)

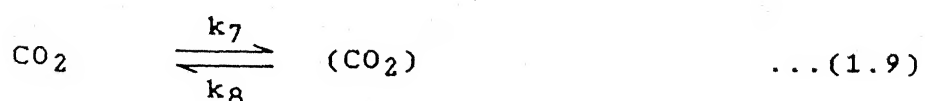
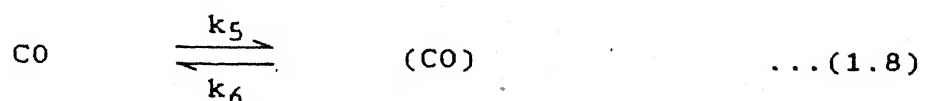
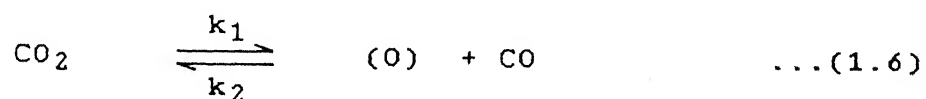
one of the reactants has to be adsorbed. This mechanism may be represented as shown in Fig.1.4. It is not necessary that A is not atall adsorbed, it is only postulated that adsorbed A molecule does not react. Reidal(54) has shown that the second mechanism can be applied to certain atoms and radical combinations. But as a whole the Langmuir- Raidal mechanism is not as common as Langmuir - Hinshelwood.

Gadsby et al.(8,10) measured the rates of gasification of coal char and coconut char in CO_2 and CO-CO_2 mixture in temperature range of 973-1103K and at pressure range of 10-760 Hg. They fitted the rate with an equation of the form

$$\text{rate} = \frac{I_1 P_{\text{CO}_2}}{1 + I_2 P_{\text{CO}} + I_3 P_{\text{CO}_2}} \quad \dots(1.5)$$

where I_1, I_2, I_3 are three constants dependent of temperature. Subsequently more investigators have employed the above rate equation.

Reif(14) made a comprehensive review of gasification reaction of carbon and summarized the various proposed reaction mechanisms as:



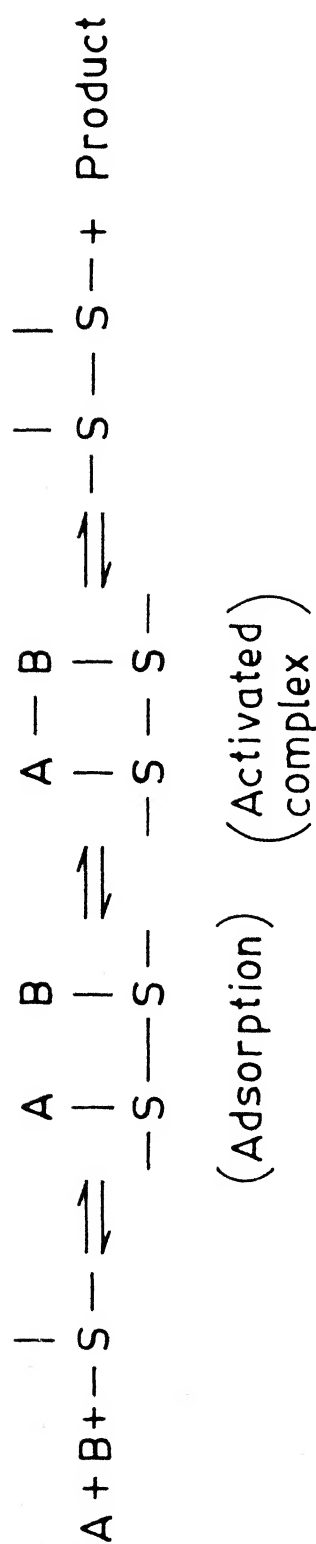


Fig. 1.3. Langmuir - Hinshelwood mechanism for a reaction :
 $A + B \rightarrow \text{Product} \quad (52)$

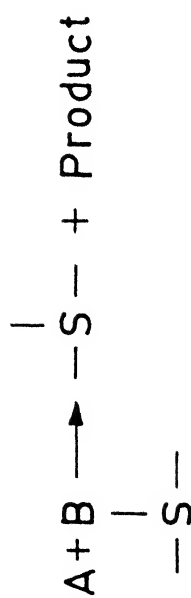
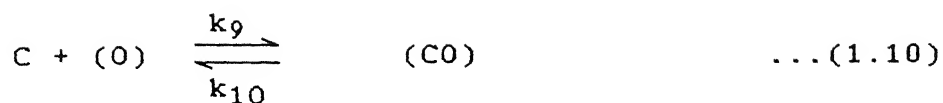


Fig. 1.4. Alternative Langmuir mechanism for a reaction :
 $A+B \rightarrow \text{Product} \quad (52)$



where bracketted terms indicate adsorbed species on the carbon surface.

The above equations i.e. Eq.1.6 - Eq.1.11 represent elementary steps of surface reaction. Different workers have arrived at the overall reaction by suitable combination of some of the above elementary steps. Some such combinations are:

Eq.1.6 -----> Eq.1.7

Eq.1.6 -----> Eq.1.10 -----> Eq.1.8

Eq.1.9 -----> Eq.1.11

Reif(14) had shown that it is possible to arrive at the rate equation (Eq.1.5) by several such combinations. Therefore, he tried to eliminate some of these mechanisms using evidence from literature as well as his own experimental work. According to him no evidence was available to substantiate the possibility of reaction 1.10. Therefore it could be discarded. Some workers(7) had reported that adsorption of CO_2 by carbon as negligible above 873K which means that reaction 1.9 and 1.11 are not applicable. These left Reif with three reaction i.e. Eq.1.6 to Eq.1.8. There has been a general agreement amongst various investigators that the forward reaction of Eq.1.6 to Eq.1.7 are valid in the absence of CO and above 873K. However, experiments have also established that CO has more than usual retarding effect on the rate of oxidation of carbon by CO_2 . The mechanism of retardation by CO can be reverse of reactions 1.6 and 1.7 and reaction 1.8. With the help of

his experimental findings, Reif(14) concluded that the retardation by CO was due to the reversible nature of reaction 1.6. Therefore Reif proposed the mechanism as:

(i) Reversible oxygen-exchange between gas phase and carbon surface



(ii) Transfer of carbon from solid phase to gaseous phase i.e. gasification of carbon

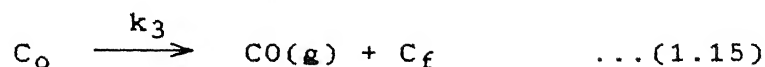
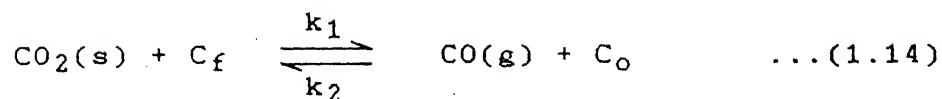


where (O) stands for occupied site by chemisorbed oxygen on carbon surface.

In Reif's mechanism it was concluded that the forward and backward steps of reaction 1.12 take place rapidly, i.e. the reaction is reversible. But the reaction 1.13 is irreversible and its reverse step has no significant effect. The retarding effect of carbon monoxide on the gasification reaction was accounted by the reverse step of reaction 1.12. It is because as the concentration of CO increases in the gas phase, the fraction of site covered by chemisorbed oxygen decreases. The rate equation 1.5 is consistent with the above mechanism. Subsequent studies (19,23,24) established the soundness of Reif's mechanism.

Ergun(19) considered the mechanism of surface reaction in detail based on literature evidences and came to agreement with the conclusions reached by Reif(14) earlier. However, he modified the approach somewhat and rewrote the equations in terms of surface sites

in the following manner as proposed in Langmuir-Hinshelwood mechanism.



where C_o and C_f refer to the occupied and free sites respectively on carbon surface. Equation 1.14 is reversible and equation 1.15 is irreversible and slow. On the basis of literature findings Ergun(19) ruled out any significant adsorption of inert gases, carbon, CO, CO_2 on the carbon surface. Therefore, reaction sites were considered as either free or occupied by an adsorbed oxygen atom. Hence the rate expression given by Ergun may be briefly described as noted below.

$$\begin{aligned} \text{Overall rate } (r_g) &= \text{rate of step (2) i.e. reaction 1.15} \\ &= k_3 \text{C}_o \quad \dots(1.16) \end{aligned}$$

where C_o is the concentration of sites occupied by oxygen atom. The value as C_o can be determined by applying steady-state approximation.

At steady state,

$$\begin{aligned} \text{rate of reaction 1.14} &= \text{rate of reaction 1.15} \\ &\dots(1.17) \end{aligned}$$

where C_o is constant

$$\begin{aligned} \text{Hence } r_g &= k_3 \cdot \text{C}_o \\ &= k_1 \cdot p_{\text{CO}_2} \cdot \text{C}_f - k_2 \cdot p_{\text{CO}} \cdot \text{C}_o \quad \dots(1.18) \end{aligned}$$

where C_f denotes concentration of free carbon sites on the surface.

$$\text{Now, } \text{C}_o + \text{C}_f = \text{C}_T \quad \dots(1.19)$$

where C_T is the total number of carbon sites on the surface. Combining Eq.1.18 and Eq.1.19

$$C_o = k_1 \cdot C_T \cdot PCO_2 / (k_3 + k_1 \cdot PCO_2 + k_2 \cdot PCO) \dots (1.20)$$

or

$$\text{rate } (r_g) = k_1 \cdot k_3 \cdot C_T \cdot PCO_2 / (k_3 + k_1 \cdot PCO_2 + k_2 \cdot PCO) \dots (1.21)$$

By proper rearrangement of terms, Eq.1.21 reduces to Eq.1.22, which may be written as:

$$r_g = \frac{I_1 \cdot PCO_2}{1 + I_2 \cdot PCO + I_3 \cdot PCO_2} \dots (1.22)$$

$$\text{where } I_1 = k_1 \cdot C_T \dots (1.23)$$

$$I_2 = k_2 / k_3 \dots (1.24)$$

$$I_3 = k_1 / k_3 \dots (1.25)$$

which is nothing but the rate equation (Eq.1.5) used by Gadsby et al.(8,10) to fit their experimental data.

According to Ergun(19) k_1, k_2, k_3 should be same for same form of carbon irrespective of the source. However $I_1 = k_1 \cdot C_T$ and since C_T is the total active sites on carbon surface and would depend upon the source, I_1 would vary. It is also expected that the equilibrium constant of reaction 1.14, viz.

$$K_e = k_1 / k_2 \dots (1.26)$$

be independent of the source of carbon. Ergun(19) carried out experimental measurements of rate of gasification in fluidized bed in temperature range of 973-1673K at atmospheric pressure and verified the validity of the above rate equation and the conclusions of. Mentser and Ergun(24) subsequently measured the oxygen uptake on carbon black at 923, 1073, 1123K using CO-CO₂ gas mixtures.

Fig.1.5 shows the variation of equilibrium constant (K_e) of oxygen-exchange reaction as a function of temperature. The fact that the data obtained on three types of carbon, viz. cyclon graphite, activated graphite and activated carbon yielded the same value of K_e . This was taken as confirmation of the above mechanism.

Fig.1.6 shows $\log k_3.C_T$ as function of $1/T$ for the above three types of carbon. All of them yielded activation energy of 247 kJ/mol. This was taken as a confirmation of the point that k_3 is the same for all types of carbon having coplanar bonds irrespective of the origin, particle size, porosity and crystallinity. The difference in the reaction rates of carbons of different variety was ascribed to difference in number of active sites.

Grabke(23) proposed another two step mechanism which is very much similar to the mechanism discussed above. But he utilized the concept of "Stationary oxygen activity" ' a_o ' on the carbon surface.



Here also, Grabke(23) neglected the influence of the reverse step of reaction 1.28 on the overall rate because experiments showed no detectable transfer of carbon from gaseous phase to solid phase.

Turkdogan and co-workers(26,28,29) carried out very comprehensive investigations on rate of gasification of carbon by CO_2 . They employed thermogravimetry technique for measurement of rate of weight loss as function of time which constituted the basis of rate

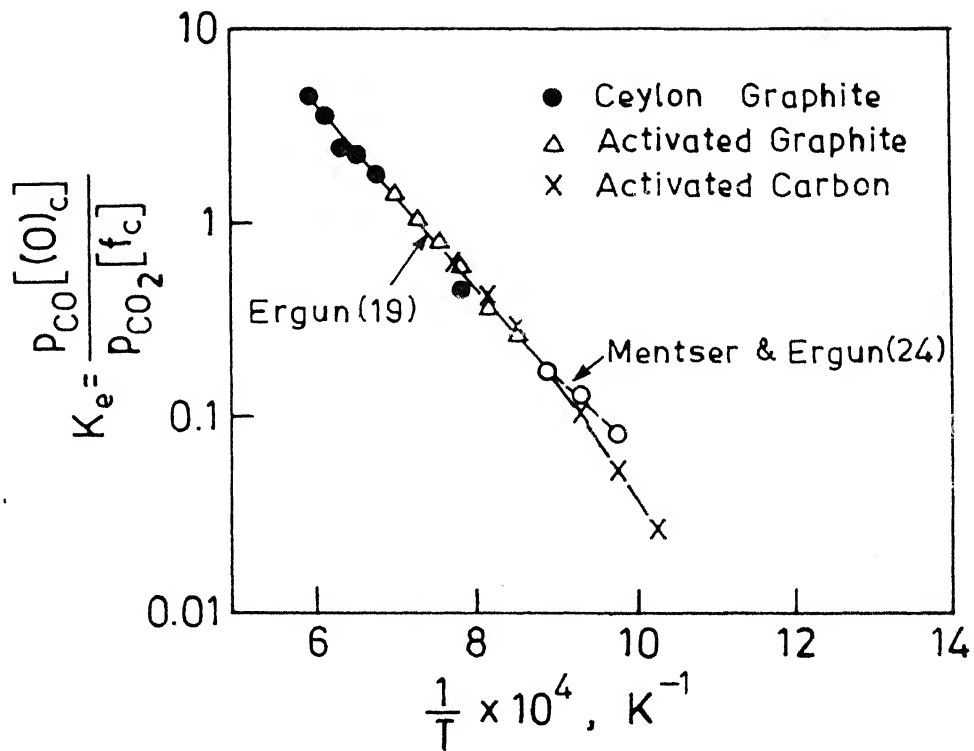


Fig. 1.5. Equilibrium constant K_e for oxygen-exchange reaction as a function of temperature. (24)

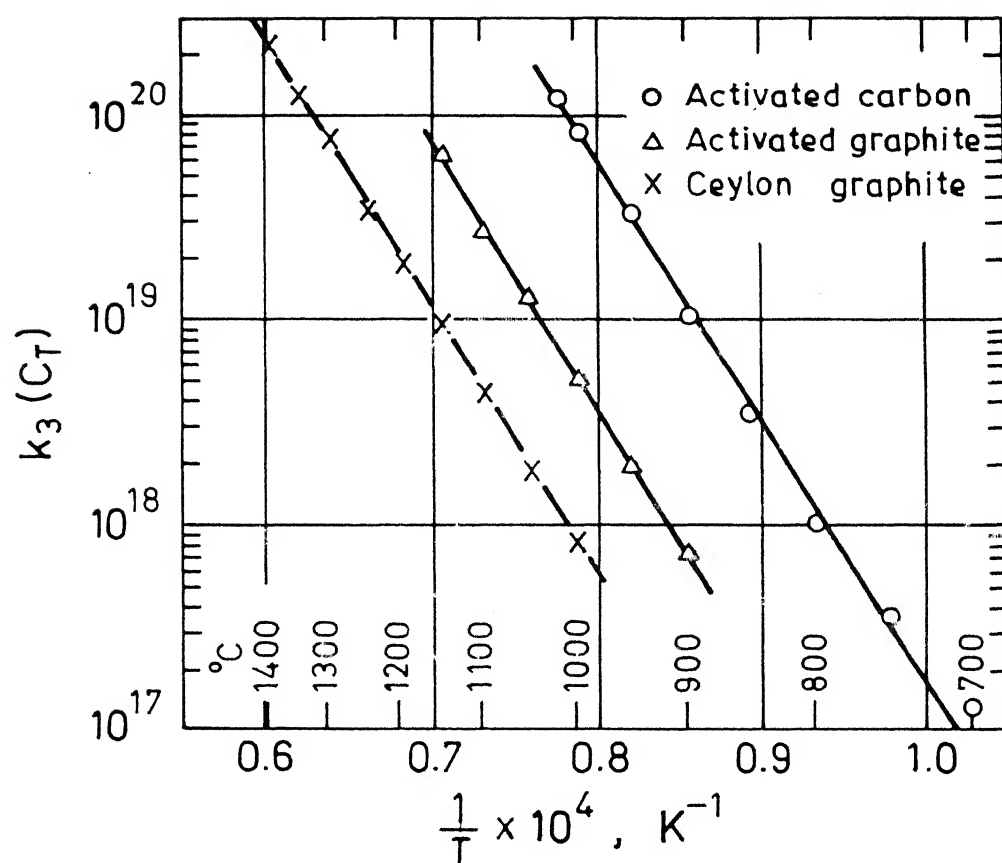


Fig. 1.6. Constants of gasification step as a function of temperature
(Activation energy : 247 kJ/mol) (19)

data. Measurements were carried out on coconut char, electrode graphite and metallurgical coke with particles of varying sizes. Gases employed were CO_2 , CO-CO_2 and CO-CO_2 - He mixture. The temperature ranged from 973-1673K and the pressure was varied over a wide range.

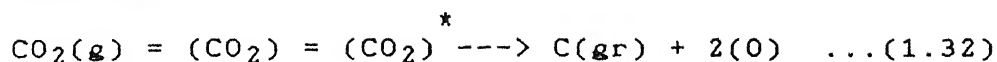
From the nature of experimental data and microscopic observations of partially reacted samples, Turkdogan et al.(26) tried to ascertain whether the extent of "burning" of carbon was uniform all through or varied from surface to core. Theoretically, as stated before, complete internal burning means that rate is exclusively controlled by chemical reaction step. On the basis of these, they selected such combination of temperature and particle size for further work which according to them gave exclusively chemically controlled rate.

Turkdogan et al.(29) stated that none of the previous interpretations seemed to account satisfactorily for their observed effects of pressure and gas compositions on the rates. Therefore they proposed a new mechanism, which assumed existence of the following adsorption equilibrium on the surface

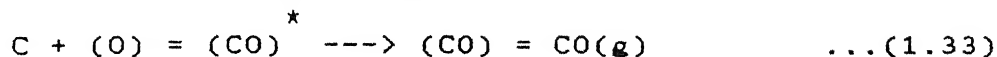


They also assumed that carbon monoxide is the main adsorbed species. Therefore fraction of vacant sites was approximated as $(1 - \theta_{\text{CO}})$, where θ_{CO} is the fraction of sites occupied by carbon monoxide. On the basis of the above they proposed the following rate mechanism which is radically different from the mechanisms discussed already.

(i) Dissociation of CO_2 on the carbon surface and resulting oxygen exchange



(ii) Gasification of carbon



where the asterix represents activated complexes of the species and $\text{C}(\text{gr})$ means carbon in solid form. Turkdogan et al.(28,29) proposed that the carbon monoxide inhibition on the overall rate takes place in two ways:

(a) it covers the surface of carbon by strong chemisorption

(b) it increases the activity coefficient of $(\text{CO}_2)^*$

Based upon their reaction mechanism, Turkdogan et al.(29) proposed two completely different rate equations for gasification. In presence of sufficient amount of carbon monoxide, the resistance of reaction(1.32) \gg resistance of reaction(1.33) and thus reaction(1.32) becomes rate controlling. Under this situation

$$\text{Rate} = \frac{\theta_1 [(\text{PCO}_2) - (\text{PCO}_2, \text{e})]}{1 + (\text{PCO}/\theta_{\text{CO}})} \quad \dots(1.34)$$

where θ_1 is rate constant and θ_{CO} is activity coefficient for a solution with fixed number of sites. On the other case, when amount of CO present in the gas phase is sufficiently low, then the resistance of reaction(1.33) \gg resistance of reaction(1.32) and then

$$\text{Rate} = \theta_2 (\text{PCO}_2)^{\frac{1}{2}} \quad \dots(1.35)$$

where θ_2 is a constant.

A more general statement, according to them, should be, for

a given CO-CO₂ mixture, resistance of reaction(1.32) >> resistance of reaction(1.33) at a low pressure, and resistance of reaction(1.33) >> resistance of reaction(1.32) at high pressure.

A search of literature reveals that the above rate equations have not been used by other workers subsequently. This has resulted into confusion. The following criticisms can be made about the approach of Turkdogan and co-workers. They have never documented the extent of disagreement of their experimental data with Langmuir - Hinshelwood type rate equation. In their mechanism, Turkdogan et al.(29) assumed adsorption of C,CO₂ and CO on the carbon surface but previous workers(7,13) had found very negligible adsorption of C,CO₂, and very slow adsorption of CO. In derivation of rate expressions Turkdogan et al. assumed formation of two activated complexes, one in equilibrium with CO₂ and other in the reverse direction. The net rate was taken to be the differences in decomposition rates of the two complexes. The concept of two activated complexes appears to be speculative.

Rao and Jalan(32) tried to show similarities among various rate equations reported in literature. The rate equation of Ergun(19) is:

$$r_g = \frac{I_1 p_{CO_2}}{1 + I_2 p_{CO} + I_3 p_{CO_2}} \quad \dots(1.22)$$

Dividing the numerator and denominator on right hand side by I₂,

$$r_g = \frac{(I_1/I_2) p_{CO_2}}{(1/I_2) + p_{CO} + (I_3/I_2) p_{CO_2}} \quad \dots(1.36)$$

Rao et al. computed I_2 values from Wu's(11) data and found that the term $(1/I_2)$ can be neglected. Thus Eq.1.36 transforms to

$$r_g = \frac{(I_1/I_2) PCO_2}{PCO + (I_3/I_2) PCO_2} \quad \dots(1.37)$$

Dividing Eq.1.37 by PCO

$$r_g = \frac{(I_1/I_2) (PCO_2/PCO)}{1 + (I_3/I_2) (PCO_2/PCO)} \quad \dots(1.38)$$

Eq.1.38 resembles the rate equation proposed by Grabke(23) which can be stated (at (PCO_2/PCO) ratio greater than 2.0) as:

$$r_g = \frac{k_2 (PCO_2/PCO)}{1 + X (PCO_2/PCO)} \quad \dots(1.39)$$

Comparison of Eq.1.38 and Eq.1.39 reveals that k_2 is equivalent to the term (I_1/I_2) and X is equivalent to (I_3/I_2) . Rao et al.(32) compared the (I_3/I_2) values, calculated from Wu's data with that of 'X' values reported by Grabke over a temperature range and found very good agreement amongst them. At low (PCO_2/PCO) value (<2.0), Eq.1.38 may be approximated as:

$$r_g = (I_1/I_2) (PCO_2/PCO) \quad \dots(1.40)$$

which is analogous to Grabke's rate expression

$$r_g = k'K_e (PCO_2/PCO) \quad \dots(1.41)$$

where K_e is the equilibrium constant of the oxygen-exchange reaction and k' is the rate constant of the forward step of gasification

reaction.

Rao et al. also pointed out similarity between rate equation of Turkdogan et al. (28,29) for (p_{CO_2}/p_{CO}) less than 9.0 with that of Eq.1.22. Under condition of complete internal burning i.e. under chemical control, gas composition will be uniform through out the sample and will be equal to the bulk gas composition. As according to Turkdogan et al. total gas pressure was 0.96 atmosphere,

$$p_{CO_2} = 0.96 - p_{CO} \quad \dots(1.42)$$

Substituting Eq.1.42 into Eq.1.22 and rearranging

$$r_g = [I_1/(1 + 0.96 I_3)] p_{CO_2}/[1 + (I_2 - I_3)/(1 + 0.96 I_3) p_{CO}] \quad \dots(1.43)$$

Comparison of Eq.1.34 and Eq.1.43 shows that at negligible p_{CO_2} , θ_{CO} employed by Turkdogan et al is nothing but $(1 + 0.96 I_3)/(I_2 - I_3)$. Rao et al. (32) rendered Eq.1.35 i.e. the rate expression at low p_{CO} as proposed by Turkdogan et al to be doubtful proposition for their data. Table 1.2 compiles the values of θ_{CO} calculated by the present author through correlation of Turkdogan et al and through the functional correlation of θ_{CO} and I_2, I_3 established by Rao et al.

Table 1.2: Comparison of θ_{CO} values calculated two ways

Temp., K	I_2, atm^{-1} (Rao & Jalan)	I_3, atm^{-1}	$\theta_{CO} = \frac{1+0.96I_3}{I_2 - I_3}$	$\theta_{CO} = \frac{5940}{T} + 3.36$ (Turkdogan et al)
1173	620	2.69	5.80×10^{-3}	2.49×10^{-2}
1223	214	2.40	1.56×10^{-2}	4.0×10^{-2}
1273	804	2.16	3.92×10^{-2}	6.2×10^{-2}
1323		1.95	9.40×10^{-2}	9.34×10^{-2}

It is evident from the above table that the relation $\theta_{CO} = (1 + 0.96 I_3)/(I_2 - I_3)$ holds good only at 1323K and considerable disagreement exists among the values at lower temperatures. The following comments can be made on the above findings. There exists a considerable amount of scatter in $\log \theta_{CO}$ vs. $1/T$ plot in work of Turkdogan et al. and the plot was drawn with only few data points. So question can be raised how far θ_{CO} values are reliable. Again true comparisons can probably not be made because of difference in experimental condition of Wu(11) and Turkdogan et al.(28,29). The latter employed CO_2 and $CO - CO_2$ gas mixture at 0.96 atmosphere whereas Wu used inert gas alongwith CO_2 at 1.03 atm. pressure. On the other hand the relation of θ_{CO} and I_2, I_3 may be valid only at high temperature because $p_{CO_2, e}$ may have appreciable influence on the rate equation(Eq.1.34) and thus can not be neglected at low temperature.

Turkdogan et al(29) found that the temperature dependence of θ_2 was same irrespective of the type of carbon and obtained an activation energy of 290 kJ/g-atom C. Same statement holds good for dependence of θ_1 with temperature also. Fig.1.7 shows $\log \theta_1$ versus $1/T$ for graphite, metallurgical coke and coconut char as reported by Turkdogan et al. They found the activation energy to be 252 kJ/g-atom C irrespective of type of carbon. This is in excellent agreement with the activation energy of 247.8 kJ/g-atom C reported by Ergun(19). The independence of activation energy on the nature of carbon had also been found by Ergun.

In a recent publication Wu et al.(50) have made a fresh calculation of Wu's(11) unpublished data and have compared the findings with other investigators. Wu had employed a differential

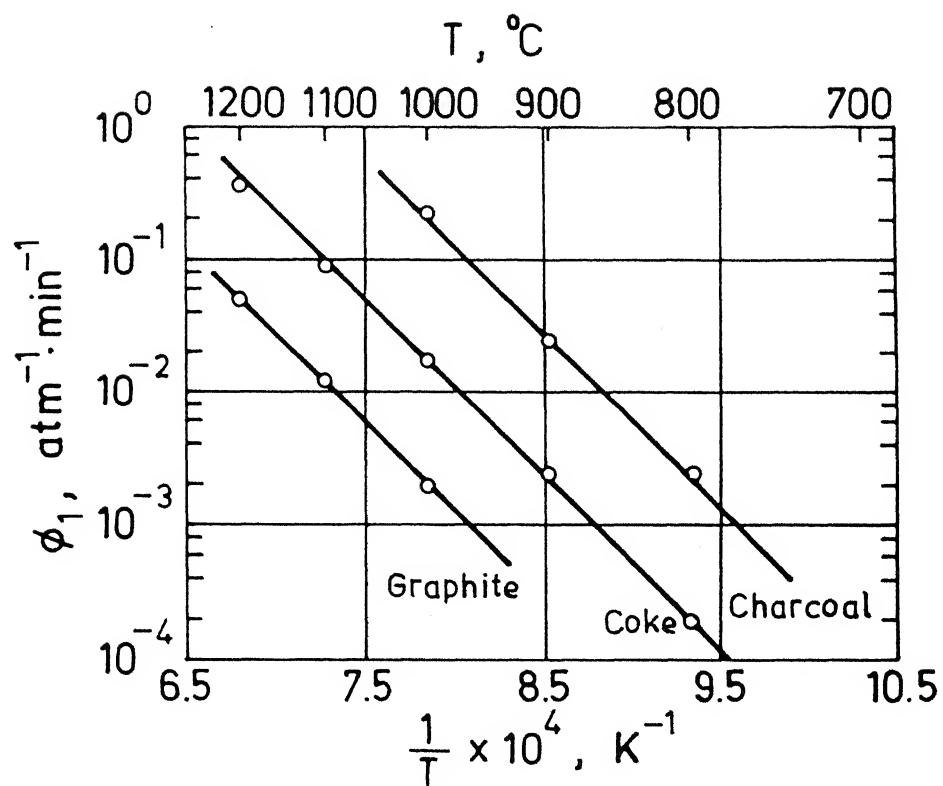


Fig. 1.7. Temperature dependence of the rate parameter ϕ_1 for oxidation in CO-CO₂ mixtures. (29)

reactor i.e. single layer of carbon to avoid mass transfer effect. Graphite of 50-60 mesh size was used and rate was measured by intermittent monitoring of weight. Wu et al found that the reaction rate varied with progress of gasification and thus they have tried to deal with the initial rate. They have fitted their data with an equation of the following form

$$r_g/r_0 = 1 + C.F \quad \dots(1.44)$$

where $r_g = - \frac{dW_c/dt}{W_c}$

F = fraction of carbon gasified

r_0 = rate at F = 0

C = a constant

It was found by Wu et al(50) that the value of 'C' ranged between 11 to 18.5 and an average value of 14 gave a reasonably good fit. They found that a fairly consistent value of r_0 (within $\pm 5\%$) could be obtained from the following expression

$$r_0 = (1/15t) \ln [(1 + 14F)/(1 - F)] \quad \dots(1.45)$$

They have also tried to confirm the validity of Langmuir-Hinshelwood rate equation with their data on graphite and calculated the rate constants I_1 , I_2 , I_3 alongwith specific rate constants of oxygen exchange step as well as gasification step. Table(1.3) compiles the value of rate constants of Langmuir-Hinshelwood rate equation for different workers.

It is evident from Table(1.3) that absolute values of I_2 , I_3 as well as the ratio of I_3/I_2 vary widely for different workers except for Wu et al(50) and Grabke(23). It has been already mentioned that the term 'X' used by Grabke is analogous to (I_3/I_2) . The matching of

(I_3/I_2) of Wu et al and that of 'X' of Grabke can be attributed to the fact that both of them employed graphite for their rate studies. It is apparent from Table(1.3) that I_2 , I_3 and the ratio (I_3/I_2) depends upon the type of carbon used and also may be on the experimental conditions. So the conclusion drawn by Rao et al(32) that I_2 and I_3 are intrinsic rates and insensitive of the type of carbon, seems doubtful.

Wu et al(50) have pointed out that if the oxygen-exchange mechanism is correct then equilibrium constant of the step should be same atleast for same type of carbon. Fig.(1.8) presents the equilibrium constants (K_e) as a function of temperature for different workers. It may be noted from Fig.1.8 that equilibrium constants of Wu et al.(11,50), Grabke(23) are in significant disagreement with those of Ergun(19) and Lewis(12). Lewis and Wu et al used same type of coke. Wu et al. attributed the disagreement to the reliability of rate measurement techniques i.e. differential bed reactor, fluidized bed reactor. They also have cast doubt on the validity of mechanism involving an oxygen exchange step.

Standish et al(49) have carried out kinetic studies and SEM analysis of wood char particles of 10 - 34 mm size in temperature range of 1173 - 1273K under atmospheric pressure using thermogravimetric technique. The gas composition was varied from 100% CO_2 to 20% CO_2 and rest was N_2 . They fitted their kinetic data through a 'global' rate equation correlating effect of temperature, gas composition and particle size on rate.

$$\frac{dW_c}{dt} = 2.1 \times 10^{-3} \exp(210.3/RT) (CO_2)^{0.71} (R_o)^{-0.81} \dots(1.46)$$

Table 1.3 Values of I_2 , I_3 and their ratios for different workers at various temperatures

Worker	Gadsby et al. (10)	Lewis et al. (12)	Wu(11)	Wu et al. (50)	Grabke(23)
Carbon	Coconut shell char	Coke	Coke	Electrode graphite	Graphite
Size	8- 10 B.S sieve	20- 200 mesh	50- 60 mesh	50- 60 mesh	
Method	Fixed bed	Fluidized bed	Differential	Differential	
Temperature	1007 - 1102	1075 - 1366	1089 - 1311	1144 - 1131	
Pressure	0.013- 1.0	1.0	1.026	1.026	
I_{02}	$10^{-7.9}$	$10^{-1.9}$	$10^{-5.4}$	$10^{-8.67}$	
E_2	-191.1	-64.68	-169.26	-258.05	
I_{03}	$10^{6.5}$	$10^{-0.6}$	$10^{-1.52}$	$10^{-0.81}$	
E_3	126.42	-26.88	-25.62	-30.42	

CALCULATED VALUES

Temp.	I_2	I_3	I_3/I_2	I_2	I_3	I_3/I_2	I_2	I_3	I_3/I_2	$X=I_3/I_2$
1173	3.76	7.82	2.08	9.30	3.91	0.42	127.80	0.43	0.003	0.006
1223	1.69	13.26	7.83	7.10	3.49	0.49	63.06	0.39	0.006	0.015
1273	0.81	21.56	26.56	5.54	3.15	0.57	32.88	0.35	0.011	0.036
1323	0.41	33.81	82.25	4.40	2.86	0.65	18.01	0.32	0.018	0.080

Units : Temperature in K, Pressure in atmosphere⁻¹, E in kJ/mol

$$I_1 = I_{01} e^{-E/RT}$$

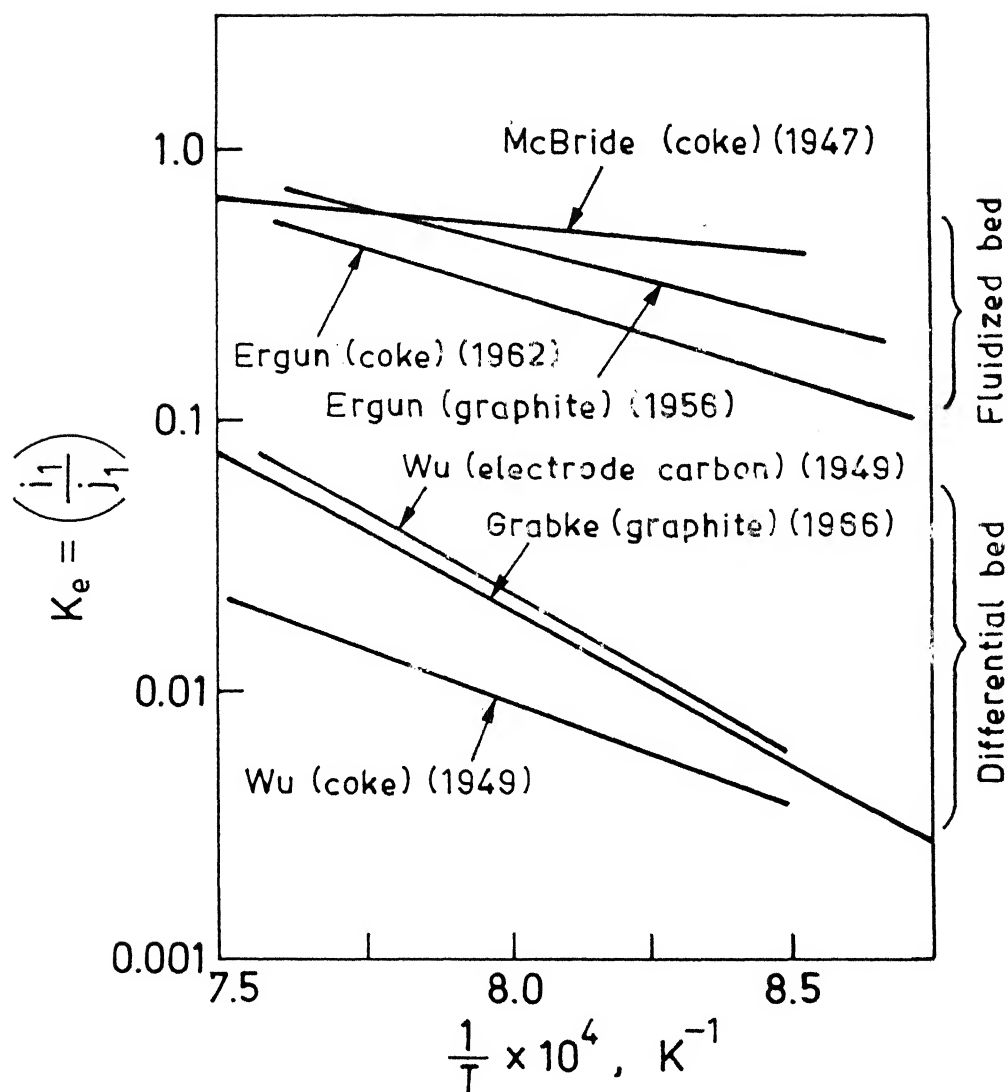


Fig. 1.8. Equilibrium constants K_e for oxygen exchange reaction (50)

where $\frac{dW_c}{dt}$ = rate of weight loss

R_0 = initial particle radius

The order of reaction with respect to gas composition is an apparent order and not true order. Fractional order,

$$\text{i.e. rate} \propto p_{\text{CO}_2}^n \quad \dots(1.47)$$

where n is a fraction, has been reported by other workers also. Standish et al.(49) have reviewed the same. Groeneveld et al(80) found that gasification kinetics of charcoal in CO_2 - N_2 gas mixture could be represented by the equation

$$-\frac{dX_B}{dt} = k C_A^m C_B^n \quad \dots(1.48)$$

De Groot and Shafizadeh(81) also found that their rate data of Douglas fir and cottonwood char in CO_2 could be conveniently fitted into rate expression

$$-\frac{dX_B}{dt} = k W_0 (p_{\text{CO}_2})^{0.6} \quad \dots(1.49)$$

Turkdogan et al.(29) reported that in presence of very low amount of CO

$$\text{rate} \propto (p_{\text{CO}_2})^{0.5} \quad \dots(1.50)$$

The more frequently encountered value of n is around 0.5 and the reasons for the same have been reviewed by Smith(82). However, the above said equations (Eq.1.47 - Eq.1.49) are essentially empirical in nature and are concerned with 'global rate' without distinguishing the rate controlling mechanism. Standish et al(49) have advocated the use of 'grain model' which included shrinking core model (SCM), grainy

core model (GCM) and uniform conversion model (UCM). Advantage of the grain model is that they need no detailed knowledge of pore structure. SEM analysis of Standish et al indicates that their data satisfactorily follow SCM.

According to the basic definition, the term 'activation energy' is the energy barrier associated with an elementary step. It does not apply to the overall reaction rate when more than one kinetic steps are jointly controlling the rate. So from fundamental point of view the term 'activation energy' can not be applied without this precaution. To express the energy barrier of an overall process, it should at least be called as 'apparent activation energy' or a better way of expressing it may be by the term 'temperature co-efficient' because it gives the temperature dependence of rate. But many workers use the term indiscriminately. For the time being and for the following discussion, the term activation energy has been accepted keeping in view the above limitation of the term.

Activation energy for gasification of carbon by CO_2 has been found to vary in a wide range of 210 - 375 kJ/mol. It depends upon the type of carbon used. Different workers have used different rate expressions which would yield variety of activation energy values. Heat and mass transfer limitations are found to have pronounced effect on activation energy. Literature evidence shows that catalytic effect on a reaction can significantly bring down activation energy value. However, for purely chemical control, non-catalysed gasification reaction activation energy should not be below approximately 275 kJ/mol. In view of such a large activation energy, temperature has a very significant influence on rate of gasification. A 100°C rise of

temperature can increase the rate by an order of magnitude.

1.2.4 Mass and heat transfer limitations on rate

It has already been mentioned that the kinetic steps of gasification reaction include transportation of the reactant and product gases to and from the reaction sites respectively. Although surface reaction primarily controls rate of gasification of carbon, it is expected that the reaction kinetics may be affected by mass transfer limitation depending upon the conditions. Some workers (17,18,20,21) under specific experimental conditions noticed significant effect of mass transfer step on gasification kinetics. In a comprehensive review, Walker et al.(21) discussed the role of transfer of reactant and product on gas-carbon reaction. Fig.1.9 schematically presents the temperature dependence of rate. As shown in Fig.(1.1), the reactant gas viz. CO_2 and product gas viz. CO , have to be transported through external boundary layer as well as through the pores of carbon. The term 'mass transfer' here includes both of them. According to Rossberg(18) three distinct regions may be identified. Role of diffusion on each region may be described in brief as follows:

Region 1: At low temperature, as the reaction is generally chemically controlled, mass transfer does not play any significant role in determining the kinetics of the reaction. At this stage, the whole porous body experiences attack from CO_2 of uniform composition that prevails in the bulk and thus each unit volume of carbon participates in the reaction in the same rate (i.e. uniform internal reaction).

Region 2: At high temperature the resistance offered by mass transfer steps for reactant and product gases are no more negligible.

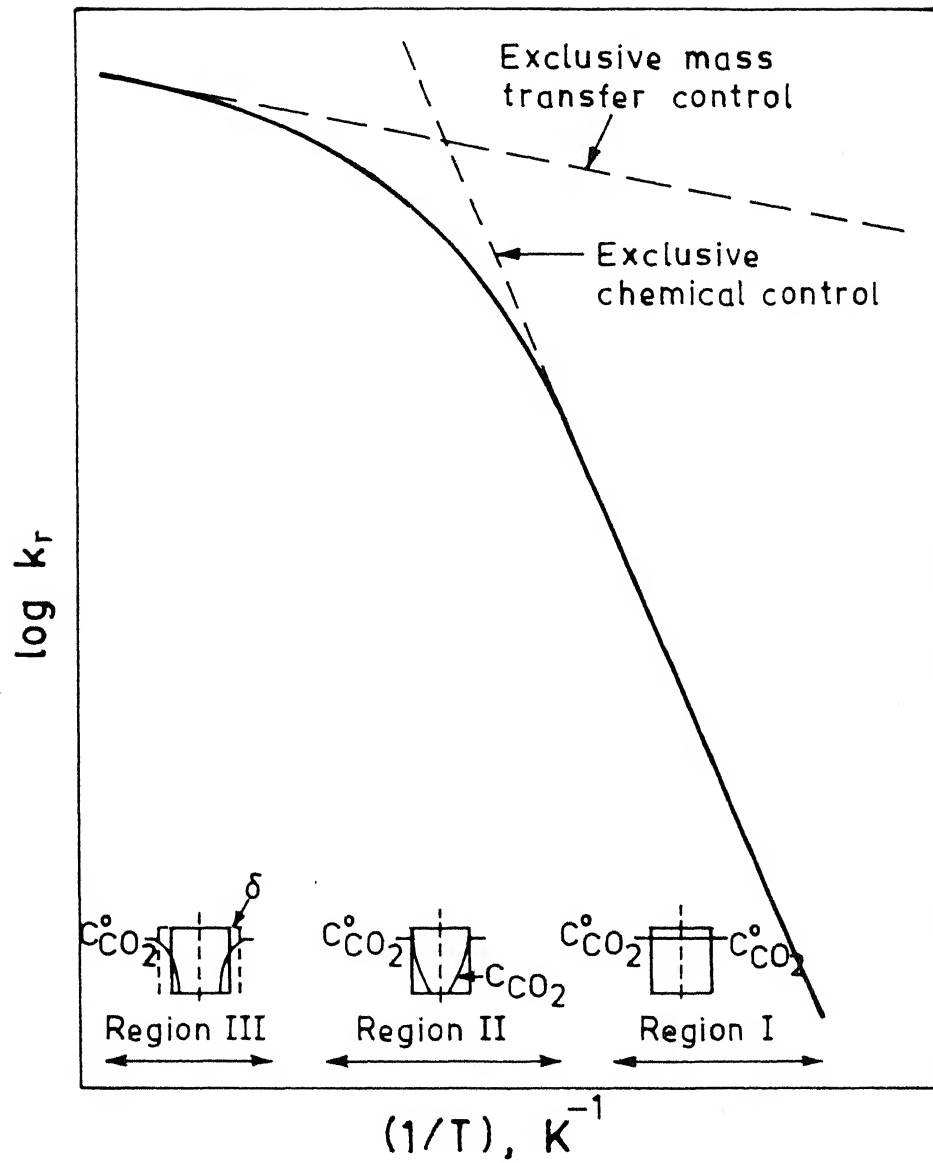


Fig. 1.9. Temperature dependence of mass transfer for C-CO₂ reaction in porous carbon pellet. (32)

With increase of temperature the rate of the chemical step of a reaction increases rapidly but the relative increase in the mass transfer steps are much less as shown in Fig.(1.9). Thus the mass transfer and chemical reaction rates become comparable and the gas composition in the porous solid varies considerably from that of the bulk composition. Under this situation each unit volume does not register the same rate of reaction as is in the case of region 1.

Region 3: At still higher temperatures beyond region 2, the chemical step becomes much faster compared to mass transfer and for any practical purpose, offers no resistance to the progress of the reaction. The surface concentration of reactant gas becomes a fraction of bulk concentration and penetration takes place to a limited extent only. Thus the reaction virtually becomes confined to the surface.

So it is apparent from the above discussion that mass transfer is expected to play an important role in the gasification reaction at high temperature as well as intermediate temperatures and its significance can not be ignored. As the particle size increases, the diffusional path length also increases and chance of mass transfer controlling the rate becomes more. At high temperature an exclusive chemical control reaction can be achieved only by the use of very small particles. On the other hand at lower temperature, due to relative slowness of chemical reaction rate, one can have exclusive chemical control even for somewhat larger particles of carbon.

Many investigations (26,32,49,55,58,77) have been carried out to find out the influence of particle size on the gasification rate of carbon. Rao et al.(32) found that at 1269K, time for 50 pct. burn off increases from 65 minutes to 85 minutes when the initial

weight of the pellet was increased from 0.25 gm to 1.08 gm and the corresponding rates for carbon black decreased from $8.34 \times 10^{-3} \text{ min}^{-1}$ to $6.03 \times 10^{-3} \text{ min}^{-1}$. Standish et al.(49) have also found a fractional dependence of rate on particle size. In other words they have reported that with increase of particle size, time for complete conversion also increases. But Ergun(55) found that variation of particle size of metallurgical coke from approximately 0.2 to 1 mm did not affect the gasification rate in steam at 1 atmospheric pressure and upto 1473K.. Van Heek et.al.(83) also observed no effect of particle size when size of bituminous coal particle was varied from about 0.1 to 1.4 mm in steam at 10 atmospheric pressure and temperature upto 1023K. Literature reports that effect of particle size on gasification of coal char is complex (54) and has been found to range from nil(57) to 35 folds(58).

Turkdogan et al.(58) and Tien and Turkdogan(77) performed quite extensive and systematic study on the effect of particle size on gasification rate for different types of carbon. Fig.1.10 presents experimental rate of gasification of coke spheres at various temperatures as a function of particle diameter. Turkdogan et al.(26) also tried to distinguish the regions of 'complete internal burning', 'partial internal burning' etc. as a function of particle size. Fig.1.11 shows the logarithm of rate of gasification per particle against logarithm of sphere diameter for electrode graphite at 0.96 atmospheric pressure and various temperatures. They found that, as expected, at lower temperature the zone of chemical control is extended upto higher particle size than at higher temperature.

So an observed reaction rate may be associated with mass transfer

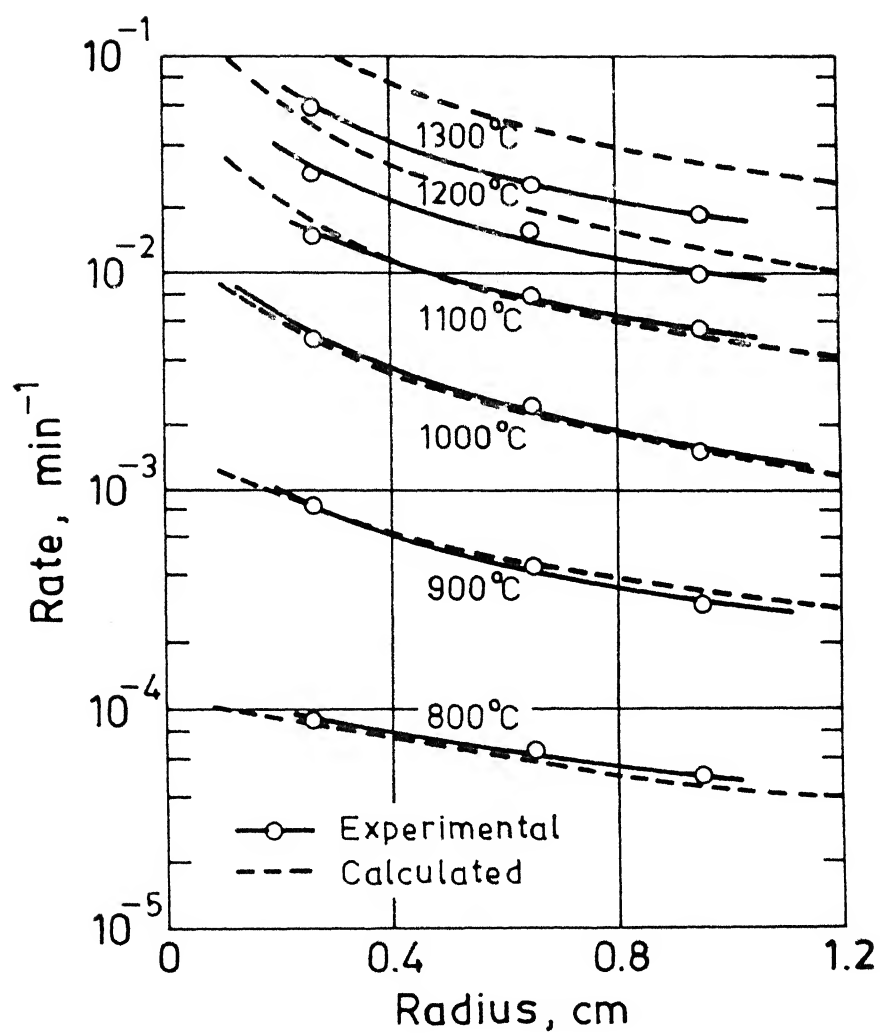


Fig. 1.10. Effect of particle size on rate of oxidation of coke spheres in CO₂. (77)

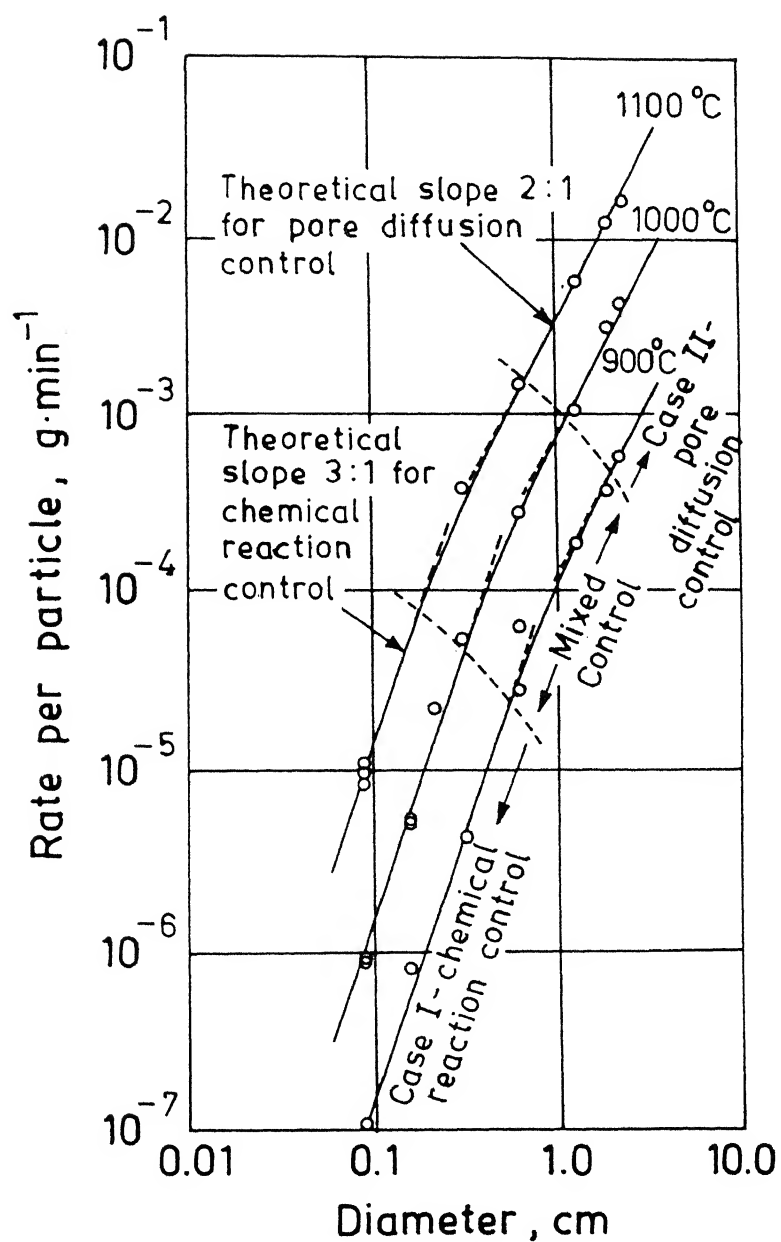


Fig. 1.11. Rate of oxidation of electrode graphite as a function of particle diameter in CO_2 . (26)

limitation depending upon the experimental conditions and thus may not represent true chemical reaction rate. It is always preferable to eliminate the mass transfer effect, if present, from the observed rate because it is much easier to interpret data when only chemical aspect of a reaction has been considered. One way of avoiding mass transfer limitation is by proper choice of set of experimental conditions where complete diffusion of both reactant and product gases is ensured. But this calls for extensive and careful experimentation. A better way may be to determine the extent of mass transfer limitation quantitatively by mathematical analysis.

If a reaction is free from mass transfer limitation i.e. sample is exposed to uniform gas composition throughout the volume, the rate is called 'intrinsic chemical reactivity'. A term 'effectiveness factor' is used to account for the extent of mass transfer limitation on a reaction rate and can be defined as the ratio of actually observed rate to that of intrinsic rate. Mathematically

$$\eta = \frac{\text{Observed rate}}{\text{Intrinsic rate}} \quad \dots(1.51)$$

where η = effectiveness factor

Due to non-availability of mathematical models, early workers could not calculate effectiveness factor. Roberts and Shatterfield(76) first presented a workable model for this purpose and the same has been subsequently used by number of workers (32,42,84). Later on, based on their own rate expressions, Tien and Turkdogan(77) developed a mathematical model to calculate effectiveness factor. As Fig.1.10 shows, the calculated curves (dotted lines) agreed fairly well with the experimental observations. Ghosh and Ajmani (79) compared

the two procedures of calculation mentioned above. In order to make such comparisons it was necessary to take same values of chemically controlled rates and these were taken from the work of Turkdogan and Vinters(28). The conditions of their calculation are listed in Table 1.4.

Table 1.4 Conditions used by Ghosh et al.(79) for effectiveness factor calculation

Diameter of sample (cm)	Thickness of sample (cm)	Porosity	Density (gm/cc)
1.0	0.25	0.5	0.9
2.0	0.25	0.5	0.9
2.0	0.50	0.3	1.2
2.0	0.25	0.3	1.2

Fig.1.12 presents one such comparison of the two methods graphically. Ghosh et al. observed that the two methods match sometime, but agreement is quite poor in many cases. They further noticed that there is no systematic variation of the results obtained by the two methods and concluded that the mathematical treatment proposed by Roberts et al.(76) and Tien et al.(77) do not yield same results. Details of the procedures of effectiveness factor calculation by the two methods mentioned above would be presented later.

Alam and DebRoy(74) and Szekeley et al.(85) presented two other methods of effectiveness factor calculation. According to Alam et al., the effectiveness factor can be calculated from an expression of the following form:

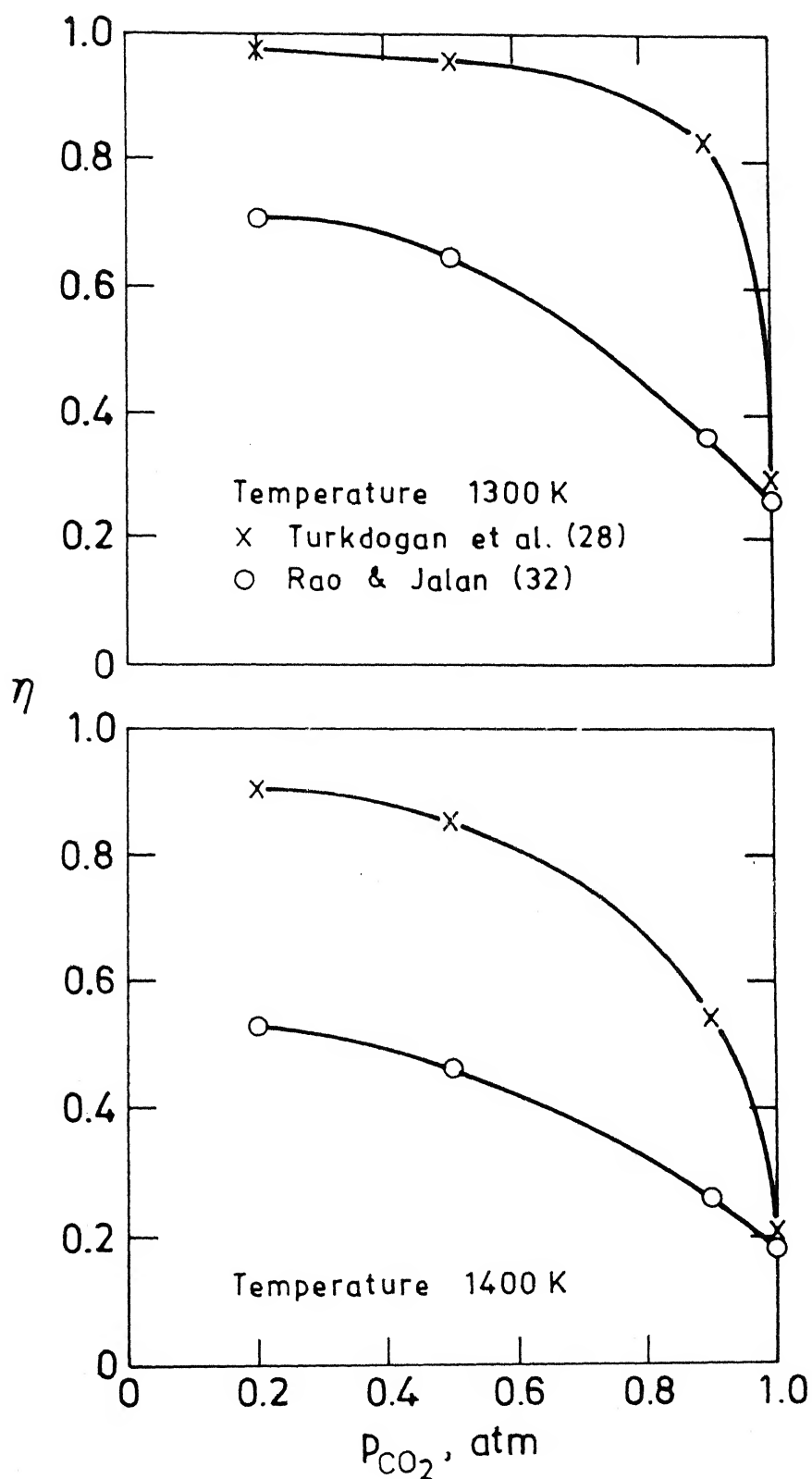


Fig. 1.12. Comparison of effectiveness factors, calculated by two methods (sample dia = 2.0 cm and thickness = 0.25 cm). (79)

$$\eta = \frac{1}{K_v R T L (1/K_g + L \coth \theta / \theta D_e)} \quad \dots (1.52)$$

where K_v = intrinsic reaction rate constant, $\text{gm-mol/cm}^2 \text{ s}$

R = universal gas constant, $\text{gm-cm}^2/\text{s}^2 \text{ gm-mol K}$

T = temperature, K

L = characteristic length of the pellet, cm

K_g = gas phase mass transfer coefficient, cm/s

D_e = effective diffusivity of CO_2 , cm^2/s

and $\theta = L (K_v R T / D_e)^{-1/2}$

According to Alam et al. the intrinsic rate constant K_v is affected by numerous factors including the nature and concentration of the defects. They also advocated that as pore size distribution changes with time, the value of effective diffusivity should also be calculated as a function of reaction time. Thus the value of effectiveness factor keeps on changing as the gasification reaction proceeds.

Szekely et al.(85) redefined the effectiveness factor in a slightly different manner than the conventional definition. They took

$$\bar{\eta} = (r_g^{F,d}) / (r_g^{o,d}) \quad \dots (1.53)$$

where $r_g^{o,d}$ = the initial rate of reaction, which may be modified by diffusional effects

$r_g^{F,d}$ = the rate of reaction at a particular value of burn-off F .

and $\bar{\eta}$ = effectiveness factor which represents the net effect of structural changes on the reaction.

They also pointed out that in a catalysed gasification reaction as the concentration of catalysts will increase with increase

of burn off, the value of $\bar{\eta}$ may be greater than 1. Skekely et al.(85) arrived at the same conclusion as Alam and DebRoy(74) that effectiveness factor value is a function of burn-off.

Carbon gasification reaction is endothermic in nature. So if the rate of heat transfer through the material is not rapid enough, the centre temperature of the sample is expected to be lower than that of the surface. The temperature difference between the surface and the centre will be high with large particle size. Extent of temperature drop will also depend upon the rate of reaction, because higher rate of reaction will demand more heat transfer to the reaction site from the surrounding. Again at higher temperature as the reaction rate is greatly enhanced, it may be expected that temperature difference will be significant. Thus for large particle size and at high temperature there may exist a significant temperature gradient from surface to centre depending upon the thermal conductivity of the bed. Porous and powdery mass are more prone to the temperature gradient due to poor thermal conductivity. As the reaction rate has exponential dependence on temperature, the difference of surface and centre temperature may cause significant variation in rates and thus rate may be partly heat transfer controlled. The observed rate under partial heat transfer control will be different from that of the rate, if it is intrinsic. Magnitude of heat transfer limitation can be accounted for by 'non-isothermal effectiveness factor,' defined in the same way as expressed for isothermal effectiveness factor (Eq.1.51).

Rao et al.(32), in view of probable non isothermal effect on rate, tried to measure the true temperature of the pellet. They inserted thermocouple in a bed of carbon black particle and found that

the actual bed temperature was quite low in comparison to the control temperature. For example when the control temperature was at 1223K, the bed temperature increased rapidly from around 1161K to 1208K ($+2^{\circ}\text{C}$) within around 5 to 6 minutes and got stabilized at that temperature. They presented a curve showing the actual temperature of the carbon bed against furnace temperature.

Tien and Turkdogan(78) measured the extent of temperature variation of the surface and the centre of a 2.2 cm diameter x 5 cm thick metallurgical coke sample under CO_2 atmosphere. They found that upto around 20 pct. burn off, the centre temperature rapidly dropped by around 7°C . With progress of gasification, both surface and centre temperature decreased continuously. But the extent of temperature drop during reaction of carbon with carbon dioxide reported by them(78) for cylindrical sample was widely off from what they had reported in previous publication(77) for coke sphere.

Tien and Turkdogan(78) also presented a mathematical formulation to calculate the heat transfer effect on gasification reaction. Though the formulation and procedure are quite sound but the model suffers a serious drawback of dimensional inconsistency of the governing equations which render their calculations doubtful. A detailed discussion in this regard will be presented later.

1.2.5 Surface area

Different types of carbon inherently contains pores, varying in amount and size (10 \AA° to more than 500 \AA°).

Pores can be classified into the following groups(59):

- (a) micropores (diameter $< 10 \text{ \AA}^{\circ}$)
- (b) semi micro or transitional pores (diameter $\approx 10\text{-}300 \text{ \AA}^{\circ}$)

(c) macropores (diameter $> 300 \text{ \AA}$)

Microporosity in carbon arises due to imperfections in the structure. Some micropores are really molecular sieves. High specific surface area (m^2/g) of carbon like that in coconut char is attributed mainly to the presence of micropores.

Numerous investigators have determined pore surface area of various forms of carbon viz. char, coal etc. Some of these have been reviewed by Johnson(56), Turkdogan et al.(30) and Anderson et al.(86). The most common technique of surface area measurement is by BET using adsorption of nitrogen gas at liquid nitrogen temperature (-196°C). However, for carbonaceous material, BET measurements have also been carried out extensively by carbon dioxide adsorption at dry ice temperature (-78°C) or even at room temperature. Nitrogen adsorption and carbon dioxide adsorption often gave differing results when specific surface area is very large due to presence of extensive micropores.

Johnson(56) reviewed the salient features of surface area measurement. From literature findings he stressed more reliability on surface area values measured by carbon dioxide adsorption rather than by nitrogen adsorption. Penetration of nitrogen into micropore structure of carbonaceous materials is apparently limited by slow and activated diffusion process and thus gives lower value of surface area. Surface area thus measured at most reflects the area of macropores and transitional pores. For partially gasified chars, presence of more open micropores may lead to capillary condensation and thus abnormally high value of apparent surface area. On the other hand higher temperature of carbon dioxide facilitates activated

diffusion in micropores and capillary condensation is prohibited by the low relative adsorption pressure. Table 1.5 presents some surface area values of different types of carbon both by nitrogen and carbon dioxide adsorption.

Table 1.5 Surface area values of different types of carbon

Type of carbon	Surface area (m^2/gm)		
	$\text{N}_2(\text{liquid})$	$\text{CO}_2(\text{liquid})$	
Spheron 6	111.4	123.8	
Graphon	93.0	75.0	
Lampblack 8	46.7	175.4	ref.(86)
Activated carbon	1369.0	1292.0	
Metallurgical coke	3.0	-	
Electrode graphite	1.30	-	
Coconut char	-	1050.0	ref.(30)
Wood char	348.0	-	
Wood char	-	350.0	

Turkdogan et al.(30) carried out an extensive investigation of the problem of BET surface area measurement by nitrogen adsorption technique. They confirmed that erroneously high surface area at very low relative pressure of nitrogen gas is due to capillary condensation and also at high relative pressure due to capillary filling phenomena. They evolved a technique which according to them, eliminated both the errors. Few of their measured values of surface area of different types of carbon are already listed in Table 1.5. It may be noted from Table 1.5 that the surface area of coconut char both by nitrogen adsorption and carbon dioxide adsorption are close, thus confirming reliability of the technique. A scan of literature has further revealed that the investigators in recent years have been using both

CENTRAL LIBRARY
KAROL
108433

nitrogen BET(60,74,85,87) as well as carbon dioxide BET(88,89).

Rate of gasification $[- \frac{dW_c/dt}{W_c}]$ varies with carbon burn

off(i.e. the extent of gasification). This aspect has received attention from several investigators(30,50,59,74,85). But the nature of variation of rate reported by various workers does not follow the same trend. However, in a large number of cases it has been found to increase to a maximum at around 40 to 60 pct. burn off and then decrease again.

In order to explain this, many workers determined changes in pore surface area with burn off(30,50,59,60,74,85). Some typical patterns are shown in Fig.1.13. It may be noted from Fig.1.13 that in most of the cases, the surface area first increases with increase of burn-off and then decreases. It is the general view of the workers(30,85) that at the initial stage of reaction, the micropores once unavailable become accessible to the gas and thus gives rise to increase in surface area. But with progress of gasification, the micropores collapse to bigger size of pore resulting in decrease of surface area. It may also be noted from Fig.1.13 that effectively there is no change in surface area of metallurgical coke and electrode graphite with progress of conversion. For formed coke a diametrically different behaviour has been reported by Szekely et al.(85). They found that the surface area of formed coke increased continuously with increase of burn off. The reason put forward by Szekely et al. behind this is that they used tar as a binder to make formed coke and on gasification tar tends to produce very finely divided carbon particles. This may cause the high surface area of formed coke.

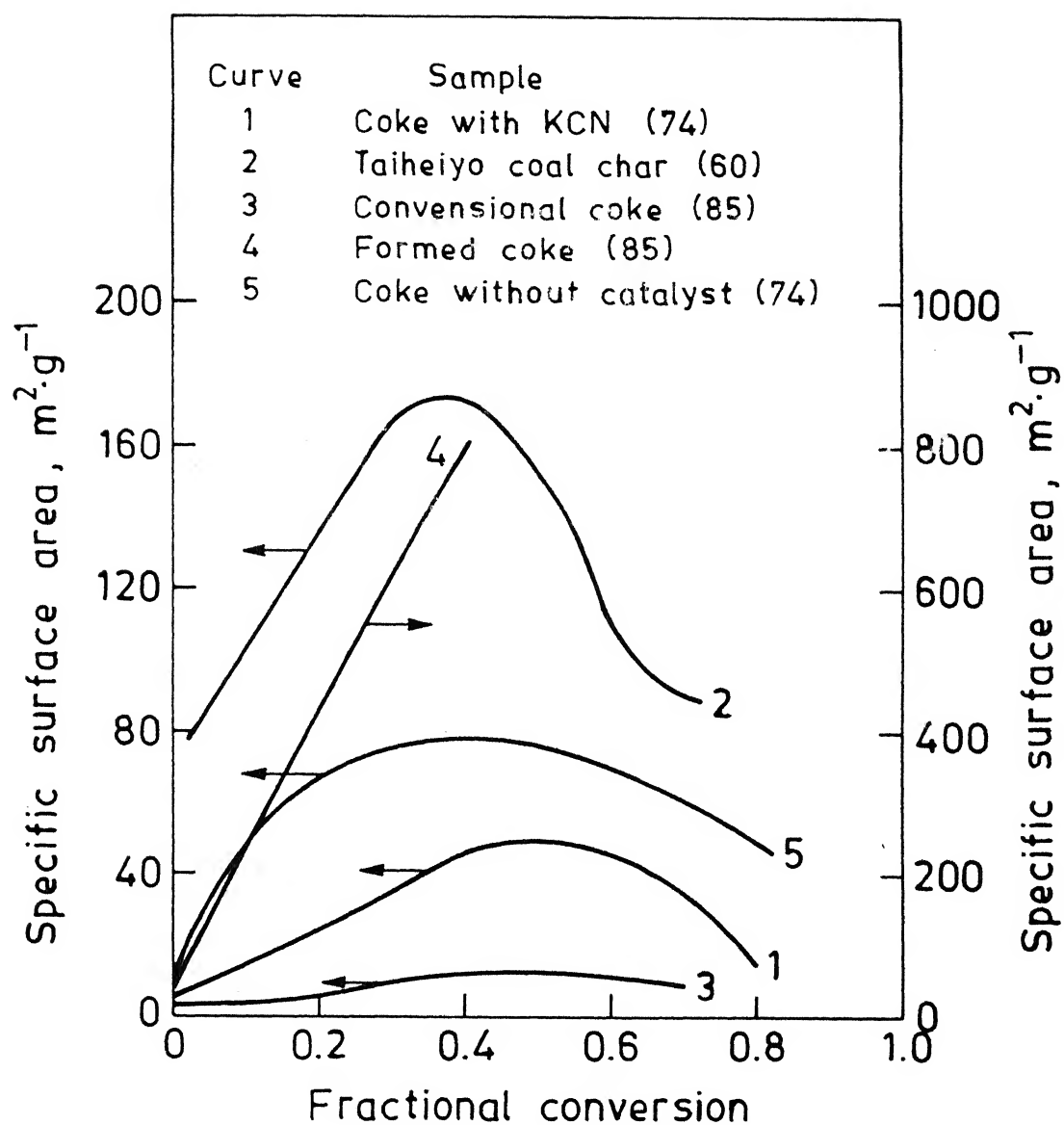


Fig. 1.13. Specific surface area vs. fractional conversion curves for different investigators.

Connected pore volume and pore size distribution are generally measured with the help of mercury penetration porosimeter(30,74,85) by measuring the pressure required to fill the pores with mercury. The measurement of pore size distribution is associated with the assumption of cylindrical or slit like geometry of pore section. But as in most of the carbon the pore texture is irregular, Turkdogan et al.(30) pointed out that pore volume is the more relevant parameter to be determined from mercury porosimeter rather than the pore size distribution. However, Alam et al.(74) and Szekely et al.(85) used the same technique for measurement of pore size distribution also.

There exists a sharp disagreement among workers(74,85) whether micropores or macropores dominate the change in pore volume with conversion. Alam and DebRoy(74) found that the pores of $0.05\text{ }\mu\text{m}$ to $1.0\text{ }\mu\text{m}$ or larger size increased with increase of coke conversion and contribution of larger pores ($>10\text{ }\mu\text{m}$) decreased with increase of burn off upto 40 pct. After 40 pct. burn off enlargement of small pores accounted for decrease of specific surface area. On the other hand Szekely et al.(85) reported that pore size larger than $35\text{ }\mu\text{m}$ contributed maximum towards the change in porosity of sample and change of porosity due to fine pores ($<0.032\text{ }\mu\text{m}$) was found to be negligible.

From above discussion it is established that surface area as well as porosity of a carbon sample undergoes change during gasification. The effective diffusivity of a porous material is a function of the total porosity. Thus several investigators(29,50,85) advocated that the effective diffusivity of the bed should be

determined as a function of reaction time. Turkdogan et al.(30) preferred to measure the effective diffusivity experimentally whereas Alam et al.(74) calculated the same from the following expression

$$D_{eff} = \frac{\epsilon^2}{\sqrt{3}} \times D \quad \dots(1.54)$$

$$\text{and } D = \left(\frac{1}{D_b} + \frac{1}{D_k} \right) \quad \dots(1.55)$$

where D_{eff} = effective diffusivity

D_b = bulk diffusivity

D_k = Knudsen diffusivity

ϵ = fractional porosity

By and large the change of $\left[-\left(\frac{dW_c/dt}{W_c} \right) \right]$ with burn off has been correlated with change in pore surface area. The parameter 'specific reaction rate' i.e. the rate per unit surface area has been found to be independent of burn off(60,74,89). Fig.1.14 presents specific reaction rate as a function of conversion for different types of carbon. It may be noted from Fig.1.14 that Adsehiri et al.(60) found very good constancy of specific reaction rate for all types of char. Same behaviour has been reported by Alam and DebRoy(74)[Fig.1.15] for uncatalysed coke. Pattern of variation of specific rate for coke doped with catalyst is somewhat different and will be discussed in the later section in connection with catalysis of gasification.

In order to tackle the problem of dependence of gasification rate on physical parameters like surface area, porosity etc. some workers have recently tried to formulate empirical equation giving relationship of $\left[-\left(\frac{dW_c/dt}{W_c} \right) \right]$ with fractional conversion(50,85,89).

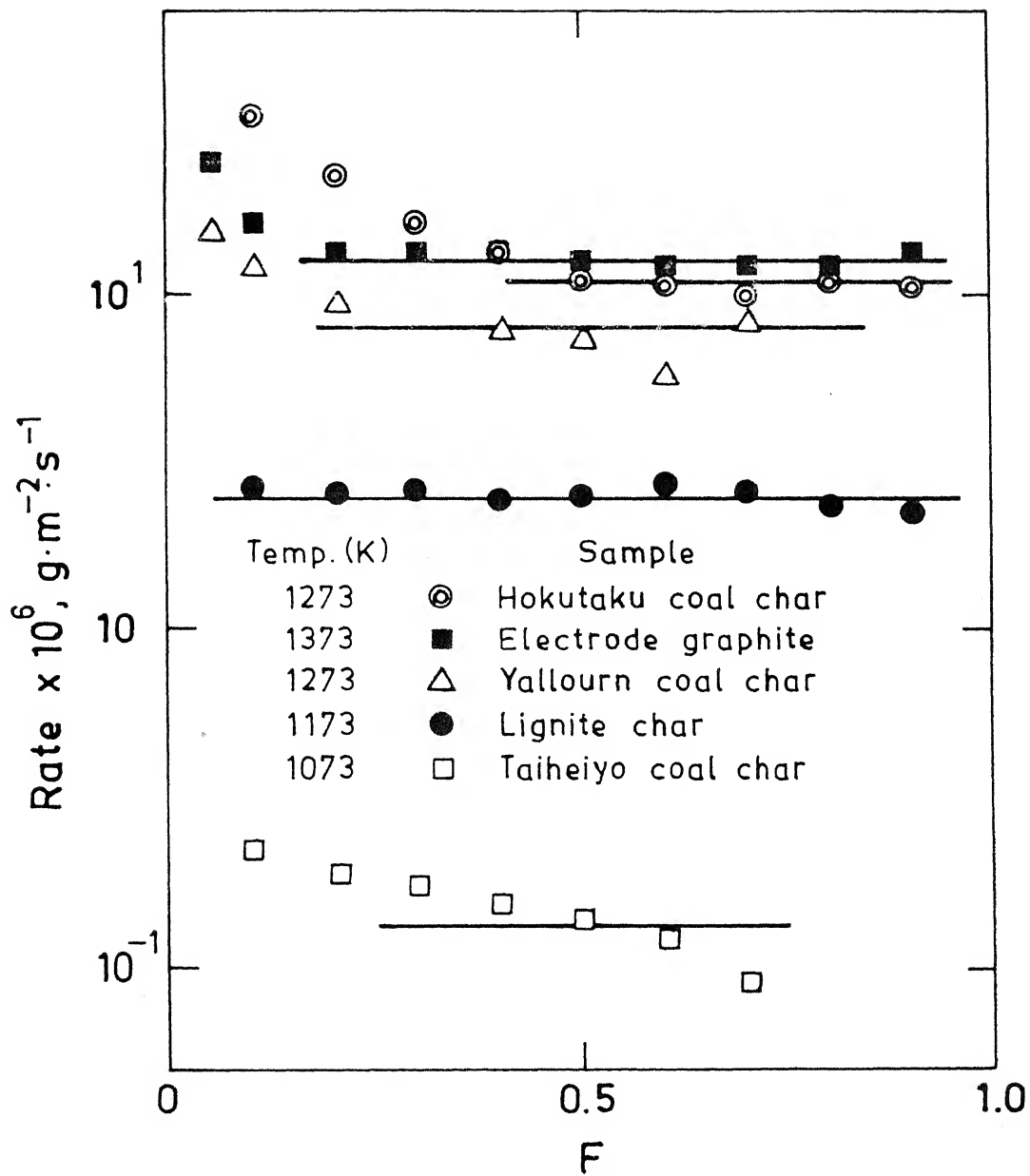


Fig. 1.14. Rate of gasification per unit surface area vs fractional conversion. (60)

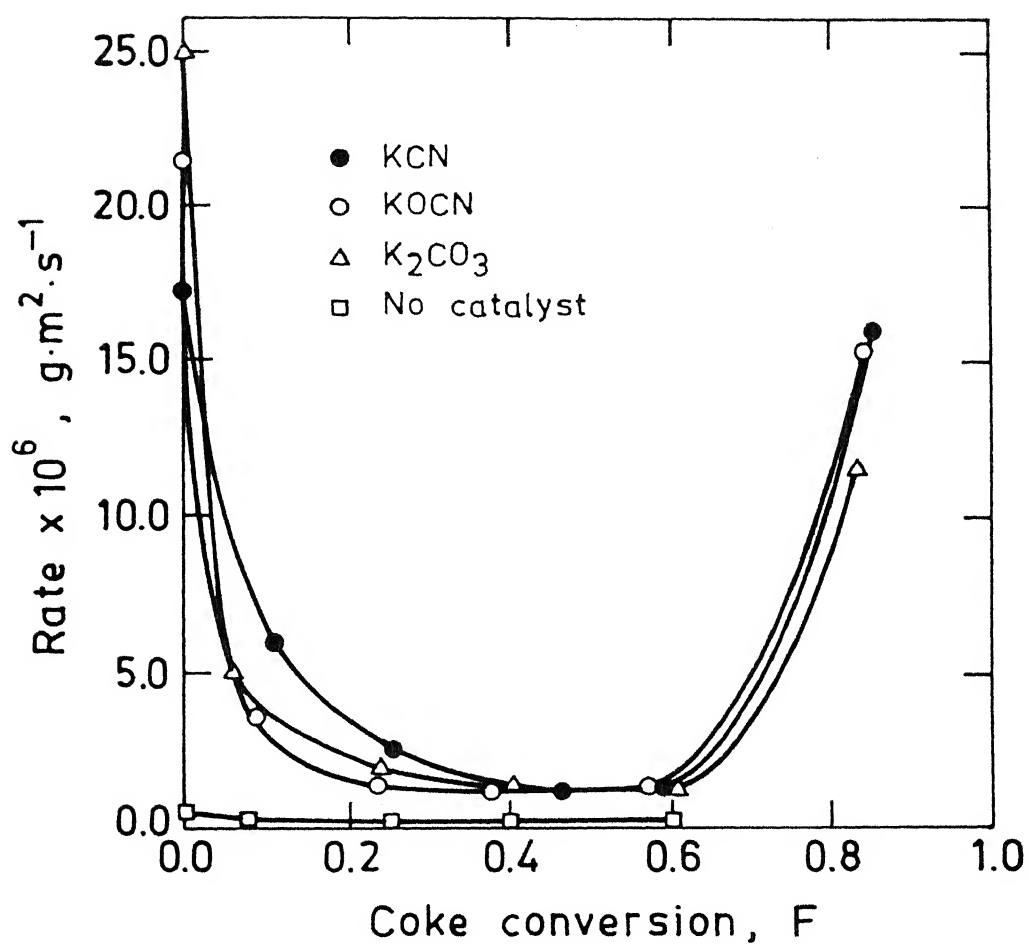


Fig. 1.15. Rate per unit surface area vs. fractional conversion of coke at $T=1123$ K. (74)

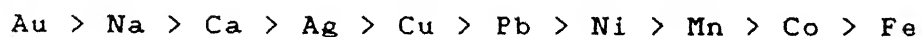
However, there is no unanimosity about these.

Turkdogan et al.(30) tried to correlate reaction rate with surface area for different types of carbon. Fig.1.16 presents the logarithm of rate (fractional weight loss per unit time) of gasification of carbon at 1373K against the logarithm of total surface area (m^2/gm) of unoxidized sample. It may be noted that the rate is proportional to the specific surface area for pyrolytic graphite, electrode graphite and coke. However, for coconut char, actual rate is much lower than extrapolated rate. They ascribed this behaviour of coconut char to predominance of micropores in it. According to them gases do not diffuse into the micropores easily. So micropores basically remain inactive during gasification reaction.

1.2.6 Catalysis of gasification reaction

Gasification reaction of carbon is found to be influenced quite significantly by foreign elements or compounds.

Many investigations have been carried out on catalytic gasification of carbon. Investigators have found that transition metal, alkaline earth metal etc. greatly enhance the reaction rate. A comparative study on the relative activity of various types of metal catalysts was carried out by Letort et al.(68) in the combustion of graphite in air at 773K in presence of 0.12% catalyst. They presented the following series in increasing order of catalytic activity.



But one thing must be borne in mind that the relative activities are by no means Universal but depend strongly on the particular experimental conditions like size and porosity of catalyst particles (and thus their surface area), chemical state of the

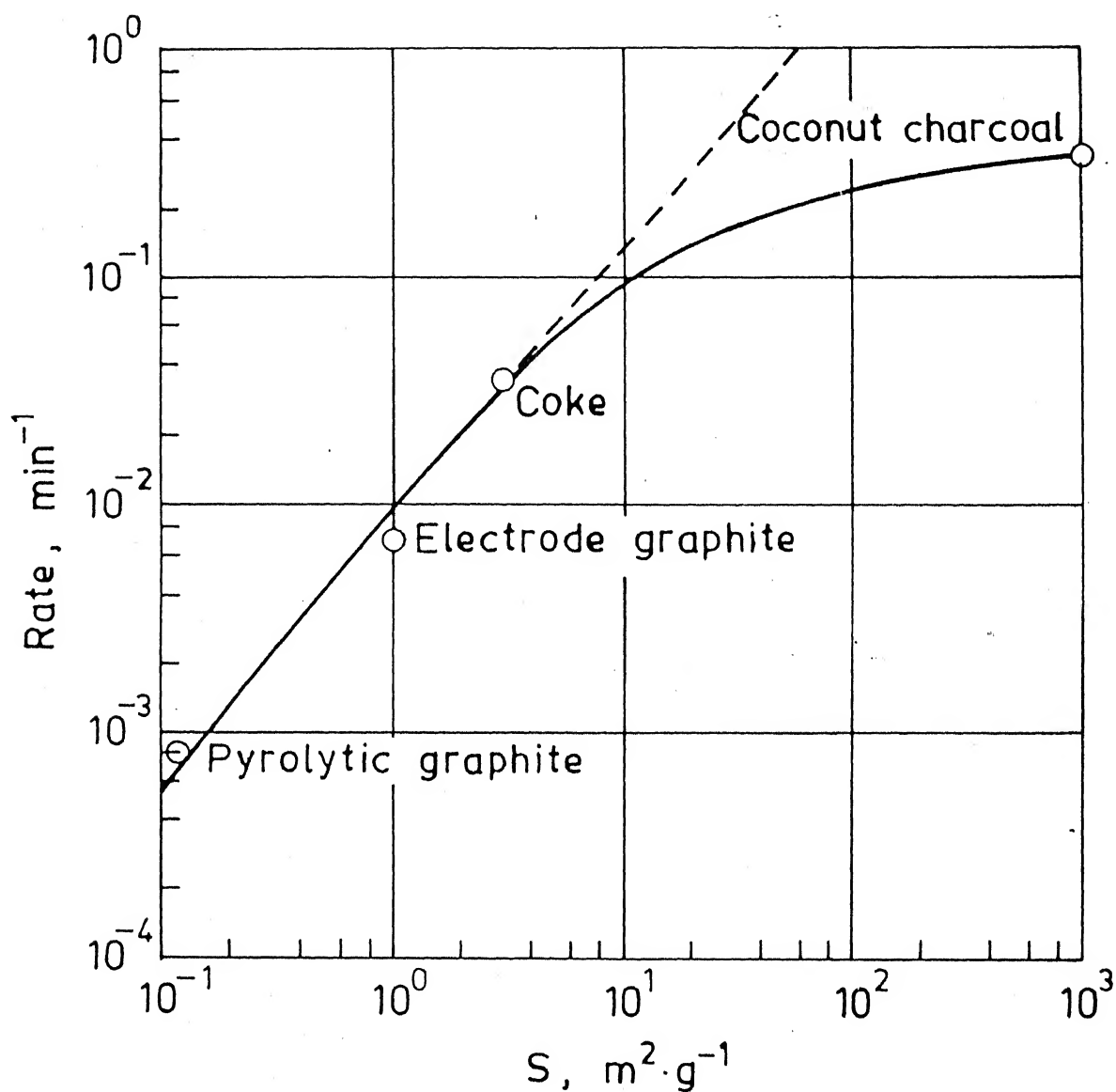


Fig. 1.16. Rate of oxidation in CO_2 at 1373 K related to internal surface area (BET) of unoxidized carbons. (30)

catalyst, intimacy of contact between catalyst and carbon surface etc. On the other hand sulphur bearing compounds have proven to be inhibitors of gasification reaction.

Walker et al.(64) compiled various aspects of catalytic reaction of carbon. The theories advanced to account for the experimental findings of catalytic gasification fall broadly into two categories. In brief they can be described as follows:

(a) Oxygen transfer mechanism

This mechanism was first proposed by Neumann et al.(90) and then by Milner et al.(91) to explain catalytic gasification reaction. The scheme proposed by Milner et al. may be presented as:



where RO represents metallic oxides.

Vestola and Walker(65) expressed views similar to the above in principle, and differed only in the chemical entity of the intermediate compounds. Catalysts on the carbon surface are regarded as oxygen carriers by an oxidation - reduction cycle. Elements or compounds which do not undergo such cycle under the experimental conditions can not exhibit any catalytic effect.

(b) Electron - transfer mechanism

The electronic theory of catalysis of gas-carbon reaction envisages a transfer of electrons between two solid phases. Long and Sykes(66,67) proposed that oxygen atom gets adsorped at the active sites of the carbon network and changes the distribution of π -bond. This oxygen - carbon bond is very weak and readily decomposes to carbon monoxide.

Turkdogan and Vinters(69) studied the rate of gasification of iron impregnated graphite granules (<0.01 to 2.1% Fe) in $\text{CO} - \text{CO}_2$ mixture at temperature range of $973 - 1273\text{K}$ and at pressures of 0.03 to 1 atmosphere. They also carried out gasification of iron impregnated coconut char and coke. Other catalyst elements like Ag, Cu, Cr, Zn, Ni, Co were used for study of gasification of graphite granules in air. They observed that even with less than 0.01% iron, the rate of reaction of graphite in $\text{CO} - \text{CO}_2$ gas mixture at $973 - 1273\text{K}$ increased by a factor of 2000 . Presence of 2% impregnated iron enhanced the gasification rate at 1073K by a factor of around one million. One interesting feature of their study is that they observed marked decrease of catalytic capability of transitional metals beyond 20 to 50 pct. conversion. However, hydrogen treatment of partially reduced graphite revived the catalytic effect. This finding is in accordance with what has been reported by Walker et.al.(64). Work by Mehrotra and Sinha(42) shows that there exists a marked difference in degree of catalysis of iron on the gasification reaction. They used $0 - 15\%$ iron for oxidation of carbon black in carbon dioxide atmosphere in the temperature range of $1073 - 1273\text{K}$. They observed only $2.5 - 3.0$ times rate enhancement with 15% iron which is insignificant as compared to what was reported by Turkdogan et al.. The reason for such a huge difference of extent of catalysis by iron can be explained in the following manner. Turkdogan et al. used impregnated iron in the carbon sample. With impregnation, iron atoms got incorporated into the structure of carbon and were finely disseminated at molecular level resulting into a very large Fe - C contact area. On the other hand, Mehrotra and Sinha employed a mechanical mixture of iron and carbon.

Thus iron - carbon contact area was much less than that of impregnation. So for catalytic effect, the more important factor is the contact area rather than the amount. To support this point, low rank coal may contain(59) relatively high amount of alkaline oxide in the structure. Presence of catalyst cations like Ca^{2+} , Na^+ , K^+ etc. (i.e. exchangeable cation) in high proportion in lignite char is probably the cause of high reactivity. Lignite coal contains carboxyl functional groups in their structure and exchangeable cations are thought to be present with these carboxyl groups. So the cations are intimately mixed and uniformly distributed in the carbonaceous matrix and thus catalyses gasification reaction more effectively. Treatment of char with acids (HCl , HF) removes the exchangeable cations and thus demineralized chars are less reactive than original chars. Concentration of carboxyl functional groups decrease with increase of coal rank. Therefore, inherent catalytic effect may not be significant for higher rank coals.

Otto et al.(70) found that 0.001 - 1 atomic percent of Pb can increase the gasification rate of graphite by around 5 order of magnitude, primarily because of massive increase of density of reaction sites. Based on absolute reaction rate theory, they found that site density was consistent with geometry of graphite crystal and postulated that every carbon atom in the structure can be transformed into a reaction site.

Many investigations(47,71-75) on catalytic effect of alkali metal compounds have been reported recently. From their kinetic data on gasification of carbon in carbon dioxide with 5 weight pct. of K_2CO_3 , Wigmans et al.(72) found the electron transfer mechanism to be

valid to explain the catalytic effect of K_2CO_3 . According to Cerfontain et al.(73), the difference of extent of catalytic effect of Na,K is due to the difference in amount of chemisorbed oxygen on the carbon surface. Freund(46,47) has found that even though Ca,K catalysed the gasification reaction to a significant extent, they do not show any appreciable effect on decomposition of carbon - oxygen complex and exhibit the same activation energy for both catalytic and uncatalytic gasification reaction. Thus he has concluded that enhancement of gasification reaction of carbon is due to increase of active carbon sites in presence of catalysts. This finding is in accordance with the report of Otto et al.(70).

Alam and DebRoy(74) have made a very comprehensive study on gasification of coke in carbon dioxide using KCN, KOCN and K_2CO_3 as catalysts. They have observed that the potassium bearing compounds enhance the rate quite significantly. They have also noticed that extent of enhancement do not depend upon the anionic constituents i.e. KCN, KOCN and K_2CO_3 have same degree of catalysing effect. They have explained their catalysis data on the basis of oxidation - reduction cycle mechanism i.e. Redox mechanism of precursors. With the help of micrographs of partially reacted coke sample, they have found potassium to be evenly distributed in the carbon matrix. They have attributed the extensive covering of surface by potassium to the transport of the same to the interior of small pores via gaseous medium either in elemental form or as volatile compound. Alam et al.(74) have also measured the vapourization loss of potassium as a function of carbon burn off. Molar K/C ratio has been found to decrease at the initial stage (upto around 40%) of coke conversion and after that the ratio

increases. The increase of molar K/C ratio at the advanced stage of burn off has been explained by faster rate of gasification over the rate of loss of potassium. They have tried to normalize the gasification rate per unit amount of potassium as a function of coke conversion. To eliminate the effect of structural parameter, they have plotted gasification rate of coke per unit surface area against coke conversion. Few such plots for doped sample have been shown in Fig.1.15. It may be noted from the figure that behaviour of specific rate for catalysed samples are somewhat different from uncatalysed sample. Rate is found to decrease first at the initial stage, then remain constant upto around 60% burn off, and finally increase again.

1.2.7 Summary and conclusions on kinetics of reaction of carbon with carbon dioxide

(i) The kinetics of reaction of carbon by carbon dioxide is characterized by:

(a) a large variation in rate by several orders of magnitude depending on nature of sample and experimental conditions,

(b) a high activation energy in the range of 210 - 375 kJ/mol,

(c) significant inhibition of rate by CO, which is the product of the reaction,

and (d) significant catalysis and inhibition by a number of elements and compounds.

(ii) The above features have confirmed that the rate of the reaction is primarily controlled by slow surface chemical reaction step. However, it has also been found that mass transfer partially controls the rate under some circumstances such as large particle size

and high temperature. Heat transfer limitation may also affect the rate to some extent.

(iii) In view of the importance of surface reaction step, several investigators have tried to eliminate mass transfer resistance by experimental design. Some have attempted to calculate effectiveness factor mathematically and thus to eliminate mass transfer resistance to find out true (i.e. intrinsic) surface chemical reaction rate. Comparison of procedures based on formulations of Roberts and Satterfield(76) and Tien and Turkdogan(77) shows that they do not yield the same result.

(iv) Rate of surface chemical reaction per unit mass of carbon may be designated as r_g . Its dimension is time^{-1} (i.e. sec^{-1} or min^{-1}). The following rate equation has been accepted by most of the investigators:

$$r_g = \frac{I_1 p_{\text{CO}_2}}{1 + I_2 p_{\text{CO}} + I_3 p_{\text{CO}_2}} \quad \dots(1.5)$$

This can be derived on the basis of Langmuir-Hinshelwood type of rate mechanism. Out of all the detailed mechanisms, based on the above, Reif's(14) mechanism has been accepted in general. The rate mechanism and equations proposed by Turkdogan et al.(29) are radically different and have not found acceptance.

(v) Rao et al.(32) tried to show that I_2 and I_3 of Eq.(1.5) are independent of nature of carbon. Examination of recent literature does not support this.

(vi) Carbon samples are highly porous. Pore surface areas are determined by BET technique based on adsorption of N_2 or CO_2 and range

between 1 - 1400 m²/gm. It appears that, if due precautions are taken, both adsorbents give approximately the same results even in samples with very large specific surface area due to micropores.

(vii) r_g has been found to be proportional to specific surface area(S) by and large. Therefore, S is one of the most important parameters contributing to kinetics of the reaction.

(viii) S has been found to undergo dynamic change with progress of gasification reaction. It typically increases first, exhibits a maxima and then decreases again. The rate of surface chemical reaction(r_g) as defined before, also changes with fractional conversion. Change of S has been found to explain this change of r_g fully or partially.

(ix) Several empirical equations have been proposed to quantify the relationship between r_g and fractional conversion. However, there is no generally accepted formula.

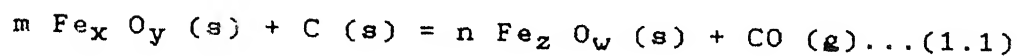
(x) Several metals and their compounds have been found to exhibit catalytic effect on rate of gasification. The effect is quite large if the catalyst is present in finely disseminated form especially at molecular level.

(xi) No satisfactory mathematical analysis is yet available to predict influence of combined heat and mass transfer resistance on reaction rate.

(xii) Several investigators have not attempted to find out chemical reaction rate separately. Instead they have proposed empirical 'global' rate expressions. These typically yield a fractional order dependence of rate on p_{CO} .

1.3 Literature Review on Carbothermic Reduction

It has already been mentioned that considerable extent of reduction of iron oxide by solid carbon may take place in blast furnace, at least at the lower part of the stack. This solid-solid reduction of iron oxide and carbon is generally termed as 'direct reduction' and may be rementioned as



where x,y,z,w are having their usual significance as described before.

1.3.1 Direct reduction versus reduction via gaseous intermediate

Kinetically, a solid-solid reaction is expected to be much slower compared to a gas-solid reaction. This is because of the following two reasons:

(a) solid-solid contact area is much smaller than that of gas-solid one,

(b) solid state diffusion is much more activated compared to gas-solid diffusion.

Therefore, it is more likely that the reduction of iron oxide by carbon will go through two stages i.e. reduction of iron oxides by CO and gasification of carbon by CO₂ (Eq.1.2, Eq.1.3). Till middle of seventies, controversy existed whether carbothermic reduction takes place directly or via gasification of carbon. But now it has been Universally accepted that reduction of iron oxide by solid carbon takes place via two stage mechanism. Following observations may be cited in support of the statement.

Many investigators (92,93,107-109,112) tried to measure the rates of true 'direct reduction' of iron oxide by carbon at

temperature range of 973 - 1423K by continuously evacuating the reaction chamber. They assumed that evacuation of chamber would result in elimination of product gas phase substantially and thus making the extent of gas-solid reactions (Eq.1.2 and 1.3) negligible. Rao (110) measured the reduction of hematite by carbon under inert gas flushing. Rate data observed by Rao was lower than what had been found under evacuated condition (92,93,107-109,112). Baukloh et al.(92) and Prasad et al.(109) used powder mixture of iron oxide and carbon, pressed into pellets, and found appreciable rates of carbothermic reduction even upon evacuation of chamber which should eliminate the product gases. Actually it may not be the case. Abraham and Ghosh (111) had shown that for a pellet size of around 1 cm. and pore diameter of the order of 10μ , the pressure inside the pellet should be at least 10 mm Hg in order to allow flushing of product gases (CO and CO_2) of carbothermic reduction out of the pellet into the evacuated chamber. This is because Knudsen diffusion predominates in pores at low pressures. So in reality, the rate of carbothermic reduction observed by investigators may not be the true direct reduction rate but was quite significantly affected by the presence of gas phase.

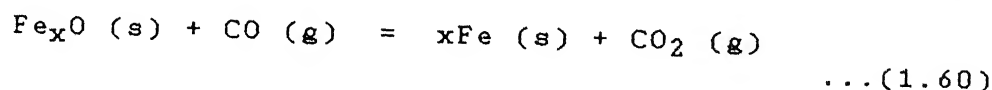
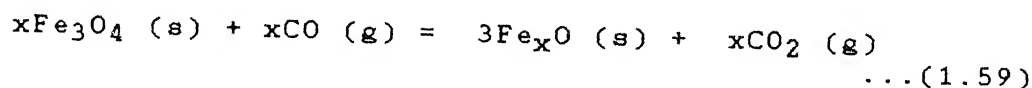
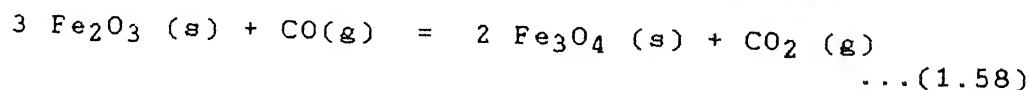
Here it is worth mentioning the following points to substantiate the two stage mechanism of carbothermic reaction:

- (a) lowering of particle size of carbon increases the reduction rate,
- (b) elements or compounds which enhance gasification of carbon also increase the rate of carbothermic reduction.

From the above discussion, it can be concluded that carbothermic reduction takes place through gaseous intermediate i.e. via

gasification of carbon.

Reduction of iron oxide takes place stagewise i.e. higher oxides get converted to lower oxides and finally get reduced to iron. The reaction 1.2 can be of any of the following:



1.3.2 General feature of carbothermic reduction

Numerous investigations on fundamental aspects (110,113-126) as well as on practical application (127-131) of reduction of iron oxides by carbon have been carried out in last 2-3 decades. As the scope of this thesis, which will be discussed later on is limited to fundamental aspects, no special mention has been made regarding the processes related to application.

Tables 1.6 and 1.7 compile the salient features like experimental conditions, mode of reduction, activation energy etc. of carbothermic reduction carried out by different workers. It is a general finding that iron oxide reduction takes place stagewise (Table 1.7) i.e. higher oxide is first reduced to lower oxide and finally is iron produced. But Seaton et al. (124) have reported that reduction of hematite and magnetite with bituminous coal char at the temperature range of 1073 - 1473K under inert gas flow did not take place stagewise. They found that magnetite, wustite and iron were present at early stages of reduction. This has been attributed by them to the temperature gradient which lead to a condition where conversion of

wustite to iron was possible near the surface and the core mixture of hematite, magnetite and wustite.

Kinetic study of carbothermic reduction of iron suffers from two major difficulties:

(a) as the solid reductant i.e. carbon is present along with oxide, the sample can not be gradually heated to reaction temperature. This is because reduction reaction can start at around 973K,

(b) the weight loss suffered by a carbon-oxide mixture is the sum total of weight losses due to removal of oxygen from oxide and weight loss due to gasification of carbon. To calculate the rate of reduction, it becomes essential to separate the weight loss of each of above types. Rao(110) attempted to separate these two with the help of some theoretical considerations. But this approach suffers from some untenable assumptions. On the other hand Bicknese and (113), Otsuka and Kunii (114), Gokhale and Ghosh (122), Abraham Ghosh (123) measured the amount of gas generated as well as analysed the gas composition as a function of time with the help of either gas chromatograph or oxygen sensor.

If the volumetric flow rate (\dot{Q}) of gas generation and composition of the product gases are known, one can find out the rate of weight loss of carbon (\dot{w}_C) and oxygen (\dot{w}_O) in the following manner.

$$\dot{Q}_{CO} = \dot{Q} \cdot X_{CO} \quad \dots(1.61)$$

$$\dot{Q}_{CO_2} = \dot{Q} \cdot X_{CO_2} \quad \dots(1.62)$$

where \dot{Q}_{CO} , \dot{Q}_{CO_2} are volumetric flow rates and X_{CO} , X_{CO_2} are volume fractions of carbon monoxide and carbon dioxide respectively.

$$\dot{w}_O = 16 (\dot{Q}_{CO} + 2 \dot{Q}_{CO_2}) / 22,400 \text{ gm/sec} \quad \dots(1.63)$$

Table 1.6 Experimental conditions and salient features of carbothermic reduction

Reference Particle Sizes Nature of Particle Compaction Atmosphere Temp. Amount Mode of Comments															
C		Fe ₂ O ₃		C		Fe ₂ O ₃		range C/Fe ₂ O ₃		Temp. Amount		heating		Comments	
1	2	3	4	5	6	7	8	9	10	11					
Otsuka and Kunii (114)	Fine(20μ, 66% <5μ) 67μ 124μ 190μ	Fine 57μ	Electrode graphitite (99.8%C) 31%pore volume	Pure Fe ₂ O ₃ (=4.79 gm/cc)	=0.8 by hand normally; only in some special expts. 770Kg/cm ²	N ₂ at 200cc/sec at STP	1050-1150	7 to 30 wt% C (Std=0.8 g Fe ₂ O ₃ 0.2g C)	Insertion in to hot zone	Bentonite added in some expts, most 1100°C, no pressing					
Abraham (3)	-200,+ 230 mesh USS(62-74μ)	Pellet micro-pellet (2mm) powder (-325 mesh)	Low ash electrode graphite	pure Fe ₂ O ₃ (certified)	hand, 50 psi also hand	Stagnant CO-CO ₂	880-1018 (mic-rope-11let at 970 940-1040)	1-1.5g C/O ratio 2.0	gradual heat insert-ion with initial N ₂ flow in 2 steps - do -	gradual powder mix. in the form of broken pellets					
Gokhale et al. (122)	-200 mesh	-325 mesh 5mm dia	- do -	Rajhara ore(also pure Fe ₂ O ₃) for comparison	hand	- do -	933-1076 (1gm. iron ore + 0.4gm. gr.po-wder								
Bicknese et al. (113)	-100 to 325 mesh	-12,+16 mesh (1 to 2 mm)	activated coconut charcoal	pure FeO (synthetic and natural)	hand	(180 cc/min) flowing CO at 0.008 mole CO per g. FeO per min.	1150	75pct. oxide + 25pct. charcoal by wt.	insert-ion into face	data for fig.3					

Table :1.6 (Contd.)

1	2	3	4	5	6	7	8	9	10	11
Rao (110)	-325 mesh (5 to 50μ)	less than 1μ	Pure am- orphous carbon	pure Fe ₂ O ₃	hand press	600cc/ min argon	850 - 1087	1gm. total samp- le mostly Fe ₂ O ₃ + amorp. carbon nothing stated; seems to be inse- rtion 1.3cm. dia. approx. 80% concen- trate + 20% char	Inserti- on of sample basket	
Seaton et al. (124)	-325 mesh	80% passi- ng th- rough -325 mesh. also (lime+ sili- ca) -325 mesh	Bitumi- nan co- al char (5.78% volati- le, also H ₂ O and ash	hemat- ite conce- ntrate & magne- tite conce- nyrate	hydro th- ermal ag- glomerat- ion then dried	N ₂ 900cc/ min (STP)	800- 1200			
Fruehan (119)	-200 mesh	-200 mesh (<74μ)	Coconut charcoal and meta- llurgic- al coke (devol. at 600°C)	Pure Fe ₂ O ₃ prepa- red FeO (by CO- CO ₂) also NiO	Pressed into cylinder =2.6g/ cm ³	Flowing Ar or He (1 lit/ min) also at diff. pressures (0.1 to 15 atm) some expts. in stagnant gas also naut gas	900- 1200	Perha- ps sa- mple inse- rtion into hot zone (noth- ing stated)	12.5% C for FeO 16% C for varying Fe ₂ O ₃ pressure total wt. (0.1-15 approx. 1 atm) pre- gm. (0.7 ssure cm. deep, build up mostly; inside sometim- pellet es pell- measured ets (0.6 in some to 1.4 stagnant C/Fe O	Also expts under varying pressure total wt. (0.1-15 approx. 1 atm) pre- gm. (0.7 ssure cm. deep, build up mostly; inside sometim- pellet es pell- measured ets (0.6 in some to 1.4 stagnant C/Fe O
Sriniv- asan & Lahiry (121)	-300 mesh	-300 mesh	Graphi- te (95.3% f.c)	Hematite cu) (68.34% total iron) total iron)	Spherical gas expt. 2 pellets (0.5) hand rol- ling usi- ng moist- ure and then dry- ing (also bentonite 1.5%)	flush (31x10 ⁻⁶ m/s) (720 cc min) (STP)/	925- 1060	Sample inser- tion	2 3 mol.ra- tio 3 to 8, pellet 10-12 mm. dia.	

Table -1.6 (Contd.)

1	2	3	4	5	6	7	8	9	10	11
P.C.Ghosh & S.N.Tiwari (116)	-60 mesh	-60 mesh (<200 μ)	South Indian Lignite coke (67.9% f.c), 10.6% Vol. 6.7% moist)	Gua hema-tite iron ore (55.2% Fe)	3/4 inch. dia mixed pellet by disk tainer pelletiser air dried and at 120°C	Pellets mixed in sea- ed con- tainer	900 - 1100°C	Insertion into hot zone	15 to 35% coke (by wt.)	

Table 1.7 Experimental conditions and salient features of carbothermic reduction for powder mixture

Ref and year	Stage wise redn	Stages in rate	Activation energy kj/mol	Temp. variation during expt. (°C)	Gas Composition, %CO	Index of rate	Mechanism and rate-controlling step	Role of mass transfer	Other comments
1	2	3	4	5	6	7	8	9	10
Otsuka and Kunii (114)	Yes	Yes; 2	20% redn. 230 - 272 60% redn. 63 - 314	-	10% redn. - 0 30% redn. - 50 50% and above - 80	% oxygen removal per min.	gasification rate controlling; in 2nd stage, catalysis by reduced iron	-	Increasing C pct. increases rate
Abraham and Ghosh (123)	Yes	Yes; 2 but no crop	15% redn. 305, 296 50% redn. 230-not pressed 140-pressed	12°C (for expt. at 1218K)	10% redn. - 20 20% redn. - 30 40% redn. - 80	rg	- do -	-	-
Gokhale et al. (122)	Yes	Yes; 2 but not for micro pellet, crop - 60% redn. 11et	60/ redn. 209 for micro pellet, crop - 60% redn. 58.6	-	-	rg	-do- for powder mix; oxide redn. at least partially controlling for micro pellet	-	rate increases linearly with wt.% C
Fruehan (119)	Yes; (no Fe upto 35% redu.)	no diff. in 2nd stage rate if starting with Fe ₂ O ₃ or FeO redn. of Fe ₂ O ₃ faster than FeO	-	-	initially CO ₂ ; considered scatter in gas analysis in the 2nd stage; approx. CO ₂ /CO close to FeO-Fe equlm.	ln(1-f) -kt, f is carbon reacted dW _C /dt = kt W _C (min ⁻¹)	gasification controlling at high temp. indicated by result	partial mass transport for reduction of FeO by C compared with oxidization of C by CO-CO ₂ ; good agreement; press. build-up not	rate constant for reduction of FeO by C compared with oxidization of C by CO-CO ₂ ; good agreement; press. build-up not

Table 1.7 (Contd.)

1	2	3	4	5	6	7	8	9	10
Rao (110)	not clear	not cl- ear; but talks about 2nd.3rd stage someti- mes	301.5	Only a state- ment usual- ly 1-2 min. elapsed before sample attain- ed temp	-	1- ---= W_{CR} , dt R is rate parampter (min ⁻¹) ln(1.743-f) =-Rt+Const. f is frac. redn.	gasifi- cation contro- lling; in- fluence of prom- oter/in- hibitor studied	-	assump- tion that a const. frac. of CO is consum- ed to reduce Fe-oxi- de. Aga- in $\beta=1$ (assum- ed) err- oneous analys- is; rate increa- ses w/ th C/ Fe ₂ O ₃
Bicknese et al. (113)	not rele- vant, took FeO		57.8	-	since there was flow of CO also, ar- tificial CO/CO ₂ ratio could be maintained 6/1 to 18/1	m= [1-(1-R _x) ^{1/3}] rate of reduct- ion; ch- emical [(C _e -C)/C _e t] t is in min. reacti- on at oxide/ Fe int- erface	-	rate increa- ses with C/FeO ratio	
Seaton et al. (124)	NO all phas- es incl- uding Fe found even in early stage (non-uniformi- ty between co- re and surface partly respon- sible)	NO	159 - 213.5	large temp. diff. betw- een core and surf- ace for appr- ecia- bly period	-	similar to Rao; ln (1 - 0.98f)= kt (for Fe ₂ O ₃ ---> Fe ₃ O ₄) etc.-1 (min ⁻¹) pellet	rate of gasifi- cation and ra- te of heat transf- er to pellet	some heat trans- fer ana- lysis; ut- ed to reason- able agreen- ent claimed	initia- lly hi- gh rate er ana- trib- uted to pyroly- sis, V.M., X-ray invest- igation

Table 1.7 (Contd.)

1	2	3	4	5	6	7	8	9	10
Sriniv- asan and Lahiry (121)	Yes; (X-ray diff.)	NO (but talks of st- ages from active energy point)	20% redn. 418 60% redn. 285 80% redn. 56 (not rel- iable)	10 to 12°C for Wust- ite redn.	some data available, lot of scatter; shows de- creased of CO ₂ /CO ratio as redn.pro- gresses (not rel- iable, it seem)	rate rel- ated to log (df _o /dt)x60 fraction oxygen min. remove	Carbon gasifica- tion con- trolling except towards the end when Wustite redn.may be contr- olling	-	rate incre- ases with C/Fe ₂ O ₃ ratio
Ghosh and Tiwari (116)	NO all phas- es pres- ent simu- ltan- eous- ly (X-ray)	-	78.3	-	-	slope of fractio- nal redn. is time	iron oxi- de redn. controll- ing	-	no dry- ing or devola- tiliza- tion incre- se of reduc- tant incre- ases rate

$$\begin{aligned}\dot{w}_c &= 12 (\dot{Q}_{CO} + \dot{Q}_{CO_2}) / 22,400 \\ &= 12 \dot{Q} / 22,400 \text{ gm/sec} \quad \dots(1.64)\end{aligned}$$

The reaction between CO and O₂ to form CO₂ may be represented as :



Assuming equilibrium of reaction (1.65)

$$p_{O_2} = (X_{CO_2} / X_{CO})^2 / K \quad \dots(1.66)$$

where K stands for the equilibrium constant of Eq.(1.65) and p_{O₂} is the partial pressure of oxygen in the product gas. Again,

$$X_{CO} + X_{CO_2} = 1 \quad \dots(1.67)$$

If oxygen sensor is used for gas analysis, then p_{O₂} can be measured from oxygen sensor data. Then combining Eq.(1.66) and Eq.(1.67) it is possible to find out X_{CO} and X_{CO₂}. If gas chromatograph is used then X_{CO} and X_{CO₂} can be directly determined. Once X_{CO} and X_{CO₂} are known, the rate of loss of oxygen i.e. the reduction rate can be easily calculated.

The variables which are found to affect the reduction kinetics of iron oxide by carbon are (1) temperature (2) particle size of iron oxide as well as carbon (3) C/oxide ratio (4) catalyst. Their effect may be described as follows.

Temperature has a pronounced effect on the carbothermic reduction rate. It may be noted from Table 1.7 that activation energy varies over a wide range starting from 56 kJ/mol to 418 kJ/mol. It is worth mentioning here that activation energy measured at various degrees of reduction differ quite a bit from stage to stage. On an average, early stage of reduction is characterized by high activation

energy (240 - 300 kJ/mol) indicating that it is controlled by gasification reaction since activation energy for reduction reaction varies approximately between 40 - 100 kJ/mol. The second stage is associated with much lower activation energy probably due to catalytic effect of freshly produced iron. Catalytic effect of iron on carbothermic reduction will be discussed in the next section.

Particle size is another important factor which contributes quite significantly on the reduction rate. Workers (110,114,119) have found that lowering of carbon particle size enhances the rate. The effect of particle size on gasification rate has already been discussed in previous section (Sec.1.2.4). Again dependence of rate of reduction on carbon particle size is an indication that the overall rate is controlled by gasification. On the other hand Otsuka et al.(114) have noticed that decrease of iron oxide particle size also enhance the reduction. They explained this observation by better contact area of particles. They also found that variation of both iron oxide and carbon particle size did not have any significant effect on rate.

If the reduction kinetics is controlled by gasification, then it can be expected that rate will depend upon the availability of carbon. This is because if carbon is not present in the near vicinity of an oxide particle then there will be local starvation of reducing gas and reaction will proceed slower than expected. Many Workers (110,116,119,121,126) studied the effect of amount of carbon on reduction rate. Rao (110) employed amorphous carbon for reduction of hematite at the temperature range of 1123 - 1280K. They varied the $\text{Fe}_2\text{O}_3/\text{C}$ ratio from 1:1.5 to 1:9 and found that higher proportion of

carbon enhanced the reduction rate markedly. For example, he found that at 1280K the time for 50% reduction decreased from 35 to 10 minutes when $\text{Fe}_2\text{O}_3/\text{C}$ ratio increased from 1:1.5 to 1:9. Fruehan (119) found that when the percentage of coconut char was increased from 10 to 30, the rate of reduction of wustite increased from around 12 mg/min to 38 mg/min at 1273K. Observations of Srinivasan et al. (121) and Ajersch (126) also confirm that with increase in amount of carbon in the mixture of oxide and carbon enhances the reduction rate.

1.3.3 Catalytic effect of freshly produced iron in carbothermic reduction

Catalytic effect of iron produced during reaction is till now a controversy in carbothermic reduction of iron oxide. This is because the literature review shows that some workers (114,122,123) observed considerable catalytic effect where as some others (110,120) did not notice it or it was not considerable. To pin point the sources of discrepancy in this regard it is necessary to have a close look to the experimental conditions employed by different workers which is summarized in Table 1.6.

Otsuka and Kunii (114) employed powder mixtures of oxide and carbon and found that in general, the carbothermic reduction followed a two stage behaviour. The first stage (i.e. the initial stage of reduction) exhibited a large activation energy. It is expected if the overall reaction is controlled by the rate of gasification of carbon.

The second stage was accelerated considerably and exhibited low activation energy. They explained the second stage acceleration in the powder mixture by catalytic effect of reduced metallic iron on the rate of gasification, which has been discussed earlier in section

(1.2.6). But they did not get this catalytic action for all experimental conditions, like for low C/Fe₂O₃ and fine particle size or fine carbon particle and Fe₂O₃ particle above 57 μ . They observed less pronounced effect when both carbon and iron oxide particle sizes were above 67 μ .

Gokhale et al. (122) employed both pure hematite and iron ore with graphite in powder mixture as well as mixture of iron oxide/ore pellet and graphite powder in the temperature range of 1206 - 1349K. They also observed significant catalytic effect of iron in the second stage for powder mixture of iron oxide/ore and graphite. The effect was not detectable for oxide pellet and graphite powder mixture.

Abraham and Ghosh (123) studied reduction of ferric oxide with graphite. They employed four types of combinations of the oxide and graphite namely

- (a) iron oxide and graphite powder mixture
- (b) oxide pellet and graphite powder mixture
- (c) micro pellet of hematite and graphite powder mixture
- (d) iron oxide pellet separated from graphite powder bed

They found that in all the cases, reduction was stagewise. Catalytic effect of iron oxide was significant for powder mixture of oxide and graphite. No detectable effect was observed by them in other cases. Figs.(1.17) and (1.18) present two typical results of Abraham et al. as examples. Fig.(1.17) shows the variation of rate of carbon loss, rate of oxygen loss, bed temperature, gas composition etc. for iron oxide and graphite powder mixture where as Fig.(1.18) presents the same for iron oxide micropellet and graphite powder

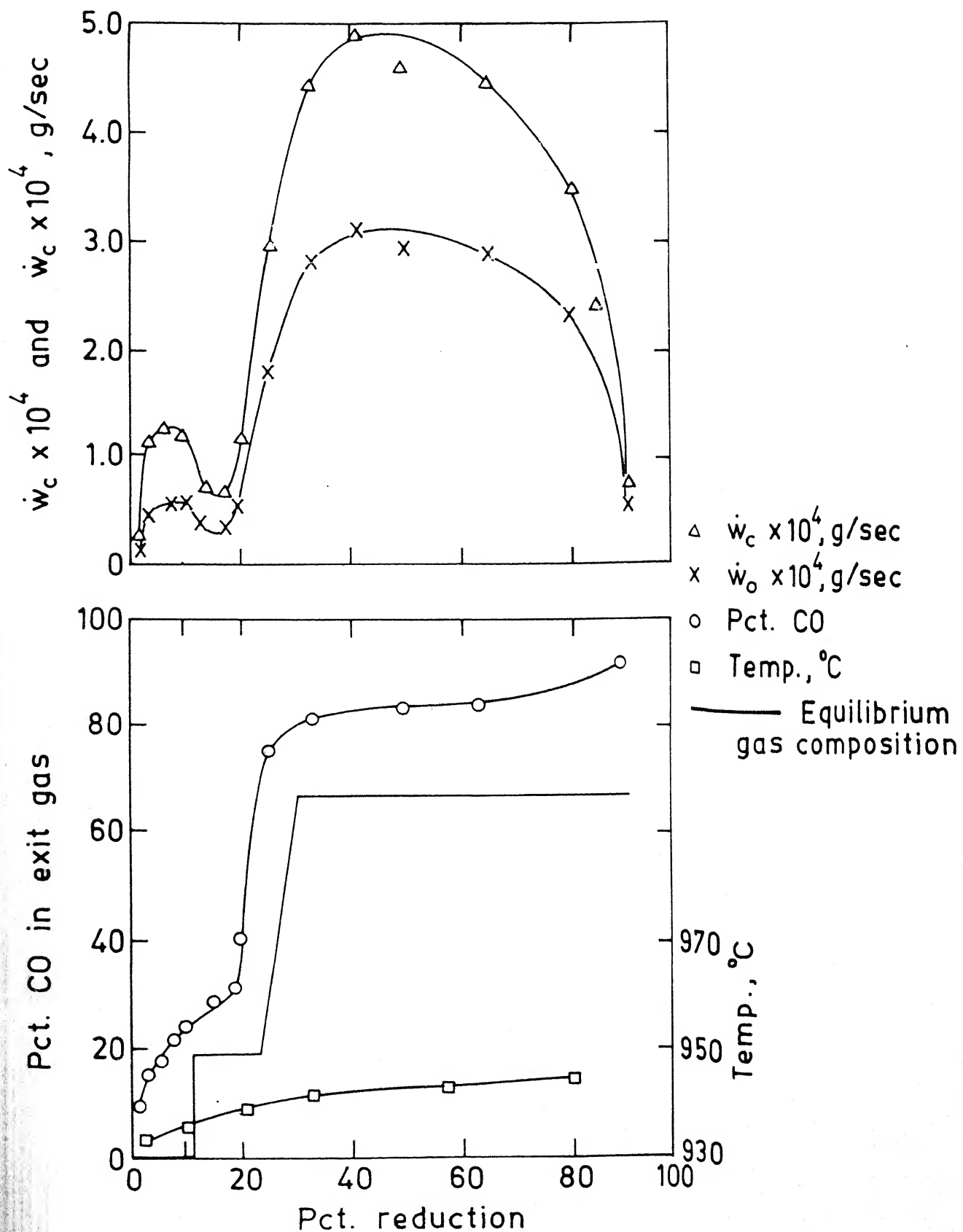


Fig. 1.17. Variation of observed and calculated parameters with fractional reduction of iron oxide and graphite powder mixture. (3)

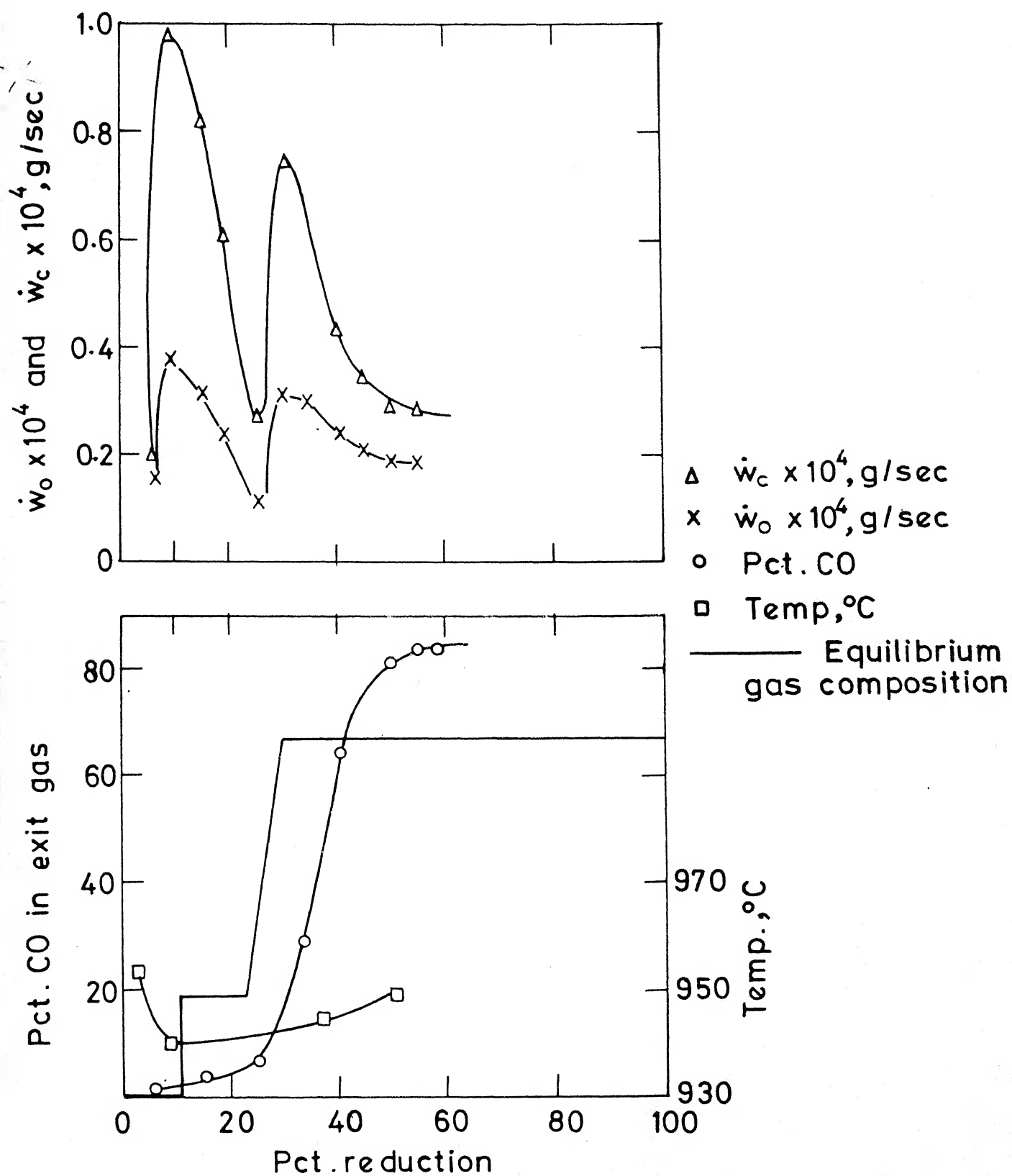


Fig. 1.18. Variation of observed and calculated parameters with fractional reduction of iron oxide micro-pellet and graphite powder mixture. (3)

mixture.

From an overall review of literature it may be concluded that except Otsuka et al.(114), Gokhale et al.(122) and Abraham et al.(123) no other worker (113,119,121,124) has observed catalytic effect. Though Rao (110) tried to show the effect of iron catalysis on reduction rate but it was not very clear. A critical analysis of the situation may be presented as follows:

Basic considerations point out that the effect of catalysis by Fe is likely to be marked if

(i) the first stage viz. $\text{Fe}_2\text{O}_3 \rightarrow \text{FeO}$ is somewhat accelerated, e.g. due to presence of volatile matter in carbon or may be by H_2O , which can produce reducing gases rapidly and lead to gaseous reduction of oxide. This was the case of Ghosh et al.(116) and Seaton et al.(124).

(ii) the reduction is not strictly stagewise but Fe is somehow present all through the course of reduction.

Basically the extent of catalysis by iron would be governed by the ratio

$$\frac{\text{Carbon surface in contact with reduced iron}}{\text{Total carbon surface reacting with gas}} \dots 1.68$$

The above ratio is likely to be influenced by the following factors

- (a) $\text{C}/\text{Fe}_2\text{O}_3$ particle size ratio
- (b) shape of the particles
- (c) degree of compaction
- (d) porosity of carbon particle

- (e) presence of bentonite or other extraneous materials
- (f) C/Fe_2O_3 quantity ratio

It has already been mentioned in connection with gasification of carbon that very effective catalysis of gasification of carbon by iron can be obtained when iron is impregnated (69) within carbon. On the other hand mechanical mixture of iron and carbon was found (42) to be ineffective in this regard. The powder mixture of iron oxide and carbon can not be compacted too much. From area of powder metallurgy(132) it is known that for mixed sizes and irregular shapes, the particle to particle contact area is more than equal sized, spherically shaped particles. Again in fine powders (less than 10 μ), the average porosity is large because of more frictional resistance to compaction due to large surface area. These observations are consistent with high porosity value in oxide-carbon mixtures. For high porosity the particle to particle contact area is low and is expected to vary by a factor of few when porosity is altered(132). This feature is likely to make catalytic effect sensitive to packing parameters.

It has been observed by Otsuka et al.(114), Gokhale et al.(122) and Abraham et al.(123) that relatively large size of iron oxide particles as compared to size of graphite suppressed the enhancement of rate at the $Fe_xO \rightarrow Fe$ stage. Bicknese et al.(113) could not detect catalytic effect because they started with FeO only.

Fruehan (119) took coconut char, coal char and metallurgical coke (partially devolatilized) as reducing material and did not find any enhancement of rate. It is quite likely that substantial amount of volatile matter released from partially devolatilized carbon would

have masked the catalytic effect of iron on the second stage. However, Fruehan ascribed this to the high reactivity of the form of carbons. But metallurgical coke is not much reactive than graphite. So absence of iron catalysis in case of metallurgical coke is a bit puzzling.

Rao (110) employed the size ratio of C/Fe₂O₃ to be around 40. He also used amorphous carbon which is perhaps more reactive. Combination of particle size ratio and high reactivity of carbon may led to less pronounced catalytic effect.

In experiments by Srinivasan et al.(121), 1.5 wt% bentonite was added to the powder mixture as binder. As Otsuka et al.(114) had observed, this might have decreased catalytic activity because bentonite would have a tendency to stick to Fe₂O₃ particles. Also retention of moisture due to improper drying may be a cause of masking of enhancement of the second stage.

1.3.4: Reaction mechanisms and rate equations

Carbothermic reduction of iron oxide has generally been found to be controlled by gasification reaction. Of course few workers have also concluded that reduction of iron oxide by CO may play an important role in determining the overall reaction rate. To elucidate this point, observations by few investigators have been discussed below:

As already mentioned, Otsuka and Kunii (114) observed a change in rate at around 33 percent reduction representing the onset of Fe_xO ---> Fe stage. They obtained the activation energy at the first stage between 230 - 272 kJ/mol and that of the second stage as low as 63 kJ/mol. Rao (110) found an overall activation energy to be

301.5 kJ/mol and no distinct stages were observed by him. Bicknese et al. (113) started with FeO and the activation energy found by them was 242 kJ/mol for FeO \rightarrow Fe stage. Study of Abraham et al. (123) on powder mixture of iron oxide and carbon showed that the activation energy at lower stage of reduction was much higher than that of the final stage. They reported the value at 15 percent reduction to be 305.2 kJ/mol where as 50 percent reduction gave activation energy of 230 kJ/mol for unpressed sample and 140 kJ/mol for pressed sample. Fruehan (119) found that the rate of reduction of iron oxide did not depend upon the starting material (i.e. hematite or wustite) and proceeded with the same rate in the last stage and give the same activation energy. This high activation energy is an indication of gasification controlled reduction reaction, at least at the first stage.

It may be possible that with advancement of reaction, the reduction of iron oxide by CO may become important and may start contributing significantly in controlling the overall reaction rate. Change of slope of rate versus reciprocal of temperature plot (118,124) indicates a probable change in control mechanism from gasification to reduction of oxide. Fruehan (119) also postulated that at high temperatures the reduction of FeO by CO may be partially rate controlling.

Experimentally, the rate controlling reaction can be best diagnosed from the analysis of the product gas which is a mixture of CO and CO₂. As stated earlier, some investigators determined gas composition either by gas chromatography (114) or by solid electrolyte cell (123) as the reaction progressed. Fig. 1.17 presents a typical

gas composition vs. pct. reduction curve (123) for mixture of graphite and Fe_2O_3 powder. Since the reduction is stagewise, viz. $\text{Fe}_2\text{O}_3 \rightarrow \text{Fe}_3\text{O}_4 \rightarrow \text{Fe}_x\text{O} \rightarrow \text{Fe}$, the gas composition in equilibrium with oxide phases at different stages would be a step function as shown.

If the actual gas composition follows the equilibrium curve for oxides, it would mean that oxide reduction by CO is much faster as compared to rate of gasification of carbon. In such a situation, rate of gasification would be exclusively controlling the overall reaction. Reverse would be true if actual gas composition lies close to equilibrium line for carbon. In Fig. 1.17, the gas composition lies in between indicating partial control by both.

Gokhale et al.(122) calculated the rate of reduction of oxide by CO theoretically and showed that it gave the correct activation energy for reduction rate in $\text{Fe}_x\text{O} \rightarrow \text{Fe}$ stage for their experiments on mixtures of micropellets of iron ore and graphite powder. These exercises demonstrate that partial control of rate by oxide reduction step cannot be ruled out.

Number of mathematical formulations (110,120,133-138) have been put forward to account for mechanisms and kinetic data of carbothermic reduction.

For solid-solid and solid-gas reactions which are basically diffusion controlled, Jander (133), Ginstling et al.(134) and Carter (135) have developed very useful correlations to describe the overall process. As detailed discussion of the mathematical model is out of the scope of this review, only the final form of their equations are presented below

$$[1 - (1 - f)^{1/3}]^2 = \frac{kt}{R_o^2} \text{ (Jandar) } \dots 1.69$$

$$[1 - 2/3 f - (1 - f)^{2/3}] = \frac{kt}{R_o^2} \text{ (Ginstling et al.) } \dots 1.70$$

$$\left\{ v - [1 + (v - 1)f]^{2/3} - (v - 1)(1 - f)^{2/3} \right\} / [2(v - 1)] = \frac{kt}{R_o^2} \text{ (Carter) } \dots 1.71$$

where R_o is the initial radius of the oxide pellet and f is the fraction reacted at time t . v is the volume ratio of the product to that of an equivalent amount of reactant. It is worth mentioning here that McKewan (139) has also proposed a very simplified but attractive mathematical model for reduction of spherical pellets of iron oxide by gases, which may be presented as

$$R_o \rho_o [1 - (1 - f)^{1/3}] = kt \dots 1.72$$

where R_o is initial radius of pellet, ρ_o is the oxygen density in the pellet. f and k have their usual significance.

Rao (110) has presented a kinetic model for carbothermic reduction of iron oxide on the basis of carbon gasification reaction as rate controlling. He separated the share of weight loss due to the oxygen loss of oxide from that of total weight loss. He also assumed that whatever CO was generated due to gasification got consumed by iron oxide for reduction. The model proposed by Rao could not explain the reaction rate at the early stage. This may be because of the abovesaid assumptions. The model is basically empirical in nature.

The mathematical analysis of Sohn and Szekely (136) is a generalized formulation for the reaction between two solid species via

a gaseous intermediate, involving net generation of gases. The model enables one to present the carbothermic reduction of iron oxide where the overall reaction is under dual control of reduction of oxide by CO and oxidation of carbon. One of the important assumptions they made is that gas composition was uniform throughout the pellet. This may be true only where no diffusional resistance to gas flow through pellet will be present. Sohn et al. characterized the system by two dimensionless parameters v_v and v_β which include the reaction rate constant, the shape and size of the reactants, the relative amounts of the solid reactants. They defined the dimensionless time of reaction as

$$z = 1/v_\beta (1 - \alpha) = k.t \quad \dots 1.73$$

where v_β represents the ratio of the activities of the two solid reactants defined simply in terms of the volume ratio and the reaction rate constant, α is the dimensionless position of the reaction front within the grain and k is the proportionality constant. Using relationship between relative amounts of the solid reactants, the fractional conversion of iron oxide (X_o) can be related to fractional conversion of carbon (X_c) as

$$X_o = 2v_v X_c \quad \dots 1.74$$

where v_v is the dimensionless parameter defining the relative molar quantity of solids. If $2v_v$ is less than 1 then carbon reacts completely and the oxide is partly reduced. On the other hand when $2v_v > 1$, then oxide is completely reduced.

Srinivasan et al.(142), in a theoretical analysis made an attempt to determine the conditions under which the reduction of iron oxide by carbon takes place according to two stage mechanism involving

gasification of carbon. They introduced the concept of minimum temperature of reduction (T_{min}). Essentially minimum reduction temperature means that at any temperature below T_{min} , the gasification reaction ceases to have any effect on the reduction and the overall reduction reaction takes place directly by solid carbon. They have used the rate expressions of Rao (32) and Ergun (19) for gasification and compared the results obtained by two rate equations under different conditions. They noticed that T_{min} increases with increase of carbon dioxide in the bulk phase. T_{min} evaluated from Ergun's expression was found to be extremely sensitive to the amount of carbon dioxide in the gas phase and was applicable only when bulk phase contains negligible amount of carbon monoxide. According to them (121), in case of hematite T_{min} evaluated through Rao's expression for gasification was applicable for all values of carbon dioxide and that for magnetite and wustite reduction will be valid only at low amount of carbon dioxide content.

Tien and Turkdogan (120) performed a mathematical analysis of rates of reaction of metal oxides and carbon mixtures. The rate equation derived took into account the rate of carbon gasification reaction, the diffusive and viscous flow of reactants and products viz. carbon monoxide and carbon dioxide through the packed bed where a pressure gradient exists. They criticized the mathematical formulation of Rao (140) which predicted that carbon dioxide pressure build up at 2 cm. below the surface of the powder mixture would be more than 20 atmosphere at 20 percent reduction stage. With the aid of their (120) mathematical model, Tien et al. concluded that for a 2 cm. deep bed the pressure build up at the bottom of the bed would be negligible.

They also demonstrated that if the furnace gas is neutral then the rate of reduction would be lower than if the reaction chamber contains carbon dioxide. They attributed this lowering of rate with neutral ambient gas to the back diffusion of inert gas into the interparticle pores of the solid mixture. They found that at lower temperature and/or with carbon of low reactivity, the composition of the furnace gas had a greater effect on the rate of reduction within the bed, because of the greater effect of back diffusion.

1.4 Plan of work

The literature review presented in sections 1.2 and 1.3 show that substantial informations are available on gasification of carbon and carbothermic reduction of iron oxides. But still some anomalies and gaps exist in literature. It may be noticed from literature review that most of the workers have tried to determine the rate controlling step(s) of carbothermic reduction from the activation energies. Though the above approach is alright in some cases, a more appropriate way may be direct comparison of reduction rate obtained experimentally and the rate predicted from gasification data. If gasification is the rate controlling step for the overall reaction then it is expected that rates of carbon loss evaluated from both reduction and gasification should match. Very few investigators have made any effort in this direction. Again literature review shows that attempt of Abraham et al (123) to correlate the reduction rate and gasification rate yielded a very significant quantitative disagreement.

The reasons for the disagreement were considered to be :

(a) measured rate of gasification of graphite in CO_2 was erroneous, which is evident from low activation energy reported by them.

and/or (b) their extrapolation of the rate of gasification of graphite in CO_2 to CO-CO_2 mixture, using some extrapolation formula available in literature. It may not be correct.

Again, many investigators have reported that gasification rate of carbon in iron oxide and carbon powder mixture is greatly enhanced by freshly produced iron. But catalysed gasification reaction will not allow quantitative correlation with reduction rate properly. So precautions have to be taken so as to either eliminate or minimize the catalytic effect. It has also been documented in literature that highly reactive form of carbon may not be significantly catalyzed from freshly produced iron.

Again in carbothermic reduction, carbon experiences a varying atmosphere of CO-CO_2 mixture. So for correlation purpose, the following are the requirements

(a) experimental data on rate of gasification in CO_2 and CO-CO_2 gas mixture,

(b) experimental data on rate of carbon loss and rate of oxygen loss in carbothermic reduction,

(c) precautions to avoid catalytic effect of freshly produced iron.

It may be noted from literature review that Rao et al (32) concluded that I_2 , I_3 of Langmuir-Hinshelwood rate expression are universal in nature. But from further examination this conclusions appears to be doubtful and thus needs attention.

It has been established by many workers that the gasification kinetics may be significantly influenced by heat and mass transfer limitations and thus the experimentally observed rate may be lower than the intrinsic chemically controlled rate.

On the basis of the above, the followings were decided:

(a) to determine the gasification rate of graphite in CO_2 to check the data of Abraham et al.

(b) since high reactive form of carbon is supposed to experience little influence from freshly produced iron, it was decided to employ coconut char as carbonaceous material for carbothermic reduction. As mentioned, for correlation purposes, it is necessary to determine rate of gasification of coconut char in CO_2 , CO-CO_2 and $\text{CO}_2\text{-Ar}$ gas mixtures

(c) heat and mass transfer analysis of gasification reaction

(d) to carry out weight loss as well as product gas analysis experiments during carbothermic reduction. Again as no information is available on simultaneous measurement of weight loss and gas analysis, effort should be made in this direction

(e) carbothermic reduction being endothermic in nature, it is desirable to have the history of the bed temperature during reaction

(f) it being a fundamental study, it was decided to employ pure iron oxide and carbon

(g) to express all the experimental data in analytical form and development of required computer programs

(h) numerical solution of the differential equations in connection with heat and mass transfer analysis

Keeping the above in mind, the following schedule was planned to be executed i.e.

(1) to design and fabricate the thermogravimetry set up with all probable precautions

(2) to make char from coconut shell in the laboratory itself

(3) to fabricate the required set-up for char making

(4) to design and fabricate a special thermogravimetry apparatus for simultaneous measurement of weight loss as well as to perform product gas analysis with the help of a gas chromatograph

(5) to design and fabricate the reaction cell with gas out-let for simultaneous measurements

(6) a thermogravimetry set-up for measurement of reactivity of coconut char in CO-CO₂ atmosphere because the former being highly poisonous gas, experiments can not be conducted with a open top arrangement

(7) to perform different types of experiments under various operating parameters

(8) to compare the results of the mathematical models available for mass transfer and heat transfer analysis and development if necessary

(9) computer programs to calculate the intrinsic rate of gasification after eliminating heat and mass transfer effects theoretically

(10) to compute the instantaneous rate of carbon loss and oxygen loss from carbothermic weight loss data with the help of product gas composition, measured with the help of the gas chromatograph and to develop the required computer program

(11) to compare the experimental rate of reduction with that of the rate predicted from gasification data for the present set of study

and to attempt to remove the anomaly reported by Abraham et al.

(12) to interpret the results obtained there of.

CHAPTER 2

APPARATUS

The objective of the present investigation included the following sets of experiments:

- (i) gasification of graphite in pure carbon dioxide
- (ii) preparation of coconut char from coconut shell
- (iii) gasification of coconut char in pure carbon dioxide, carbon dioxide-monoxide gas mixtures and simultaneous gas composition measurement by gas chromatograph
- (iv) carbothermic reduction of hematite by coconut char
- (v) analysis of product gas during carbothermic reduction by gas chromatograph.

2.1 Apparatus for Measurement of Gasification Rates of Graphite in Pure Carbon Dioxide

Gasification rates of graphite were measured in a conventional thermogravimetry set-up, designed and fabricated in the laboratory according to the specific requirements. The set-up consisted of the following components:

- (i) gas train to purify, control and measure the flow rate of carbon dioxide, monoxide and inert gas,
- (ii) the thermogravimetry apparatus with furnace, reaction chamber, temperature measurement and control unit, facility for continuous measurement of weight loss.

2.1.1 Gas train

The basic purpose of the gas train was to closely monitor the flow rate of the gases and to purify them from the probable impurities present. Fig.(2.1) shows the line diagram of the train. The detailed description of the train is noted in Table 2.1.

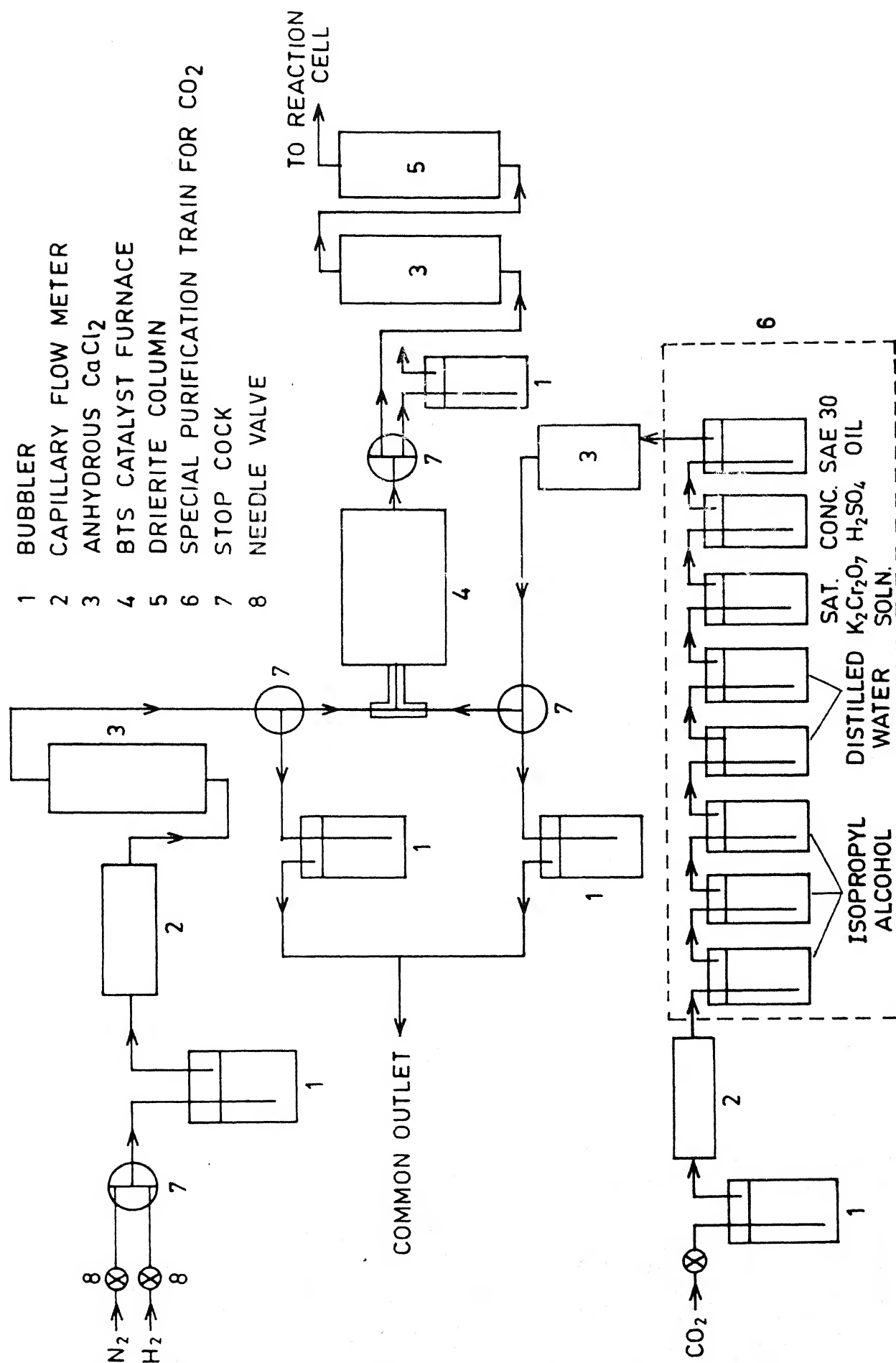


Fig. 2.1. Schematic representation of the gas-train.

Table 2.1 Gases used and their functions

<u>Gas</u>	<u>Function</u>
Argon	Flushing of the reaction chamber before and after the experiments to ensure an inert atmosphere in the chamber
Carbon dioxide	To provide oxidizing atmosphere for gasification of carbon
Hydrogen	To regenerate BTS catalyst periodically by the reaction: $\text{Cu}_2\text{O} + \text{H}_2 = 2 \text{Cu} + \text{H}_2\text{O}$

Commercial argon is pure enough for flushing purpose. The impurities generally present in it are moisture and oxygen. To ensure complete removal of these impurities, the inert gas was passed through the reagents, presented in Table 2.2

Table 2.2 Reagents used for purification of inert gas

<u>Reagent</u>	<u>Function</u>
Anhydrous CaCl_2	To remove moisture
Alkaline pyrogallol	To remove oxygen
Concentrated H_2SO_4	To remove moisture and alkaline vapour
BTS catalyst	To remove oxygen
Drierite (CaSO_4)	To remove moisture

As mentioned earlier, carbon dioxide was used to oxidize the carbon. Commercially available carbon dioxide is a byproduct of fermentation of molasses and may contain a number of impurities like vapour of alcohols, aldehydes, ketones etc. alongwith moisture. The purification system (Baccus train (143)) employed for removing the impurities consisted of a number of scrubbers through which the impure

carbon dioxide was made to pass through. The outcoming gas was found to be odourless and atleast 99% pure. The rest was air. The scrubbing reagents used and their purposes are given in (Table 2.3).

Table 2.3 Scrubbing agents for carbon dioxide purification

<u>Scrubbing agent</u>	<u>Purpose</u>
Isopropyl alcohol	To remove aldehydes, ketones
Distilled water	To remove alcohol
Concentrated $K_2Cr_2O_7$	To oxidize ammonia and sulphur compounds
Concentrated H_2SO_4	To remove alkaline compounds
Compressor oil (SAE 30)	To absorb oxidation product

The carbon dioxide gas was passed through a bubbler and a capillary flowmeter where the flow rate of gas was registered. From flowmeter, carbon dioxide entered the Baccus train. The reagents in the unit could be used only for 10-12 runs in succession. Therefore, a standby unit was also fabricated and kept ready with required reagents for replacement. Gas emerging out of the Baccus train then entered an anhydrous $CaCl_2$ column and finally into the reaction chamber via BTS catalyst furnace, $CaCl_2$ column and drierite tower. BTS catalyst, manufactured by BASF, West Germany is nothing but finely divided copper, deposited on a suitable ceramic substrate. Due to very high surface area, the copper particles have high efficiency to remove oxygen at relatively low temperature.

Drierite has a low equilibrium residual water vapour content and therefore was used after the last anhydrous calcium chloride column in the gas train.

2.1.2 Thermogravimetry set-up

Fig.(2.2) presents the schematic diagram of the thermogravimetry (TG) set-up used for reactivity study. It consisted of a vertical furnace, a mullite tube as reaction chamber, the housing of sample holder, gas inlet and outlet pipes, thermocouples for controlling and measurement of temperature, sample hanging assembly and a single pan semi-micro balance (Sartorius make) with readability of 10^{-5} gm for continuous recording of instantaneous weight.

A Kanthal wound vertical furnace of 53 cm length was used in the study. A mullite tube of 62 cm length and 5 cm internal diameter was employed as the reaction chamber. The mullite tube reaction chamber was fitted with two brass flanges (one at the top and the other one at the bottom) to provide air tight fitting covers. Both the flanges were having copper coil brazed on them for water cooling. Silicone rubber gaskets and high temperature sealants were employed to make the set-up gas tight.

While designing the TG assembly, the following precautions were taken into consideration:

(i) the entire gas should sweep past the surface of the carbon sample. However, it should do it smoothly and without creating any dead zone. The stainless steel gas outlet tube with its hood over the sample holder was to serve this purpose (Fig.(2.2)). In order to make the arrangement precise, the tube was kept aligned by a stainless steel(S.S) guide tube and the position of the hood was made adjustable by a threading arrangement.

(ii) one problem in precise thermogravimetry work, specially in flowing gas is vibration of the hanging assembly which lead to

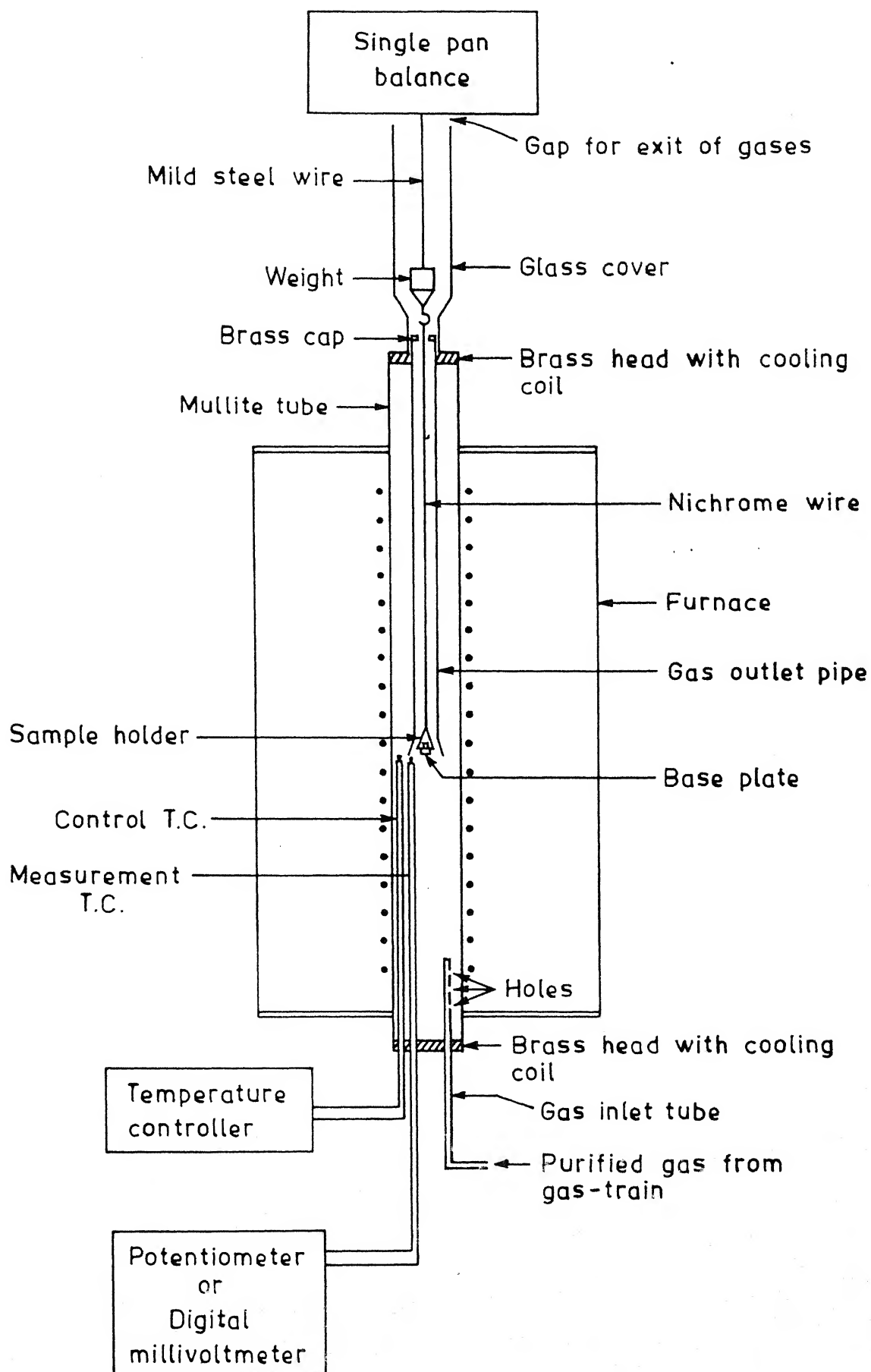


Fig. 2.2. Thermogravimetry set-up.

fluctuation in the reading of the balance and consequent difficulties. In order to minimize it, the following steps were taken in addition to the proper outlet arrangements.

A glass cover was provided on the gas outlet pipe. The main purpose of the glass tube was to prevent any forced vibration to the hanging assembly due to external disturbances such as thermal convection. The single pan balance was placed on a wooden platform with a central hole. An inconel rod having a cylindrical weight at its lower end was connected to the balance. The sample bucket holder was suspended to the constant temperature zone of the reactor tube with the help of flexible nichrome wires through a hook in the cylindrical weight of the inconel rod. The sample bucket holder was a circular platform with cylindrical protrusion at the bottom, having holes at the edge to enable fixing of hanging wires. This arrangement was found to be quite satisfactory.

(iii) during gasification reaction, the weight loss of carbon sample should be only due to the oxidation of carbon by carbon dioxide. But it was found that weight loss of sample was quite substantial in argon atmosphere. The reasons for the weight loss in inert atmosphere might be by demineralization/devolatilization of sample, oxidation by residual oxygen in argon or by oxidation in presence of back diffused air in the reaction chamber. The gas train of the inert gas was sufficiently equipped to scavenge out the impurity oxygen in it and the weight loss could not be accounted by the demineralization/devolatilization of the sample. So precautions were taken to cut down the back diffusion of air in the reaction chamber.

Open end of the glass tube, placed over the S.S gas outlet tube was sealed with a copper disc having a central hole in it to allow the inconel rod connecting the balance to pass through. A copper tube around 8 cm long was attached around the hole of the copper disc to reduce the effective cross sectional area of the opening. This arrangement was found to cut down the back diffusion of air which was confirmed by weight loss measurement in argon gas.

(iv) errors in temperature measurement and control were minimized. The furnace had about 6 cm long uniform temperature zone, where the sample could be conveniently located. One of the two thermocouples was used for temperature control and the other one for measurement of reaction temperature. Through some trials, it was found that the temperature control was better if the control thermocouple was placed inside the reaction chamber rather than near the outer surface of the mullite tube. Therefore, the control thermocouple was placed inside the chamber.

The furnace was controlled by a Leeds and Northrup model 6260 Electromax temperature controller actuated by chromel - alumel thermocouple. A power supply circuit consisting of temperature controller, variable autotransformer, resistors and relay allowed significant improvement in the temperature control. The measurement thermocouple was connected to either a Leeds and Northrup model 8686 millivolt potentiometer or to a Digital millivoltmeter (3 $\frac{1}{2}$ digits, Vaishesika make) to measure the actual temperature of reaction. Both the thermocouples were calibrated against standard Pt/Pt-10% Rh thermocouple. The digital millivoltmeter was also calibrated from time to time against precision Leeds and Northrup potentiometer. The

potentiometer was again checked against a reference voltage source and found to be quite accurate.

(v) it was necessary that the gas temperature and the sample temperature should not differ much for an isothermal study. This necessitated that the flowing gas should have opportunity to get preheated to the reaction temperature before coming in contact with the carbon sample. Heat transfer calculations pointed out that a separate preheating furnace was not necessary. However, in order to ensure attainment of temperature, the gas was introduced through a specially designed inlet tube (Fig.(2.2)). A copper tube of 2.5 mm internal diameter was closed at the top and three holes were made at the side wall, one beneath the other. The copper tube was positioned through one of the bottom holes such that the holes of the copper tube were facing the furnace tube wall. This served as gas inlet tube. The incoming gas was forced through the holes of the tube and was thus made to impinge on the heated wall of the furnace. This would also result in a swirling motion in the gas. Due to these, there would be better heat transfer between the furnace wall and the gas resulting in improved preheating efficiency.

2.2 Char Making Apparatus

The purpose of this set-up was to prepare char from crushed coconut shell which would be subsequently used for gasification study as well as for reduction of iron oxide. This was necessary since the char available in the market was found to have poor reactivity and would not meet requirement. This set-up also consisted of :

- (i) gas purification train
- (ii) char making furnace

2.2.1 Gas purification train

Char was prepared in flowing argon gas. The purpose of argon was to provide a neutral atmosphere during charring. As mentioned earlier, the common impurities present in argon are moisture and oxygen. The reagents used for purification were anhydrous CaCl_2 and BTS catalyst. Fig.(2.3) shows the schematic diagram of the whole set-up.

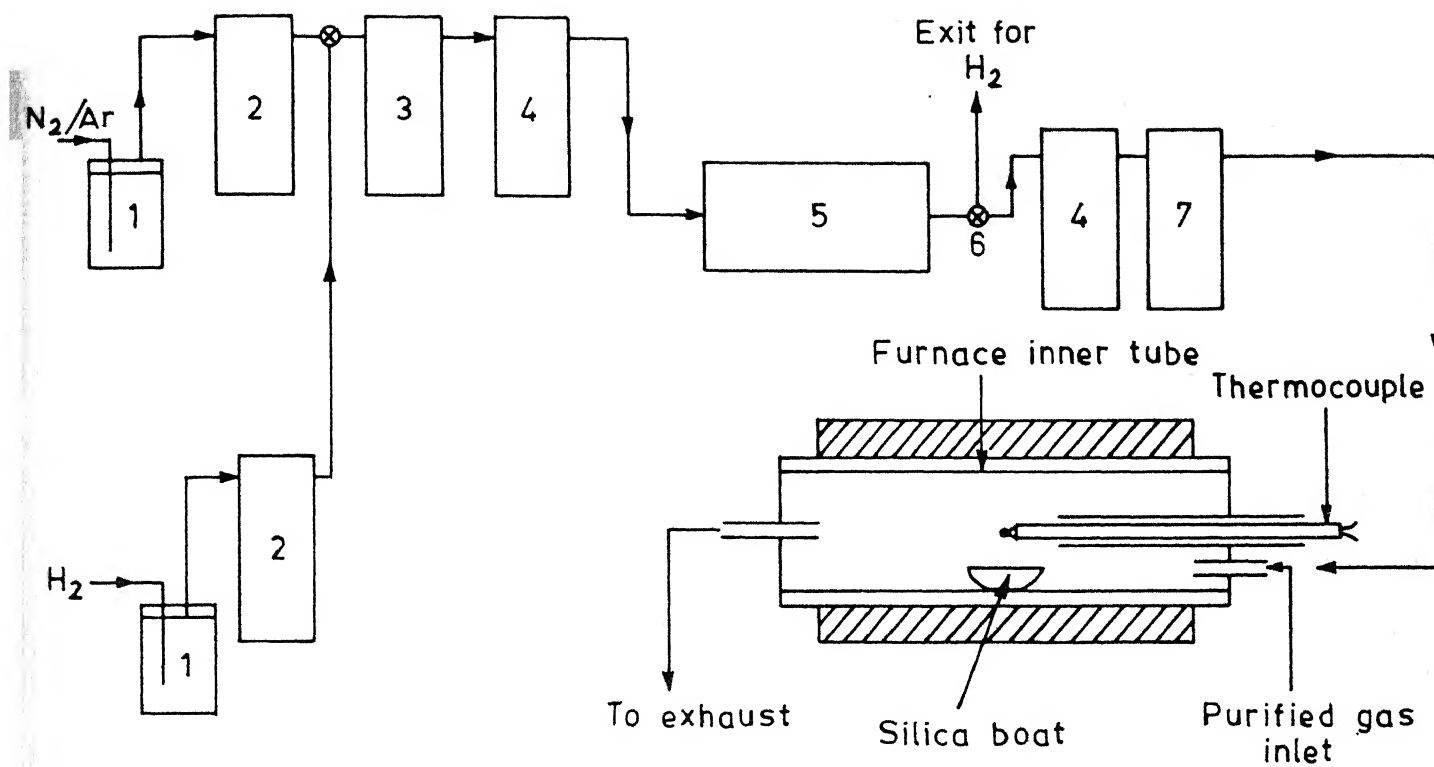
2.2.2 Char making furnace

A Kanthal wound horizontal furnace of around 50 cm length was used for heating the reaction chamber. The charring chamber was mullite tube of 55 cm long and 5 cm inner diameter mullite tube. Both ends of the tube was fitted with water cooled brass flanges. One chromel-alumel thermocouple was put inside the reaction chamber through a hole in the gas inlet side. This thermocouple was used for both control of the furnace and for measurement of temperature. Leeds and Northrup make model 6260 Electromax controller was used for controlling the furnace temperature.

One condenser was connected just after the char making furnace at the outlet end to condense the evolved volatile matter during charring.

2.3 Apparatus for Carbothermic Reduction

In a mixture of iron oxide and carbon, the weight loss is due to both loss of oxygen and carbon. In order to determine degree of reduction of oxide from weight loss data, investigators have made assumptions or have made auxilliary measurements such as simultaneous determination of gas composition or determination of total iron content in the reduced mass. Literature review of carbothermic



- 1 Bubbler 2 Capillary flowmeter 3 Glass ball mixer
 4 Anhydrous $CaCl_2$ 5 BTS catalyst furnace
 6 Stop cock 7 Soda lime tube

Fig. 2.3. Char making apparatus.

reduction of iron oxide shows that very few studies have been made where simultaneous measurement of weight loss and the product gas analysis have been done.

Here a scheme for simultaneous measurement of weight loss and on-line analysis of product gas of carbothermic reduction was planned. For this purpose the TG set-up described in Sec.2.1.2 was employed after modification of the assembly. The need for modification arose since a TG assembly which allows continuous weight loss measurement without any opening at the top, for connection to balance, was not available in the laboratory.

Fig.(2.4) presents a schematic view of the modified TG set-up, designed and fabricated for this purpose. The modification consisted of :

(i) fabrication of a special cylindrical chamber, made of inconel which would be hanging freely from the balance and would contain the sample inside,

(ii) fabrication of an outer metallic rectangular chamber alongwith a brass isolation valve. This isolation valve was kept closed most of the time during experiment. It was opened intermittently to free the suspension rod for noting down the weight.

Dead volume of the entire chamber was drastically cut down through proper design so that the gas chromatograph hooked up with the outlet determines CO and CO₂ of the product gas without much of a time lag. The entire hanging chamber was kept in inert atmosphere maintained by flowing purified argon.

The arrangement is explained below in details and shown in Fig.(2.4) and Fig.(2.5).

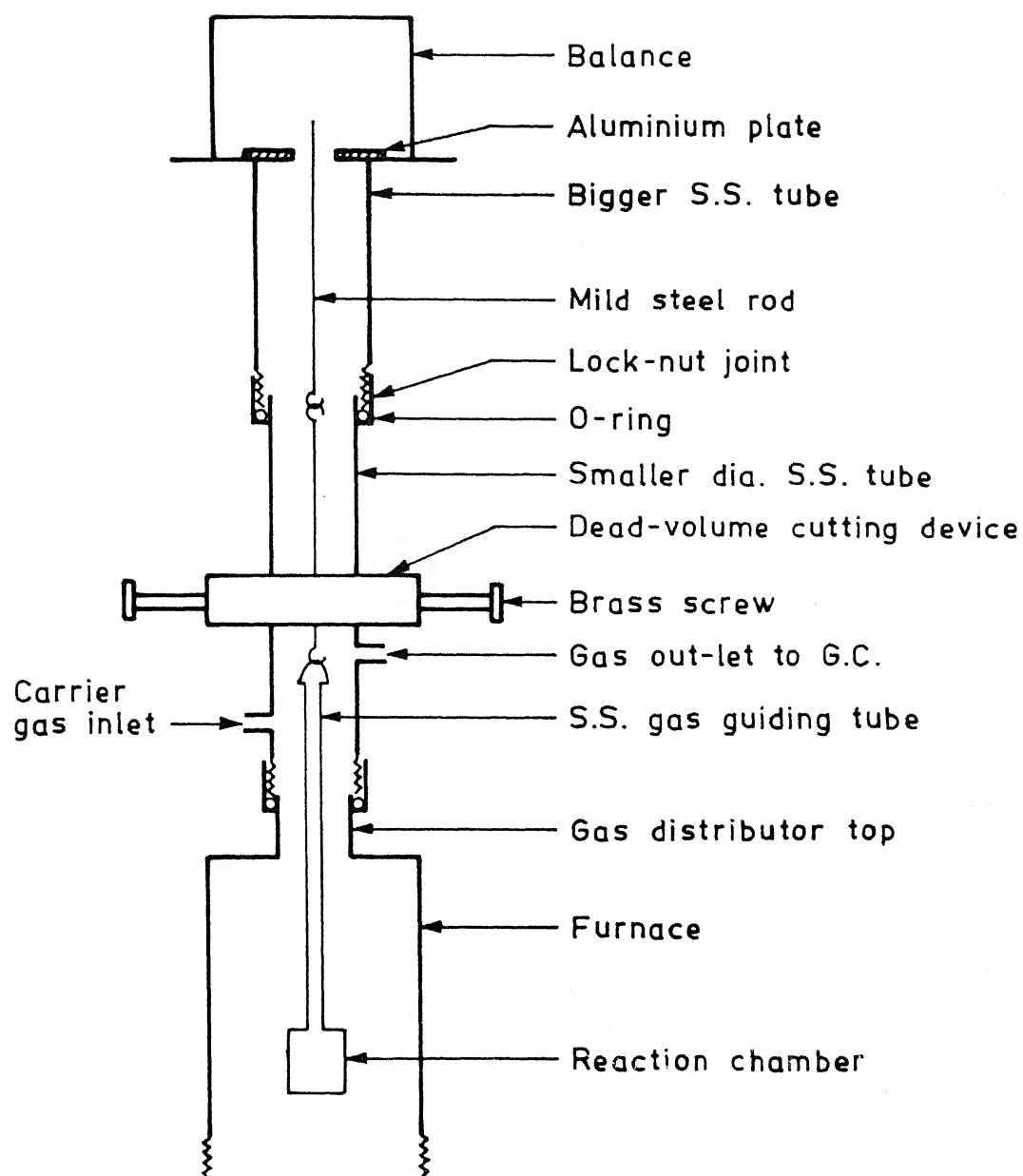


Fig. 2.4. Modified TG set-up.

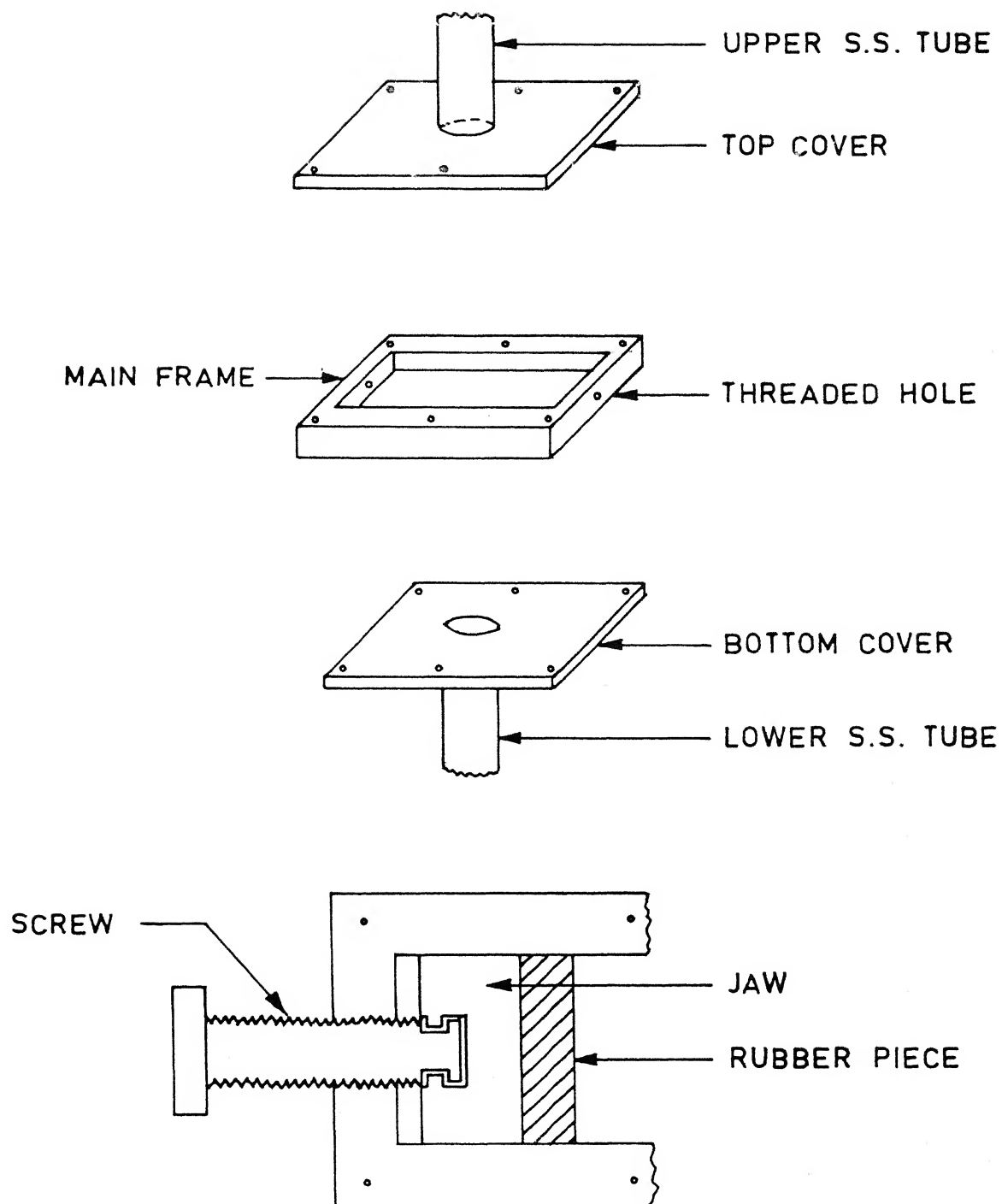


Fig. 2.5. Different parts of dead volume cutting device.

Analysis of the product gas was done with the help of gas chromatograph made by Chromatography and Instrument Company, Baroda. Result of the analysis was registered in the form of peaks on a continuous chart paper. Digilog make dual pen strip chart recorder was employed for this purpose.

One inconel made cylindrical bucket of 1 cm internal diameter and 2.5 cm long served as reaction chamber. One cylindrical alumina crucible, containing the mixture of oxide and char was kept in the bucket. The top of the inconel bucket was covered by a threaded inconel lid, having a central hole with thread. One stainless steel tube was screwed with the bucket cover to guide the product gas outside the reaction chamber. The length of this tube was so adjusted that its open face ended just below the outlet hole of tube 3. The whole assembly i.e. the bucket alongwith the stainless steel gas outlet tube was hanged from the balance by hooking it to the inconel rod.

For achieving gas tightness between the top of the furnace tube to the bottom of the balance platform, a set of S.S tube (tube 1, tube 2, tube 3 in Fig.(2.4)) were connected to one another with lock-nut joints with rubber O-rings. This allowed sliding of the tubes for opening the top of the furnace or for adjustments by loosening the nut. Tube 1 had an internal diameter of 2.2 cm to give an idea of the size.

The exposed end of the tube 3 was brazed onto the dead volume cutting device. Fig.(2.5) presents the sketch of the abovesaid arrangement. It consisted of one main frame and two covers. The main frame was a rectangular block of brass having a rectangular hollow

space in it. The facing sides of the hollow space were perfectly parallel and smooth. Two brass jaws having exact fitting in the hollow space was made to move along the side walls of the hole with the help of two brass screws. The brass screws were fixed to the jaws by jam nuts and could move through threaded holes in the smaller arms of the rectangular main frame. Two high temperature rubber pieces were pasted against the facing sides of the jaws so that when the brass screws were turned full in clockwise direction, the jaws would press against each other tightly without damaging the inconel rod. Two brass covers were fitted on both sides of the main frame with the help of screws. Both the covers were having central holes smaller than internal diameter of tube 2. The upper cover was brazed with the open end of tube 2.

Tube 3 of diameter same as that of tube 2 was fixed with lower brass plate cover. Open end of this tube was connected with the gas outlet tube of the furnace chamber by lock-nut arrangement. Tube 3 was having two small holes on the opposite walls, one slightly below the other. Two small diameter copper tubes were fixed with the holes. The lower hole served as the inlet of an inert carrier gas and the upper one acted as an outlet of the mixture of the product gas and the carrier gas. When the jaws of the dead volume cutting device was pressed tightly against each other, the gas mixture was forced to get diverted to the gas chromatograph.

Unfortunately, the assembly described above did not work satisfactorily. The details of the problems and the probable causes will be discussed later. But at this stage it is worth mentioning that it was decided to decouple the weight loss measurement and the product

gas analysis during carbothermic reduction of iron oxide. An auxilliary set-up was made for gas analysis. However, the modified TG set-up described above was found to be very useful for kinetic study of coconut char gasification in CO-CO₂ gas mixture since the former is poisonous and could not be employed straight with an open top arrangement.

2.4 Gas Analysis Set-up

For this part of study, the horizontal furnace described in Sec.2.2.2 was used. A fused silica tube of 31.5 cm long and 0.9 cm internal diameter served as the reaction chamber as well as the sample holder. Fig.(2.6) shows the arrangement. A chromel-alumel thermocouple was inserted into the silica tube so that the tip of the thermocouple just touched the sample bed. This enabled registering of the temperature history of the bed as reaction proceeded. One elbow glass joint was fixed with the silica tube by polythene tube. Precaution was taken so that no gas could leak through the joint. The other end of the glass elbow was connected to the inlet of the gas chromatograph through polythene tube. There were two holes at the bent of the elbow joint so that two wires of thermocouple could come out which in turn were connected to a digital millivoltmeter. The two holes were sealed with the help of high temperature silicone sealant. Two thermocouple wires were isolated from each other by fine silicone rubber tubes.

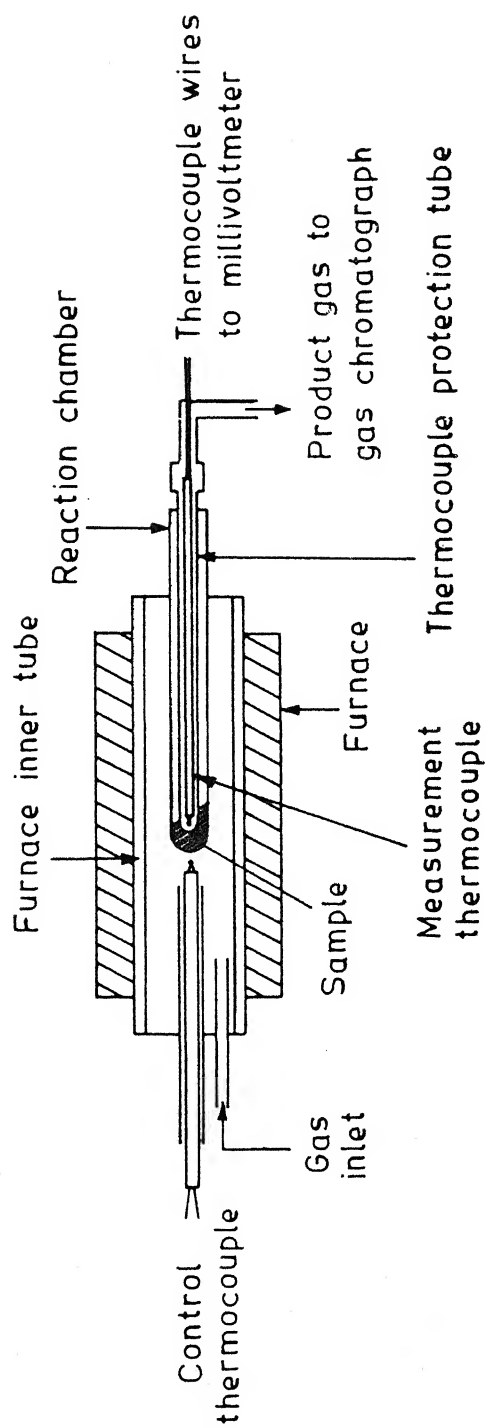


Fig. 2.6. Apparatus for product gas analysis and bed temperature measurement.

CHAPTER 3

MATERIAL PREPARATION AND EXPERIMENTAL PROCEDURE

As the title of the chapter suggests the content will be divided into two main parts viz. how the materials for different types of experiments were prepared and secondly the procedure for conducting the experiments.

3.1 Material Preparation

The starting raw materials for the experimental studies were:

Graphite	Low ash, electrode grade graphite rod of 5 cm diameter
Coconut char	Prepared in the laboratory by charring crushed coconut shell
Iron oxide (Fe_2O_3)	Reachim make, USSR

3.1.1 Preparation of graphite powder

A 5 cm diameter electrode grade graphite rod was machined on lathe to produce coarse sized graphite powder. Precautions were taken to avoid contamination like oil, dirt etc. from lathe. Coarse graphite powder was then ground in porcelain mortar and pestle to finer sizes. Porcelain mortar and pestle was carefully cleaned by acetone before use. The fine graphite powder was then screened to - 170 + 200, - 200 + 230, - 230 + 270 mesh size using USS screen. Intermittantly the powder was heated in oven to remove moisture to avoid sticking. The sized fractions were then treated with magnet to remove any accidental iron contamination, heated in oven at around 110°C for 12-18 hours, and finally stored in desiccator for further use.

3.1.2 Preparation of coconut char

The starting material for preparation of coconut char was coconut shell. First the coconut shells were crushed with the help of clean iron mortar and pestle. Silica crucible of 20 cm diameter and 10 cm depth was then filled with the crushed coconut shell. The char making furnace (Sec.2.2.2) was maintained at around 1000°C . Before putting the crushed shell in the furnace, argon or nitrogen was passed through the reaction chamber at a flow rate of 1 lit/min. for at least 10 minutes to ensure neutral atmosphere. The gas flow was continued and was slightly increased while introducing the sample in or withdrawing it out of the furnace. This was done to prevent the back diffusion of air in the furnace chamber.

Coconut shell was allowed to devolatilize for one hour under continuous flow of inert gas. At the end of stipulated charring time, the gas flow was again increased and the sample was withdrawn to the cooler part of the furnace. There the char sample was allowed to cool down under inert atmosphere for around 10 minutes. Finally the crucible was taken out and the last stage cooling was done in desiccator.

Char thus produced was then ground with the help of properly cleaned porcelain mortar and pestle and sieved to - 200 + 230 mesh size fraction by USS screen. Here also intermittent heating of char was done to prevent balling and thus better separation. The sized fraction of char was again heated at 1000°C using the same procedure described above. Recharring of sized char was done to ensure complete devolatilization. Dead charring was necessary to make sure that during gasification study, sample did not undergo any weight loss due to

devolatilization. Finally the sized char was kept in glass bottle and stored in desiccator.

3.1.3 Preparation of iron oxide + coconut char powder mixture pellet

Iron oxide used for carbothermic reduction was first ground in a clean porcelain mortar and pestle and sized to - 325 mesh size. This powder and coconut char of - 200 + 230 size were used for preparation of composite pellet. Proportion of powders were so adjusted that the mixture gave a stoichiometric C/Fe_2O_3 ratio equals to 2. Powder mixture was taken in a porcelain crucible and thoroughly mixed with the help of a stainless steel spatula. Jerks were avoided subsequently to prevent segregation.

A hand operated hydraulic press was used for pellet preparation. Small amount of the powder mixture was carefully transferred in a stainless steel die. Steel plunger of 1.25 cm diameter was fitted into the die and pressure applied was 4.8 tons/sq.cm, for one minute. Pellets were kept in oven at around $100^{\circ}C$ to avoid moisture adsorption. Each pellet was divided into four almost equal pieces when subjected to carbothermic reduction study.

3.1.4 Preparation of iron oxide micro pellets

Little amount of iron oxide powder of - 325 mesh size was taken in a watch glass and was mixed with few drops of distilled water to form a paste. Small portion of the paste was picked up at the flat end of a spatula and was hand rolled to small spherical shape. Rolling of moist iron oxide was quite difficult because the paste used to get dried up very fast and crumbled into powder. An alumina boat containing the spherical pellets was kept at the low temperature zone

of a horizontal furnace for two hours and then slowly introduced to the hot temperature zone. Firing of the pellets was done at a temperature of 925°C for another two hours. Then the alumina boat was withdrawn to cooler part of the furnace and was allowed to undergo furnace cooling to room temperature. This was done to avoid chance of breaking or cracking of the pellets due to thermal shock. Each and every pellet was then filed to around 2 mm diameter spherical pellet and were stored in an oven at 100°C .

3.2 Experimental Procedure

The scheme consisted of two types of experiments. As the gasification of carbonaceous material plays an important role in determining the rate of carbothermic reduction, it was carried out first. Next experimental study was of carbothermic reduction of iron oxide. The whole experimental schedule consisted of the following sets:

- (i) reactivity study of graphite in pure carbon dioxide
- (ii) reactivity study of coconut char in pure carbon dioxide
- (iii) reactivity study of coconut char in carbon dioxide-monoxide and carbon dioxide-argon gas mixtures
- (iv) trials for simultaneous measurement of weight loss and product gas analysis in carbothermic reduction
- (v) carbothermic reduction of iron oxide-coconut char powder mixture
- (vi) carbothermic reduction of iron oxide micropellet-coconut char powder mixture
- (vii) product gas analysis and bed temperature measurement of (v) and (vi)

(viii) bed temperature measurement during gasification of graphite and coconut char

3.2.1 Reactivity study of graphite in pure carbon dioxide

Graphite powder sample of varying sizes (namely - 170 + 200, - 200 + 230, - 230 + 270 mesh) were taken in a properly cleaned cylindrical 1.0 cm i.d. stainless steel bucket. The depths of the buckets were varied from 0.2 cm to 0.5 cm to see the effect of bed depth on the gasification kinetics. Before putting the graphite powder, the bucket was cleaned with acetone and was accurately weighed. Preweighed bucket was then filled with graphite powder and was compacted in a fabricated compaction unit. Fig.(3.1) presents the schematic view of the compaction unit. Bucket, containing the powder sample was placed under the copper plunger and compaction was carried out by placing required weight on the brass plate. Bed height after compaction could be measured by measuring the extent, the plunger went inside the bucket. Outer surface of the bucket was then cleaned and bucket was weighed accurately to find out the amount of sample taken.

The set-up described in Sec. 2.1.2 was used for this set of study.

The reaction chamber of the furnace was maintained at desired temperature. The BTS catalyst furnace temperature was kept at 180°- 200°C. Reaction chamber was flushed with the purified argon for atleast 15 minutes to remove air and thus ensuring neutral atmosphere. After flushing, the top inlet of the furnace was opened and the sample holder was hanged inside the chamber by hooking it with the inconel rod coming from the balance. Argon flow was continued for another 10

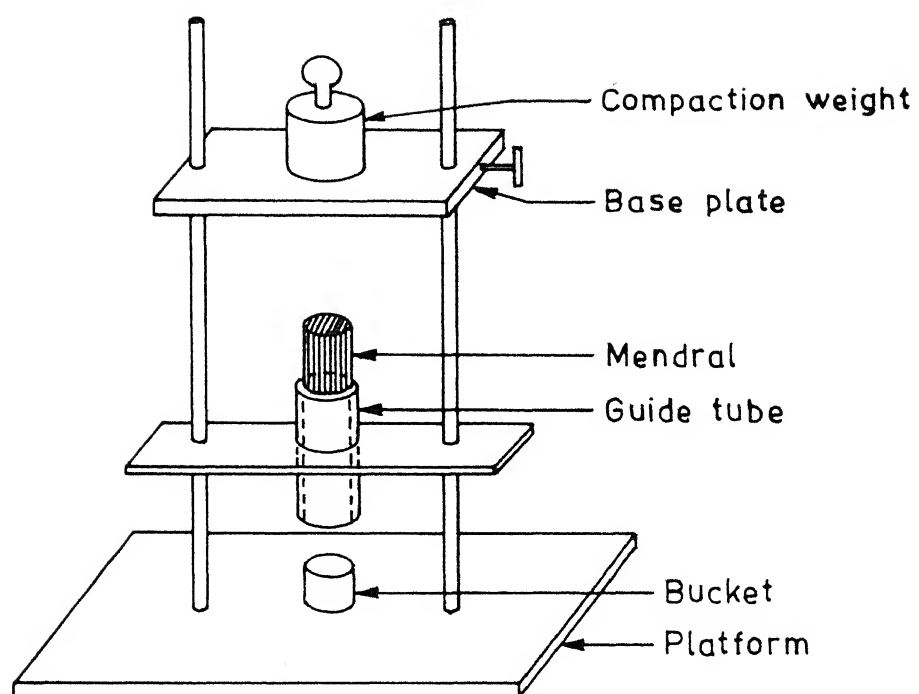


Fig. 3.1. Schematic representation of the compaction unit.

minutes. Then the furnace top was reopened and the sample bucket containing graphite powder was kept carefully on the flat surface of the sample holder and was slowly introduced into the constant temperature zone of the reaction chamber. The top of the furnace was then closed and the single pan balance was released. The weight of the assembly under argon atmosphere was recorded. While the top of the reaction chamber was open, the inert gas flow was increased slightly to minimize the back diffusion of air. After inserting the sample, argon gas was passed for another 10 minutes for two reasons: firstly to allow sufficient time for temperature stabilization of the sample and secondly to allow removal of any moisture that might have got adsorbed during handling of sample. Immediately after 10 minutes of argon flow, the weight of the hanging assembly alongwith the sample was registered. This weight was taken as zero time weight. Argon flow was then gradually cut-off and flow of carbon dioxide at required flow rate was set in. Instantaneous weight of the sample was recorded every 5 minutes. Gasification experiments with graphite were conducted for one hour. Then the carbon dioxide gas flow was cut off and the argon flow was switched on simultaneously.

Few blank runs were conducted in argon to find out the extent of weight loss suffered by graphite due to demohisturization or devolatilization (if any). Another probable reason of weight loss in argon may be by oxygen coming either as impurity in argon gas or by air, coming to the chamber by back diffusion. Experimental procedure for blank runs were exactly similar to the reactivity study with following differences:

- (a) no carbon dioxide gas was used

(b) during gasification, weight of the sample after 10 minutes of argon flow was taken as zero time weight where as for blank runs, weight immediately after putting the sample in reaction chamber was taken as zero time weight.

All the experiments were repeated atleast twice to check reproducibility. Moisture played a very important role during reactivity study. When the moisture content of the atmosphere was high, the reactivity value found to be low and at one stage black shoots of carbon started coming out alongwith the gas. This problem was overcome by drying the samples before subjecting to gasification.

3.2.2: Reactivity of coconut char in pure carbon dioxide

The apparatus used here was same as graphite reactivity study and the procedure followed was also identical. The only noted difference between the two sets of experiments was that when coconut char was used for gasification, there was quite a bit of bed swelling thus causing instability. Swelling was pronounced when the bed was compacted, and may be due to two reasons (a) expansion of entrapped air and (b) high rate of generation of carbon monoxide due to faster rate of reaction of coconut char. Compacted bed offered more resistance to the outcoming gas as well. To avoid the abovesaid problem, the amount of sample taken was less so as to accommodate any expansion of bed and no compaction was done. The bucket was filled with coconut char and few tappings were given to make the upper surface even. Bed was found to be pretty stable this way.

3.2.3 Trials for simultaneous measurement of weight loss and product gas analysis in carbothermic reduction

Apparatus described in Sec.2.3 was used for this purpose. As

mentioned earlier the basic aim of this trial was to measure the weight loss of the sample and at the same time to analyse the product gas so as to enable one better representation of carbothermic reduction. The procedure followed was as described below:

The reaction chamber at the desired temperature was flushed with purified argon, flowing at a rate of 1 lit/min for at least 10 minutes before putting any sample inside. Mixture of carbon sample of - 230 + 270 mesh size and iron oxide (hematite) of - 325 mesh size was taken out of the oven and was transferred to a clean and preweighed cylindrical alumina crucible. The C/Fe₂O₃ stoichiometric ratio of the powder mixture was kept at 2.0. Carbon amount was kept higher than the stoichiometric amount so that the reduction kinetics was not affected by starvation of carbon at any stage. Each time around 0.5-0.6 gm of mixture was taken for the study. The crucible was then enclosed in the inconel cylindrical sample holder. The lower part of the stainless steel gas guide tube was then screwed with the bucket. Furnace top was opened and the sample holder alongwith the stainless steel tube was introduced into the furnace halfway. The second part of the gas guide tube was screwed with the top of the first part. The whole assembly was hanged from the inconel rod. The top of the furnace was then closed and the argon flow was diverted to the gas inlet of tube 3 to act as a carrier of the product gas to the gas chromatograph. Argon flow rate was reduced to 300 cc/min. Weight of the whole assembly was recorded after one minute of inserting the sample. It was found that within first one minute the extent of reaction was nominal and it was taken as zero time weight. Then onwards attempts were made to measure weight loss and perform gas

analysis alternatively. To do so, the long brass screws of the dead volume cutting device were turned clockwise and the internal jaws were pressed against each other to prevent the product gas from going up and thus forcing the gas to pass through the gas chromatograph. Gas was injected to the gas chromatograph with the help of an auto gas sampler for 10 seconds. Then immediately the brass screws of the device were turned anticlockwise to allow the rod from the balance to hang freely. Weight of the assembly was registered at that time instant. But unfortunately the assembly did not work satisfactorily. The main problem faced was that gas chromatograph did not sense the gas composition variation in a workable manner. The probable reasons identified were:

(i) there might be heavy dilution of the product gas by flowing inert gas

(ii) leakage of the product gas through the joints of the gas guide tube and the sample holder

It was difficult to remove the probable causes of non-functioning of the system and retain precautions simultaneously. Thus it was decided to decouple the two measurements. The procedure for gas analysis experiments will be discussed in the later part of this chapter.

3.2.4 Reactivity study of coconut char in carbon dioxide-monoxide and carbon dioxide-argon gas mixtures

The modified thermogravimetry set-up described in Sec. 2.3 was used for this part of reactivity study. Coconut char was taken in 0.2 cm deep, 1.0 cm i.d. cylindrical stainless steel bucket. The bucket was cleaned with acetone and dried. Char sample was taken out

of the oven everytime and was carefully weighed in the preweighed bucket. The procedure was same as that described in Sec.3.2.1 for reactivity measurement of graphite in pure carbon dioxide. The differences between the two procedures are quoted below.

Instead of pure carbon dioxide, as was the case for previous reactivity study of graphite and coconut char here three different mixtures of CO-CO₂ and CO₂-Ar containing 20%, 50%, 80% CO₂ and rest either CO or Ar were used. During the experiments, when the argon flow was on, the gas mixtures of required compositions were developed in the gas train through a bypass. Flow rate of gas mixtures used was 1 lit/min. Exactly after 10 minutes of heating of sample in argon atmosphere the weight of the assembly was noted down. Inert gas was then slowly switched to a gas outlet in the gas train and the CO-CO₂ or CO₂-Ar mixture was simultaneously diverted to the furnace. Weight of the sample after one minute of CO-CO₂ flow was taken as zero time weight. Weight loss measurements were carried out in the same way as described in Sec.3.2.3.

Two capillary flowmeters were used to obtain the gas mixture of required composition. One of the flowmeters was calibrated by using pure CO₂ and the other one by CO and Ar.

3.2.5 Weight loss measurement of coconut char and iron oxide powder mixture

Apparatus described in Sec.2.3 was used for this part of the study. Sample holder described in Sec.2.3.2 was employed to serve as reaction chamber. Initially a mechanical mixture of iron oxide and coconut char powder of -325 and -200 +230 mesh size respectively were

used. But it was found that the bed was unstable and powder had a tendency to come out of the alumina crucible. To avoid the problem of swelling of bed, powder mixture was pelletized by a hand operated hydraulic press. Each pellet was then cut into almost equal four parts. Procedure of pellet preparation has already been described in Sec.3.1.3. 0.5-0.6 gm of this pellet was taken in clean, preweighed cylindrical alumina crucible. This crucible alongwith the sample was enclosed in the inconel sample holder. The procedure of this set of experiments was same as described in Sec.3.2.3. But here only the weight loss measurement was carried out.

3.2.6 Weight loss measurement of coconut char powder and iron oxide micro pellet mixture

The set-up employed for this study was the same as that used for powder mixture as described in Sec. 2.3.

0.3 to 0.35 gm of iron oxide micropellet of approximately 0.2 cm diameter was weighed in a preweighed alumina crucible. Coconut char of required weight was taken in the crucible to make the C/Fe_2O_3 stoichiometric ratio of 2.0. Char was taken in such a manner that all the iron oxide micropellets were fully surrounded by carbon. Alumina crucible was then carefully transferred into the inconel sample holder so that the crucible suffered minimum jerk. Otherwise it may result in some segregation. Same procedure as described in Sec. 3.2.3 was followed to carry out the experiments.

3.2.7 Product gas analysis and bed temperature measurement for carbothermic reduction (Sec.3.2.5 and Sec. 3.2.6)

The purpose of this set of experiments was to continuously analyse the composition of the gas produced during carbothermic reduction and to obtain the temperature history of the bed throughout

the experiment. The apparatus used for this purpose has been described in Sec. 2.4.

Experiments were conducted for both powder mixture and micropellet-powder mixture systems. Sample of chosen type was taken in the silica tube reaction chamber. Before putting the sample in, the silica tube was first cleaned with dilute hydrochloric acid and then thoroughly washed under running water. The tube was then rinsed with soap solution. The tube was again washed under running water. Finally it was cleaned by acetone and then dried. When iron oxide micropellet and coconut char powder mixture was used as sample, then micropellet and char was put alternatively to ensure that char surrounded each iron oxide micropellet.

After putting the sample in the silica tube, the open end of the same was closed with the gas outlet assembly. Thermocouple, going through the polythene tube connecting the silica tube and the elbow glass joint was so adjusted that the tip touched the sample bed. The thermocouple was connected to the digital millivoltmeter. The open end of the elbow joint was connected to the gas chromatograph. Then the silica tube was slowly pushed into the furnace, operating at the required temperature. The length of the silica tube was such that the sample bed remained in the constant temperature zone. Gas sampling started immediately after the gas was found to bubble through the bubbler, connected to the exit end of the gas chromatograph. Sampling continued at a suitable interval of time till the gas evolution stopped.

As mentioned before, the composition of the product gas was analysed by calculating the area of the peaks registered on the strip-

chart recorder. The gas chromatograph was calibrated against pure carbon dioxide and monoxide as well as for mixtures of various proportion of the two gases. Gas mixtures of known compositions were monitored through two precalibrated capillary flowmeters. Hydrogen was employed as the carrier gas of the chromatograph. It was found that impurities in commercial hydrogen affected the smooth functioning of the chromatograph and thus was purified by adding anhydrous CaCl_2 column and BTS catalyst furnace in the carrier gas line. Silicagel column was employed for analysing the product gas mixture. The temperature of the column was maintained at 130°C and the bridge current used for all the experiments was 190 mA. During calibration, a number of sampling was done for each composition to check the reproducibility. Use of an auto gas sampler ensured uniformity of gas sampling. Area under the peaks was measured by dividing each peak into number of triangles and each triangle area was calculated by employing standard formula. This was found to be quite satisfactory method of peak area calculation. A master graph was generated by plotting the peak area against composition of the gas mixture and subsequently, this plot was used to analyse the product gas of carbothermic reduction. Fig. (3.2) presents the plot of area versus gas composition for CO-CO_2 mixture. Bed temperature was continuously monitored by the digital millivoltmeter. Measurement of temperature was also stopped when gas ceased to evolve.

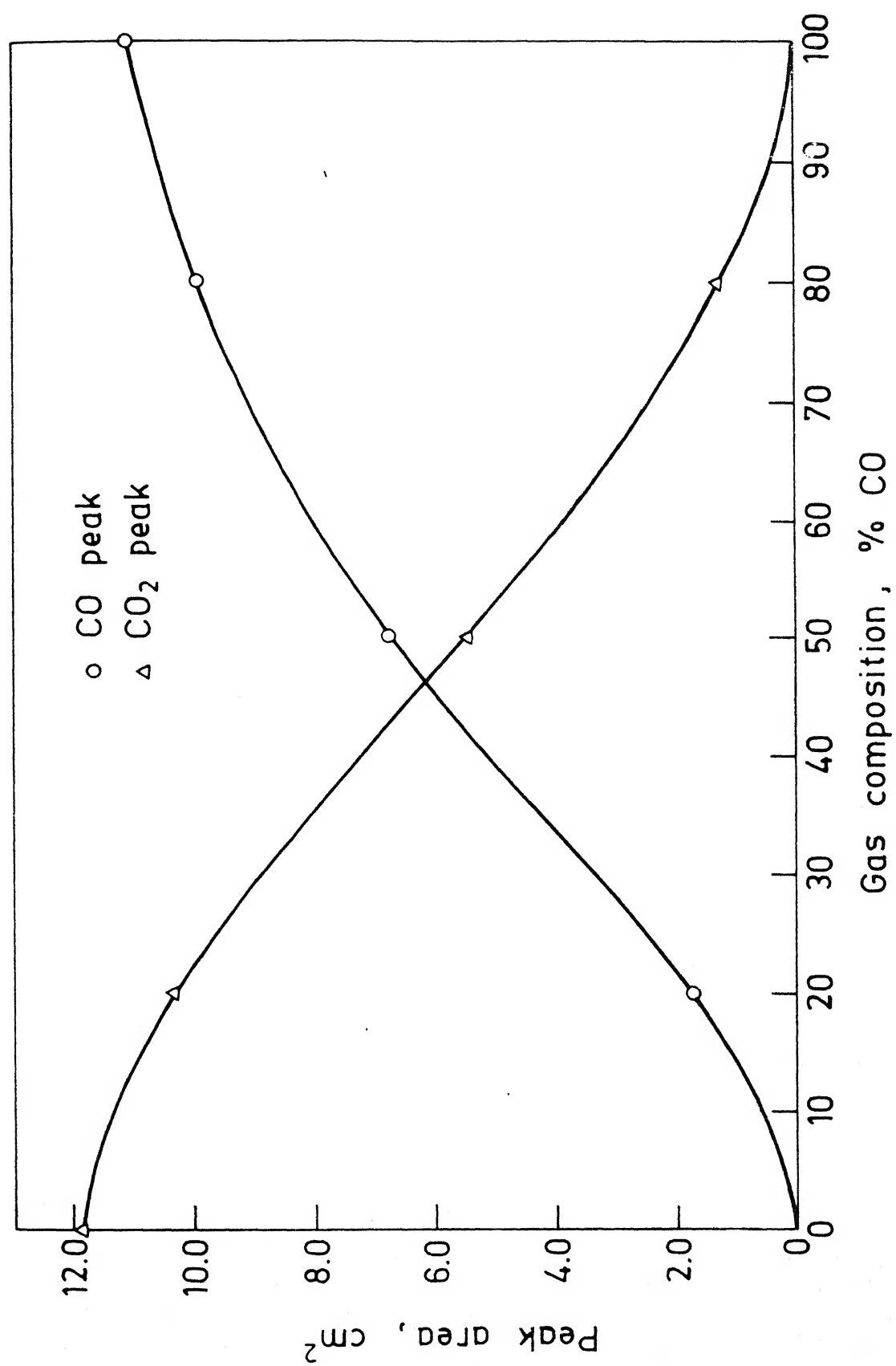


Fig. 3.2. Gas chromatograph calibration curves for CO-CO₂ mixture at room temperature (305 K).

CHAPTER 4

RESULTS ON REACTIVITY MEASUREMENTS IN PURE CO₂, CO - CO₂ AND CO₂-Ar MIXTURE

It has already been stated in the literature review that significant anomalies do exist in the reported values of the rate constants of Langmuir - Hinshelwood type rate equation, obtained by different workers (Table 1.3). Again it has been mentioned in the plan of the work that there is a mismatch in the gasification rate of graphite in CO₂ and rate of carbon loss predicted from carbothermic reduction of iron oxide by graphite as reported by Abraham(3). So the purpose of these measurements was:

(i) to redetermine the gasification rate of graphite used by Abraham in carbon dioxide
and (ii) to determine reactivity of coconut char in CO₂, CO - CO₂ and CO₂-Ar gas mixtures. Coconut char was used for this set of study because graphite was found to be not suitable for further studies in carbothermic reduction due to its low reactivity.

The extent of oxidation of a given type of carbon may be affected by a number of independent variables like (a) flow rate of gas, (b) particle size of carbon, (c) temperature, (d) compaction pressure of the bed, (e) height of the powder bed etc. Experiments were conducted to find out the effect of the abovementioned parameters on the rate of gasification.

4.1 Effect of experimental variables

Table (4.1) - (4.3) summarize the various experimental conditions employed for gasification study of graphite and coconut char.

Table 4.1 Experimental conditions for measurement of
gasification rate of graphite in pure CO₂

Expt.No.	Temp (K)	Flow rate of CO ₂ (lit/min)	Compaction pressure (PSI)	Particle size (ASTM)	Bed depth (cm)	Fractional bed poro- sity
1	1283	1.0	50	-200 +230	0.38	0.46
2	1283	2.0	75	-200 +230	0.40	0.46
3	1283	2.0	100	-200 +230	0.39	0.51
4	1283	2.0	75	-230 +270	0.25	0.51
5	1283	2.0	50	-200 +230	0.47	0.49
6	1243	1.0	50	-200 +230	0.19	0.52
7	1243	1.5	50	-200 +230	0.19	0.52
8	1243	2.0	50	-200 +230	0.18	0.52
9	1222	1.5	100	-200 +230	0.42	0.46
10	1222	1.5	100	-230 +270	0.16	0.52
11	1222	1.5	50	-200 +230	0.22	0.51
12	1222	1.5	50	-200 +230	0.27	0.46
13	1222	1.5	50	-200 +230	0.47	0.49

Table 4.2 Experimental conditions for measurement of
gasification rate of coconut char in CO₂

Expt.No.	Temp. (K)	Flow rate of CO ₂ (lit/min)	Particle size (ASTM)	Bed depth (cm)	Fractional bed porosity
14	1283	2.0	-200 +230	0.09	0.46
15	1280	2.0	-200 +230	0.17	0.65
16	1280	2.0	-200 +230	0.19	0.66
17	1280	2.0	-200 +230	0.24	0.63
18	1280	1.5	-200 +230	0.28	0.47
19	1280	1.0	-200 +230	0.31	0.51
20	1246	1.5	-200 +230	0.10	0.55
21	1214	1.5	-200 +230	0.19	0.65
22	1214	1.5	-200 +230	0.22	0.57
23	1214	1.5	-200 +230	0.28	0.61
24	1204	1.5	-200 +230	0.10	0.57
25	1151	1.5	-200 +230	0.15	0.67
26	1151	1.5	-200 +230	0.22	0.54
27	1151	1.5	-200 +230	0.28	0.60
28	1081	1.5	-200 +230	0.12	0.57
29	1081	1.5	-200 +230	0.17	0.55
30	1081	1.5	-200 +230	0.26	0.57

Table 4.3 : Experimental conditions for measurement of gasification rate of coconut char in CO₂-Ar gas mixtures

Expt.No.	Temp (K)	Gas composition (Vol %)		Bed depth (cm)	Fractional bed porosity
		CO ₂	Ar		
31	1283	80	20	0.09	0.54
32	1283	50	50	0.08	0.47
33	1283	20	80	0.10	0.54
34	1246	80	20	0.11	0.57
35	1246	50	50	0.12	0.53
36	1246	20	80	0.10	0.56
37	1204	80	20	0.09	0.51
38	1204	50	50	0.11	0.53
39	1204	20	80	0.11	0.52
40	1151	80	20	0.10	0.56
41	1151	50	50	0.08	0.46
42	1151	20	80	0.09	0.55

Table 4.4 Experimental conditions for measurement of gasification rate of coconut char in CO-CO₂ gas mixtures

Expt .No.	Temp (K)	Gas composition (volume percent)		Bed depth (cm)	Fractional bed porosity
		CO ₂	CO		
43	1285	80	20	0.13	0.60
44	1285	50	50	0.10	0.51
45	1285	20	80	0.11	0.56
46	1246	80	20	0.12	0.57
47	1246	50	50	0.10	0.48
48	1246	20	80	0.10	0.51
49	1204	80	20	0.11	0.43
50	1204	50	50	0.09	0.50
51	1204	20	80	0.11	0.53
52	1145	80	20	0.12	0.58
53	1145	50	50	0.12	0.53

4.1.1 Gas flow rate

Gasification trials were made at three different flow rates at 1283 K and 1243 K for graphite and at 1280 K for coconut char. In case of graphite at 1283 K, it was found that the weight loss was higher as the flow rate was increased from 1.0 lit/min to 2.0 lit/min. But graphite oxidation was not affected by flow rate at 1243 K. However, it was noted that though increase of flow rate increased the weight loss for coconut char at 1280 K, but the effect was only marginal.

Therefore, in order to minimise flow rate dependence of rate, CO₂ flow rates of 2.0, 1.5 and 1.0 lit/min were chosen for studies on: (i) graphite at higher temperature, (ii) graphite below 1243 K, coconut char at 1280 K, and (iii) coconut char at lower temperature, respectively. Experiments with coconut char in CO - CO₂ gas mixture were conducted at a gas flow rate of 1.0 lit/min. As the presence of CO in the gas stream is expected to slow down the gasification rate considerably, lower flow rate was sufficient for this purpose.

4.1.2 Particle size

As our main objective of the gasification study of graphite in CO₂ was to redetermine the rate and compare it with what was reported by Abraham et al.(110), most of the experiments were conducted by using the same particle size (- 200 + 230 ASTM) as was used by them. Only few experiments were performed to have a qualitative idea about the particle size effect. Fig.(4.1) presents the percentage weight loss as a function of time for two particle sizes at 1283 K and 1222 K for graphite, and Fig.(4.2) presents the

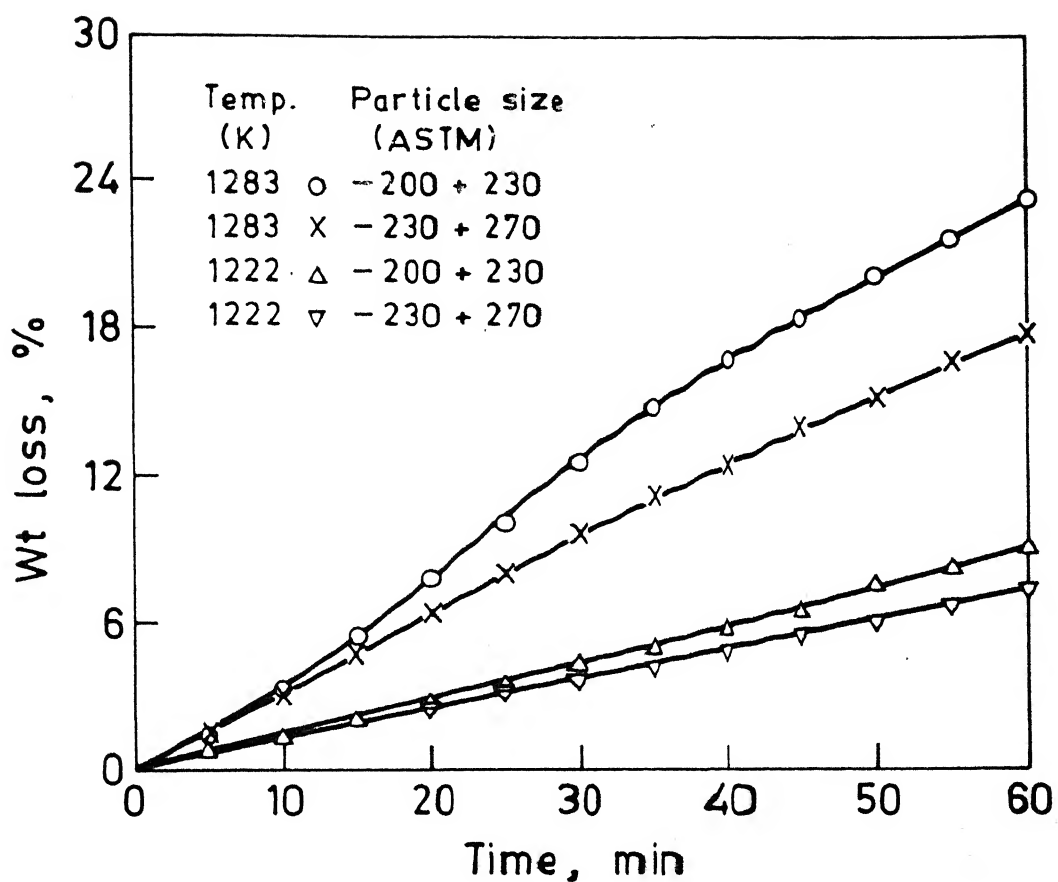


Fig. 4.1. Effect of particle size on weight loss of graphite in CO_2 .

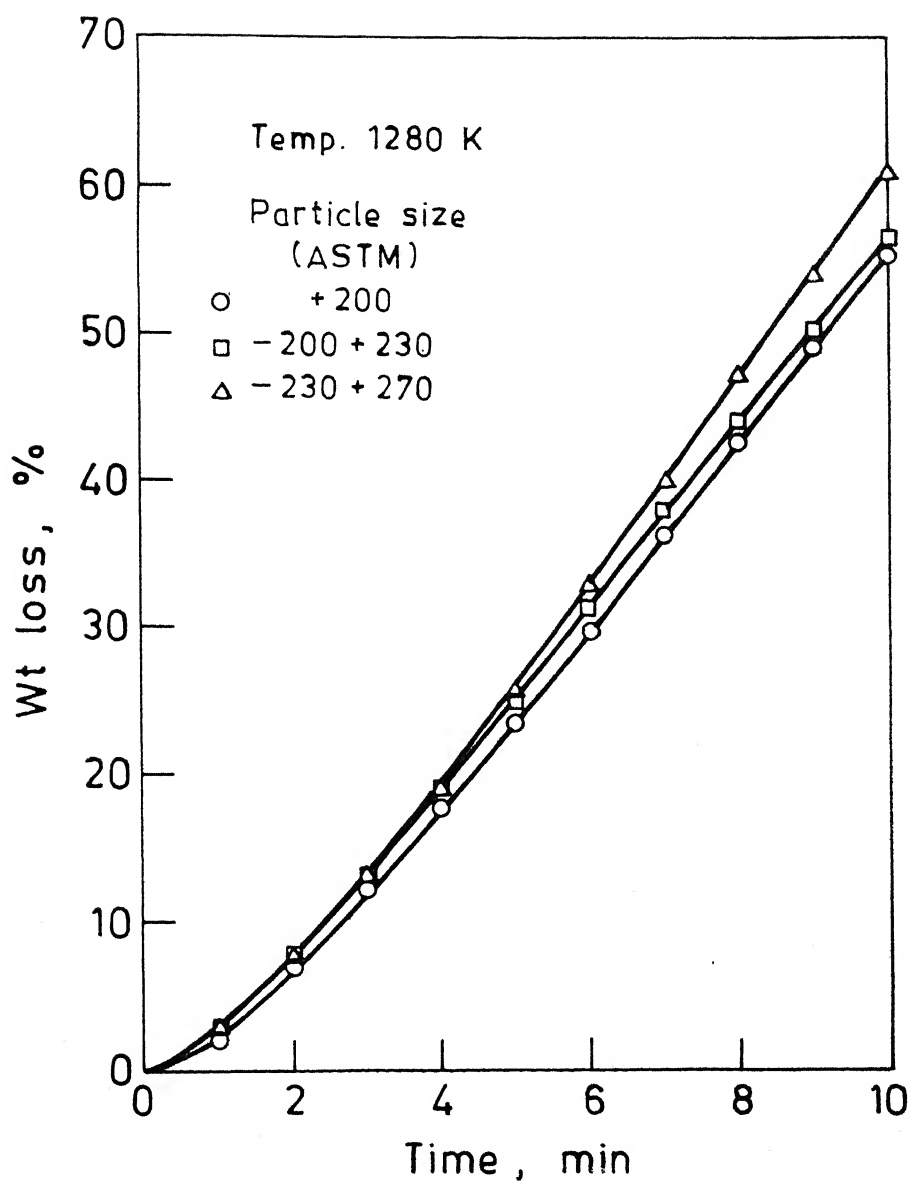


Fig. 4.2. Effect of particle size on weight loss of coconut char on CO_2 .

same for coconut char at 1280 K at three different particle sizes. It may be noted from Fig.(4.1) that at higher temperature, the extent of weight loss is slightly higher with coarser particle size but at lower temperature, both the particle sizes exhibited almost same extent of weight loss for graphite. Fig.(4.2) shows that there was no significant effect of particle size on weight loss as a function of time for coconut char. No discussion is attempted here since the same will be done after various calculations in later chapter.

It should be mentioned here that gasification study of coconut char in CO - CO₂ mixture was conducted only with the particle size of - 200 + 230 ASTM.

4.1.3 Compaction pressure

Fig.(4.3) presents the percentage weight loss vs. time curves for various compaction pressures at two temperatures for graphite. It may be noted from the figure that at higher temperature low compaction pressure gave a slightly lower amount of weight loss but at 1222 K, compaction pressure had practically no effect on weight loss.

It has already been mentioned that powder bed of coconut char had a significant swelling tendency during gasification study and expansion of bed was more pronounced when bed was compacted. That is why no compaction was given to the powder bed of coconut char.

4.1.4 Bed depth

As gasification is a gas-solid reaction, the diffusion of reacting gas to the reaction site or the product gas away from the site through porous solid is expected to influence the reaction rate. Experiments were conducted with different bed depth to find its effect

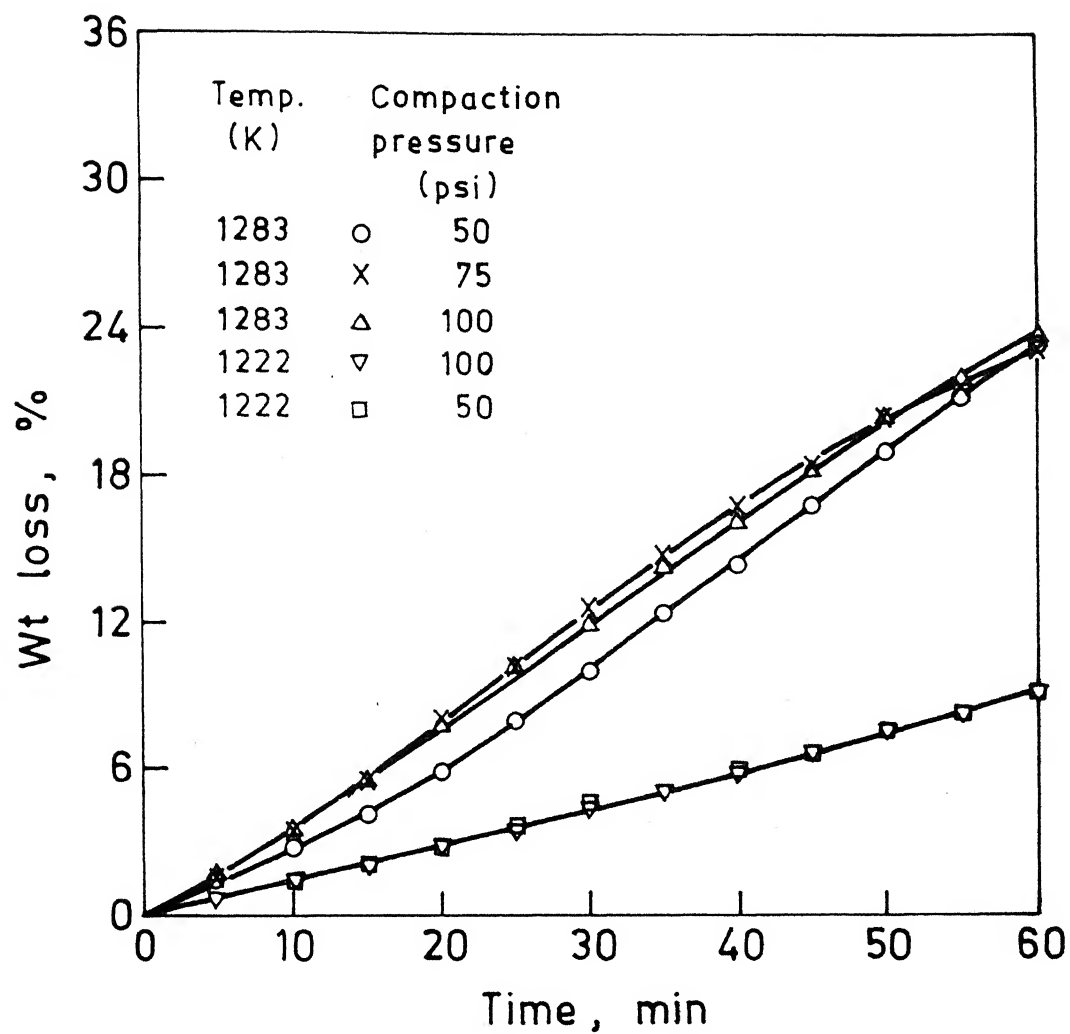


Fig. 4.3. Effect of compaction pressure on weight loss of graphite in CO_2 .

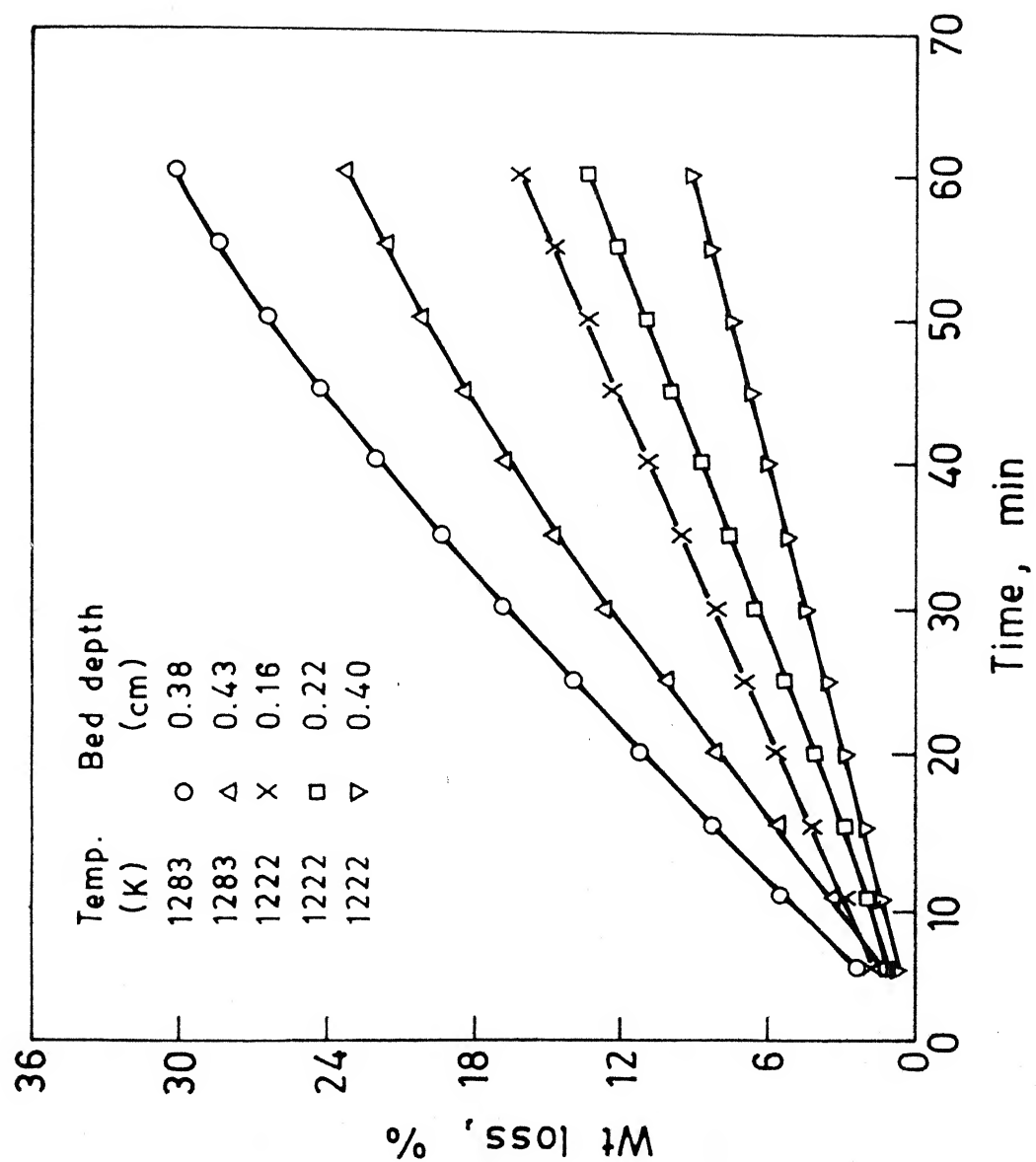


Fig. 4.4. Effect of bed depth on weight loss of graphite in CO_2 .

on gasification rates of both graphite and coconut char. Fig.(4.4) presents the effect of bed depth on weight loss of graphite at 1283 K and 1222 K. Fig.(4.5) gives the percentage weight loss as a function of time at various bed depths and temperatures for coconut char. It may be noted from the figures that bed depth affects the extent of weight loss or in other words the rate of gasification quite considerably. Again discussions on this aspect will be presented in subsequent chapter.

4.1.5 Concentration of carbon monoxide

Literature review reveals that CO is a very strong inhibitor of gasification reaction and even a small proportion of CO in the gas retards the rate significantly. During carbothermic reduction of iron oxide, the carbonaceous materials actually experience a varying environment of CO - CO₂ gas mixture. Thus it is important to find out the effect of CO on gasification kinetics. In the present study, due to inherent low reactivity of graphite, coconut char was employed as reducing agent in carbothermic reduction and gasification experiments were performed in CO - CO₂ gas mixtures for coconut char only. Effect of carbon monoxide was examined at 4 temperatures in a 0.2 cm bucket and - 200 + 230 ASTM particle size. Fig.(4.6) and Fig.(4.7) present percentage weight loss vs. time curves for different gas compositions at different temperatures. It may be noticed from those figures that through out the experimental temperature range, effect of CO is quite pronounced.

4.2 Measurement Errors

4.2.1 Errors in temperature measurement

Trials were performed to find out conditions for best

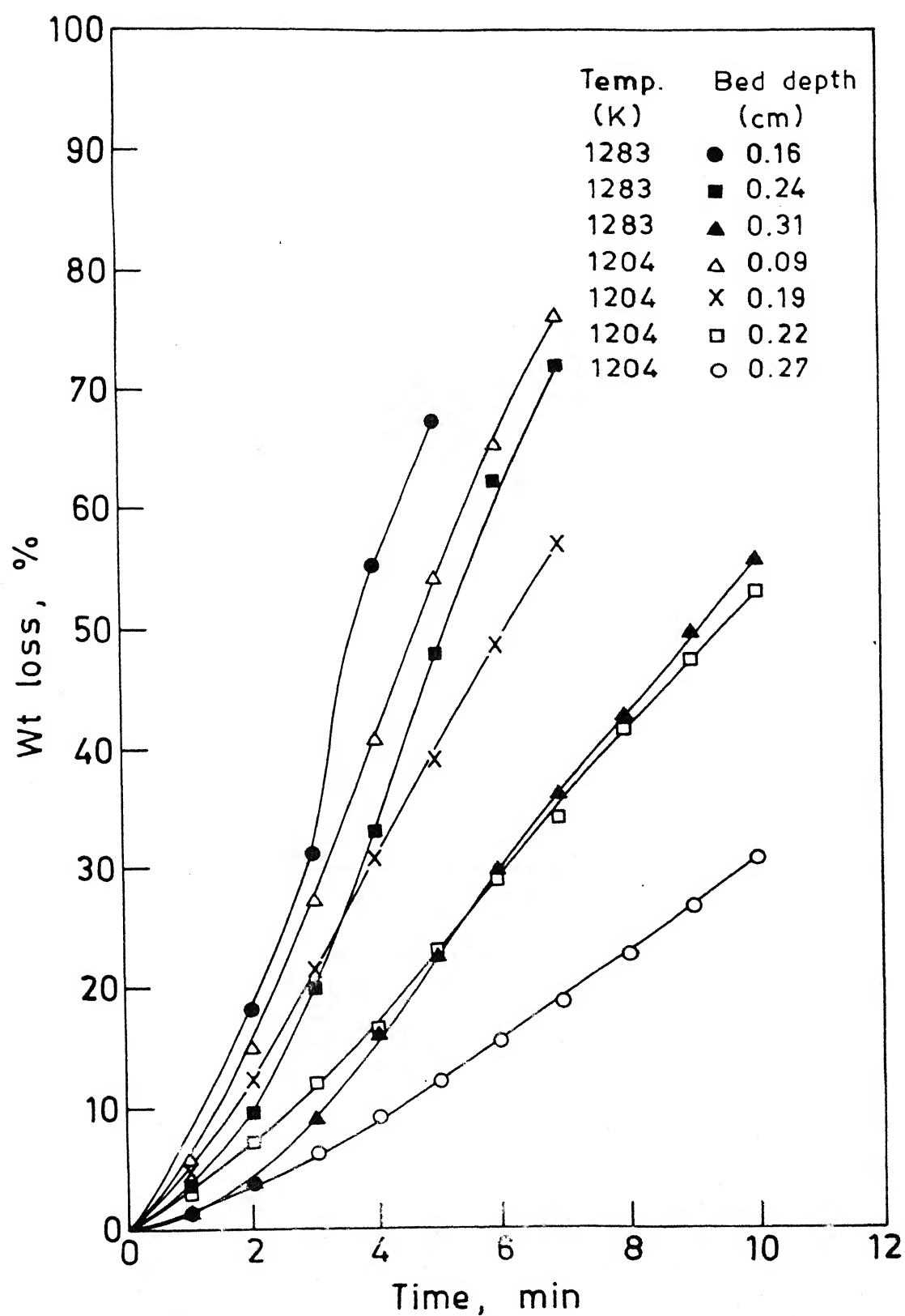


Fig. 4.5. Effect of bed depth on weight loss of coconut char in CO_2 .

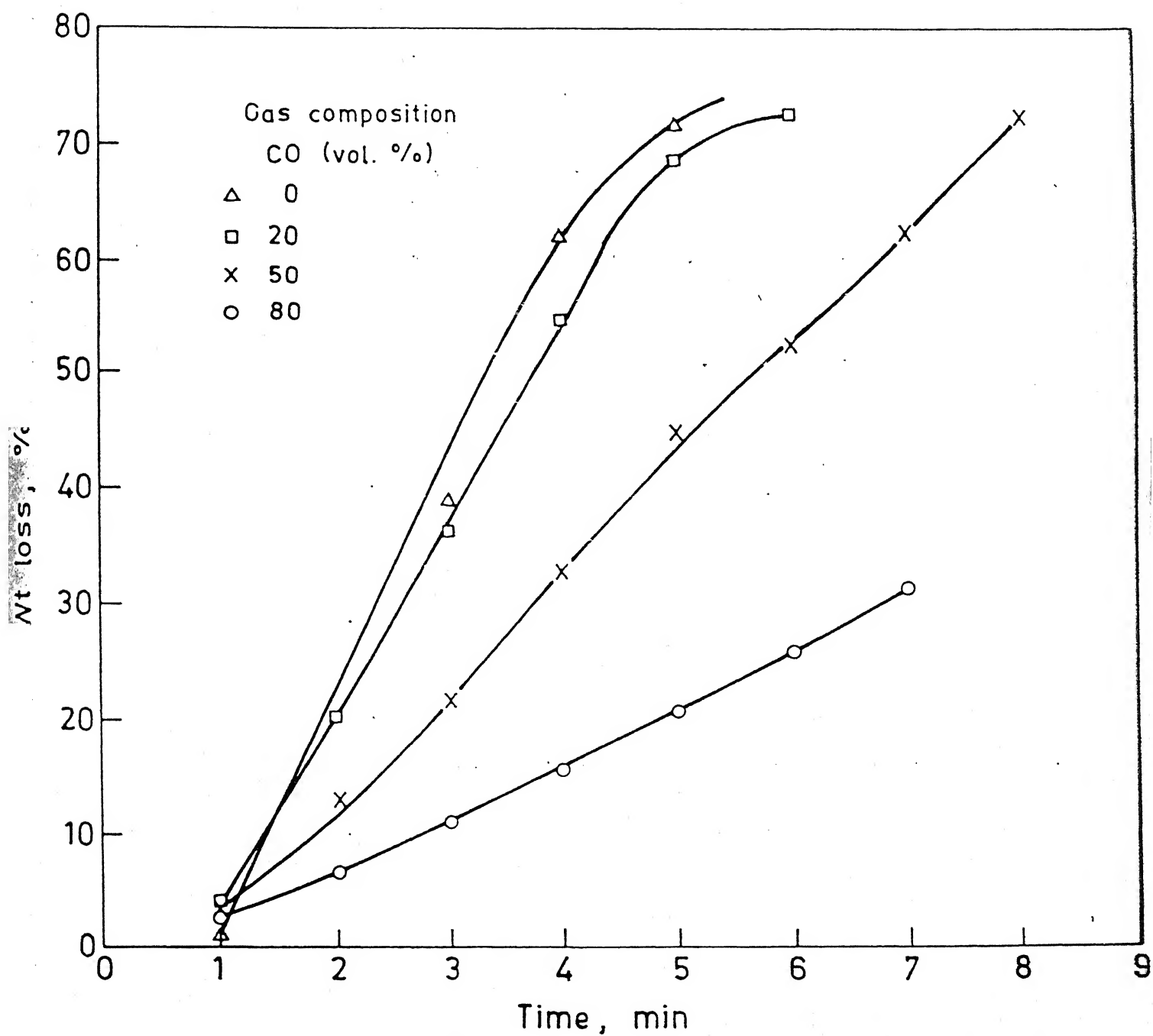


Fig. 4.6. Effect of CO on weight loss of coconut char at 1280 K

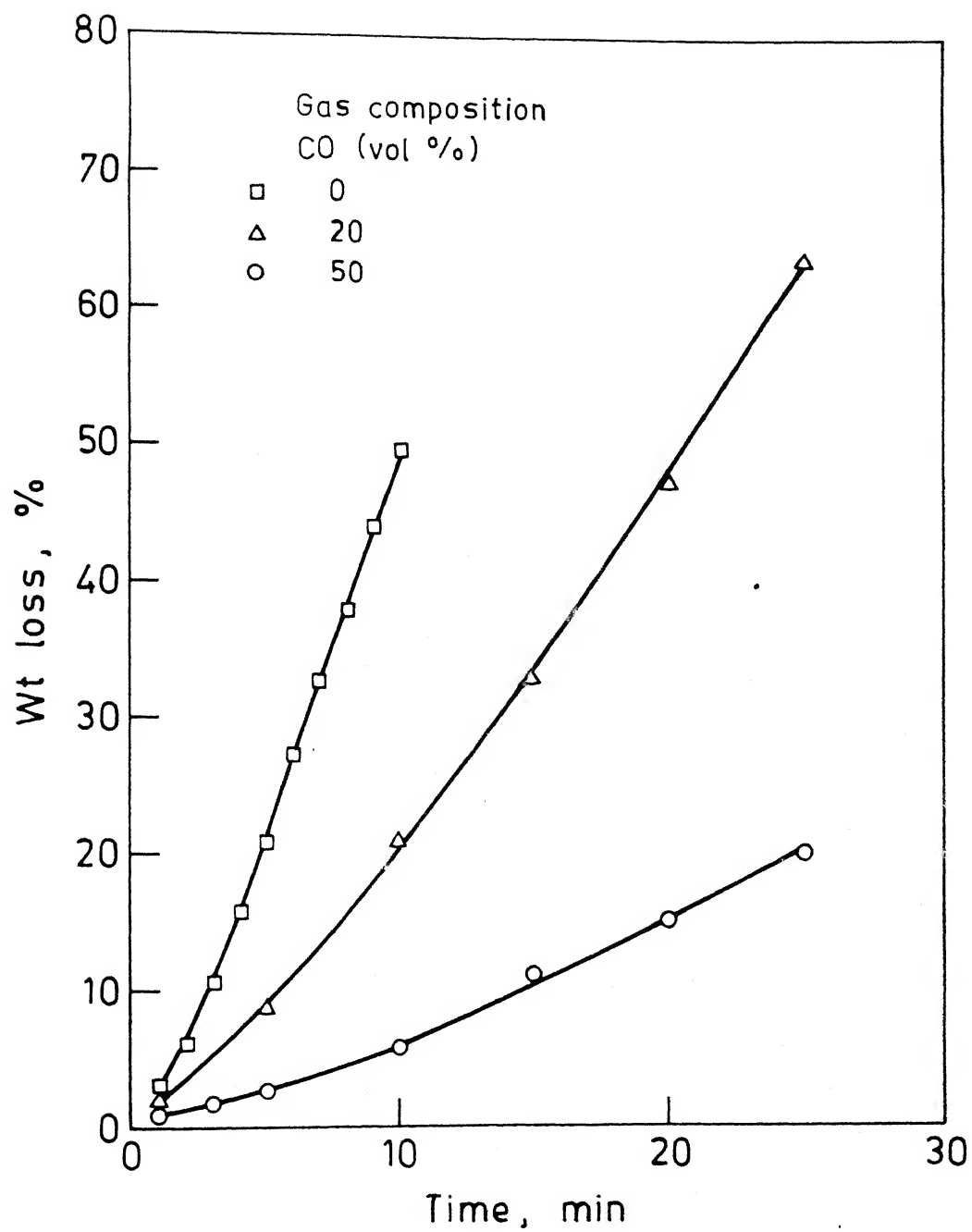


Fig. 4.7. Effect of CO on weight loss of coconut char at 1151 K.

control of the furnace temperature and it was decided to place the control thermocouple inside the reaction chamber. The furnace control was found to be accurate within $\pm 2^{\circ}\text{C}$ at the constant temperature zone. The measurement thermocouple was placed within 1 - 2 cm below the sample holder in the constant temperature zone and thus expected not to give any serious difference in the actual reaction temperature and the measured temperature.

Since the thermocouples were calibrated against standard thermocouple and the measuring instrument also checked against precision potentiometer from time to time, the other sources of error in temperature measurement were small and the overall temperature measurement error may be taken as $\pm 2^{\circ}\text{C}$.

4.2.2 Errors in flow measurement

It has already been mentioned in Sec.(2.1.1) that capillary flowmeters were employed for monitoring the flow of the reacting and inert gases. All the flowmeters were duly calibrated with actual gases for which the flowmeters were to be used. Calibration of flowmeters were done with the help of standard wet gasmeter (Toshniwal make). During calibration of flowmeter with CO_2 gas, liquid column was found to have stability problem. It was due to high Joule - Thomson effect on CO_2 gas when it passed through constrictions. Heating of the gas regulator with the help of a heating tape was found to stabilize the liquid head completely. Mixtures of CO and CO_2 , developed through the capillary flowmeters are expected to have an error of $\pm 3\%$ as a rough estimate.

4.2.3 Error in weight loss measurement

The balance used for thermogravimetry measurements had a

readability of 10^{-4} gm after precautions were taken for damping vibration of the hanging assembly. It was found that the nichrome wires and the stainless steel bucket suffered oxidation and thus weight of the hanging assembly changed from run to run. Auxilliary experiments were carried out to determine the extent of nichrome wire and bucket oxidation in inert and carbon dioxide gases. It was observed that oxygen pick-up of wire and bucket both in inert and CO_2 atmosphere was negligible and the oxidation took place primarily when the hot bucket alongwith wire was taken out of the furnace after completion of a run. Thus oxidation of stainless steel bucket and nichrome wires did not incorporate any error in the weight loss measurement during gasification studies in CO_2 . But same was not true when the stainless steel bucket was exposed to the $\text{CO} - \text{CO}_2$ gas mixture. The bucket underwent an oxidation - reduction cycle and contributed quite significant error in the weight loss. For this reason, gasification of coconut char in $\text{CO} - \text{CO}_2$ gas mixture was carried out in inconel buckets.

To check reproducibility of weight loss data, each experiment was repeated atleast two times. Fig.(4.8a) and Fig.(4.8b) illustrate the nature of reproducibility. It was found that gasification experiments on graphite were highly reproducible. Here data sets showing agreements within 2% were accepted. But experiments with coconut char were associated with reproducibility of less degree of accuracy. Repeat experiments reproducible within 5 - 7% were accepted for reporting.

4.3 Procedure for Rate Calculation

As stated in Sec(1.2.2), the instantaneous rate of

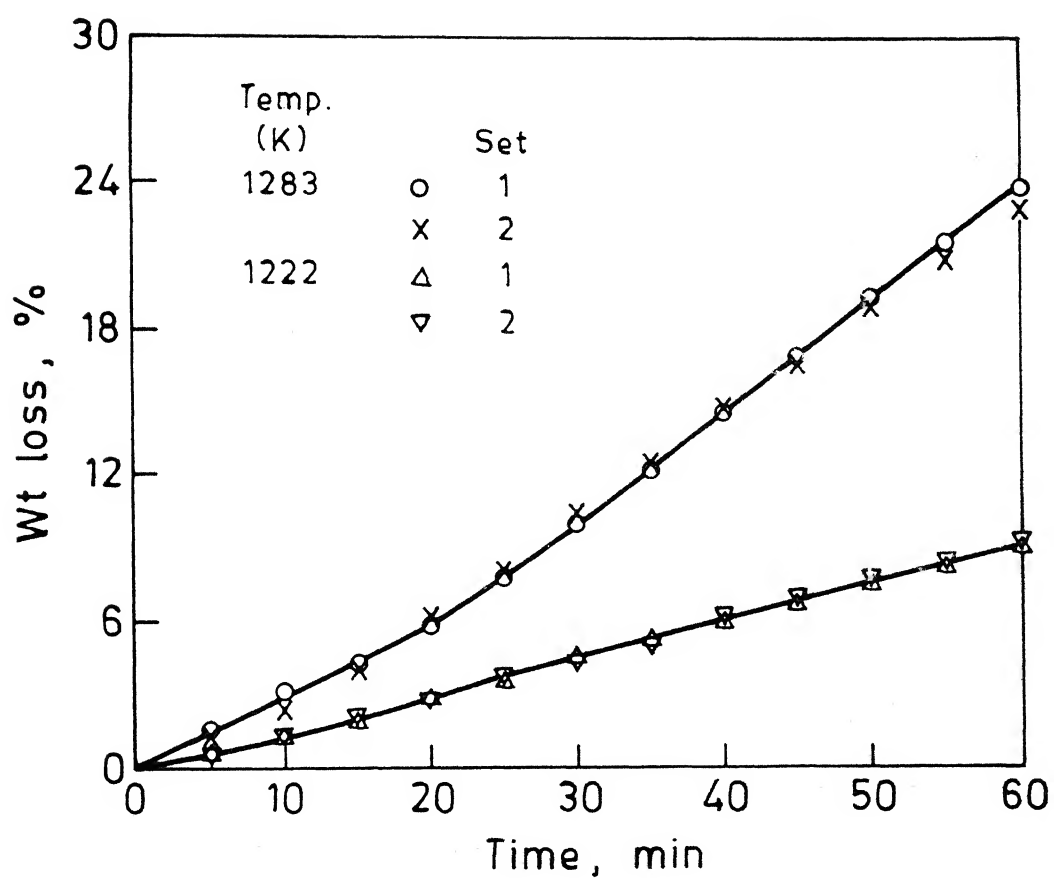


Fig. 4.8a. Reproducibility of weight loss data of graphite in CO_2 .

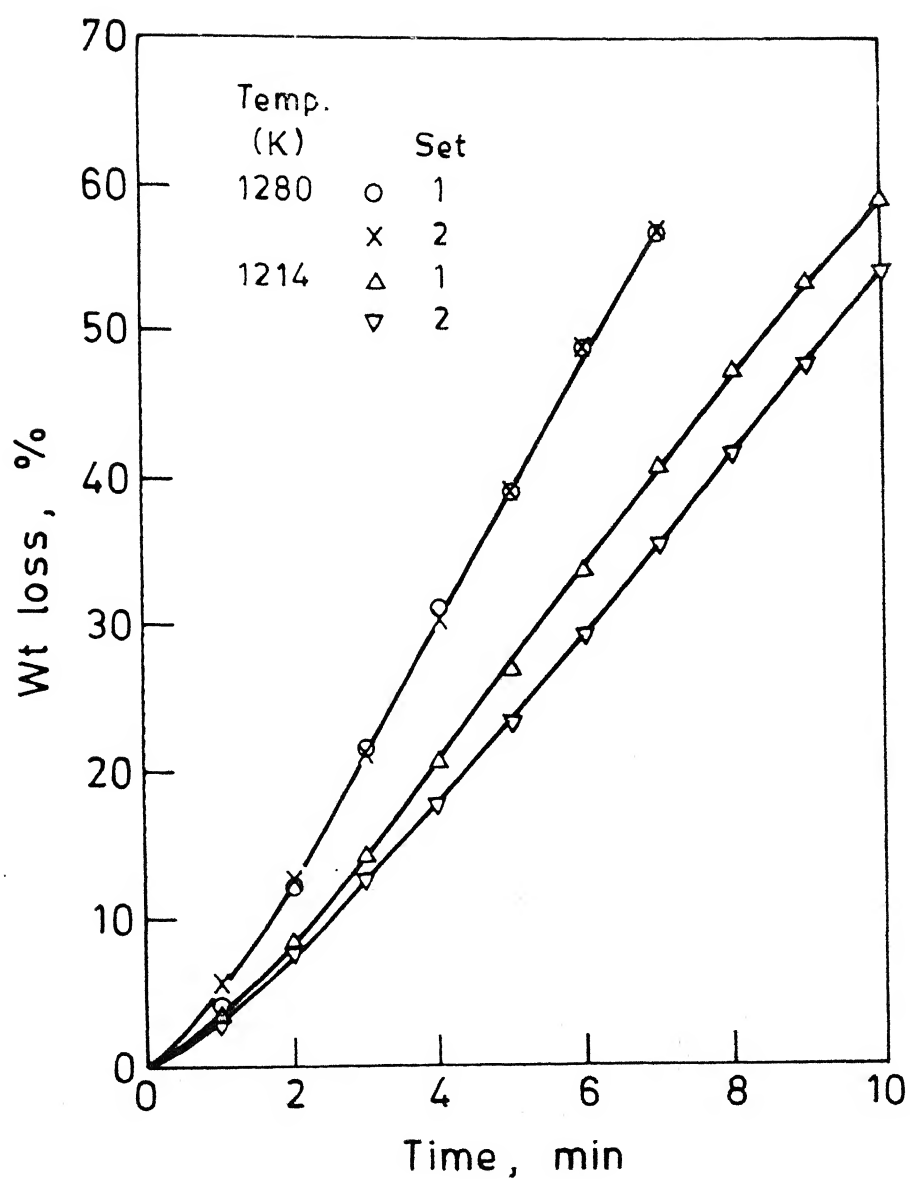


Fig. 4.8b. Reproducibility of weight loss data of coconut char in CO₂.

gasification per unit mass of carbon (r_g) may be defined as:

$$r_g = \left[- \left(\frac{dW_c}{dt} \right) / W_c \right] \quad \dots(1.4)$$

where r_g is in s^{-1}

$$\text{or } - dw_c/w_c = r_g \cdot dt \quad \dots(4.1)$$

Integrating between limits $t = 0$, $w_c = w_o$ and $t = t$, $w_c = w_c$

$$- \ln \left[\frac{w_c}{w_o} \right] = r_g [t]_0^t \quad \dots(4.2)$$

$$- \ln (w_c/w_o) = r_g t \quad \dots(4.3)$$

where w_o = initial weight of carbon (gms)

Eq.(4.3) which is the integrated form is convenient for determination of r_g , and several investigators have used this. However, it assumes that r_g is independent of time. This is hardly justified as literature review and present experimental data point out. Therefore it was decided to employ Eq.(1.4) as the basis for determination of r_g and in this approach r_g depends on time of reaction.

As CO_2 reacts with carbonaceous material, there will be continuous loss in weight. The weight loss, as mentioned earlier could be due to the following reasons:

(a) some weight loss due to extraneous factors such as dehydration, devolatilization, oxidation by back diffused air. It plays only a minor role.

(b) weight loss due to oxidation by CO_2 . As already stated, blank runs i.e. heating of sample only in flowing argon were carried out to find the extent of weight loss due to the extraneous factors[item(a)].

Then necessary corrections were done to the weight loss measured during gasification in the following manner.

Weight loss in blank experiments is about 5 pct. of weight loss in actual gasification studies. Therefore it was not serious. Even then corrections were incorporated as follows.

If w_{Ar} denotes the weight loss of sample after 10 minutes in the blank run then initial weight of sample in gasification study is

$$w_3 = (w_c - w_{Ar}) \quad \dots(4.4)$$

Weight loss after 10 minutes in the blank run was subtracted since argon was also passed for 10 minutes in the gasification experiments before commencing CO_2 flow. As the carbon samples contained some impurities, actual amount of carbon available for gasification was

$$w_0 = w_3 \times \text{fixed carbon} \quad \dots(4.5)$$

Blank runs were carried out for the same extent of time as was for gasification experiments. Actual weight loss at any time instant was calculated by subtracting the weight loss of the sample in the blank run from the weight loss recorded in gasification study at that time instant. So the instantaneous weight of carbon (w_c) left at any time was nothing but ($w_0 - \Delta w_c$), where Δw_c is the extent of weight loss due to gasification alone.

To find out $-(dw_c/dt)$, weight loss data was analytically expressed as a function of time. It was found that polynomial of third order could fit the data quite satisfactorily. Fig.(4.9) shows the reproducibility of the original weight loss data by the polynomial, as samples. So weight loss can now be expressed as

$$\Delta w_c = a + bt + ct^2 + dt^3 \quad \dots(4.6)$$

Eq.(4.6) was then differentiated at any time instant to get the rate

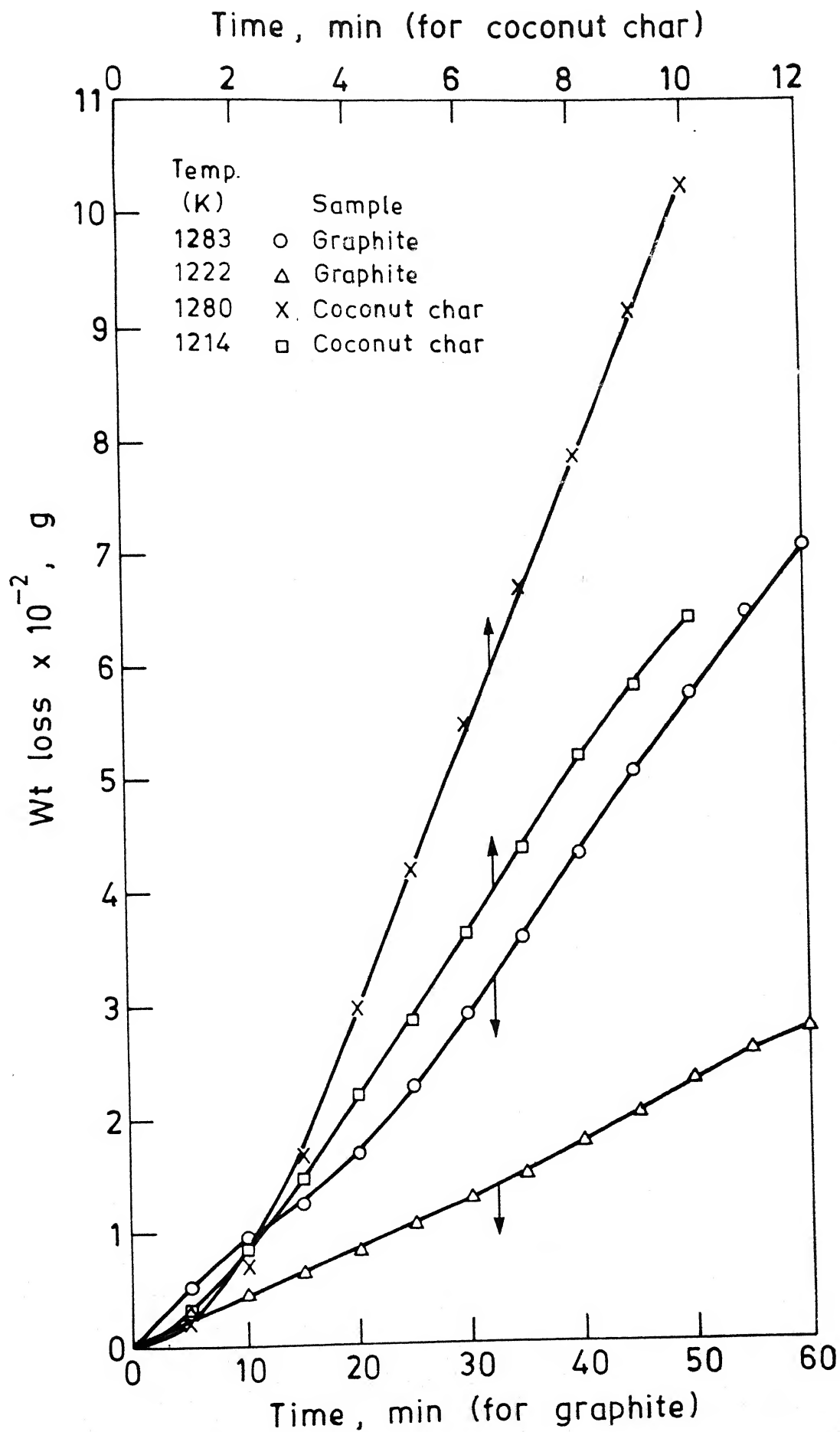


Fig. 4.9. Polynomial fitting of weight loss data in CO_2 .

of weight loss and instantaneous rate at any time was calculated by dividing the rate of weight loss by the weight of carbon at that time instant.

Fig.(4.10) present few sample curves of instantaneous rate as a function of time. It may be noticed from the figure that the instantaneous rates for both graphite and coconut char vary as a function of time and no well defined steady state region could be identified.

Literature review (Sec.1.2.5) shows that the structure of sample undergoes dynamic changes with the progress of burn off and the rate of reaction depends upon the structure of the sample. Therefore, efforts have been made by many workers to correlate instantaneous rate with that of percentage burn off i.e. fractional conversion, as change in structure is expected to be related to fractional conversion (F), which therefore is a more fundamental parameter than time.

$$F = \Delta w_c / w_c = 1 - w_c / w_0 \quad \dots(4.7)$$

Figs.(4.11a) and (4.11b) present few sample curves for instantaneous rate versus fractional conversion for graphite and coconut char. It may be noted from Figs.(4.11a) and Fig.(4.11b) that there is no uniform pattern of variation of the instantaneous rate versus fraction conversion curves for graphite and coconut char. Literature review reveals that number of workers (30,50,59,74,85) have reported instantaneous rate as a function of percentage burn off. There also no definite trend of variation could be noticed. However, in many cases, it has been found that rate reached the maxima at around 60 percent burn off and then decreased again. Investigators (30,50,59,60,74,85) have tried to correlate the variation of rate with

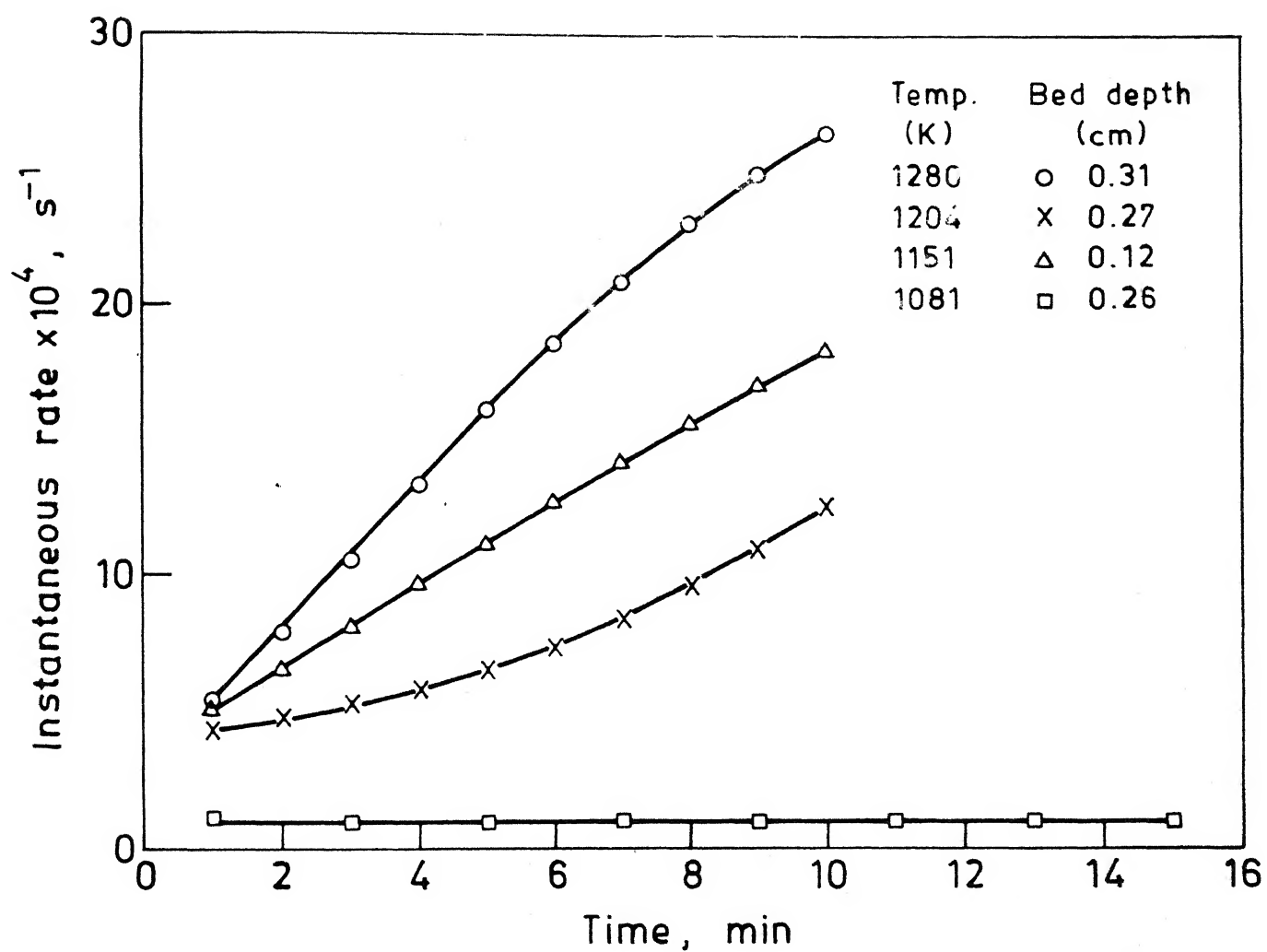


Fig. 4.10. Instantaneous rate vs. time for coconut char in CO_2

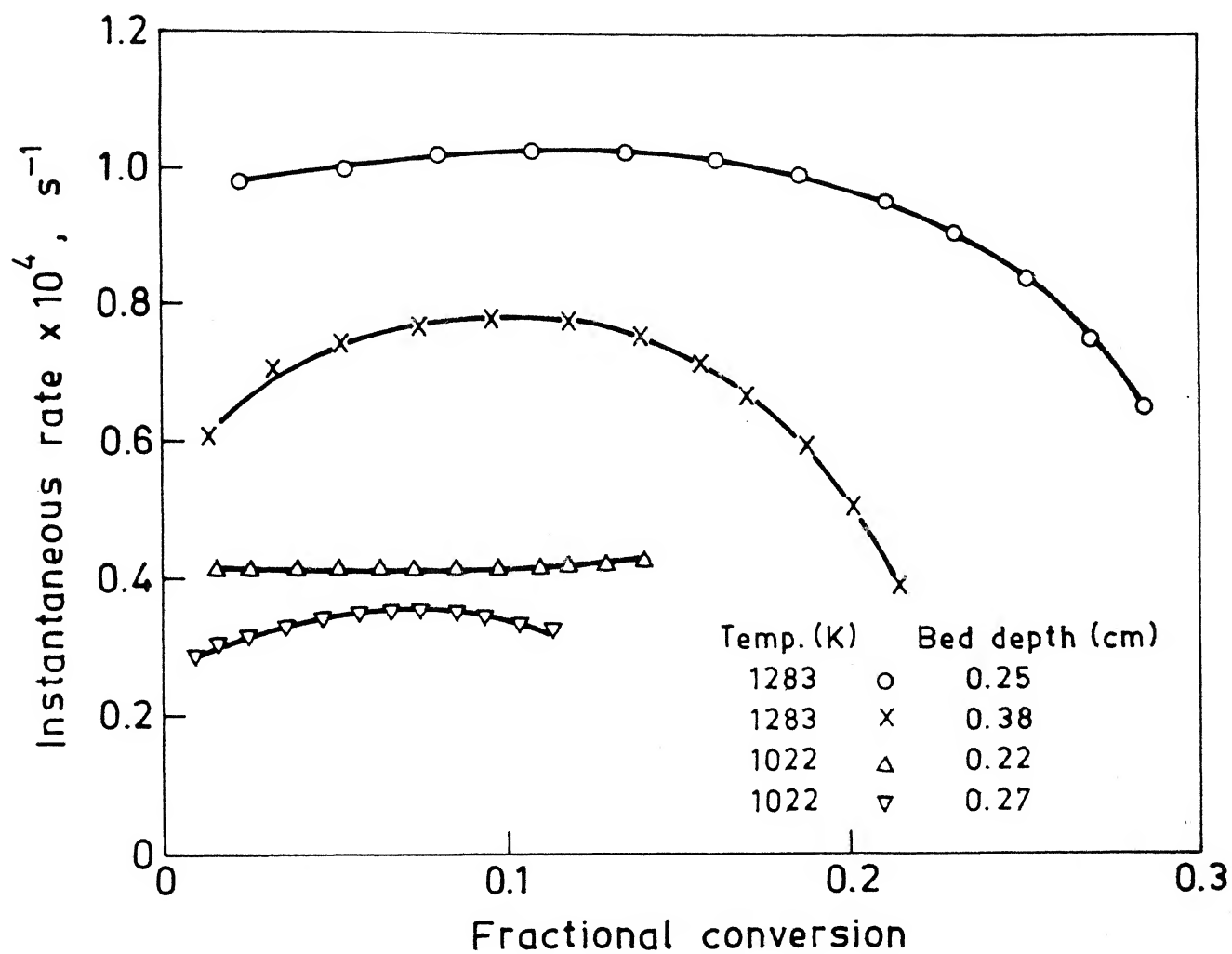


Fig. 4.11a. Instantaneous rate vs. fractional conversion curves for graphite in CO_2 .

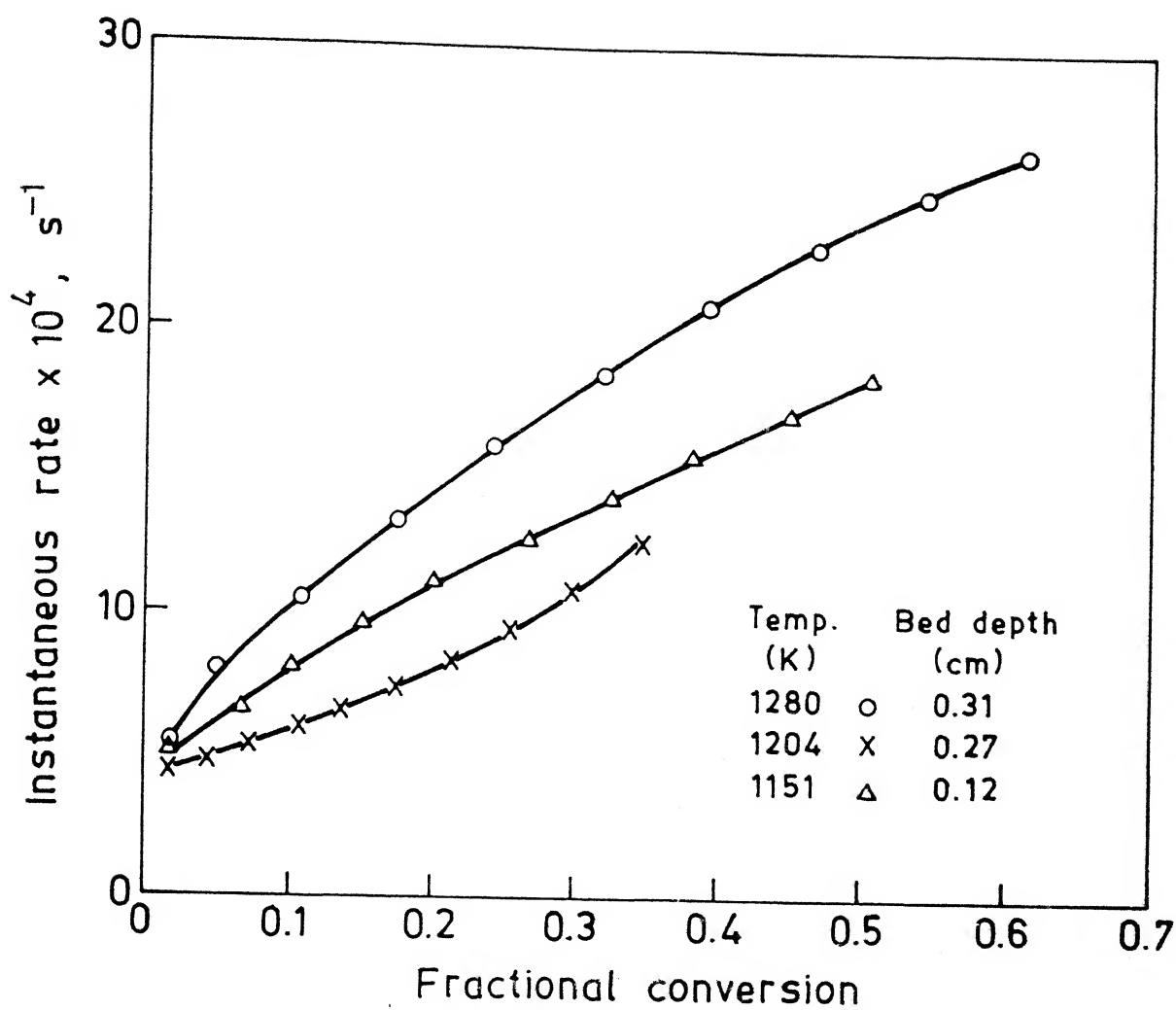


Fig. 4.11b. Instantaneous rate vs. fractional conversion curves for coconut char in CO_2 .

the change in surface area.

Several equations have been proposed in literature to correlate the rate of gasification and the fractional conversion. But these are empirical correlations only and are of different types. No universal formula exists in this regard which has been generally accepted.

From a fundamental point of view it is desirable to work with initial value of r_g , since the characteristics of the bed is known only initially. However it requires some time to flush out inert gas from furnace chamber. Therefore it was decided to find r_g at 5 percent conversion (i.e. $F = 0.05$) as representative value of r_g for further calculations since it is expected that the bed characteristics such as bed height, bed porosity etc. would be essentially the same as initial.

It was then tried to see whether the ratios of instantaneous rates and rate at 5% conversion as a function of fractional conversion would yield any uniform pattern at all experimental conditions. Figs.(4.12a) and (4.12b) present such sample curves for both graphite and coconut char. It may be noticed from the figures that there is no uniform behaviour of variation of the curves. But on an average, the ratio of rates first increase with increase of burn off upto a peak value and finally decrease with further increase of conversion.

Table (4.5) - Table (4.8) present the rate data of gasification measured at 5% conversion both for graphite and coconut char under various experimental conditions.

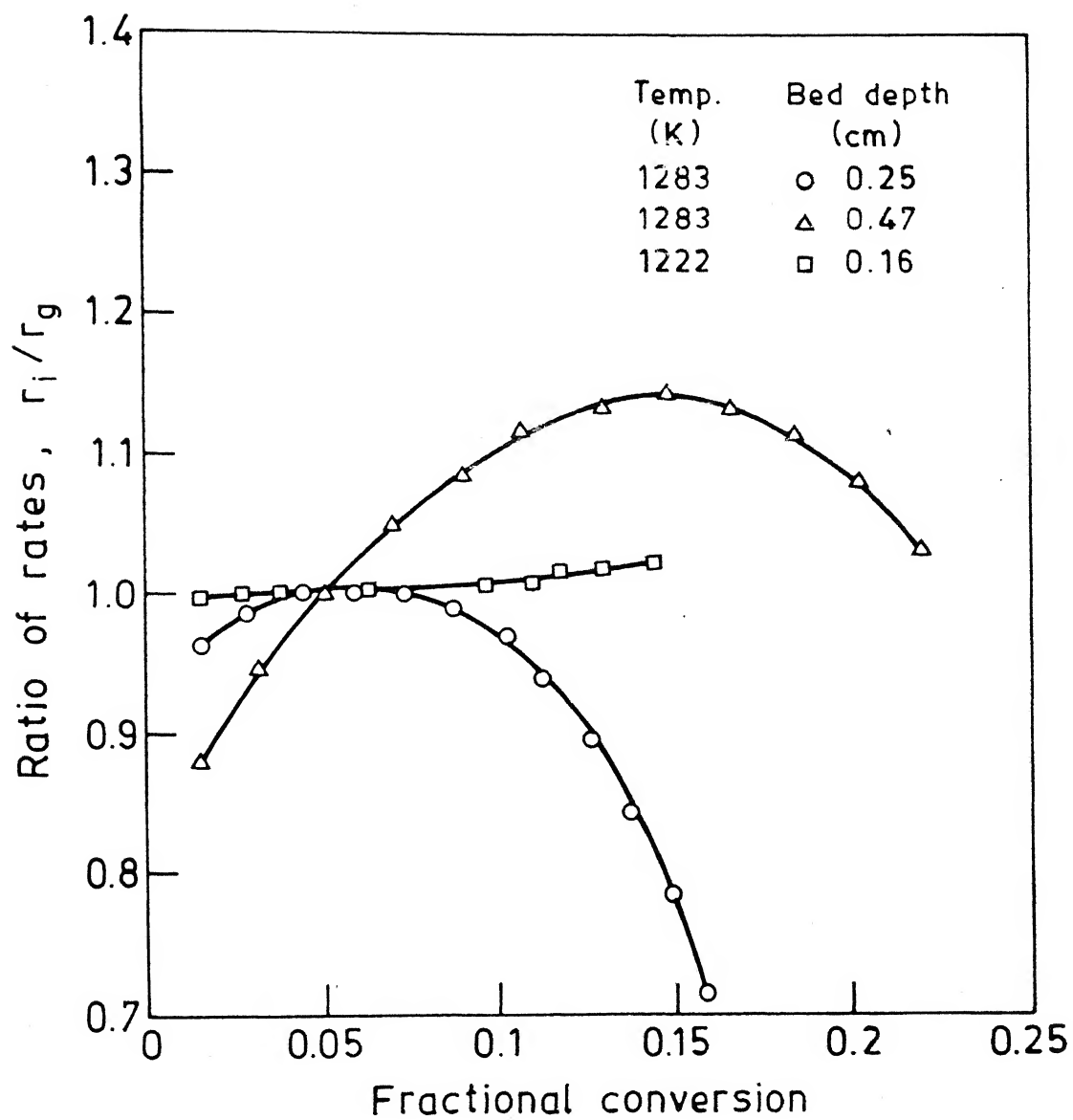


Fig. 4.12a. Ratio of rates (r_i/r_g) vs. fractional conversion for graphite in CO_2 .

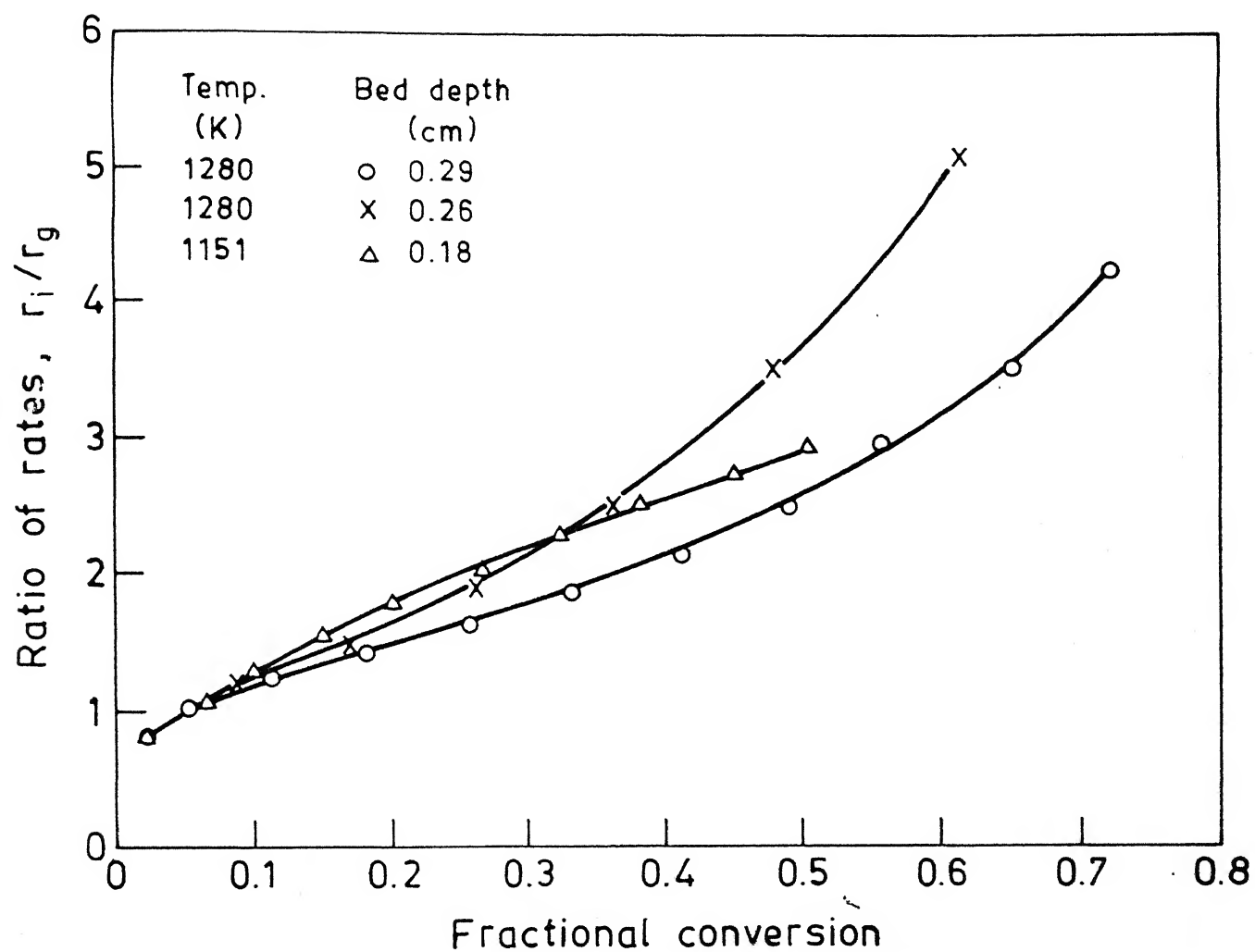


Fig. 4.12b. Ratio of rates (r_i/r_g) vs. fractional conversion for coconut char in CO_2 .

Table 4.5 Rate of gasification of graphite in pure CO₂

Experiment No.	Temperature (K)	Bed depth (Cm)	$r_g \times 10^4 (\text{Sec}^{-1})$
1	1283	0.38	0.74
2	1283	0.40	0.58
3	1283	0.39	0.66
4	1283	0.25	1.00
5	1283	0.47	0.51
6	1243	0.19	0.78
7	1243	0.19	0.86
8	1243	0.18	0.82
9	1222	0.42	0.22
10	1222	0.16	0.41
11	1222	0.22	0.41
12	1222	0.27	0.35
13	1222	0.47	0.20

Table 4.6 Rate of gasification of coconut char in pure CO₂

Experiment No.	Temperature (K)	Bed depth (cm)	$r_g \times 10^4$ (Sec ⁻¹)
14	1283	0.09	35.0
15	1280	0.17	22.5
16	1280	0.19	17.2
17	1280	0.24	11.2
18	1280	0.28	9.4
19	1280	0.31	7.6
20	1246	0.10	24.0
21	1214	0.19	15.0
22	1214	0.22	8.9
23	1214	0.28	5.0
24	1204	0.10	12.0
25	1151	0.15	6.2
26	1151	0.22	4.7
27	1151	0.28	3.6
28	1081	0.12	1.4
29	1081	0.17	1.1
30	1081	0.26	1.0

Table 4.7 Rate of gasification of coconut char in CO₂- Ar gas mixture

Experiment No.	Temperature (K)	Gas composition(Vol.%)		Bed depth (Cm)	$r_g \times 10^4$ (Sec ⁻¹)
		CO ₂	Ar		
31	1283	80	20	0.09	28.0
32	1283	50	50	0.08	20.2
33	1283	20	80	0.10	11.7
34	1246	80	20	0.11	19.5
35	1246	50	50	0.12	12.7
36	1246	20	80	0.10	6.6
37	1204	80	20	0.09	10.00
38	1204	50	50	0.11	6.5
39	1204	20	80	0.11	3.7
40	1151	80	20	0.10	4.5
41	1151	50	50	0.08	3.3
42	1151	20	80	0.09	2.2

Table 4.8 Rate of gasification of coconut char in CO₂- CO gas mixture

Experiment no.	Temperature (K)	Gas composition(Vol.%)		Bed depth (Cm)	$r_g \times 10^4$ (Sec ⁻¹)
		CO ₂	CO		
43	1283	80	20	0.13	21.33
44	1283	50	50	0.10	13.2
45	1283	20	80	0.11	5.0
46	1246	80	20	0.12	17.5
47	1246	50	50	0.10	10.5
48	1246	20	80	0.10	4.0
49	1204	80	20	0.11	9.65
50	1204	50	50	0.09	6.10
51	1204	20	80	0.11	2.20
52	1151	80	20	0.12	3.68
53	1151	50	50	0.12	1.57

CHAPTER 5

CALCULATION OF ISOTHERMAL AND NON-ISOTHERMAL EFFECTIVENESS FACTORS FOR GASIFICATION REACTION

5.1 Isothermal Mass Transfer Analysis

If a gas-solid reaction takes place simultaneously under chemical as well as mass transfer control, there will exist a concentration gradient along the bed and the interior will be exposed to a lower concentration of the reacting gas than the surface. This will lead to lowering of the overall reaction rate even under an isothermal condition.

As mentioned in Sec.1.2.4 effectiveness factor accounts for the mass transfer limitation of a chemical reaction and it may be stated as

$$\eta = \text{Actual reaction rate} / \text{Reaction rate without mass transfer limitation} \quad \dots(1.51)$$

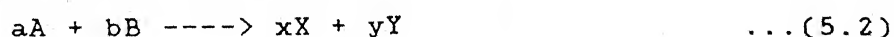
when a reaction is exclusively chemically controlled, the rate may be designated as 'intrinsic rate'.

$$\text{Intrinsic rate} = \text{Actual reaction rate} / \eta \quad \dots(5.1)$$

Two methods, one developed by Tien et al.(77) and the other by Roberts and Shatterfield (76) were used to calculate the effectiveness factor and are presented below. However, the correction of rate for heat transfer limitation will be presented in the latter part of this chapter.

5.1.1 Expression for effectiveness factor by method of Roberts and Shatterfield(76)

Roberts and Shatterfield had assumed a general chemical reaction of the following nature



According to them, the rate of the above reaction was presented as

$$r = k p_A / (1 + K_A p_A + \sum_i K_i p_i) \quad \dots(5.3)$$

The subscript i denotes any reactant or product other than A. In the gasification reaction the reactant gas is generally CO_2 and the product gas is CO. Thus Eq.5.3 can be rewritten as

$$r = k p_{CO_2} / (1 + K_A p_{CO_2} + K_2 p_{CO}) \quad \dots(5.4)$$

which is exactly similar to the rate equation derived by Reif(14) based on Langmuir-Hinshelwood adsorption isotherm.

By doing a material balance for the component A for a differential length inside the bed

$$D_A \cdot d^2 C_A / dx^2 = D_A / RT \cdot d^2 p_A / dx^2 = r \quad \dots(5.5)$$

Roberts and Shatterfield made the following assumptions for effectiveness factor calculation:

(i) The bed was treated as an infinite slab. It was exposed to the reacting gas at one end and the other end was sealed.

(ii) The effective diffusivity of all the species were constant but were not necessarily equal

(iii) Reaction took place isothermally

(iv) Ideal gas law was applicable

Material balance for any reactant other than A was presented as:

$$D_i / RT \cdot d^2 p_i / dx^2 = - V_i \cdot r \quad \dots(5.6)$$

where V is the stoichiometric coefficient. V was taken as negative for reactants other than A. Combination of Eq.5.5 and Eq.5.6 and integration subjected to the boundary conditions

$$p_A = p_{A,S} \quad , \quad p_i = p_{i,s} \quad \text{at } x = 0 \quad (\text{Exposed surface}) \quad \dots(5.7)$$

$$\text{and } dp_A/dx = dp_i/dx = 0 \quad \text{at } X = L \quad (\text{Sealed surface})$$

$$\dots(5.8)$$

yielded an equation of the following type

$$r = kp_A / \{1 + p_A [K_A - D_A \sum_i (K_i V_i / D_i)] +$$

$$\sum_i K_i [p_{i,s} + (p_{A,s} V_i D_A / D_i)]\} \quad \dots(5.9)$$

A dimensionless parameter ω was defined as

$$\omega = 1 + \sum_i K_i [p_{i,s} + (p_{A,s} V_i D_A / D_i)] \quad \dots(5.10)$$

Negative value of ω might arise for more than one reactant gas system other than A with high K_i value and very small $D_i p_s / V$ values. However, Roberts and Shatterfield considered only positive values of ω . They defined two other parameters k^* and K as

$$k'' = k^* / \omega \quad \dots(5.11)$$

$$\text{and } K = [K_A - D_A \sum_i K_i V_i / D_i] / \quad \dots(5.12)$$

K has the dimension of adsorption constant and k^* has that of rate. Incorporating ω , k^* and K , the Eq.(5.9) was transformed to

$$r = k'' p_A / (1 + K p_A) \quad \dots(5.13)$$

A modified Thiele's modulus was defined as

$$\phi_M = L (k'' RT / D_A)^{1/2} \quad \dots(5.14)$$

where L is the thickness of the slab.

Combination of Eq.5.5, Eq.5.13, Eq.5.14 and integration of the resulting equation subjected to the boundary conditions given in Eq.5.7 and Eq.5.8 yielded

$$d(Kp_A)/d(X/L) = -\sqrt{2} \phi_M [K(p_A - p_{A,o}) - \ln(1 + Kp_A / 1 + Kp_{A,o})]^{1/2}$$

$$\dots(5.15)$$

$p_{A,o}$ denoted the partial pressure of component A at the sealed surface.

According to the definition, the effectiveness factor η was expressed as

$$\eta = \sqrt{2/\theta_M} [(1+Kp_{A,s})/(Kp_{A,s})] [K(p_{A,s}-p_{A,o}) - \ln[(1+Kp_{A,s})/(1+Kp_{A,o})]]^{1/2} \quad \dots(5.16)$$

5.1.2 Expression for effectiveness factor by method of Tien and Turkdogan(77)

Based on their kinetic data on gasification of carbon by CO_2 Tien et al. developed the following mathematical model to calculate effectiveness factor.

To simplify the mathematical treatment, they assumed the following over and above what was assumed by Roberts et al.(76)

- (i) the geometrical dimension of pellet/bed remained unchanged
- (ii) the pore characteristics did not change during reaction
- (iii) steady state of reaction prevailed

Though the effective diffusivity was found to change with progress of burn off, they assumed constant value of effective diffusivity.

The total flux of CO_2 in terms of diffusive and convective flux was presented as

$$J_{CO_2} = D_e/RT \nabla p_{CO_2} + p_{CO_2}/P (J_{CO} + J_{CO_2}) \quad \dots(5.17)$$

from stoichiometry of the gasification reaction

$$J_{CO} = -2J_{CO_2} \quad \dots(5.18)$$

Eqs.(5.17) and (5.18) yielded

$$J_{CO_2} = D_e \cdot P/[RT(P+p_{CO_2})] \cdot \nabla p_{CO_2} \quad \dots(5.19)$$

where P is the total pressure = $p_{CO} + p_{CO_2}$. From conservation of mass under steady state condition,

$$\nabla J_{CO_2} = R_1 \quad \dots(5.20)$$

where R_1 is the local rate of oxidation

According to Tien et al., the isothermal rate(R) was presented as:

(i) In presence of sufficient amount of CO in the gas stream

$$R = \theta_1(p_{CO_2} - p_{CO_2,e})/[1 + (p_{CO}/\theta_{CO})] \quad \dots(5.21)$$

and (ii) when the amount of CO in the gas stream tends to zero

$$R = \theta_2 (p_{CO_2})^{\frac{1}{2}} \quad \dots(5.22)$$

The parameters θ_1 , θ_2 of Eqs.5.21 and 5.22 are rate parameters and θ_{CO} of Eq.5.21 is a thermodynamic parameter for chemisorption of CO.

In order to derive θ_1 and θ_{CO} , Eq.5.21 may be rearranged as

$$(p_{CO_2} - p_{CO_2,e})/R = 1/\theta_1 + 1/\theta_1 \cdot \theta_{CO} \cdot (p_{CO}) \quad \dots(5.23)$$

Plotting $(p_{CO_2} - p_{CO_2,e})/R$ against p_{CO} at a particular temperature should give a straight line. The slope and intercept of the straight line will yield the values of θ_1 and θ_{CO} .

Incorporating dimensionless pressure and distance, Eq.5.20 was transformed to

$$R_d = (D_e.P)/(RT.r) \cdot 1/(1 + Y_g) (dY/dX)_g \quad \dots(5.24)$$

where R_d = rate relative to external geometric surface area

$$Y = \text{dimensionless pressure} = p_{CO_2}/P \quad \dots(5.25)$$

$$P = \text{Total pressure} = p_{CO_2} + p_{CO} \quad \dots(5.26)$$

$$X = \text{dimensionless distance} = x/r \quad \dots(5.27)$$

Subscript 's' denotes the values of the parameters at the surface.

The concentration profile of the bed was calculated from the following generalized differential equation

$$1/X^C d/dX[\{X^C/(1+Y)\} dY/dX] = E[Y/(a-Y)] \quad \dots(5.28)$$

where $C = 0$ for rectangular, 1 for cylindrical and 2 for spherical coordinate. The dimensionless parameters

$$a = (1 + k_2 P) / (k_2 P), \quad \dots(5.29)$$

$$\text{and } E = (RTr^2 k_1) / (D_e P k_2) \quad \dots(5.30)$$

k_1 and k_2 were expressed as

$$k_1 = \theta_1 \cdot \rho / 12 \quad \dots(5.31)$$

$$\text{and } k_2 = 1/\theta_{C0} \quad \dots(5.32)$$

Integration of Eq.5.28 subjected to the following boundary conditions, i.e.

$$\text{at } X = 0 \quad (dY/dX) = 0 \quad \dots(5.33)$$

$$X = 1 \quad Y = Y_s \quad \dots(5.34)$$

yielded

$$(dY/dX)_s = (1+Y_s) \sqrt{2E \ln \left\{ \frac{(a-Y_0)^m (1+Y_0)^n}{(a-Y_s)^m (1+Y_s)^n} \right\}} \quad \dots(5.35)$$

$$\dots(5.36)$$

where $m = a/(1+a)$

$$n = 1/(1+a) \quad \dots(5.37)$$

Introducing expression for $(dY/dX)_s$ in Eq.5.28 and dividing it by $R_0 = r.R_L$, Tien et al. presented the expression for effectiveness factor as

$$R_d/R_0 = \eta = \sqrt{2/E} [(a-Y_s)/Y_s] \sqrt{\ln \left\{ \frac{(a-Y_0)^m (1+Y_0)^n}{(a-Y_s)^m (1+Y_s)^n} \right\}} \quad \dots(5.38)$$

where R_o = intrinsic isothermal rate

5.1.3 Procedure for effectiveness factor calculation

It was tried to calculate the effectiveness factors for the present set of study by using the expressions presented in Sec.5.1.1 and Sec.5.1.2 respectively for Roberts et al.(76) and Tien et al.(77). The procedures of calculation are presented below.

Calculation of effective diffusivity

The overall diffusivity in a straight round pore may be obtained from the following relation

$$1/D = 1/D_k + 1/D_b \quad \dots(5.39)$$

where D = overall diffusivity

D_k = Knudsen diffusivity

D_b = bulk diffusivity

The bulk diffusivity can be calculated by using the following equation (104) which reads as

$$D_b = D_{CO - CO_2} = 0.0018583 \frac{T^{3/2} (1/M_{CO} + 1/M_{CO_2})^{1/2}}{P \sigma_{CO - CO_2}^2 \Omega_{CO - CO_2}} \quad \dots(5.40)$$

where M_{CO} , M_{CO_2} = molecular weight of CO and CO_2 respectively

P = total pressure

$$\sigma_{CO - CO_2} = \text{Lenard-Jones parameter for CO and CO}_2 = \frac{1}{2}(\sigma_{CO} + \sigma_{CO_2}) \quad \dots(5.41)$$

Ω_{CO-CO_2} = collision integral of CO and CO_2

The Knudsen diffusivity (D_k) could be calculated from the following

equation(105)

$$D_k = 9.7 \times 10^3 \times a (T/M_{CO_2})^{1/2} \quad \dots(5.42)$$

where $a = 1/3$ (average pore radius)

In actual conditions, the pores are randomly oriented and the diffusing molecules have to travel through a rather tortuous path. So the diffusivity calculated through Eq.5.39 was modified by the correlation of Weisz Schwartz(106) to calculate effective diffusivity.

$$D_e = \epsilon^2 D/\sqrt{3} \quad \dots(5.43)$$

where D_e = effective diffusivity through pores

ϵ = fractional porosity of the bed

5.1.4 Calculation of effectiveness factor by method of Roberts and Shatterfield(76)

For a cylindrical geometry of infinite length, a dimensionless parameter ψ was defined as

$$\psi = \frac{L_c^2 RT}{D_e P_{CO_2,s}} \times R_{CO_2} \quad \dots(5.44)$$

where L_c = effective length of the bed

$P_{CO_2,s}$ = partial pressure of CO_2 at the surface

R_{CO_2} = rate of gasification in g-mol/cm³.S

The values of R_{CO_2} could be obtained from r_g using the following expression

$$R_{CO_2} = r_g \times \rho/12 \quad \dots(5.45)$$

where ρ = the bulk density of the bed

The effective length of the bed,

$$L_c = \frac{\text{volume of bed}}{\text{external surface area of bed}} \quad \dots(5.46)$$

In the present study, the sample was enclosed in a cylindrical bucket and gas could react with the sample only from the exposed top surface. Thus

$$L_c = \frac{(\pi D^2/4) \times h}{(\pi D^2/4)} = h \quad \dots(5.47)$$

Roberts and Shatterfield have presented master plots of η as a function of ψ at different i_2 values where

$$i_2 = (I_3 - 1.6 I_2) / (1 + 1.6 I_2) \quad \dots(5.48)$$

It is evident from Eq.5.48 that calculation of i_2 and subsequently the isothermal effectiveness factor by method of Roberts and Shatterfield need the values of I_2 and I_3 . According to Rao et al.(32) I_2 and I_3 should remain unchanged irrespective of the type of carbon and other experimental conditions. Srinivasan et al.(124) proposed the following expressions for temperature dependence of I_2 and I_3 ,

$$\log I_2 = 13280/T - 8.5306 \quad \dots(5.49)$$

$$\log I_3 = 1433/T - 0.7924 \quad \dots(5.50)$$

But the literature review [Sec.1.2.3] on gasification shows that there are no unique values of I_2 and I_3 which may be accepted as universal. Therefore this method could not be used.

5.1.5 Calculation of effectiveness factor by method of Tien and Turkdogan (77)

With the help of experimental rates of gasification in CO_2 - CO gas mixture, the value of ϕ_1 and ϕ_{CO} were first calculated using Eq.5.23. Next the parameters K_1 and K_2 can be found out by Eqs.5.31

and 5.32. A computer programme was developed to find out the composition profile of the bed through numerical solution of Eq.5.28 using 'Tri Diagonal Matrix' method. Eq.5.38 gives direct correlation between the ratios for complete and incomplete pore diffusion and from the ratio of the two rates the isothermal effectiveness factors were calculated.

In absence of CO in the gas stream Turkdogan et al.(29) have presented the following rate equation

$$r_g = \emptyset_2 (p_{CO_2})^{\frac{1}{2}} \quad \dots(1.35)$$

But they have advocated that under dual control, even in absence of CO in the gas stream, the following rate equation to be valid

$$r_g = \frac{\emptyset_1 (p_{CO_2})}{1 + p_{CO}/\emptyset_{CO}} \quad \dots(5.51)$$

So in absence of CO, for experiments in pure CO₂ and CO₂ - Ar gas mixtures Eq.5.51 transforms into

$$r_g = \emptyset_1 (p_{CO_2}) \quad \dots(5.52)$$

At a fixed temperature, rate versus p_{CO_2} should yield a straight line with slope of \emptyset_1 .

In absence of CO in the external gas stream, the dimensionless pressure is nothing but unity as total pressure is equal to the partial pressure of CO₂. Again under dual control, whatever small may be the amount of CO generated due to gasification reaction, it will impart a definite effect on the rate. So the \emptyset_{CO} values evaluated for CO - CO₂ gas mixtures was used to take care of effect of

carbon monoxide in the limiting case of $p_{CO} \rightarrow 0$. Rest of the procedure is same as described for CO - CO₂ gas mixture.

5.2 Non-Isothermal Analysis

It has already been mentioned that alongwith mass transfer resistance, heat transfer may also significantly affect the gasification kinetics. This will be prominent specially at high temperature, high bed depth and carbon of high reactivity.

In view of the importance of expected temperature gradient inside the porous carbon bed during gasification reaction, Tien and Turkdogan (78) presented a simultaneous heat and mass transfer analysis of the gasification process, providing a direct relationship between the isothermal and non-isothermal rates and a number of process parameters. The analysis by Tien and Turkdogan, although quite impressive from the point of view of its methodology, suffers a serious drawback as some equations presented there are either improperly stated or dimensionally imbalanced. Few typical examples have been presented in Appendix (6). Such errors, which perhaps occurred during simplification of mathematical expressions, render the final results of Tien and Turkdogan unreliable. So an attempt has been made to rectify the above mathematical treatment for non-isothermal effectiveness factor calculation and can be described as follows (94):

5.2.1 Derivation of temperature profile inside the bed

The basic differential heat transfer equation employed for the present modification to calculate the temperature profile of the bed is the same as was described by Tien et al. for one dimensional heat transfer along r direction and may be presented as

$$R_1 \Delta H = K_e \frac{d^2 T}{dr^2} \quad \dots(5.53)$$

where

$$\begin{aligned} R_1 &= \text{local rate of oxidation} \\ &= k_1 p_{CO_2} / (1 + k_2 p_{CO}) \end{aligned} \quad \dots(5.54)$$

ΔH = enthalpy change of the reaction

and K_e = effective thermal conductivity

Eq.5.54 can be further simplified as

$$R_1 = \frac{k_1}{k_2} \frac{y}{a^* - y} \quad \dots(5.55)$$

where dimensionless parameters

$$y = \frac{p_{CO_2}}{P} \quad \dots(5.56)$$

$$a^* = \frac{1 + k_2 P}{k_2 P} \quad \dots(5.57)$$

and P = total pressure = $p_{CO_2} + p_{CO}$

In case of rapid diffusion process, the heat transfer becomes rate controlling. Under such a situation, the appropriate differential equation can be obtained by combining Eq.5.53 and Eq.5.55 as follows.

$$\frac{d^2 z}{dx^2} = \frac{k_1}{k_2} \cdot \frac{r_o^2}{T_s} \cdot \frac{\Delta H}{K_e} \cdot \frac{y}{a^* - y} \quad \dots(5.58)$$

where dimensionless quantities are defined as

$$z = \frac{T}{T_g} \quad \dots(5.59)$$

$$x = \frac{r}{r_o} \quad \dots(5.60)$$

Analogous to Tien and Turkdogan, in the present analysis, the quantity $y/(a^*-y)$ has also been treated as a function of temperature alone. The exact expressions of k_1 and k_2 are difficult to handle mathematically. Therefore, it was attempted to simplify them as follows.

The values of the parameters k_1 and k_2 can be calculated from Eq.5.21 - Eq.5.23 and Eq.5.31 and Eq.5.32.

Knowing the values of k_1 and k_2 at different temperatures, it was attempted to express k_1/k_2 as $f(z)$. Initially a second order polynomial^a for $f(z)$ was tried, however, the fitted values tend to show a very small coefficient of z^2 . Therefore, for a small temperature interval, k_1/k_2 can be approximated as a straight^a line. Thus the Eq.5.58 may be rewritten as

$$\frac{d^2 z}{dx^2} = \beta (a + bz) \quad \dots(5.61)$$

$$\text{where } \beta = \frac{r_o^2}{T_g} \cdot \frac{\Delta H}{K_e} \cdot \frac{y}{(a^* - y)} \cdot x \cdot \frac{\rho}{M} \quad \dots(5.62)$$

M = molecular weight of carbon

and ρ = bulk density

The Eq.5.61 can be solved for one dimensional conduction through slab, subject to the boundary conditions:

$$x = 0 \quad \frac{dz}{dx} = 0 \quad \dots(5.63)$$

and

$$x = 1 \quad z = 1 \quad \dots(5.64)$$

In order to do this, Eq.5.61 may be restated as

$$\frac{1}{2} \frac{d}{dz} \left(\frac{dz}{dx} \right)^2 = \beta(a + bz) \quad \dots(5.65)$$

Integration of Eq.5.65 will result

$$\frac{dz}{\sqrt{\beta(2az + bz^2) + I}} = dX \quad \dots(5.66)$$

where I is the integration constant. For $b > 0$, Eq.5.66 can be integrated for the second time as:

$$X = 1/\sqrt{\beta b} \ln [2 \sqrt{\beta b (I + \beta (2az + bz^2)) + 2\beta bz + 2a\beta}] + J \quad \dots(5.67)$$

where J is the second integration constant. As the ratio of k_1/k_2 increases with increase of temperature, the condition of $b > 0$ is generally satisfied in all experiments. Utilizing the boundary conditions, the integration constants I and J may be expressed as

$$I = - \beta (2az_0 + bz_0^2) \quad \dots(5.68)$$

where z_0 is the value of z at $X = 0$, as determined by the boundary condition,

$$J = 1 - 1/\sqrt{\beta b} \ln [2 \sqrt{\beta b (- \beta(2az_0 + bz_0^2) + \beta (2a + b)) + 2\beta b + 2a\beta}] \quad \dots(5.69)$$

Finally upon combination of Eq.5.63 and Eq.5.67 - Eq.5.69

$$\sqrt{\beta} = 1/\sqrt{b} \ln \frac{\sqrt{b (-(2az_0 + bz_0^2) + (2a + b)) + (a + b)}}{a + bz} \quad \dots(5.70)$$

Eq.5.70 may be used to construct the temperature nomogram of the bed.

5.2.2 Derivation of non-isothermal rate

It was attempted to derive an expression for the non-isothermal rate, consistent with the present formulation of the problem. Analogous to Tien and Turkdogan (78) the non-isothermal rate may be defined as

$$R_{cp} = 1/r_0 \int_0^{r_0} R_1 dr. \quad \dots(5.71)$$

Utilizing Eq.5.55, Eqs.5.57 - 5.59, R_{cp} may be expressed as:

$$R_{cp} = \{y/(a^* - y)\}_s \int_0^1 (a + bz) dz \quad \dots(5.72)$$

Eq.5.67 provides the functional relationship necessary to integrate the above equation. However, owing to the complicated form, it is difficult to handle this equation conveniently. Therefore an analogous version of Eq.5.67 may be written as

$$Z = a_0 + a_1x + a_2x^2 \quad \dots(5.73)$$

where a_0, a_1, a_2 are coefficients of the fitted polynomial. Eqs.5.72 and 5.73 yield

$$R_{cp} = \{y/(a^* - y)\}_s \int_0^1 (A + Bx + Cx^2) dx \quad \dots(5.74)$$

where

$$A = a + b a_0 \quad \dots(5.75)$$

$$B = b a_1 \quad \dots(5.76)$$

and

$$C = b a_2 \quad \dots(5.77)$$

Eq.5.74 can now be directly integrated between the limits to obtain the value of non-isothermal rate.

Now non-isothermal effectiveness factor will be nothing but (R_{cp}/R) .

The mathematical procedure described above gives an analytical treatment for calculation of bed temperature profile and non-isothermal rate. However, the numerical solution of Eq.(5.61) can directly generate the temperature profile. Necessary computer programme has been presented in Appendix (7).

5.3 Calculation of Effective Thermal Conductivity

In general the thermal conductivity of a loose packed bed depends on the thermal conductivity of the gas filling the pores, thermal conductivity of the solid, the amount of void fraction present and the temperature. As the temperature increases, the particle to particle thermal radiation also increases and thus effects the thermal conductivity of the bed. Schotte (95) developed a technique to predict the thermal conductivity of a porous bed in which the gas phase present in the pores was assumed to be continuous. So if the thermal conductivity of the solid at minimum porosity is known it is possible to predict the bed conductivity for any level of porosity and type of gas filling the pores. The method developed by Schotte may be described as follows.

If the effective pore dimensions are of the same order of magnitude as the mean free path of the gas, then the true thermal conductivity of gas decreases. This happens when the particle diameter is around 1000 times greater than the mean free path of the gas. If

the diameter falls in that range then correction of the gas thermal conductivity is needed, otherwise either calculated or measured value of thermal conductivity of gas can be directly used. Deissler and Eian (96) developed a correlation for break away pressure P_b ,

$$P_b = (1.77 \times 10^{-21}) \times T / (D_p d^2) \quad \dots(5.78)$$

where

T = temperature

d_p = average particle diameter

d = mean diameter of gas molecule

If the actual pressure is greater than P_b , there is no need of any correction of thermal conductivity of gas. But if actual pressure is less than P_b , then gas thermal conductivity is corrected in the following manner

$$K_g = \frac{K_g^o}{1 + 2.03 \times 10^{-22} \left\{ (C_p/C_v) / (1 + C_p/C_v) \right\}_g \left\{ (1 - \epsilon) / \epsilon \right\} \left\{ (T K_g^o) / (P D_p d^2 C_p \mu) \right\}} \quad \dots(5.79)$$

where

K_g = corrected thermal conductivity of gas

K_g^o = uncorrected thermal conductivity of gas

C_p, C_v = specific heat at constant pressure and volume respectively

ϵ = porosity

μ = viscosity

If the conductivity of the solid of minimum porosity (K_s) is designated as 'intrinsic thermal conductivity', then having obtained

K_g , K_s is used to calculate the ratio K_s/K_g . Geiger and Pourier (97) have presented master plots for K_s/K_g vs. K_b/K_g at different porosity levels. Knowing the value of K_s/K_g and the porosity, K_b/K_g and thus K_b , the bulk thermal conductivity can be calculated. Again at high temperature, the radiative heat transfer from particle to particle has a contribution to the effective thermal conductivity of the bulk and thus needs correction. If K_r is the radiation contribution to the effective thermal conductivity of the bed then

$$K_r = \frac{1 - \epsilon}{(1/K_s) + (1/K_r^o)} + \epsilon K_r^o \quad \dots(5.80)$$

where

$$K_r^o = 0.692 \epsilon D_p (T^3/10^8) \quad \dots(5.81)$$

ϵ = emissivity of solid

Finally, the effective thermal conductivity

$$K_e = K_b + K_r \quad \dots(5.82)$$

The units of all the variables used in the above equations are in F.P.S. system.

CHAPTER 6

DISCUSSIONS OF RESULTS ON GASIFICATION REACTION

Gasification reaction, as it is well known, is an integral part of carbothermic reduction of iron-oxide. Though both graphite and coconut char were used for gasification rate measurement, graphite was not further employed for carbothermic reduction. Basically it was used to check the rate data of gasification of graphite in pure CO_2 , presented by Abraham (3). Rate data for both graphite and coconut char under various experimental conditions have already been presented in Chapter 4.

6.1 Comparison of r_g Values in Pure CO_2 with the Literature

Fig.(6.1) presents r_g (Sec^{-1}) in pure CO_2 as a function of temperature in an Arrhenius type of plot for this investigation as well as data of some other workers (3,29,32,42,50). It may be noted that it includes a few types of carbon. No data point has been shown. Only the lines have been presented. The purpose is to make an approximate comparison of r_g values. For graphite, rate values reported by Turkdogan et al.(29) in pure CO_2 was found to be almost an order of magnitude lower than those of present study. On the other hand, rate data of Wu et al.(50) for graphite appears to be atleast 2 times higher than these of the present study at 1283K, but matches quite well at 1243K. In the present study, the size of the individual graphite particle was - 200 + 230 mesh size and the bed depth listed in Table (4.5) - Table (4.8) are the heights of the powder bed used in the crucible. Particle size of graphite used by both Turkdogan et al. and Wu et al. were much larger than the present study. Lower rate

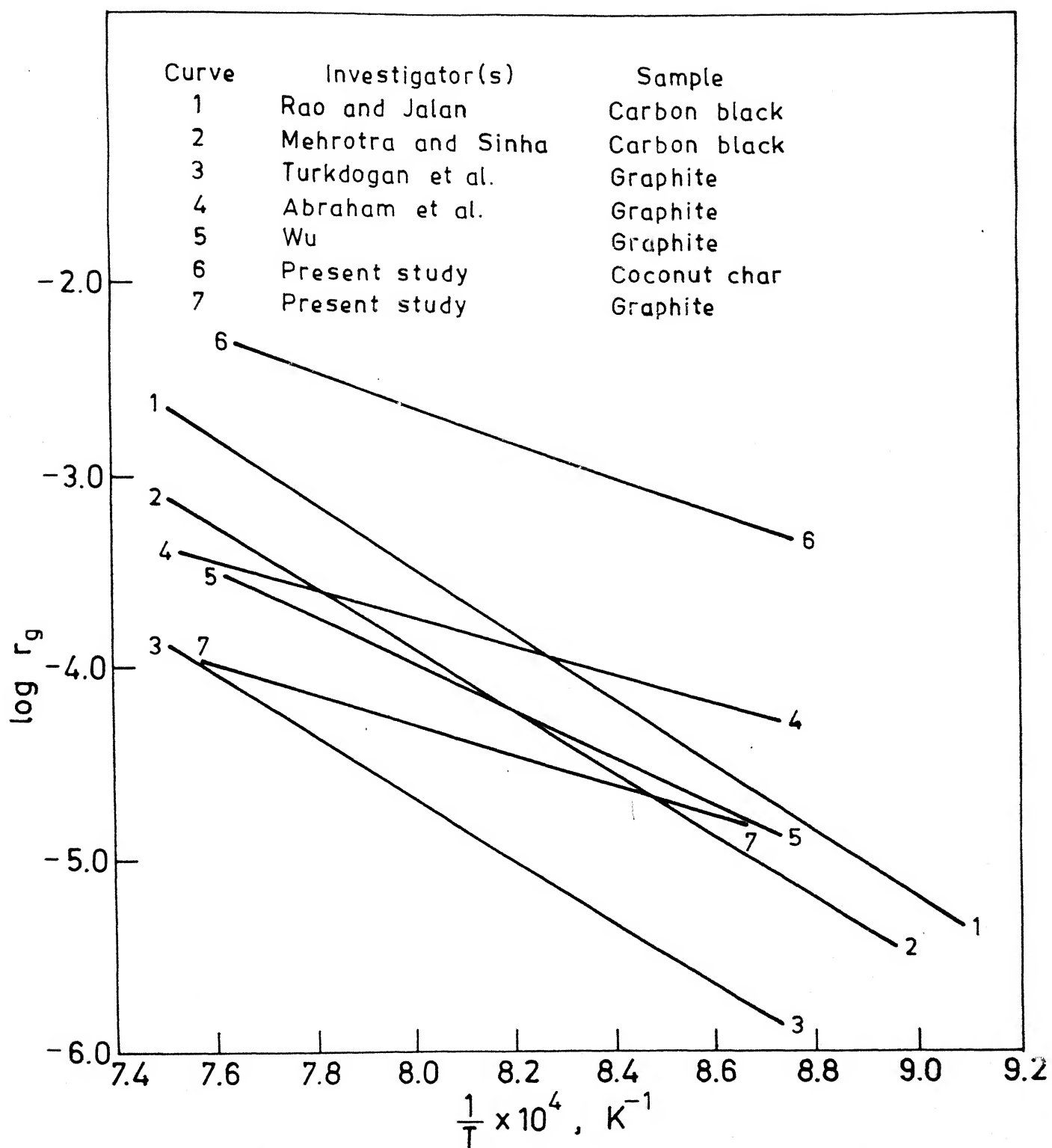


Fig. 6.1. $\log r_g$ vs. $1/T$ for different investigators.

of oxidation of graphite reported by Turkdogan et al. may be due to the reason that as the particle size was quite large, there might be appreciable amount of mass transfer resistance thus causing slow rate of reaction. But even though Wu used larger particles of graphite, their rate was higher than the present study by factor of 2, even for the lowest bed depth. Data of Mehrotra et al. (42) for carbon black was found to be comparable with the gasification rate of graphite at low temperatures. Rate reported by Rao et al. (32) for carbon black compares quite well with the present study at all the temperatures but same for Turkdogan et al. was slightly higher than graphite.

The rate of gasification of coconut char reported by Turkdogan et al. matches quite well with the results of the present investigation at 1283K. But at lower temperatures, the values for the present study are around 2 times higher.

6.2 Results and Discussions of Mass Transfer Analysis

As stated earlier the kinetics of gasification of carbon may be significantly affected by mass transfer resistance unless sufficient precautions are taken to eliminate it during experiment. So the experimentally measured rates will be lower than what it actually be if there is no mass transfer effect. Mathematical formulation and the calculation procedures of two established methods for mass transfer analysis have already been presented through Secs. 5.1.1 - 5.1.5 of Chapter 5.

6.2.1 Mass transfer analysis by method of Roberts and Shatterfield

Literature review of gasification of carbon reveals that majority of the workers have tried to establish the validity of the

Langmuir - Hinshelwood type of rate expression which may be restated as

$$K = \frac{I_1 p_{CO_2}}{I + I_2 p_{CO} + I_3 p_{CO_2}} \quad \dots(1.22)$$

where the parameters K, I_1 , I_2 , I_3 have their usual significance.

As discussed in Sec.5.1.4, the method of Roberts and Shatterfield can be used for calculation of isothermal effectiveness factor provided values of I_2 and I_3 are known.

Again literature review (Sec.1.2.3) shows that except Grabke(23) and Wu et al.(50) no one tried to estimate the parameters I_1 , I_2 and I_3 . Gadsby(10), in his modified rate expression proposed a parameter 'X' which is equivalent to (I_3/I_2) .

Rao et al.(32) have put forward the idea of universal nature of I_2 and I_3 and have presented the temperature dependence of the two parameters. But the compilation of I_2 , I_3 [Table(1.3)] clearly indicates that the values calculated for different workers vary widely and there is very little scope of justifying the concept of universal nature of I_2 and I_3 . Hence mass transfer analysis by the method of Roberts and Shatterfield could not be used for processing of results.

6.2.2 Mass transfer analysis by method of Tien and Turkdogan

The general procedure has been discussed in Sec.5.1.2. The write up here is restricted to application of same to results of gasification rate measurements in the present investigation.

In the case of coconut char, experimental rate data have been collected in pure CO_2 , $CO - CO_2$ and $CO_2 - Ar$ atmosphere.

(a) Procedure for coconut char

As mentioned in Chapter 5, parameters θ_1 , θ_{CO} for experiments in CO_2 -CO atmosphere and θ_1 for CO_2 , CO_2 -Ar atmospheres for coconut char were calculated with the help of Eqs. 5.23 and 5.51. In evaluating the parameters θ_1 and θ_{CO} for CO_2 -CO experiments, $(p_{CO_2} - p_{CO_2,e})/r_g$ values were plotted against p_{CO} at different temperatures. Fig. 6.2 presents such plots for experiments in CO - CO_2 mixtures. Fig. 6.3 shows the variation of rate as a function of p_{CO_2} at different temperatures for experiments in CO_2 - Ar mixtures. Slopes of the plots in Fig. 6.3 were used for calculation of θ_1 in CO_2 - Ar.

In calculation of θ_1 and θ_{CO} from Fig. (6.2) it was found that the plots for $(p_{CO_2} - p_{CO_2,e}) / r_g$ vs. p_{CO} have extremely small slopes and even a variation of $\pm 15\%$ of the experimental values can change the slope from positive to negative and thus the model for mass transfer calculation fails to apply. So it is obvious that for one set of data points within the experimental error range may give negative slopes for θ_1 and θ_{CO} calculation. Turkdogan et al. (29) have reported their data points to be reproducible within $\pm 15\%$ and the θ_1 , θ_{CO} values calculated by them have an error range of $\pm 50\%$. Though the model was used for the present set of calculation it appears that the model is either applicable for very selective data points of very low experimental error or even the validity of the model can be left open for questioning. So it is likely that there may be significant error in the calculated values of the rate parameters for CO adsorption.

Figs. 6.4 - 6.5 present the variation of the calculated θ_1, θ_{CO} for experiments in CO_2 - CO and θ_1 for experiments in CO_2 , CO_2 - Ar atmosphere respectively for coconut char as a function of

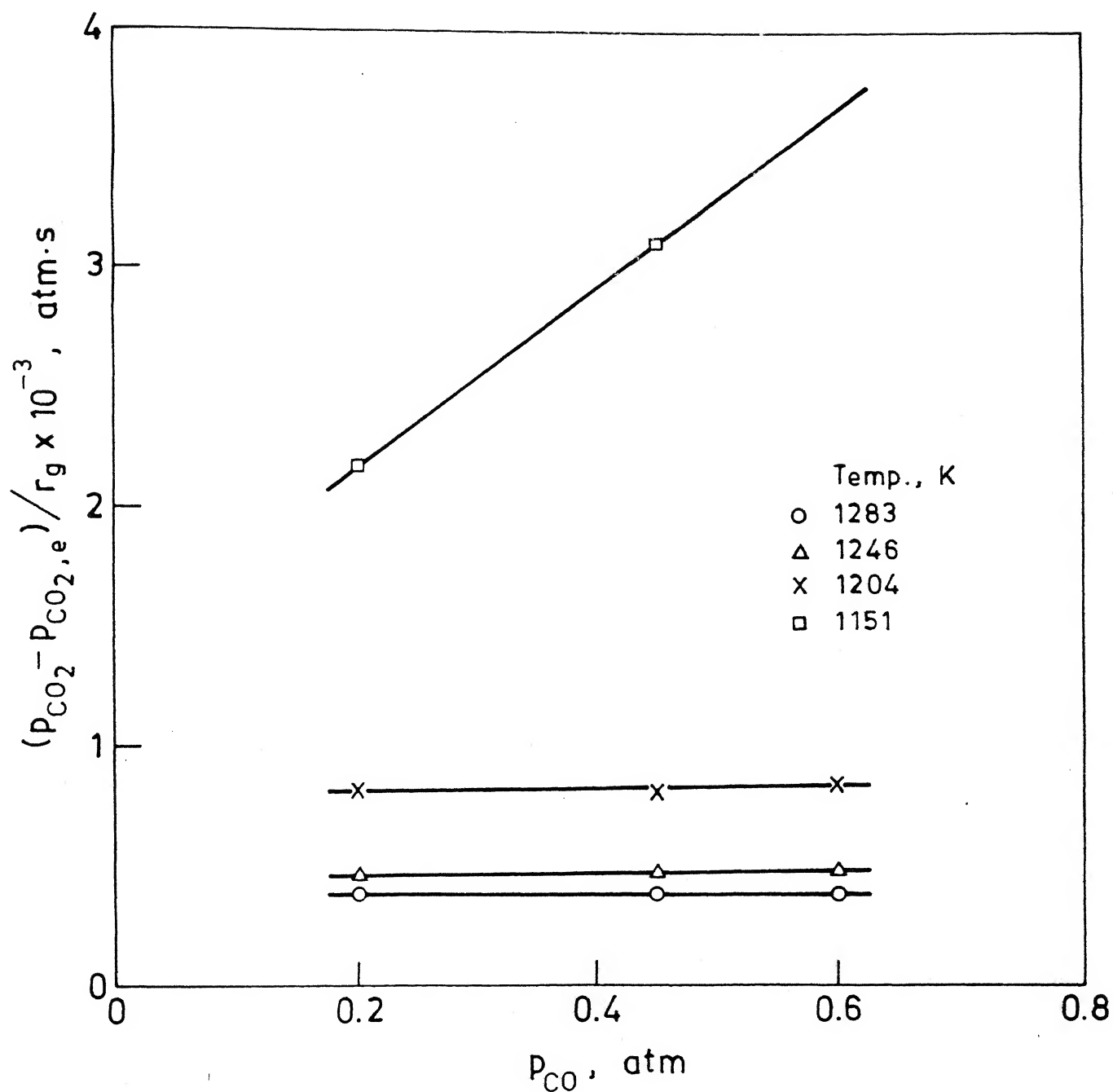


Fig. 6.2. $(p_{\text{CO}_2} - p_{\text{CO}_2,e})/r_g$ vs. p_{CO} for coconut char in $\text{CO}_2\text{-CO}$.

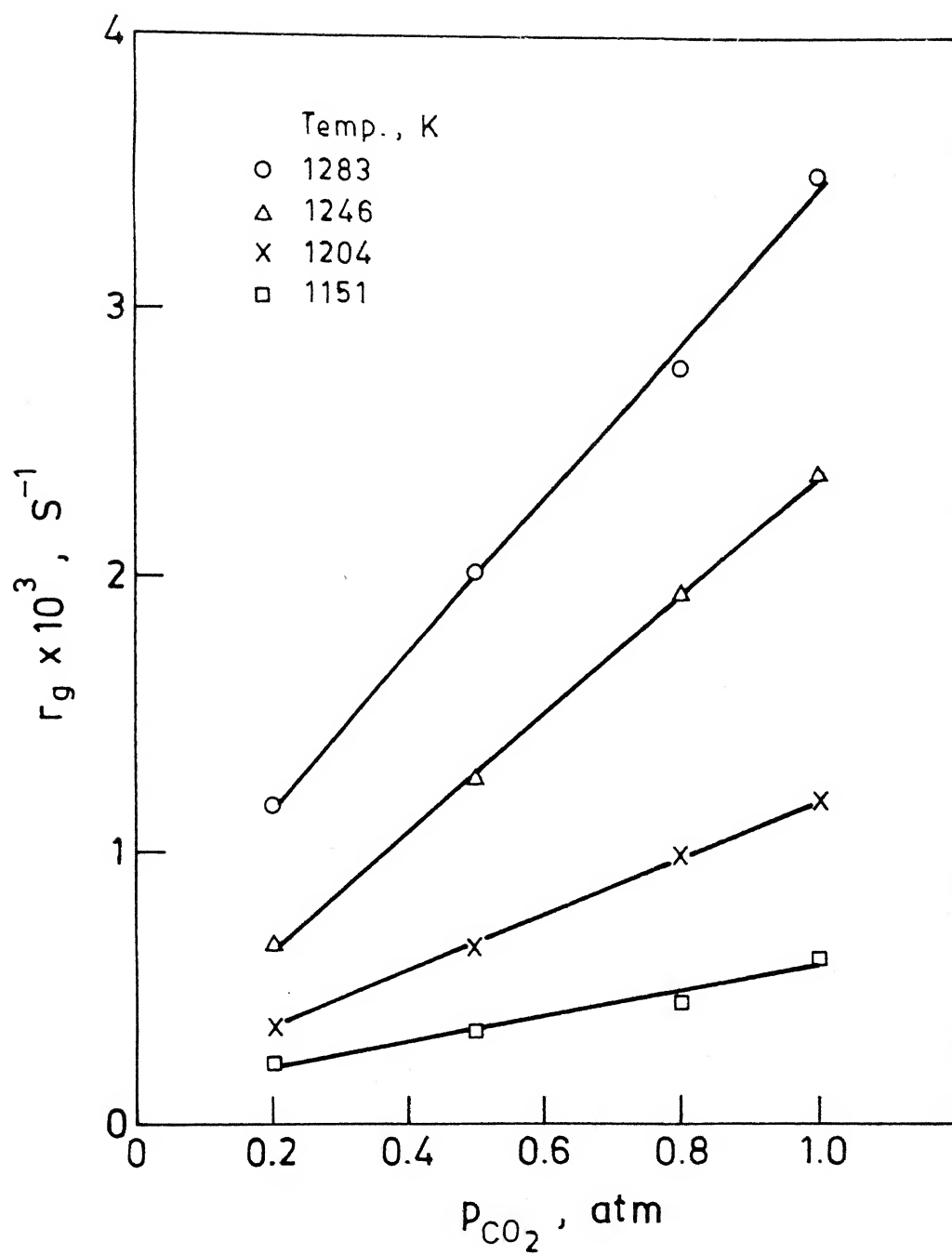


Fig. 6.3. r_g vs. p_{CO_2} for coconut char in CO_2 -Ar.

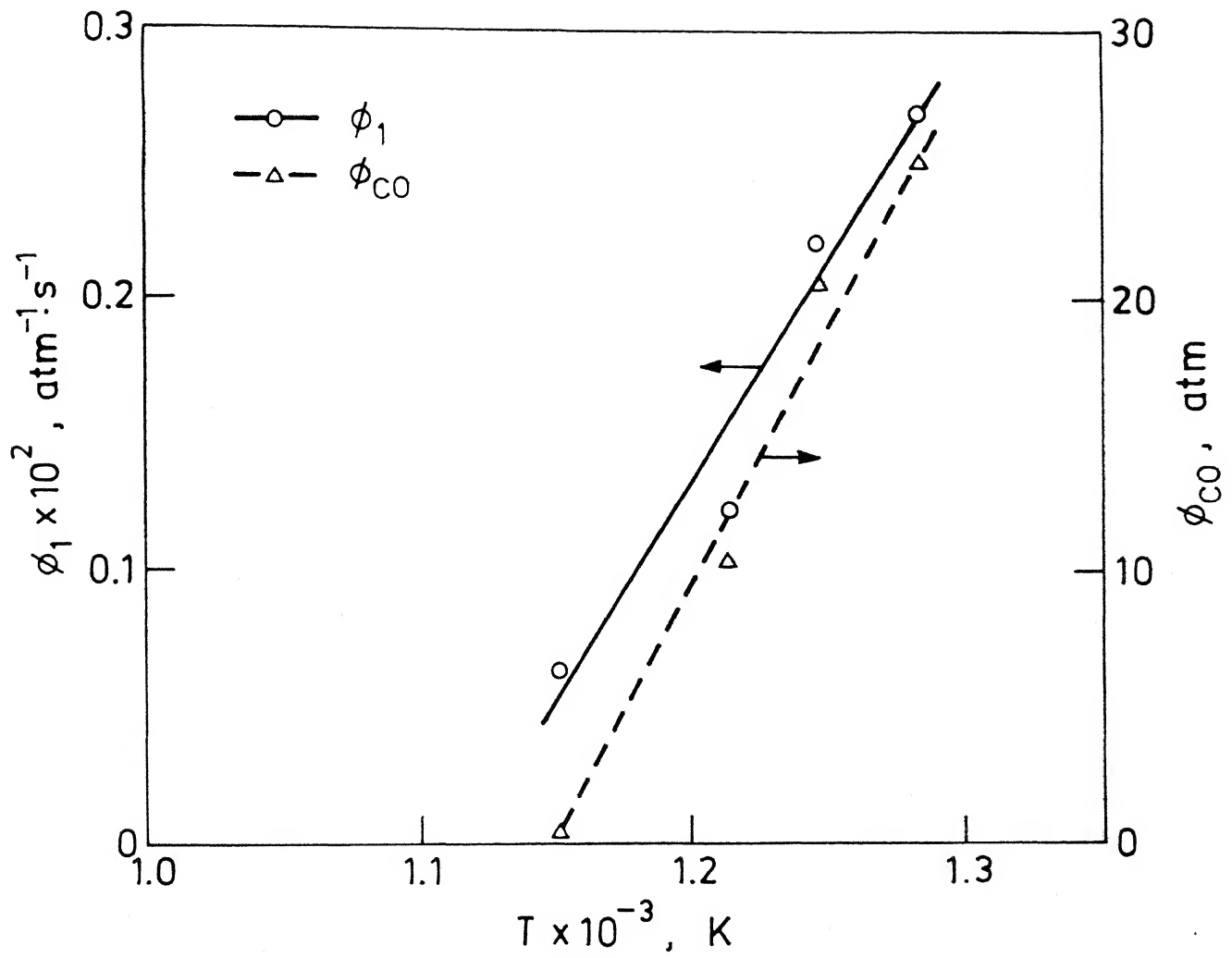


Fig. 6.4. Variation of ϕ_1 , ϕ_{CO} with temperature for coconut char in CO_2 -CO.

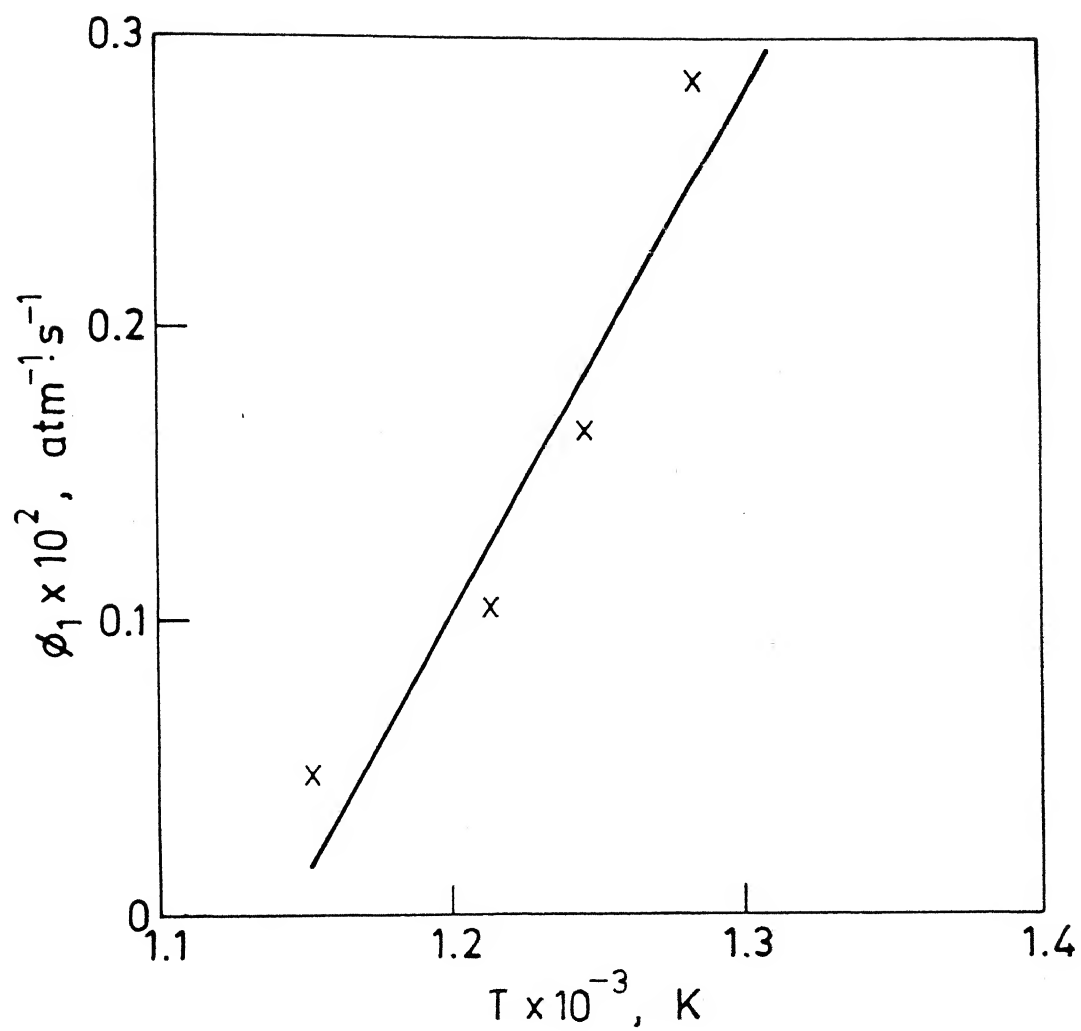


Fig. 6.5. Variation of ϕ_1 with temperature for coconut char in CO_2 and CO_2 -Ar.

temperature.

Within the limits of uncertainty of θ_1 , θ_{CO} values in CO_2 - CO atmosphere and θ_1 values in CO_2 , CO_2 - Ar atmosphere for coconut char were expressed as a function of temperature may be presented as:

(a) for CO - CO_2 gas mixture

$$\log \theta_1 = - \frac{238.56}{T} - 2.33 \quad \dots(6.1)$$

$$\log \theta_{CO} = - \frac{590.89}{T} + 2.08 \quad \dots(6.2)$$

and (b) for CO_2 and CO_2 - Ar mixture,

$$\log \theta_1 = - \frac{282.30}{T} - 2.32 \quad \dots(6.3)$$

However, in case of graphite, no experiment could be carried out in either CO_2 - Ar or CO_2 - CO gas mixtures due to extremely low rates of weight loss, and consequent limitations in reliable measurements by the experimental set up. For mass transfer analysis of measurements in pure CO_2 , only the parameter θ_{CO} is required. θ_{CO} could not be determined for graphite gasification. In calculation of mass transfer effect on oxidation of graphite in CO_2 , the correlations for temperature dependence of the θ_{CO} given by Turkdogan et al. (29), as noted below in Eq.(6.4) was employed.

$$\log \theta_{CO} = - \frac{5940}{T} + 3.46 \quad \dots(6.4)$$

6.2.3: Discussions of isothermal effectiveness factors

Tables 6.1 -6.3 present the values of isothermal effectiveness factors (η) and rates of gasification after mass transfer correction (K_c)

Table 6.1 Values of r_g , η and K_c for graphite in CO_2

Experiment No.	Temperature (K)	$r_g \times 10^4$ (S^{-1})	η	$K_c \times 10^4$ (S^{-1})
1	1283	0.74	0.45	1.64
2	1283	0.58	0.38	1.52
3	1283	0.66	0.40	1.65
4	1283	1.00	0.44	2.27
5	1283	0.51	0.42	1.21
6	1243	0.78	0.64	1.18
7	1243	0.86	0.62	1.14
8	1243	0.82	0.64	1.30
9	1222	0.22	0.49	0.45
10	1222	0.41	0.87	0.47
11	1222	0.41	0.64	0.65
12	1222	0.35	0.58	0.60
13	1222	0.20	0.50	0.40

Table 6.2 Values of r_g , η and K_c for coconut char in CO_2 and CO_2 - Ar gas mixture

Experiment No.	Vol. % CO_2	Temperature (K)	$r_g \times 10^4$ (s^{-1})	η	$K_c \times 10^4$ (s^{-1})
14	100	1283	35.0	0.60	57.9
31	80	1283	28.0	0.74	37.6
32	50	1283	20.2	0.76	26.5
33	20	1283	11.7	0.91	12.9
20	100	1246	24.0	0.62	38.7
34	80	1246	19.5	0.74	26.3
35	50	1246	12.7	0.74	17.1
36	20	1246	6.6	0.80	8.2
24	100	1204	12.0	0.68	17.6
37	80	1204	10.0	0.73	13.7
38	50	1204	6.5	0.77	8.4
39	20	1204	3.7	0.80	4.6
25	100	1151	6.2	0.76	8.5
40	80	1151	4.5	0.78	5.7
41	50	1151	3.3	0.79	4.2
42	20	1151	2.2	0.80	2.7

Table 6.3 Values of r_g , η and K_c for coconut char in CO_2 - CO gas mixture

Experiment No.	Vol. % CO_2	Temperature (K)	$r_g \times 10^4$ (S^{-1})	η	$K_c \times 10^4$ (S^{-1})
43	80	1283	21.33	0.65	32.1
44	50	1283	13.2	0.66	19.9
45	20	1283	5.0	0.72	7.0
46	80	1246	17.5	0.62	28.2
47	50	1246	10.5	0.68	15.5
48	20	1246	4.0	0.68	5.9
49	80	1204	9.65	0.63	15.3
50	50	1204	6.1	0.65	9.3
51	20	1204	2.2	0.69	3.2
52	80	1151	3.68	0.68	5.4
53	50	1151	1.57	0.70	2.3

where $K_c = r_g/\eta$... (6.5)

It may be noticed from table 6.1 that at higher temperature the values are lower than those at lower temperature. This is because of the fact that at higher temperature as the reaction rate is faster, the mass transfer limitation will play more significant role than at lower temperature. It can also be seen that in most of the cases, η values at 1243K is higher than those at 1222K. This may be explained in the following manner. In the present set of studies, the sample was enclosed from three sides and the reacting gas had access to the sample only through the top open surface. So the oxidising gas, CO_2 in the present case had to diffuse inside the powder sample bed through the interparticle pores and the reaction will basically take place at the surface of the individual carbon particle. So if the particle size (for single particle) or the bed depth (for powder bed) increases, the distance of diffusion for the reacting gas will increase and thus will give rise to higher mass transfer resistance effect. At 1243K, the bed depth of the sample was 0.19 cm where as the same did vary from 0.16 to 0.47 cm at 1222K. At 1222K, the η value found to be 0.64 with a bed depth of 0.22 cm which compares quite well with the values of η at 1243K with bed depth of 0.19 cm. Comparable η values even with higher bed depths at the two temperatures may be due to the slowness of reaction. Again at 1222K and bed depth of 0.16 cm, the effectiveness factor value was found to be 0.87 which is much higher than that of the values at 1243K. This is according to the expectation of the kinetics of the reaction.

In case of CO_2 - Ar gas mixtures, it is difficult to correlate the effectiveness factor values directly with bed depth. It

is due to the fact that with increase of proportion of Ar in the gas, the rate of gasification will automatically slow down. So with increase of Ar percentage in gas, even with same bed depth, the effectiveness factor should increase. It may be noted from Table 6.2 that at a fixed temperature, η values more or less continuously increases with decrease of partial pressure of CO_2 . But there exists no systematic variation of η with temperature.

The same conclusion can also be drawn for effectiveness factor values [Table 6.3] when coconut char was subjected to CO_2 - CO gas mixtures at different temperatures.

The probable reasons for this apparent inconsistencies in the calculated effectiveness factor values may be attributed to the following reasons:

(a) It has already been pointed out that coconut char powder bed underwent considerable swelling when it was put into the reaction chamber. This led to significant variation in the bed porosity. As a result, there may be appreciable change in the effective diffusivity of the bed. As it was very difficult to monitor the variation of porosity during reaction the present calculation is based on the bed porosity measured at room temperature. So this may incorporate some error in calculated effectiveness factor.

(b) The uncertainty of evaluation of θ_1 , θ_2 and θ_{CO} by the model of Tien and Turkdogan.

6.3 Non-Isothermal Effectiveness Factor

As discussed before, heat transfer limitation may contribute significantly to the gasification reaction at high temperature and for highly reactive form of carbon. Gasification being an endothermic

reaction, high reaction rate will demand faster rate of heat supply. If heat supply rate to the reaction site is low then there will be temperature drop in the bed and the reaction will proceed at a lower temperature. Graphite being a low reactive material, it is expected that there will be no appreciable non-isothermal effect in the temperature range of the present study and thus no heat transfer analysis has been attempted for graphite. However, detailed analysis for coconut char has been carried out. The mathematical formulation and the procedure for the non-isothermal analysis has already been stated in [Sec.5.2]. In evaluating the dimensionless parameters used in the model, θ_1 , θ_2 , θ_{CO} values calculated during mass transfer analysis (Sec.6.2) were employed.

In experiments with CO_2 - CO gas mixtures, the total pressure P is the sum of partial pressures of CO_2 and CO . But in pure O_2 and CO_2 - Ar mixture, the situation is slightly different and this aspect has already been discussed in connection with mass transfer analysis. The dimensionless parameter a^* as defined in Eq.(5.56) may therefore be transformed into

$$a^* = \frac{1 + K_2 p_{CO_2}}{K_2 p_{CO_2}} \quad \dots(6.6)$$

for experiments in CO_2 and CO_2 - Ar atmosphere.

Table 6.4 and 6.5 present non-isothermal effectiveness factor (η_T) and intrinsic chemical reaction rate (K_{CT}) for activation of coconut char, where

$$K_{CT} = \frac{K_C}{\eta_T} \quad \dots(6.7)$$

So, η_T is due to heat transfer limitation only.

Noting that K_C had been obtained by after eliminating mass transfer limitation.

Therefore K_{CT} has been obtained after correcting r_g by elimination of both mass transfer and heat transfer limitations.

It may be noticed from Table (6.4) and Table (6.5) that there is quite significant non-isothermal effect on rate at 1283K for all gas compositions, where as non-isothermal effect is found only for CO_2 and CO_2 - Ar gas mixtures at 1246K and the non-isothermal effectiveness factor ranges from 0.53 to 0.94. Again the non-isothermal effectiveness factors for CO_2 - Ar gas mixtures are much lower than those of CO_2 - CO. This is in accordance with the expected behaviour i.e. poisoning effect of CO will lower down the rate much prominently than the presence of inert argon and thus giving rise to higher value of effectiveness factor in case of CO_2 - CO gas mixture. At lower temperatures, the non-isothermal effectiveness factors turned out to be unity. This is also in accordance with what has been predicted by Bandyopadhyay et al.(94).

6.4 Activation Energy

The activation energies of gasification for graphite and coconut char were calculated by least square fitting of $\ln K_{CT}$ as a function of reciprocal of temperature. Fig.6.6 presents the Arrhenius type of plots for graphite and coconut char. The activation energies are found to be 260 kJ/mol and 250 kJ/mol for graphite and coconut char respectively. Activation energy of coconut char matches quite well with the reported value 240 kJ/mol for graphite, activated carbon by Reif (98). For high purity electrode grade graphite and medium purity activated

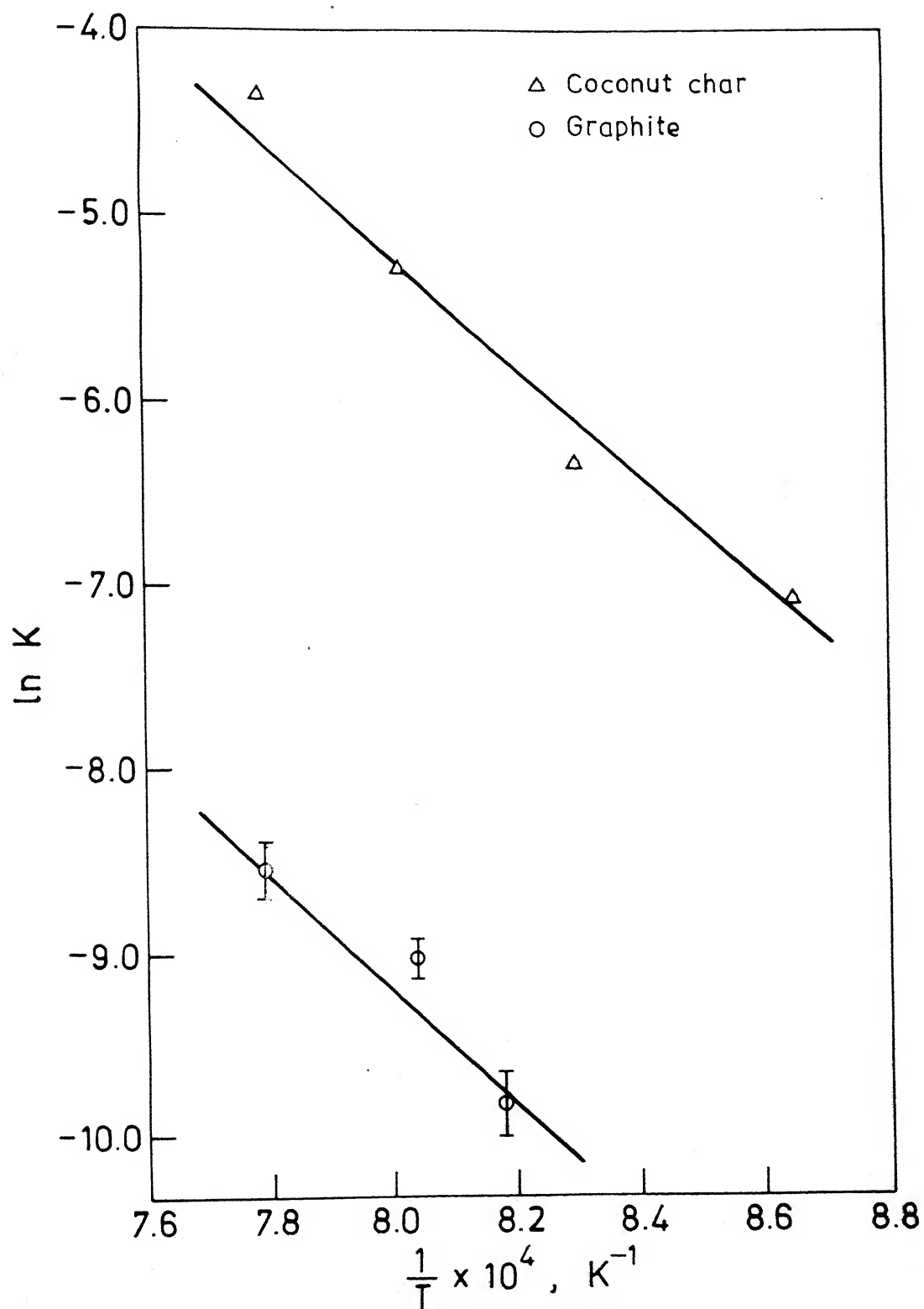


Fig. 6.6. Arrhenius plot for graphite and coconut char.

Table 6.4 Non-isothermal effectiveness factor (η_T) and intrinsic rate of gasification (K_{CT}) in pure CO_2 and CO_2 - Ar gas mixture for coconut char

Experiment No.	Temperature (K)	η_T	$K_{CT} \times 10^4$ (S^{-1})
14	1283	0.53	108.0
31	1283	0.57	65.9
32	1283	0.60	43.2
33	1283	0.66	19.5
20	1246	0.77	50.3
34	1246	0.81	32.5
35	1246	0.82	20.8
36	1246	0.94	8.7
24	1204	1.0	17.6
37	1204	1.0	13.7
38	1204	1.0	8.4
39	1204	1.0	4.6
25	1151	1.0	8.5
40	1151	1.0	5.7
41	1151	1.0	4.2
42	1151	1.0	2.7

Table 6.5 Non-isothermal effectiveness factor and intrinsic rate of gasification in CO_2 - CO gas mixture for coconut char

Experiment No.	Temperature (K)	η_T	$K_{CT-T} \times 10^4$ (S^{-1})
43	1283	0.75	42.8
44	1283	0.82	24.2
45	1283	0.87	8.0
46	1246	1.0	28.2
47	1246	1.0	15.5
48	1246	1.0	5.9
49	1204	1.0	15.3
50	1204	1.0	9.3
51	1204	1.0	3.2
52	1151	1.0	5.4
53	1151	1.0	2.3

charcoal Walker et al. (21) reported the value of activation energy to be 359.5 kJ/mol. Turkdogan et al. (29) found the activation energy to be of 288.4 kJ/mol for coconut char, electrode graphite and metallurgical coke. The value of activation energy observed by Rao et al. (32) was 332.3 kJ/mol for carbon black. Many other activation energy values have been reported in the literature. But only few have been mentioned here. Comparing the activation energy values of the literature and the present set of values, it may be noticed that except the values reported by Reif, the present values are lower than all the other cited values. In the present set of study, as heat and mass transfer corrections have been made, K_{ct} presents the intrinsic rate and thus the activation energy should be for chemically controlled rate.

6.5 Extrapolation to Zero Bed Depth

Besides all other factors responsible for giving rise to mass transfer limitation, particle size is very important to determine the extent of this effect on rate. If small particles of carbon are exposed to the reacting gas from all sides, it may be expected that the rate under this situation would represent the intrinsic chemical rate. Wu et al. (50) have employed one or two layers of thinly spreaded carbon particles for their experiment and have designated it as 'differential bed'. According to them, differential bed is superior in view of its negligible resistance to mass transfer. They, therefore, directly employed the experimentally observed rates to evaluate I_1 , I_2 and I_3 of Langmuir - Hinshelwood rate expression.

So if experimental rates at different bed depths are extrapolated to zero bed depth, it should give intrinsic rate without

the need for any heat and mass transfer correction. Figs. 6.7 and 6.8 show variation of r_g with bed depth. Values of r_g obtained by extrapolating to zero bed depth (r_g^0) are reported in Tables 6.6 and 6.7. Tables 6.6 and 6.7 also compare the rate values for graphite and coconut char respectively, obtained from zero bed depth extrapolation and the rates after heat and mass transfer corrections.

From a theoretical point of view, r_g^0 and k_{CT} (and k_c for graphite) should be equal. Tables 6.6 and 6.7 show that matching has been excellent for both graphite and coconut char. This serves as a cross-check on the entire experimental measurement as well as mass and heat transfer analysis, and shows that results can be accepted with confidence. It also demonstrates that if data are collected as function of bed depth, then extrapolation to zero depth can yield the values of intrinsic chemical reaction rate at that temperature and gas composition satisfactorily even without heat and mass transfer analysis.

6.6 Dependence of K_{CT} on Gas Composition for Coconut Char

The intrinsic rates of reaction (K_{CT}) for coconut char under various gas compositions have already been presented in Tables (6.4) and (6.5). Figs. (6.9) and (6.10) show such variation as a function of p_{CO_2} and p_{CO} for CO_2 - Ar and CO_2 - CO gas mixtures respectively. It may be seen from both the figures that the nature of the curves for both CO_2 - Ar and CO_2 - CO are same. At high temperature there is a sharp drop of rate with either 20% Ar or 20% CO. With higher proportion of Ar or CO, though there is drop of rate but the curves more or less follow a linear variation. With gradual decrease of temperature, the variation tends towards more and more linear.

Table 6.6: Comparison of rates obtained by zero bed depth extrapolation (r_g^0) with K_C for graphite

Temperature (K)	$r_g^0 \times 10^4 \text{ (s}^{-1}\text{)}$	$K_C \times 10^4 \text{ (s}^{-1}\text{)}$
1283	1.57	1.91*
1222	0.55	0.57*

* means values reproduced from Arrhenius plot.

Table 6.7: Comparison of rates obtained by zero bed depth extrapolation (r_g^0) with K_{CT} for coconut char

Temperature (K)	$r_g^0 \times 10^4 \text{ (S}^{-1}\text{)}$	$K_{CT} \times 10^4 \text{ (S}^{-1}\text{)}$
1280	96.5	93.84*
1214	29.1	26.0*
1151	9.0	8.5
1081	1.6	1.2*

* means values reproduced from Arrhenius plot.

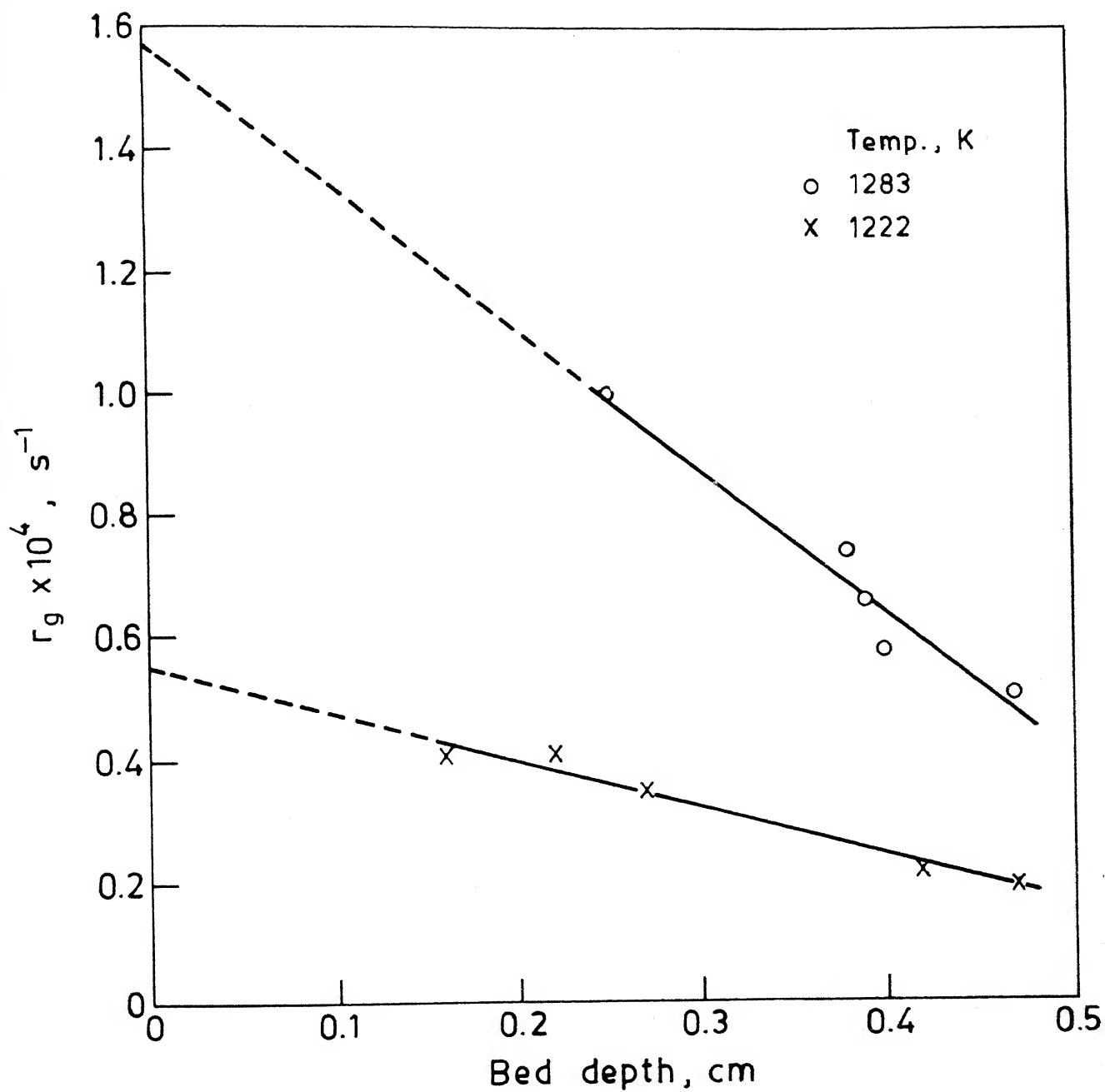


Fig. 6.7. r_g vs. bed depth for graphite in CO_2 .

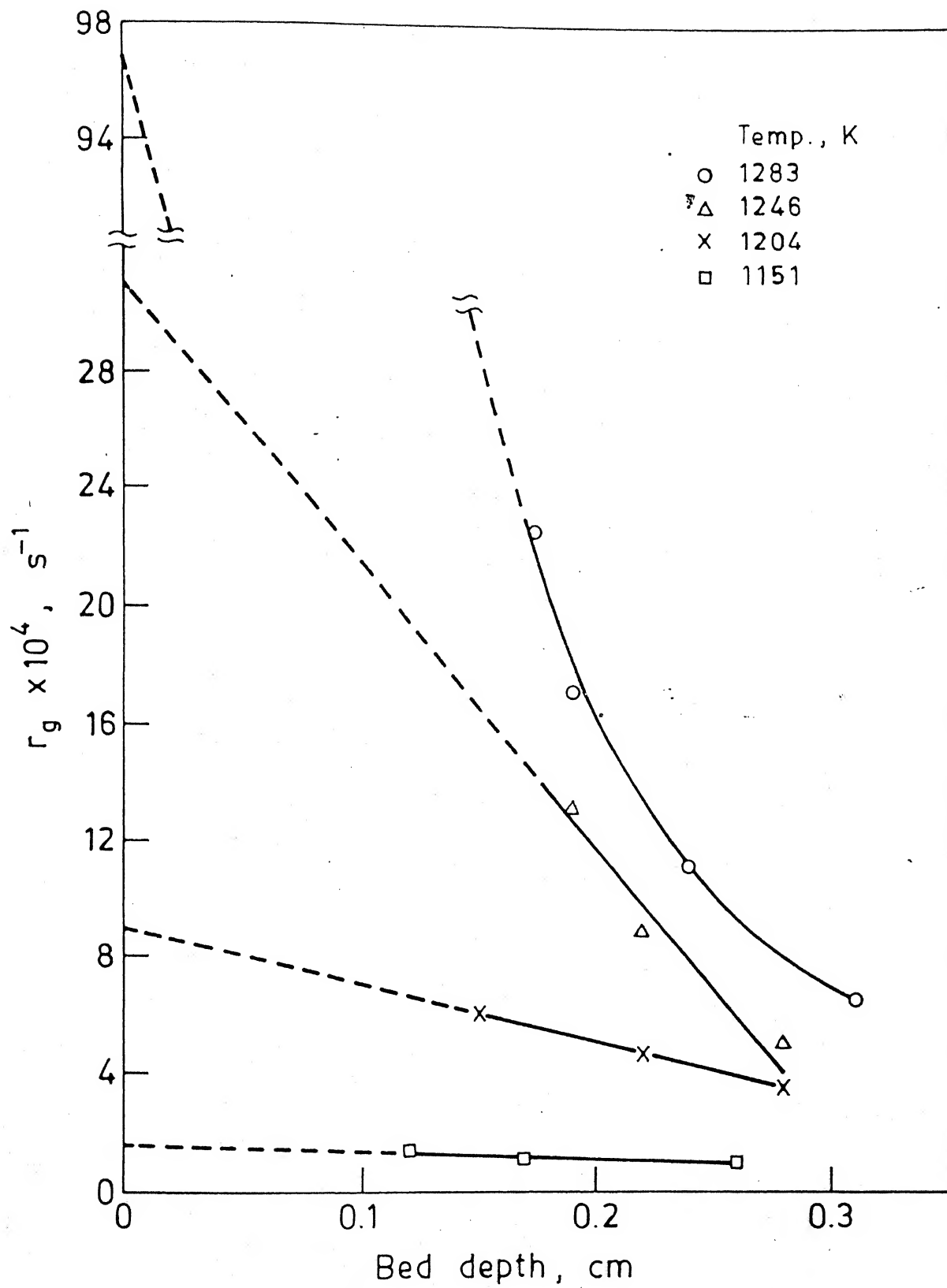


Fig. 6.8. r_g vs. bed depth for coconut char in CO_2 .

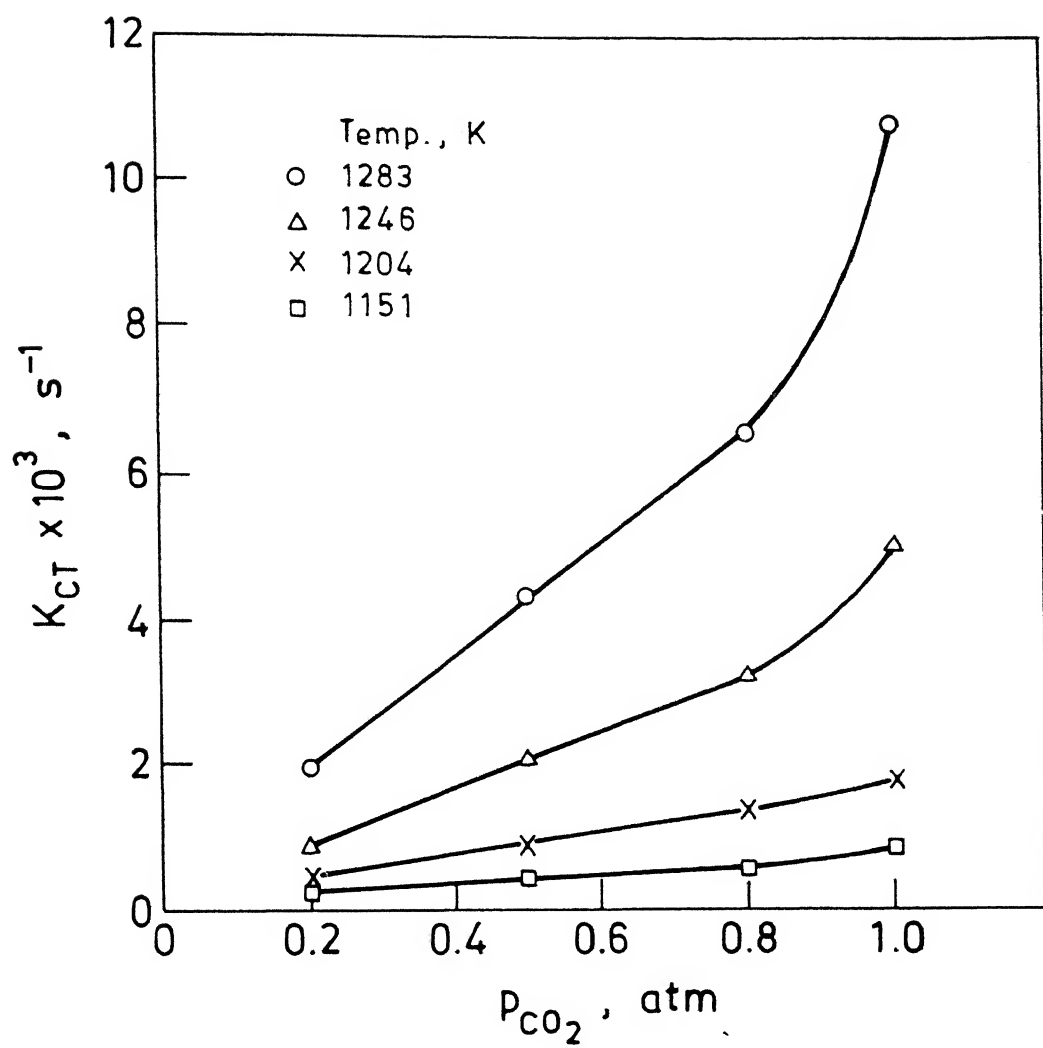


Fig. 6.9. K_{CT} vs. P_{CO_2} for coconut char in CO_2 , CO_2 -Ar.

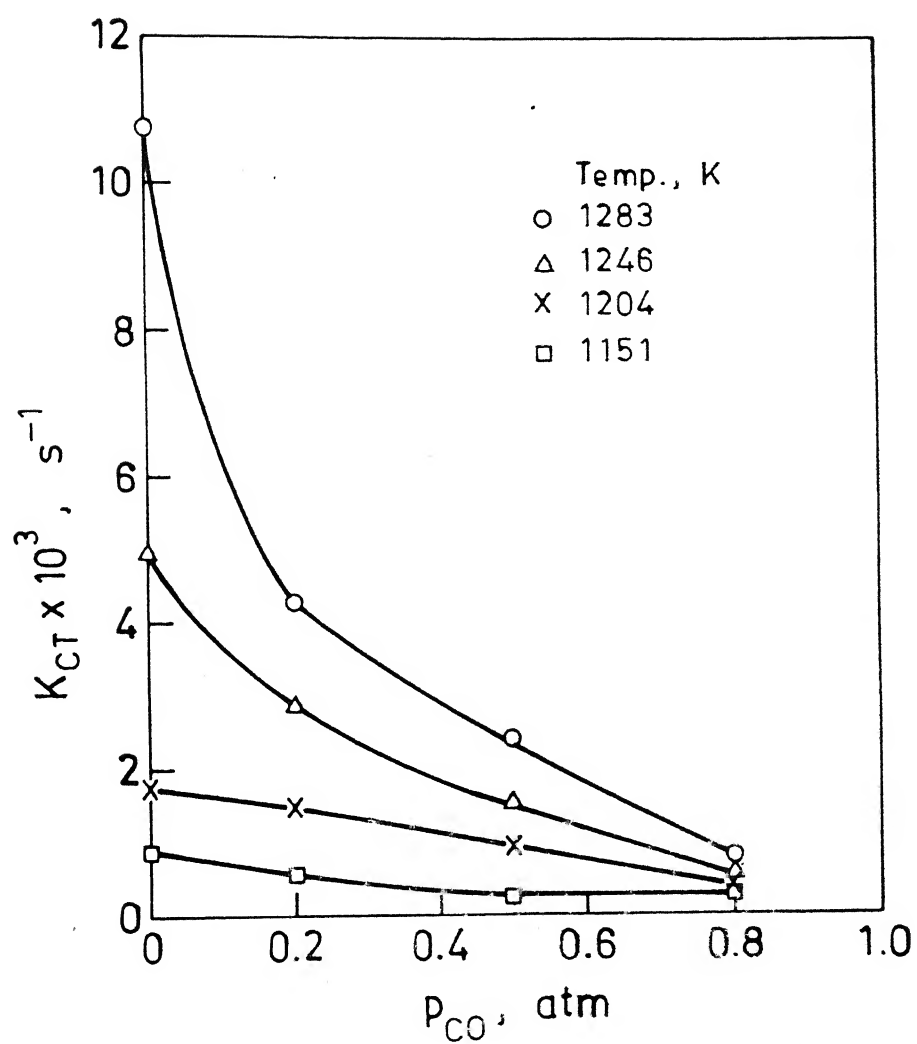


Fig. 6.10. K_{CT} vs. p_{CO} for coconut char in CO_2 -CO.

Fig.(6.11) shows the variation of ratio of intrinsic rates in pure CO_2 and $\text{CO}_2 - \text{CO}$ gas mixtures with the increase of p_{CO} in the gas stream at 1283K and 1246K as sample curves. It may be noticed that as the temperature is decreased from 1283K to 1246K, the ratios of the two rates are higher. It means that with lowering of temperature, the effect of CO on the rates was less pronounced. This is in disagreement with the finding of Turkdogan et al. (29). According to them, the effect of CO is more prominent at lower temperatures.

Literature review on gasification shows that some investigators (49,50,99) have assumed the gasification reaction to be first order reversible. If it is so, then from Eq.(5.23), rate should be proportion to $(p_{\text{CO}_2} - p_{\text{CO}_2,e})$. In the temperature range of this study, for all practical purposes, $p_{\text{CO}_2,e}$ is very small compared to p_{CO_2} and thus can be neglected. So approximately, rate should be proportional to p_{CO_2} in the case of first order reaction. But Fig.6.9 and Fig.6.10 show that at high temperatures, rates drop sharply for both 20% Ar and 20% CO in the gas stream. With higher proportions of Ar and CO, rates vary linearly with p_{CO_2} . Again at lower temperatures the rates tend to follow a linear variation at all gas compositions. If the gasification follows a first order reaction, then, rate should vary linearly for all gas compositions and all temperatures. But no such phenomenon could be established with the present set of data and thus it appears that gasification does not follow first order reaction in the present investigation.

6.7 Evaluation of Rate Parameters of Langmuir - Hinshelwood Rate Expression for Coconut Char

The rate expression given by Langmuir - Hinshelwood [Eq.1.22] directly correlates the intrinsic rate with those of the

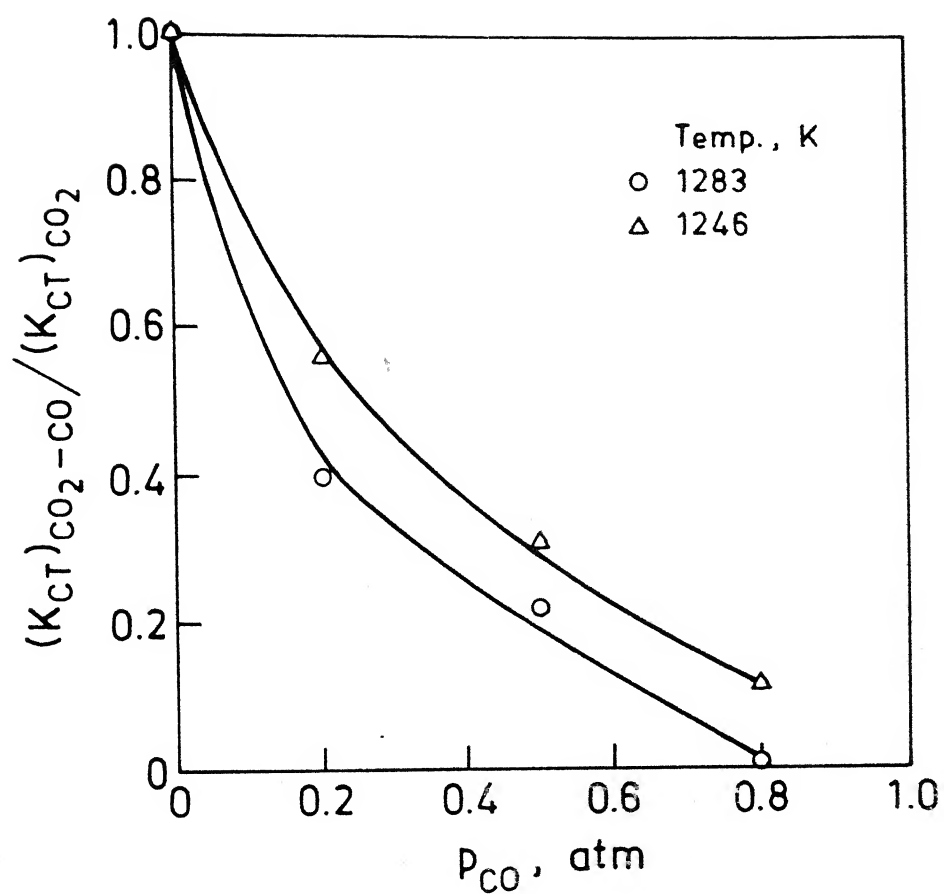


Fig. 6.11. Variation of $(K_{CT})_{CO_2-CO} / (K_{CT})_{CO_2}$ with p_{CO} for coconut char.

rate parameters I_1 , I_2 , I_3 . So with the help of Eq.1.22 it is possible to evaluate the rate parameters once the intrinsic rate is known. The procedure for the same is presented below:

Under negligible accumulation of CO, the Eq.(1.22) transforms to

$$\frac{1}{K_{CT}} = \frac{1}{I_1} \left(\frac{1}{p_{CO_2}} \right) + \frac{I_3}{I_1} \quad \dots(6.8)$$

A plot of $1/K_{CT}$ versus $1/p_{CO_2}$ at fixed temperature should give a straight line with slope of $1/I_1$ and intercept of I_3/I_1 .

When sufficient amount of CO is present in the vicinity of the reaction site, either through input gas stream or as a reaction product, then Eq.1.22 will take the following form:

$$p_{CO_2} / K_{CT} = \frac{I_2 - I_3}{I_1} p_{CO} + \frac{1 + I_3}{I_1} \quad \dots(6.9)$$

Again, at a fixed temperature, plot of (p_{CO_2}/K_{CT}) versus p_{CO} should give straight line with slope of $(I_2 - I_3)/I_1$ and intercept of $(1 + I_3)/I_1$. Combination of slopes and intercepts of Eqs.(6.8) and (6.9) will yield values of I_1 , I_2 and I_3 . After calculation of intrinsic rate of gasification, effort was made to determine I_1 , I_2 and I_3 by using Eqs.(6.1) and (6.2). Figs. (6.12) and (6.13) present the plots of $1/K_{CT}$ vs. $1/p_{CO_2}$ and p_{CO_2}/K_{CT} vs. p_{CO} respectively at different temperatures for coconut char.

Here also it may be noticed that through p_{CO_2}/K_{CT} vs. p_{CO} plots are more or less straight line, $1/K_{CT}$ vs. $1/p_{CO_2}$ plots have tendency to depart from linearity at low temperatures. However,

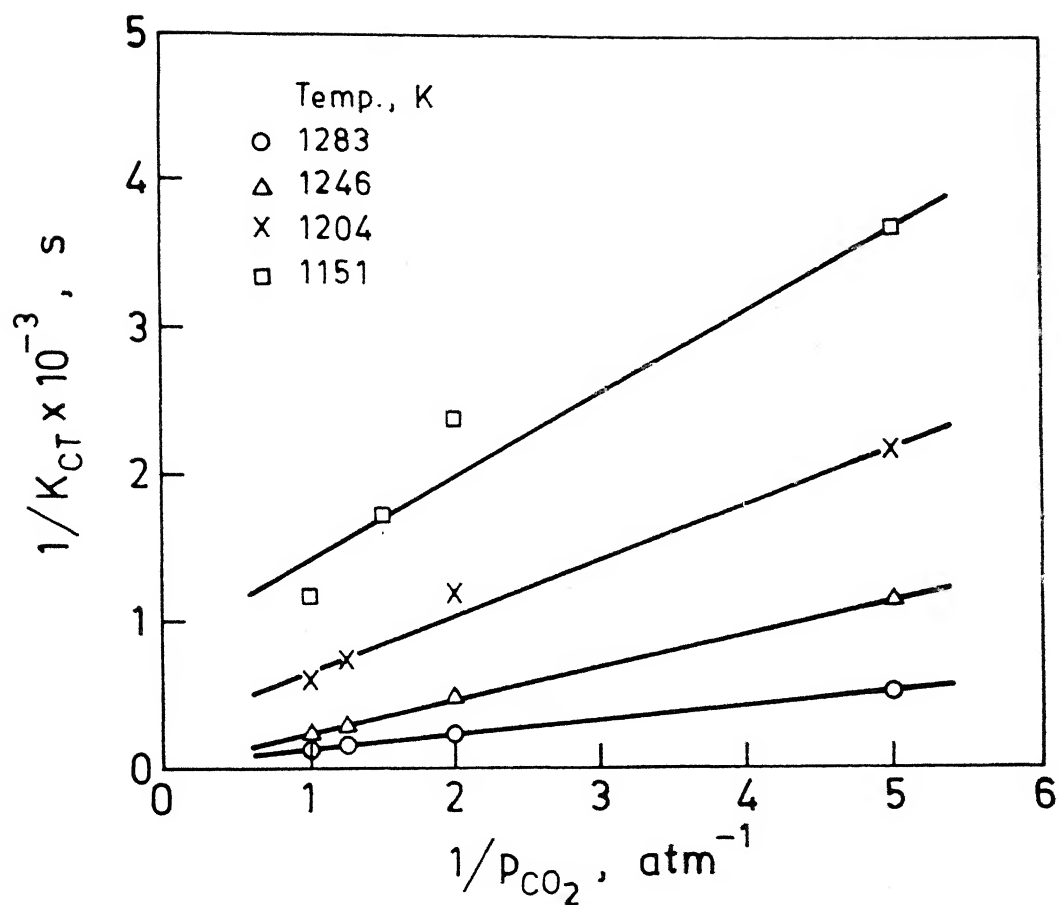


Fig. 6.12. $1/K_{CT}$ vs. $1/p_{CO_2}$ for coconut char in CO_2 , CO_2 -Ar.

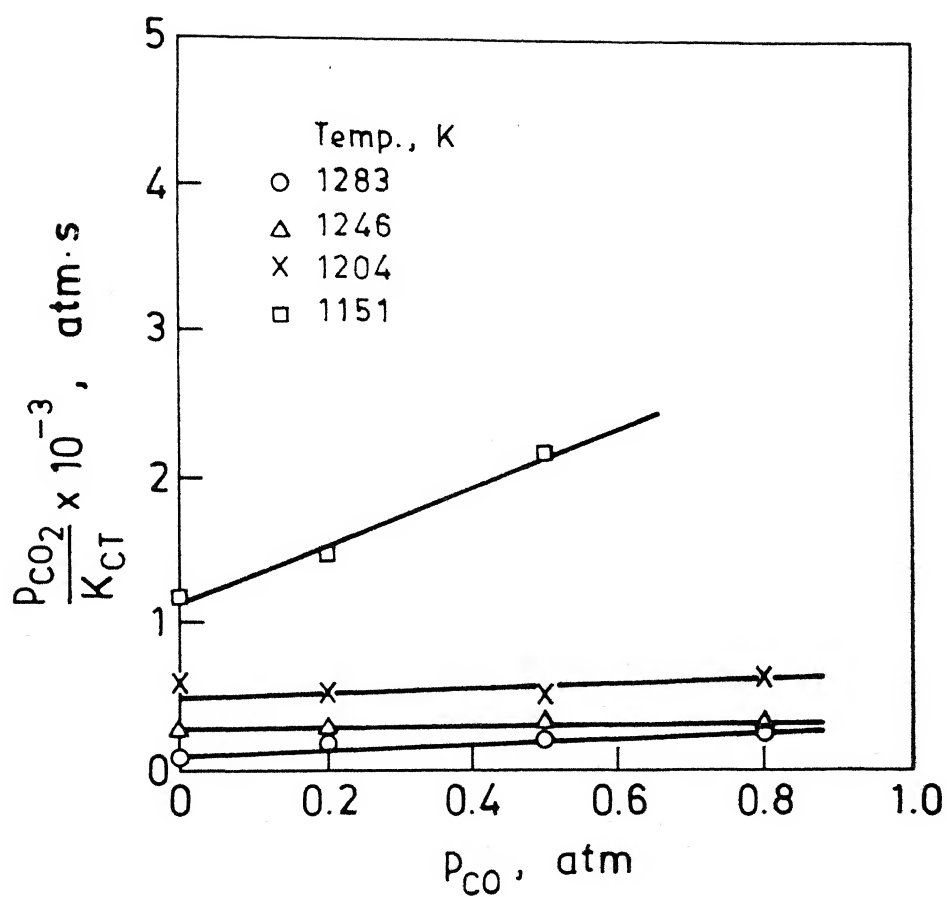


Fig. 6.13. P_{CO_2}/K_{CT} vs. P_{CO} for coconut char in CO_2 -CO.

within the limit of scatter of data, straight lines were fitted by regression analysis and from the slopes and intercepts of the plots, I_1 , I_2 , I_3 values were calculated. Fig.(6.14) presents the temperature dependence of the parameters in Arrhenius type of plots. It may be noticed from Fig.(6.14) that the values I_1 could be reasonably well fitted in Arrhenius type plot. For I_3 , scatter is more. Even then a straight line fitting of $\ln I_3$ vs. $1/T$ is approximately all right. However, for I_2 , $\ln I_2$ vs. $1/T$ does not satisfactorily yield a straight line. The values of activation energies calculated from the slopes of the I_1 , I_2 , I_3 plots are 155 kJ/mol, - 165 kJ/mol and - 251 kJ/mol respectively. Wu et al. (50) have compiled the activation energy values of I_1 , I_2 , I_3 for different workers under various experimental conditions and are reproduced in Table 6.8.

It is apparent from Table 6.8 that there exist a very wide variation of activation energies reported by different workers. Though the absolute values are differing, the activation energy values of I_1 are positive. The present value of 155 kJ/mol is lower than all the values reported in literature. Except Biederman(103), all other workers have reported negative activation energy for I_2 . The present value of I_2 matches quite well with Wu et al. (50) for coke. Again both positive and negative activation energy values for I_3 have been reported in literature and there exist a wide variation. Activation energy for I_3 determined for coconut char from the present study is found to be quite high compared to what have been reported in literature.

However, looking at the scatter of the I_2 and I_3 values in the Arrhenius plot, it appears that the activation energy values

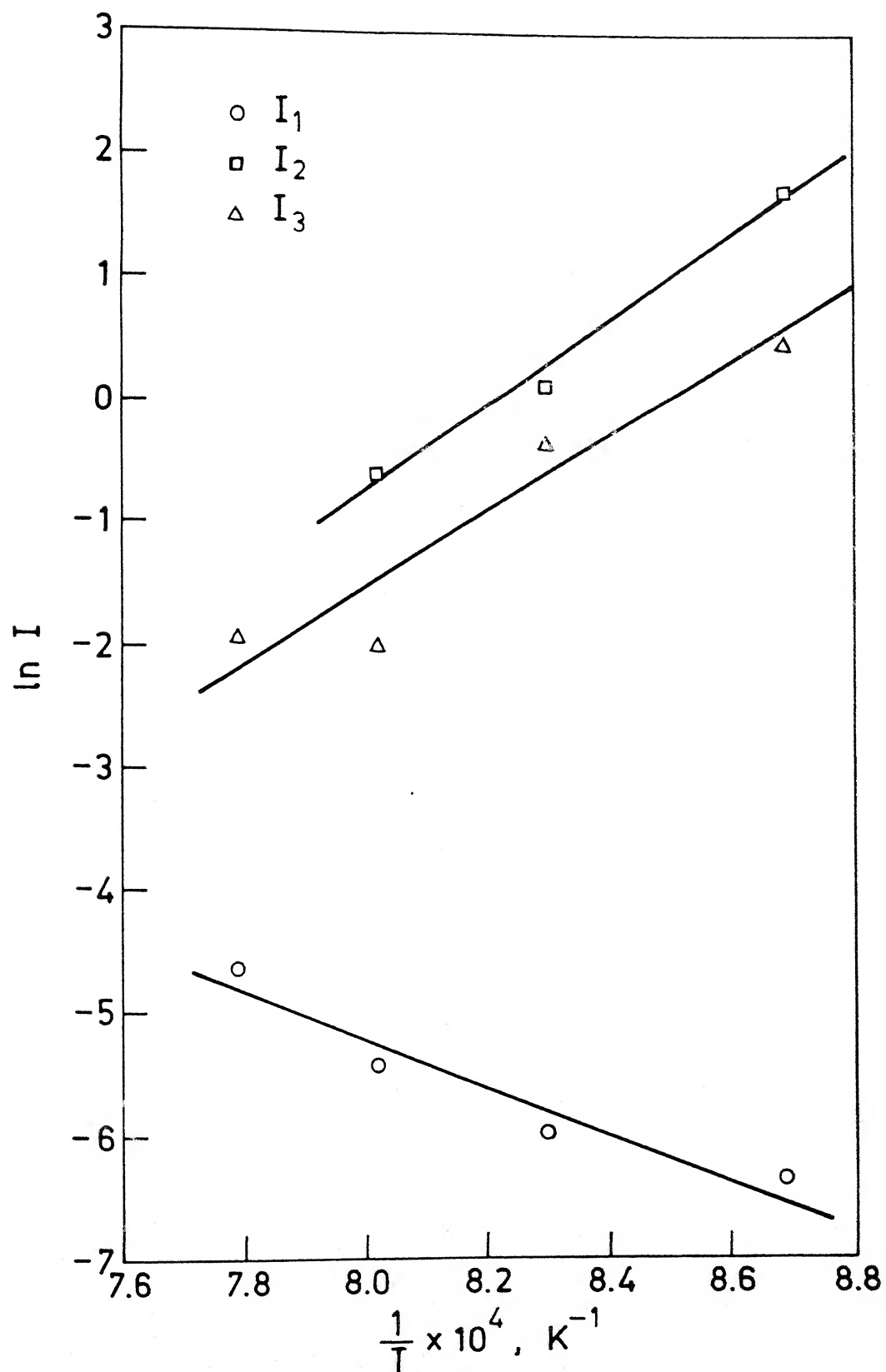


Fig. 6.14. $\ln I$ vs. $1/T$ for coconut char.

calculated for the two parameters are somewhat unreliable. In the determination of I_1 , I_2 and I_3 , it was intended to calculate transfer limitation by method of Roberts and Shatterfi. Noticing the unreliability of I_2 , no further attempt has been made in this direction.

Table 6.8: Activation energy (kJ/mol) values of I₁, I₂, I₃ for different workers

Worker	Gadsby et al (10)	Wu(50)	Wu(11)	McBridge(100)	Stranger et al(101)	Mentser et al(102)	Biederman(103)	Present study
Carbon	Coconut Char	Electrode Graphite	Coke	Coke	SP-I Graphite	Spheron-6	SP-I Graphite	Coconut char
E ₁	246.1	205.15	258.3	200.0	414.4	221.8	433.2	155.0
E ₂	-190.46	-257.19	-168.7	- 64.46	- 54.42	- 92.09	29.30	-165.0
E ₃	126.0	- 30.14	- 25.53	- 26.79	50.23	- 20.93	129.76	-251.0

6.8 Validity of Langmuir - Hinshelwood Rate Equation

Literature review on gasification reveals that many investigators(19,23,24,32) concluded that Langmuir - Hinshelwood rate equation can suitably express the gasification process. But Hedden et al.(25) and Turkdogan et al.(29) cast doubts over the validity of Langmuir - Hinshelwood rate equation. Thus further Turkdogan et al. proposed two separate rate equations [Eqs.1.34 and 1.35] to represent gasification reaction. But the criticisms made [Sec.1.2.3] about the approach of Turkdogan and co-workers may be restated as:

Turkdogan et al. never documented the extent of disagreement of their experimental data with Langmuir - Hinshelwood rate equation and the outright rejection of same seems to be questionable. In their mechanism, Turkdogan et al. (29) assumed adsorption of C, CO₂ and CO on the carbon surface. Other investigations (7,13) showed very negligible adsorption of C, CO₂ and very slow adsorption of CO. In derivation of rate expressions, Turkdogan et al. assumed formation of two activated complexes, one in equilibrium with CO₂ and other in the reverse direction. The net rate was taken to be the difference in decomposition rates of the two complexes. The concept of two activated complexes appears to be speculative. Literature review further shows that the rate equations suggested by Turkdogan et al. has not been used by other workers subsequently.

In a recent publication, Wu et al.(50) have compiled the activation energies of the fundamental steps of gasification reaction as proposed by Reif (14) and Ergun (19). These activation energies are reproduced in Table 6.9.

Table 6.9 Activation energy (kJ/mol) values of reversible oxygen steps and gasification step for different workers

Worker	Gadsby et al.(10)	Wu et al.(50)	Wu(11)	McBridge(100)	Strange et al.(101)	Mentser et al.(102)
Sample	Coconut char	Electrode graphite	Coke	Coke	SP-I Graphite	Spheron-6
E ₁₁	246.1	205.2	258.3	200.5	414.4	221.8
E _{j1}	- 70.3	- 21.9	115.1	162.8	309.7	150.7
E _{j3}	120.1	235.3	283.8	227.3	364.2	242.8

E₁₁, E_{j1} are the activation energies of forward and backward reaction of reversible oxygen exchange step respectively

E_{j3} is the activation energy of gasification step

Wu et al. have pointed out the following salient features from the activation energy values presented in Table 6.9.

The activation energy for the reverse reaction of oxygen exchange step (E_{j1}) was found to be negative for Wu(50) and Gadsby (10). Negative value of activation energy is not possible if the oxygen exchange mechanism is valid. Reif(98) suggested that the value of -70.3 kJ/mol of Gadsby et al. may be attributed to the experimental error. Again Wu et al. have shown that even an error of 5% may change the sign of E_{j1} for their experimental data. However, from negative value of E_{j1} and considerable disagreement in the calculated equilibrium constants of the oxygen exchange step for different investigators (11,19,23,50,55,100), they have expressed their doubts, that either the oxygen exchange mechanism and thus the Langmuir - Hinshelwood rate equation is not valid or the rate constants for the same have been misinterpreted.

As the literature review in Chapter 1 points out that amongst the investigators quoted, only Turkdogan and coworkers(29) had collected experimental data carefully in a wide range of gas composition in CO - CO₂ mixture. However, it is surprising that Wu et al.(50) have not used these data, and have based their conclusions on old data in limited gas composition. This makes it difficult to rely on the conclusions of Wu et al. properly.

In case of the present study, the gas composition ranged between 0% CO to 80% CO. It may be noticed from Fig. (6.12) that $1/K_{CT}$ versus $1/p_{CO_2}$ plots for coconut char have a tendency to deviate from linearity at low temperatures. Again as Fig.(6.14) indicates, the temperature dependence of I_1 , I_2 , I_3 show considerable scatter for

both I_2 and I_3 especially I_2 . On the other hand pCO_2 / K_{CT} versus pCO [Fig. (6.13)] plots show quite reasonable straight line fitting for the present investigation. $1/K_{CT}$ versus $1/pCO_2$ plots [Fig. 6.12] at high temperatures and Arrhenius plot for I_1 [Fig. 6.14] also give straight line representation of data.

If Langmuir - Hinshelwood rate mechanism is valid then one can expect linear variation under all situations. With partial fulfilment of these requirements, it is not possible to conclude with confidence whether Langmuir - Hinshelwood rate equation is valid or not. In this regard, the conclusions arising out of the present investigation tend to agree with those of Wu et al. (50).

CHAPTER 7

RESULTS AND DISCUSSIONS ON CARBOTHERMIC REDUCTION

Through literature review of carbothermic reduction, it may be noticed that reduction of iron oxide in presence of solid carbon takes place via a two stage process i.e. (a) gasification of carbon and (b) reduction of iron oxide by reducing gas, namely CO. So, for carbothermic reduction of iron oxide to take place, it is necessary that carbon has to be gasified first and thus kinetics of carbon gasification is an integral part of reduction of iron oxide by carbon. Keeping the above sequence of reactions in mind, gasification results and discussions have been presented earlier.

Again it has been pointed out in the plan of the work that comparing the activation energies of carbothermic reduction and gasification of carbon, investigators(110,121,122) have reached at the conclusion that gasification is the rate controlling step for the overall carbothermic reduction.

Many investigators(114,122,123) noticed significant enhancement of rate of carbon loss in reduction of iron oxide by carbon due to the catalytic effect of freshly produced iron. On the other hand, even with powder mixture of iron oxide and carbon, Fruehan(119) observed no catalytic effect and concluded that it was due to high reactivity of the form of carbon (coal char, coconut char) used.

In this study, coconut char has been employed as the carbonaceous material to verify the conclusion reached by Fruehan. Since it had been planned to try to predict the rate of carbothermic reduction from that of gasification rate data, efforts were required

to avoid catalysis by reduced iron since that would interfere with this exercise. This was another reason for choosing coconut char as the reducing agent.

The following combinations of iron oxide and coconut char were used for the present set of studies:

(a) iron oxide powder (-325 mesh) and coconut char powder (-200 +230 mesh) mixture

(b) iron oxide micropellet (\approx 2 mm dia.) and coconut char powder (-200 + 230 mesh) mixture.

The stoichiometric ratio of C/Fe₂O₃ was maintained to 2.0 for all the experiments so that carbon was present in excess to avoid starvation.

The experimental conditions used are summarized in Table (7.1).

Table 7.1 Experimental conditions used for carbothermic reduction

<u>Expt. No.</u>	<u>Condition</u>	<u>Temperature (K)</u>
1	1	1284
2	1	1208
3	1	1145
4	1	1078
5	2	1284
6	2	1235
7	2	1210
8	2	1145

Condition 1 : Iron oxide powder + Coconut char powder

Condition 2 : Iron oxide micropellet + Coconut char powder

7.1 Measurement Errors

Experiments on carbothermic reduction of iron oxide could be divided into two parts:

- (a) weight loss measurement
- (b) product gas analysis

Weight loss measurement experiments were carried out in the thermogravimetry set-up, described in sec.2.3. It has already been mentioned in sec.3.2.3 that efforts were made to simultaneously measure the weightloss as well as the online analysis of the product gas. But due to some problems the scheme could not be executed and thus the set-up outlined in sec.(2.4) was employed for gas analysis experiments.

7.1.1 Errors in weight loss measurements

The reaction chamber consisted of inconel bucket which contained the ceramic crucible, alongwith stainless steel gas outlet tube. The balance used for gasification study was also employed for carbothermic reduction. It was found that the weight of the gas outlet tube and the inconel bucket changed from run to run due to oxidation. Oxidation was quite apparent from the change in colour of the metallic surface. So blank runs i.e. weight change measurement of the hanging assembly alongwith the empty bucket was carried out in argon atmosphere. It was observed that there was only 0.5% weight gain in 90 minutes, which for all practical purposes can be neglected. So the oxidation of the gas outlet tube and the crucible primarily took place when they were taken out of the furnace at hot condition after completion of a run. Again a constant supply of argon was maintained in the furnace during the course of the experiments. So it is expected

that neither the gas outlet tube, nor the reaction chamber underwent any appreciable oxidation during measurements and thus did not contribute any significant error in the weight loss values.

To check the reproducibility of weight loss data, each and every experiment was repeated at least twice. It was found that the percentage total weight loss for all the experiments were reproducible within a range of ± 4 .

7.1.2 Error in gas analysis

In the case of gas analysis experiments, a single quartz tube served the purpose of both reaction chamber and the gas outlet tube. Amount of sample taken was representative of weight loss measurements. As the sample amount was low, the quantity of gas generated was also quite low. This necessitated working with the minimum possible dead volume in the quartz tube as well as in the tube connecting the gas chromatograph with gas outlet tube. This was achieved by introducing thermocouple sheath with another protection tube in the reaction chamber and flexible wires in the gas chromatograph connecting tube. With this, the final dead volume was found to be less than 5 cc which was accepted to be quite satisfactory.

Again at the initial stage of the reaction, the product gas pushed out the air entrapped in the dead volume. So the gas analysis did not give the true composition of the product gas at the early stage of reduction and hence discarded. An approximate calculation of rate of gas generation revealed that at least 1.5 minutes were necessary to make the chamber free from air.

Sampling of the product gas was started when gas bubbled through the bubbler at the exit of the gas chromatograph. As the reaction progressed, it was observed that the bubbling of the gas stopped even though the reaction was not complete. It was due to the fact that at the advanced stage of reduction, the amount of gas generated was so low that it could not overcome the path resistance of the gas chromatograph auto sampler coil. Again it was difficult to make more than two samplings for one experiment in many cases. So a number of experiments were performed at each condition to fully describe the path of the gas composition variation with time. As such, no repeat experiment was performed to check the reproducibility of the analysis but the correctness of data is beyond doubt because only one gas composition line was generated from data points of different experiments under identical conditions and they exhibited a smooth variation.

7.1.3 Error in temperature measurement

The temperature history of the bed during reduction was registered by introducing a chromel-alumel thermocouple into the reaction chamber. Initially the bare tip of the thermocouple was made to touch the bed. But it suffered from the following two disadvantages.

The thermocouple tip when directly exposed to the product gas used to break quite frequently. This caused problem in bed temperature measurement. Secondly, when the chromel-alumel thermocouple tip is exposed to CO-CO₂ gas mixture for either long time or under repeated use, the characteristic of the material changes and thus the temperature measured would be erroneous. Both the problems were avoided by putting a quartz tube of smaller diameter than the reaction

chamber, around the thermocouple. This protection tube served two purposes:

(a) it protected the thermocouple tip from the attack of the product gas

(b) it drastically reduced the dead volume of the reaction chamber

Trial runs were carried out to find the difference in the measured bed temperature with and without the protection tube around the thermocouple. It was observed that when thermocouple was covered with the quartz tube, the temperature was $2-3^{\circ}\text{C}$ lower than if the tip is not protected. So adequate correction was made in the bed temperature values measured by thermocouple with protection tube.

Again the steady state value of the bed temperature was found to be around $15-20^{\circ}\text{C}$ lower than the furnace control temperature. The experimental temperatures reported are the steady state values of the bed.

7.2 Rate Calculation Procedure

It has already been pointed out in Sec.1.3.2 that the weight loss measured during carbothermic reduction consisted of:

- (a) weight loss due to gasification of carbon
and (b) weight loss due to removal of oxygen from iron oxide.

So, to calculate the rate or the percentage reduction, it is necessary to find out the contribution of each category, mentioned above to the total weight loss. Sec.1.3.2 presents a method for the same. It may be noted that the procedure presented needs the values of the volumetric rates of gas generation as a function of time. But for the present set of studies, gas chromatograph was used to directly

estimate the gas composition at any time $t=t$. Thus the procedure of rate calculation was modified and it may be presented as below:

$$\Delta W_C + \Delta W_O = \Delta W \quad \dots(7.1)$$

where

ΔW_C = weight loss due to gasification at any time $t=t$

ΔW_O = weight loss due to oxygen removal from oxide at any time $t=t$

and ΔW = total weight loss at any time $t=t$

Differentiating Eq.7.1 with respect to time

$$\frac{dW_C}{dt} + \frac{dW_O}{dt} = \frac{dW}{dt} \quad \dots(7.2)$$

or

$$\dot{W}_C + \dot{W}_O = \dot{W} \quad \dots(7.3)$$

where

$$\dot{W}_C = \text{rate of weight loss of carbon} = - \frac{dW_C}{dt}$$

$$\dot{W}_O = \text{rate of weightloss of oxygen} = - \frac{dW_O}{dt}$$

and

$$\dot{W} = \text{rate of total weight loss} = - \frac{dW}{dt}$$

If \dot{Q} is the rate of gas generation, then

$$\dot{W}_C = (\dot{Q} \cdot X_{CO} + \dot{Q} \cdot X_{CO_2}) \times \frac{12}{22400} \quad \dots(7.4)$$

$$= \dot{Q} (X_{CO} + X_{CO_2}) \times \frac{12}{22400} \quad \dots(7.5)$$

and

$$\dot{W}_O = (\dot{Q} \cdot X_{CO} + 2\dot{Q} \cdot X_{CO_2}) \times \frac{16}{22400} \quad \dots(7.6)$$

$$= \dot{Q} (X_{CO} + 2 X_{CO_2}) \times \frac{16}{22400} \quad \dots(7.7)$$

Combining Eqs.(7.5) and (7.7)

$$\frac{\dot{W}_c}{\dot{W}_o} = \frac{X_{CO} + X_{CO_2}}{X_{CO} + 2X_{CO_2}} \cdot \frac{3}{4} \quad \dots(7.8)$$

$$\text{or } \dot{W}_o = \frac{X_{CO} + 2X_{CO_2}}{X_{CO} + X_{CO_2}} \cdot \frac{4}{3} \times \dot{W}_c \quad \dots(7.9)$$

Putting the expression for \dot{W}_o in Eq.7.3

$$\dot{W}_c \left(1 + \left(\frac{X_{CO} + 2X_{CO_2}}{X_{CO} + X_{CO_2}} \right) \cdot \frac{4}{3} \right) = \dot{W} \quad \dots(7.10)$$

$$\text{or } \dot{W}_c = \dot{W} / \left(1 + \frac{X_{CO} + 2X_{CO_2}}{X_{CO} + X_{CO_2}} \cdot \frac{4}{3} \right) \quad \dots(7.11)$$

Now knowing the values of X_{CO} and X_{CO_2} at different times(t), it is possible to calculate the instantaneous rate of carbon loss. An equivalent expression of Eq.(7.11) may be written as below to find out the instantaneous rate of oxygen loss.

$$\dot{W}_o = \dot{W} / \left(1 + \frac{X_{CO} + X_{CO_2}}{X_{CO} + 2X_{CO_2}} \cdot \frac{3}{4} \right) \quad \dots(7.12)$$

So the total carbon loss at any time $t = t$ may be given by

$$(\Delta W_C)_{t=t} = \int_0^t \dot{W}_C \cdot dt \quad \dots(7.13)$$

Hence

$$(\Delta W_O)_{t=t} = (\Delta W)_{t=t} - (\Delta W_C)_{t=t} \quad \dots(7.14)$$

Thus, the percentage reduction of iron oxide at any time(t) is

$$\text{pct. reduction} = \frac{(\Delta W_O)_{t=t}}{\text{Total removable oxygen}} \times 100 \quad \dots(7.15)$$

To utilize the weight loss data, it is essential to have the gas composition values at the same time intervals. But it was difficult to perform gas analysis exactly at the same time instants of weight loss. In order to generate the gas composition values at the required time intervals, the measured values of fraction of carbon monoxide i.e. X_{CO} was expressed analytically as a function of time. A 7th. order polynomial fitting was found to be highly satisfactory for this purpose. Thus

$$X_{CO} = a_0 + a_1 t + a_2 t^2 + \dots + a_7 t^7 \quad \dots(7.16)$$

From the fitted co-efficient values, it was possible to calculate X_{CO} at any desirable time.

Again Eq.7.13 was used to calculate the total loss of carbon at time $t=t$. To do so, it was necessary to express the instantaneous rate of carbon loss in terms of time. Here also 7th. order polynomial was found to serve the purpose quite satisfactorily.

So

$$\Delta W_C = b_0 + b_1 t + b_2 t^2 + \dots + b_7 t^7 \quad \dots(7.17)$$

Once ΔW_C was known then the oxygen loss and the percentage

reduction was calculated using Eqs.7.14 and 7.15. An adequate computer programme was developed to calculate all the parameters needed as described above and the same has been presented in Appendix (10).

7.3 Results of the Calculations

It has been mentioned in the previous section that 7th. order polynomial was used to express both the gas composition and the rate of carbon loss as a function of time and fitting was very good. Fig.7.1 presents sample plots for gas composition and the rate of carbon loss (\dot{W}_C) to show the fitting. Fig.7.2 shows the overall reproducibility of fractional reduction of iron oxide for duplicate sets of experiments. Data points in Fig.7.2 are chosen at random for all the experiments and contains the maximum limit of variation in overall reproducibility. \dot{W}_C , \dot{W}_O , and other calculated as well as measured parameters have been presented in Figs.7.3 - 7.10. It should be mentioned here that gas analysis for powder mixture of iron oxide and coconut char at 1078K was found to be erroneous due to very slow rate of gas generation and thus discarded. So \dot{W}_C and \dot{W}_O at 1078K were calculated by using equilibrium gas composition at that temperature. Again as the fitting of gas composition and \dot{W}_C was found to be extremely good, values of the parameters presented in Figs.7.3 - 7.10 are the fitted values rather than the actual values calculated from weight loss data.

7.4 Calculation Procedure of Rate of Carbon Loss from Gasification (\dot{W}_{Cp}) and the Results

In this section, an is be made to predict the rate of carbon loss in carbothermic reduction from gasification data. Gasification rates for coconut char under various gaseous environments at different temperatures are available. From the gas analysis data in cabothermic

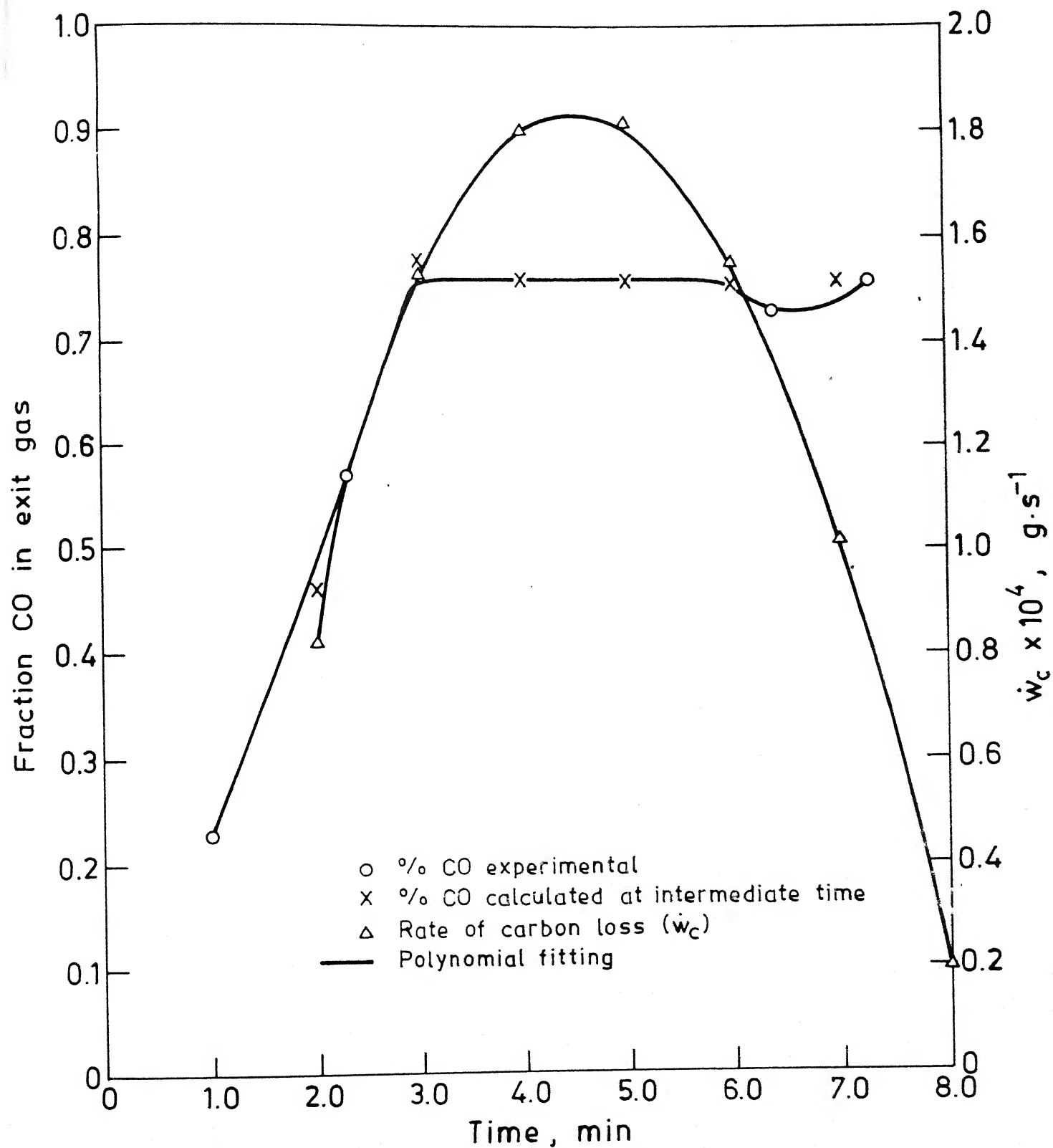


Fig. 7.1. Sample curves for exit gas composition and rate of carbon loss as function of time.

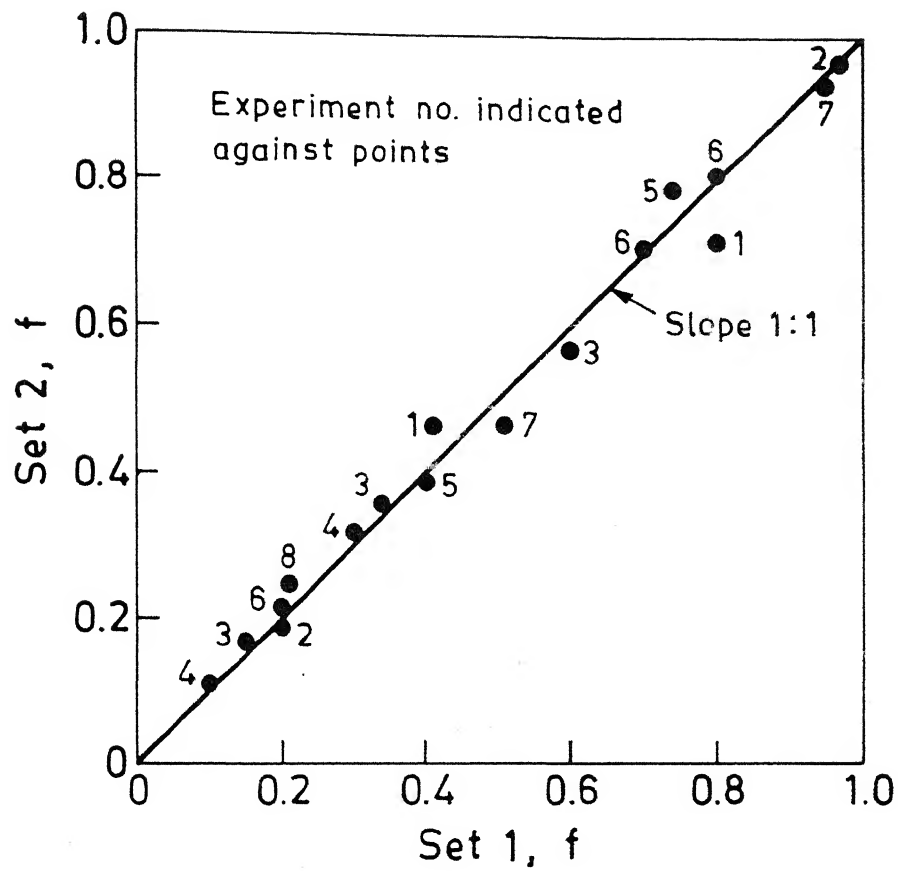


Fig. 7.2. Reproducibility of estimated fractional reduction of iron oxide amongst duplicate sets.

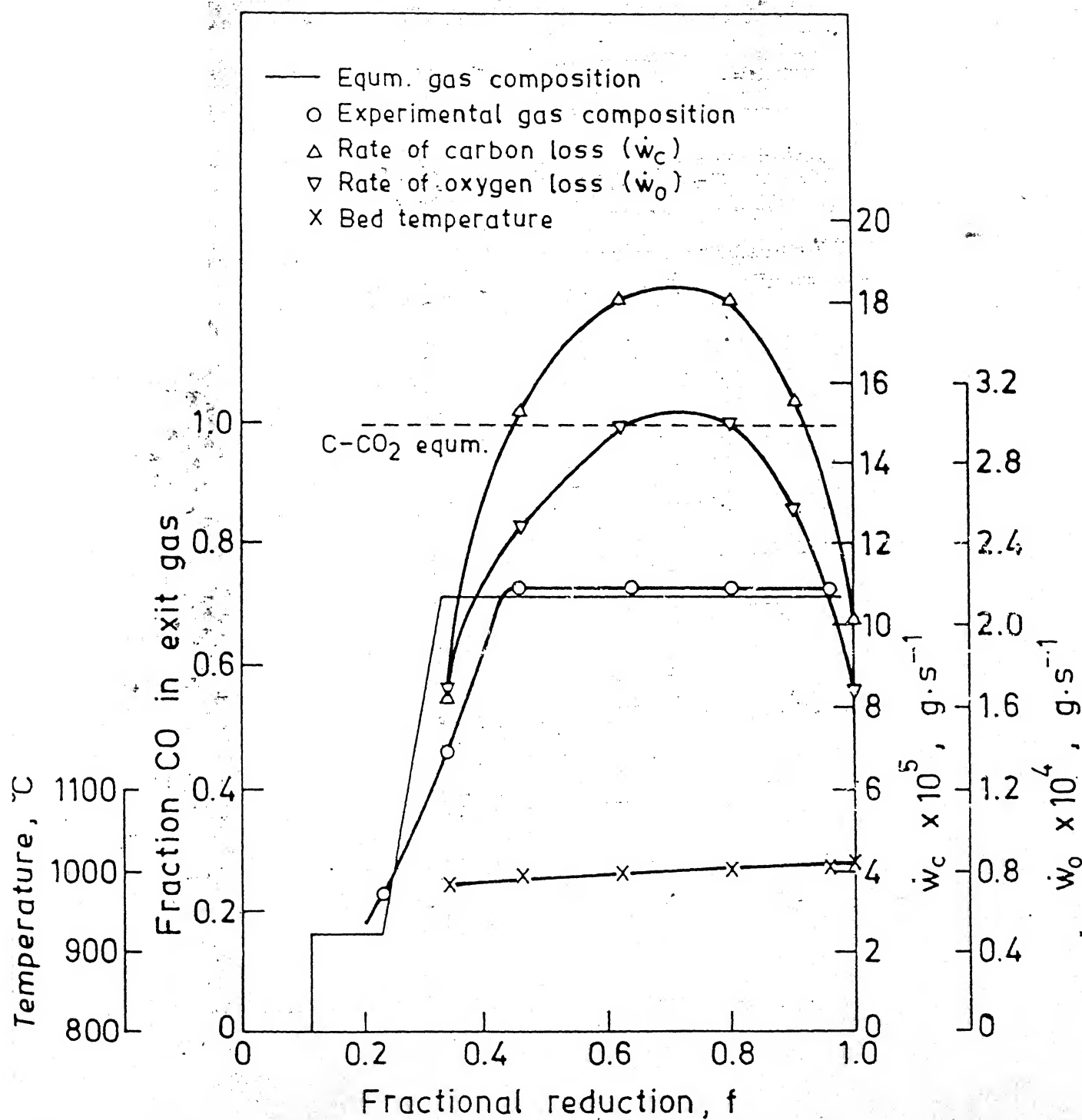


Fig. 7.3. Variation of rates, exit gas composition and bed temperature with fractional reduction (f) of iron oxide (expt. 1).

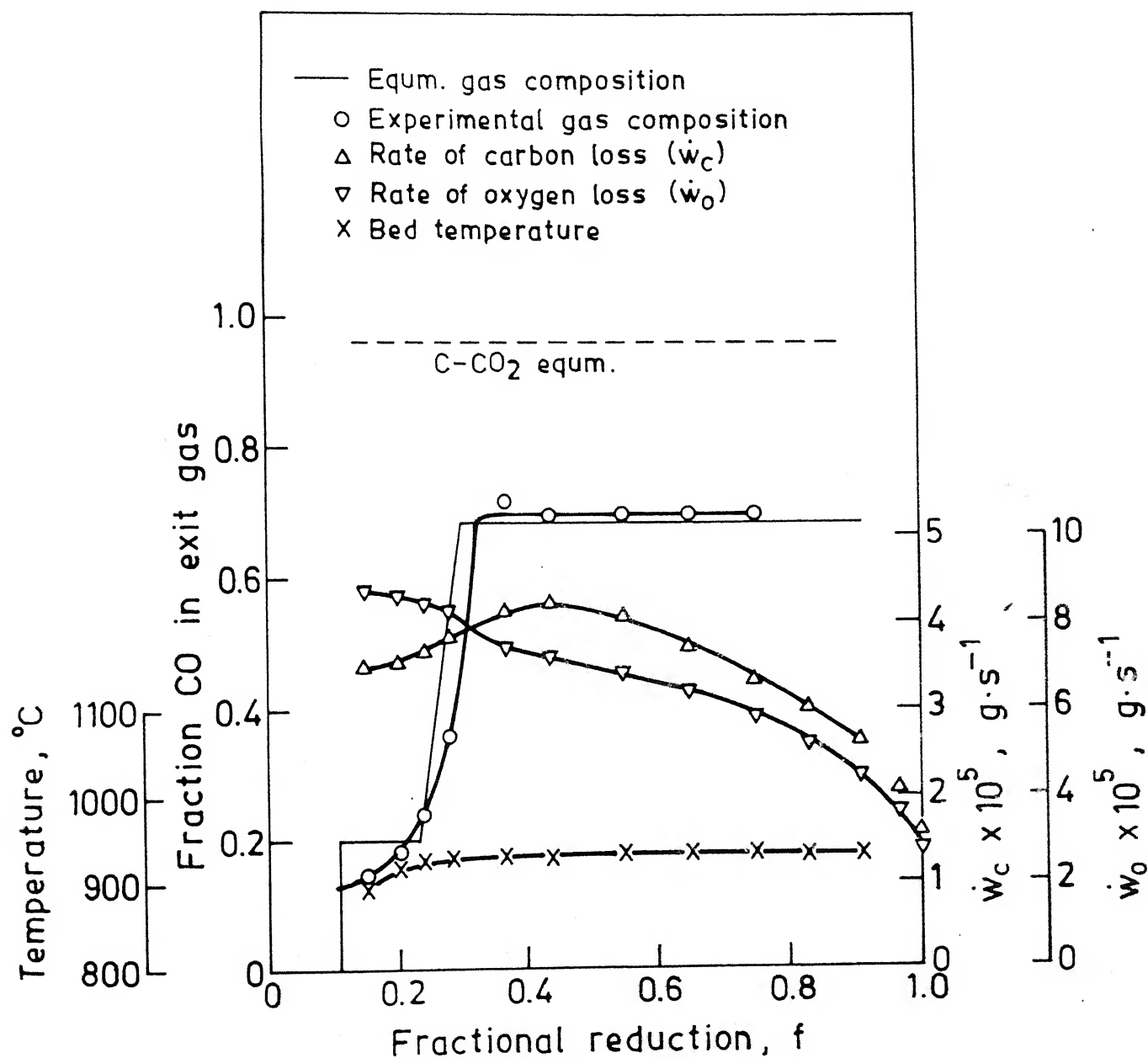


Fig. 7.4. Variation of rates, exit gas composition and bed temperature with fractional reduction (f) of iron oxide (expt. 2).

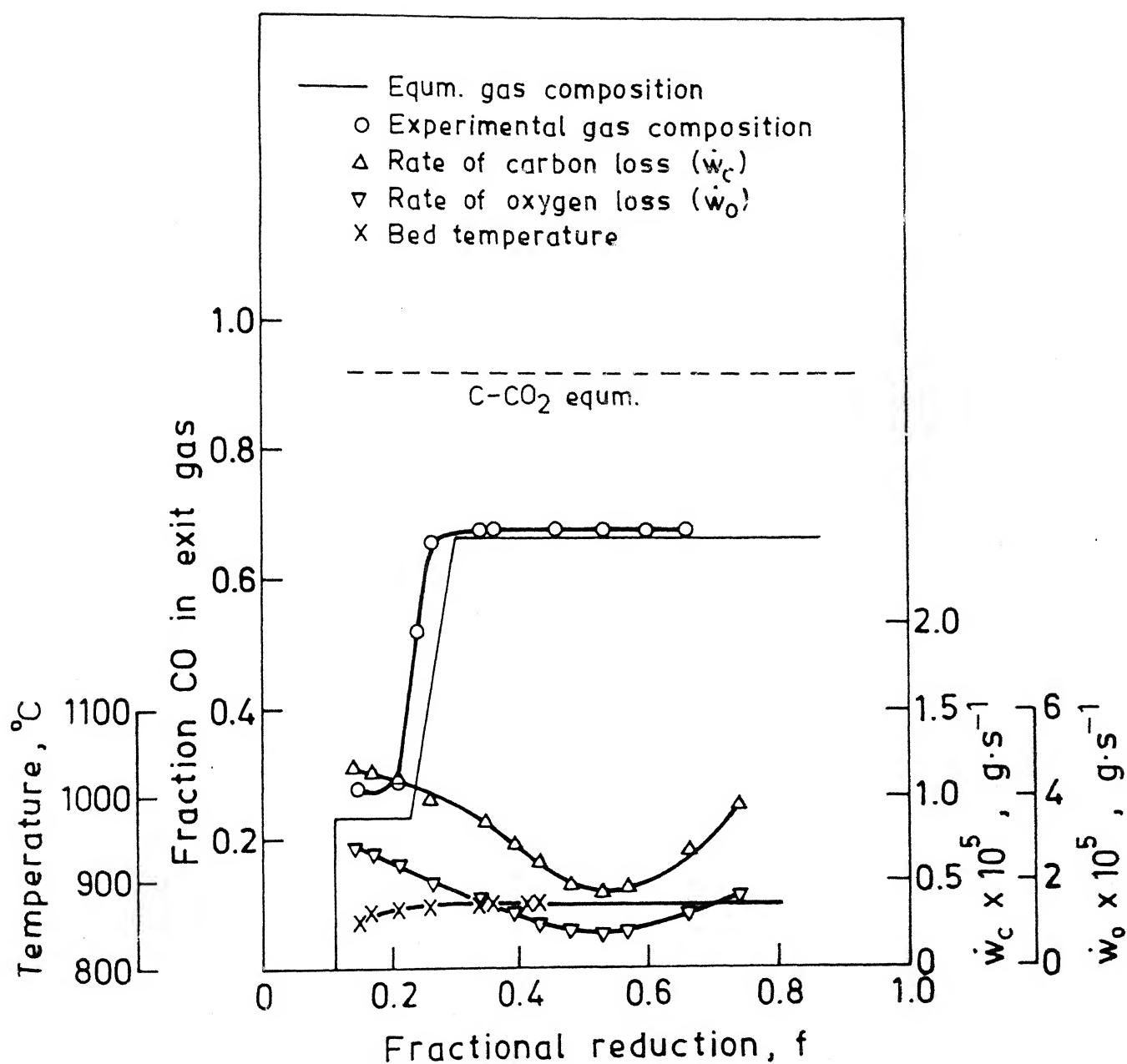


Fig. 7.5. Variation of rates, exit gas composition and bed temperature with fractional reduction (f) of iron oxide (expt. 3).

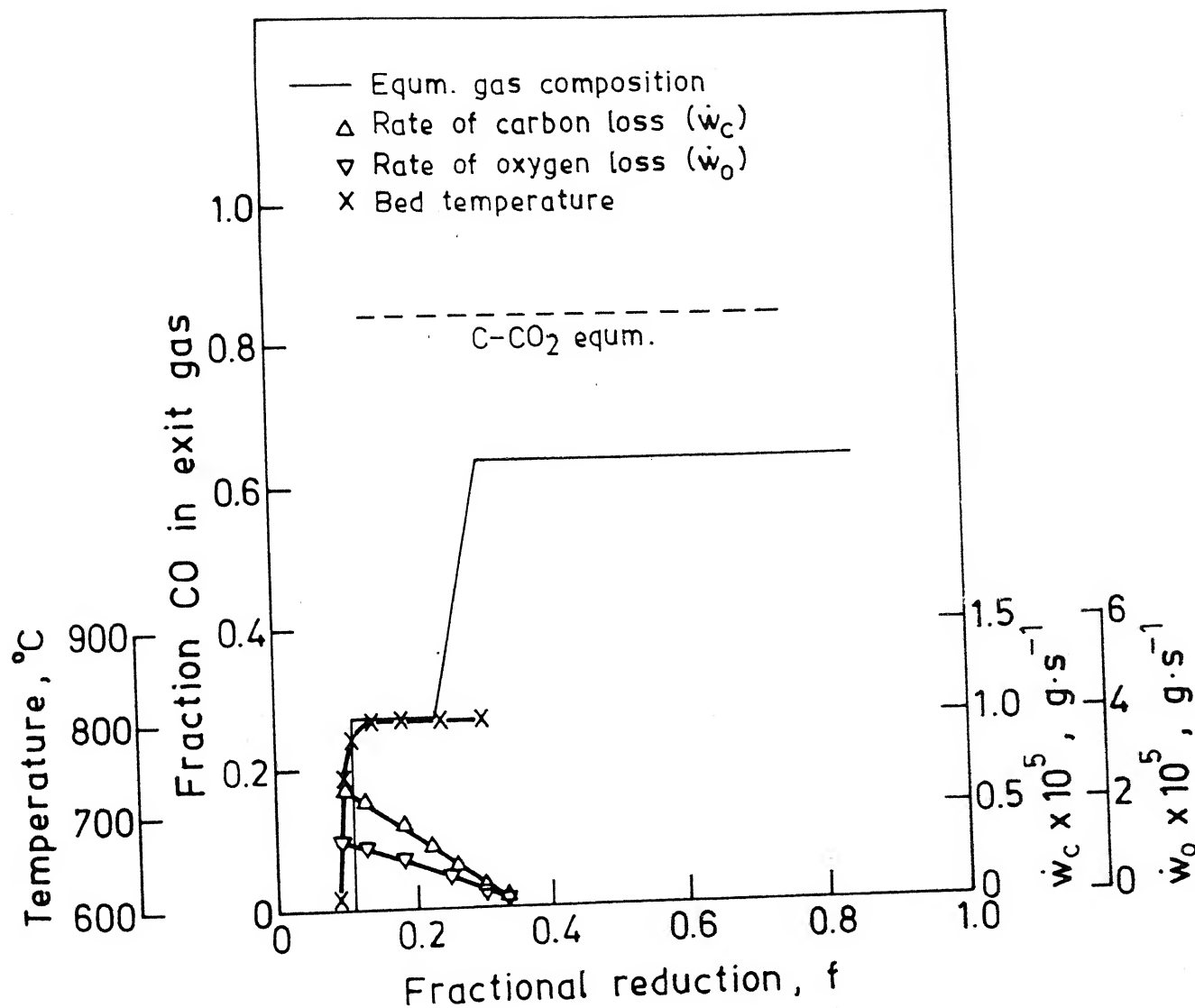


Fig. 7.6. Variation of rates and bed temperature with fractional reduction (f) of iron oxide (expt. 4).

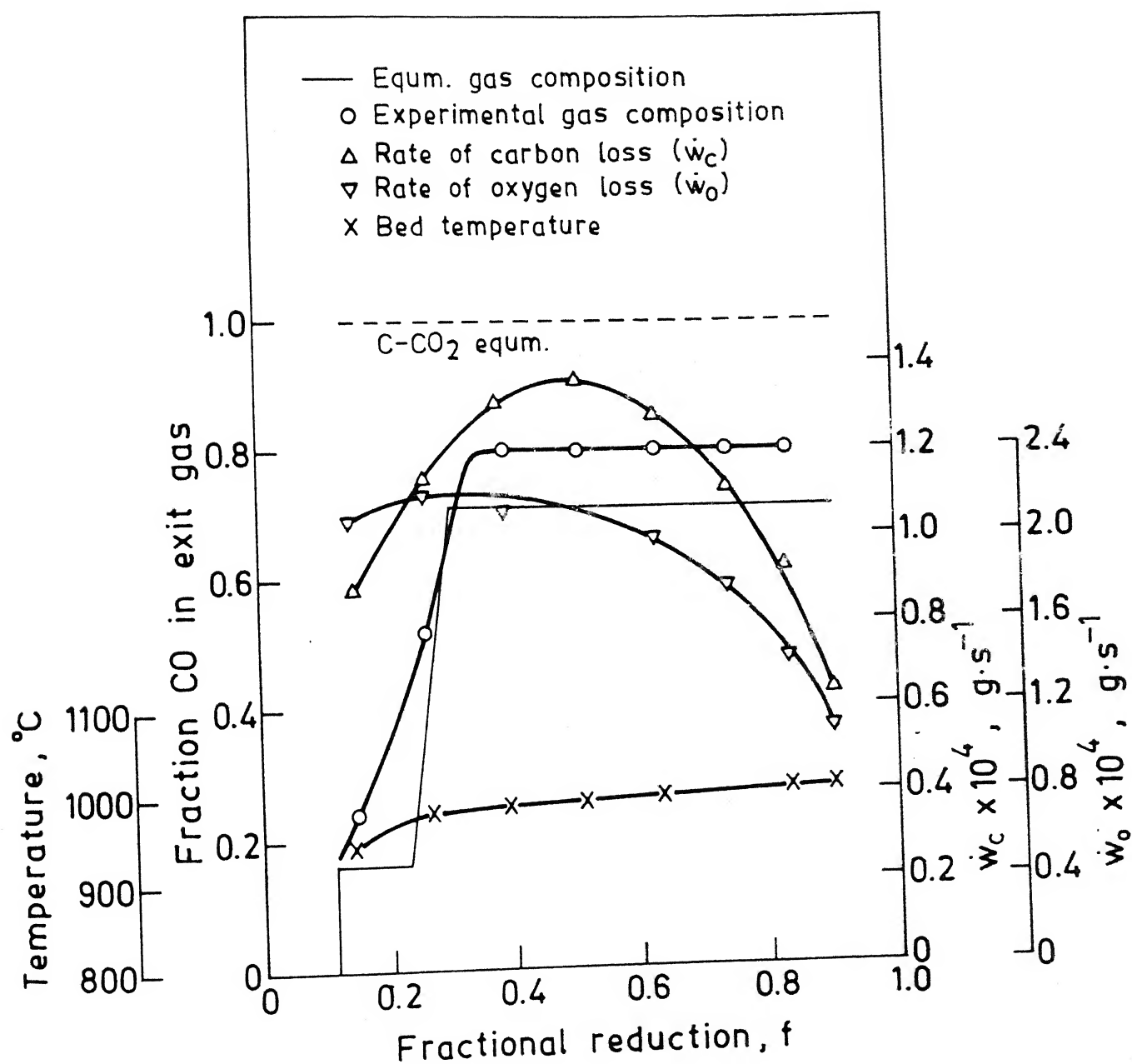


Fig. 7.7. Variation of rates, exit gas composition and bed temperature with fractional reduction (f) of iron oxide (expt. 5).

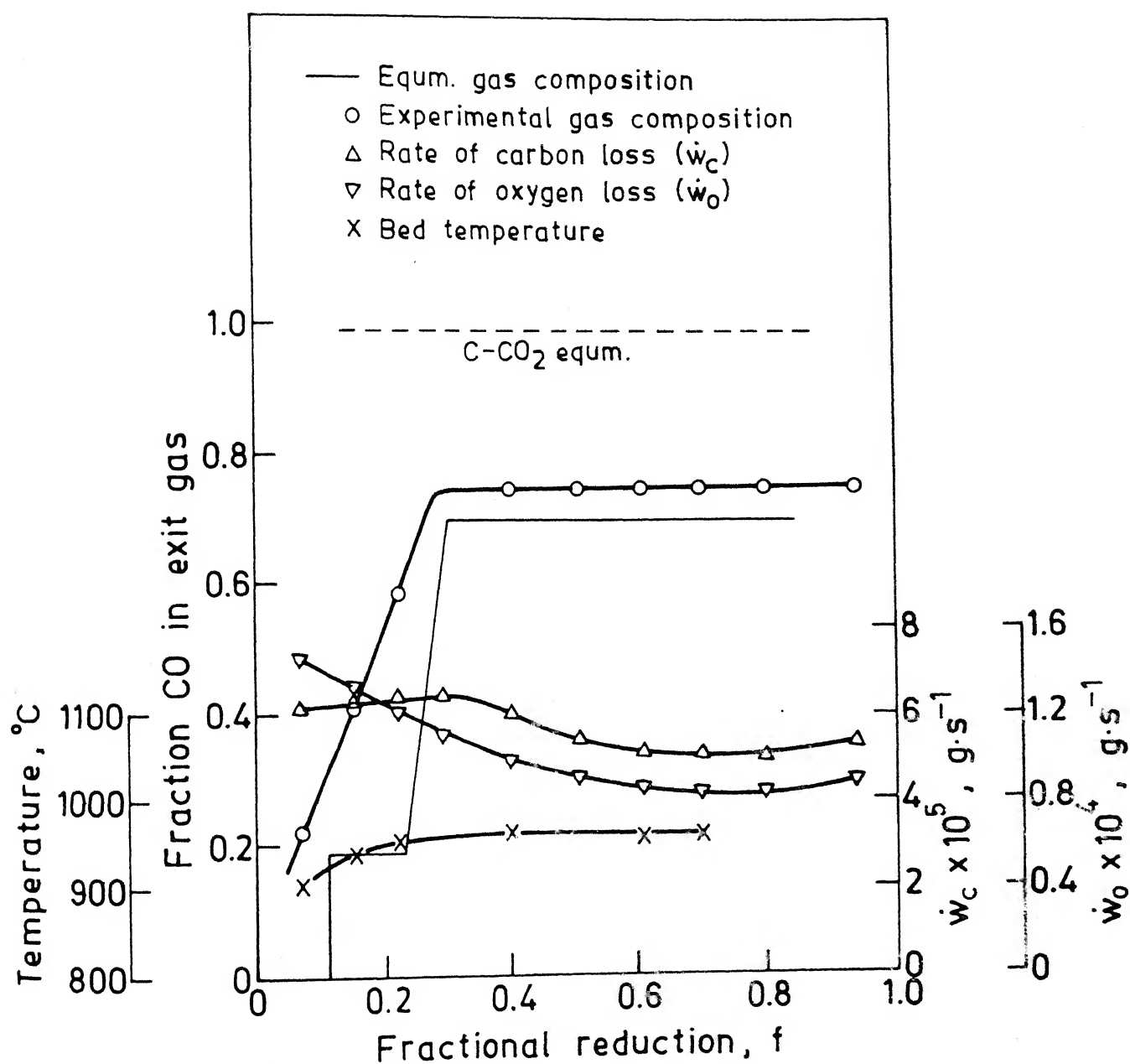


Fig. 7.8. Variation of rates, exit gas composition and bed temperature with fractional reduction (f) of iron oxide (expt. 6).

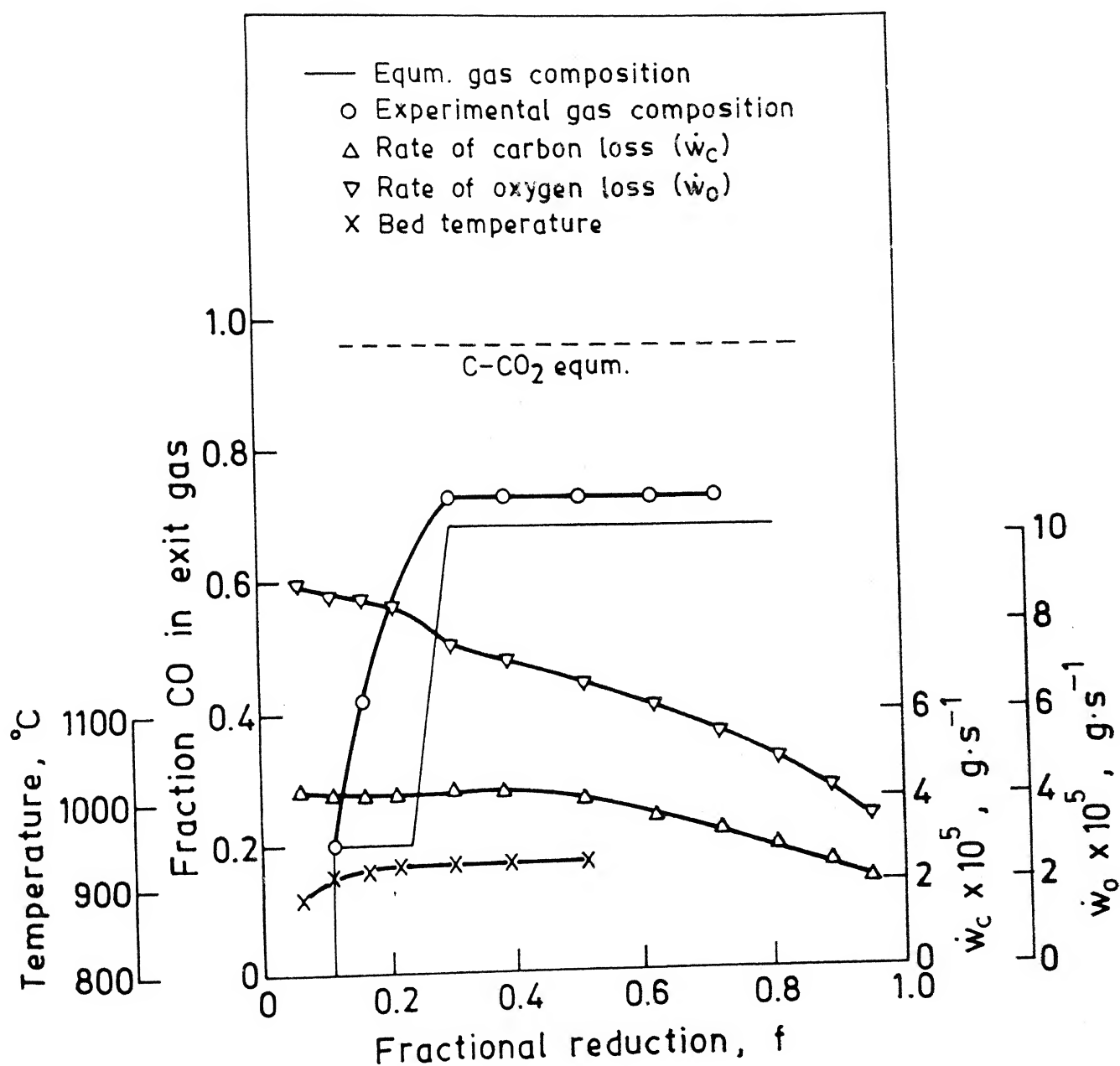


Fig. 7.9. Variation of rates, exit gas composition and bed temperature with fractional reduction (f) of iron oxide (expt. 7).

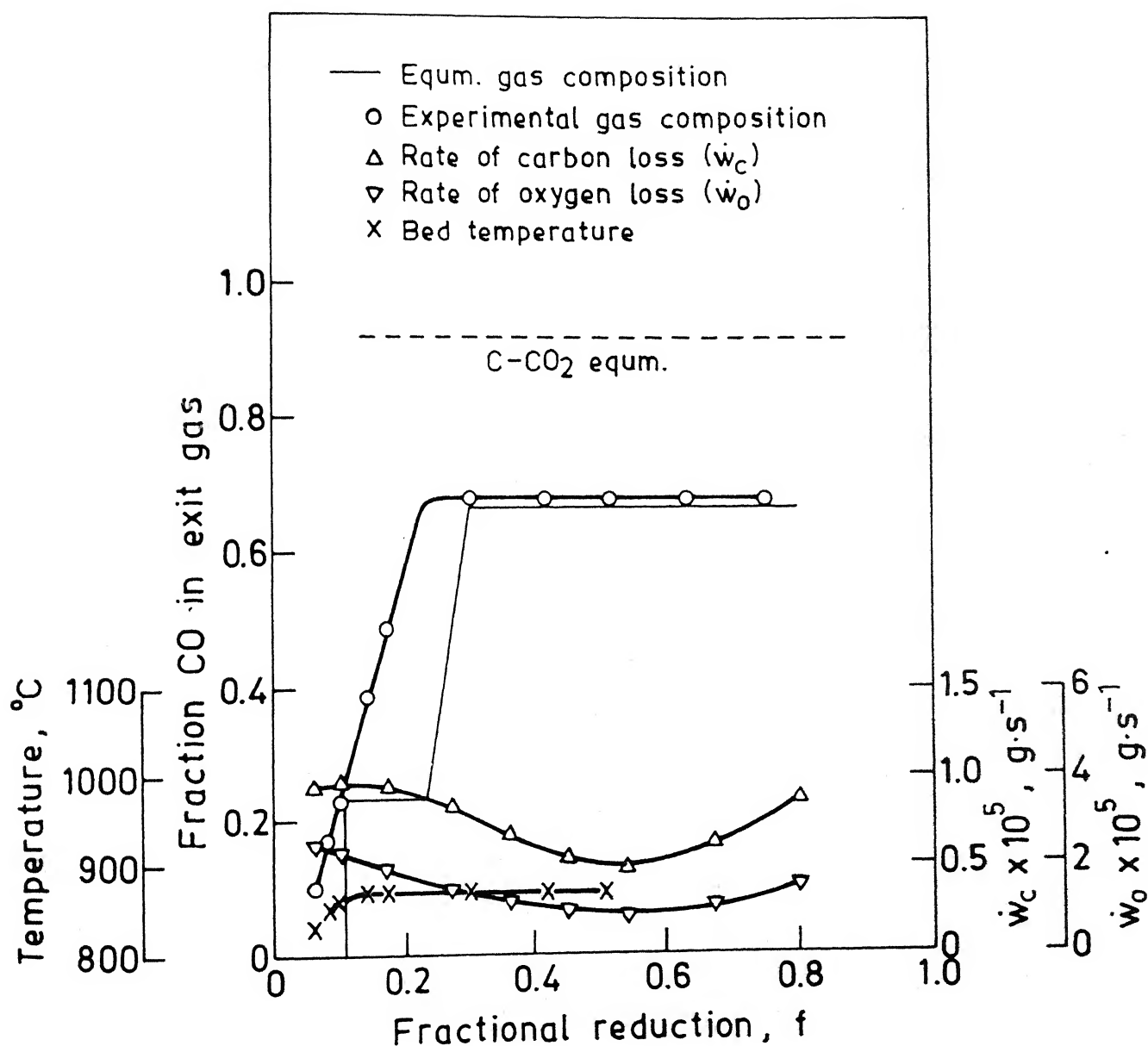


Fig. 7.10. Variation of rates, exit gas composition and bed temperature with fractional reduction (f) of iron oxide (expt. 8).

reduction, it is evident that carbon experiences a varying atmosphere of CO-CO₂ with the progress of reduction and hence proper precaution is needed to take into account the effect of gas composition on the rate at different times(t). Again the temperature of the bed was found to vary as a function of time or, in other words, is a function of fractional reduction. Thus the prediction of the rate of carbon loss in carbothermic reduction even at a fixed temperature calls for a series of rate values of gasification due to variation of bed temperature. So the predicted rate of carbon loss (g.s⁻¹) is

$$\dot{W}_{cp} = r_g (f(t) \times \emptyset (X_{CO}) \times W_c \quad \dots(7.18)$$

where $r_g (f(t))$ = rate of gasification as a function of temperature

$\emptyset (X_{CO}) = (\text{rate})_{CO-CO_2} / (\text{rate})_{CO_2}$ which is a function of X_{CO}

W_c = instantaneous weight of carbon

The \dot{W}_c calculated from the weight loss data of carbothermic reduction is associated with both heat and mass transfer limitations. So for comparison purposes, it is "more" appropriate to work with the r_g values rather than K_{CT} values.

r_g was first expressed in an Arrhenius type of plot and from the fitted coefficients, values of r_g were calculated for different bed temperatures over the experimental time intervals. Instantaneous weights of carbon were evaluated through the computer program, presented in Appendix(10). The values of the ratio of rates were obtained from the series of experiments with coconut char in CO₂ and CO-CO₂ gas mixtures(table 6.3)

\dot{W}_{cp} thus predicted have been presented in Figs. 7.11 - 7.12.

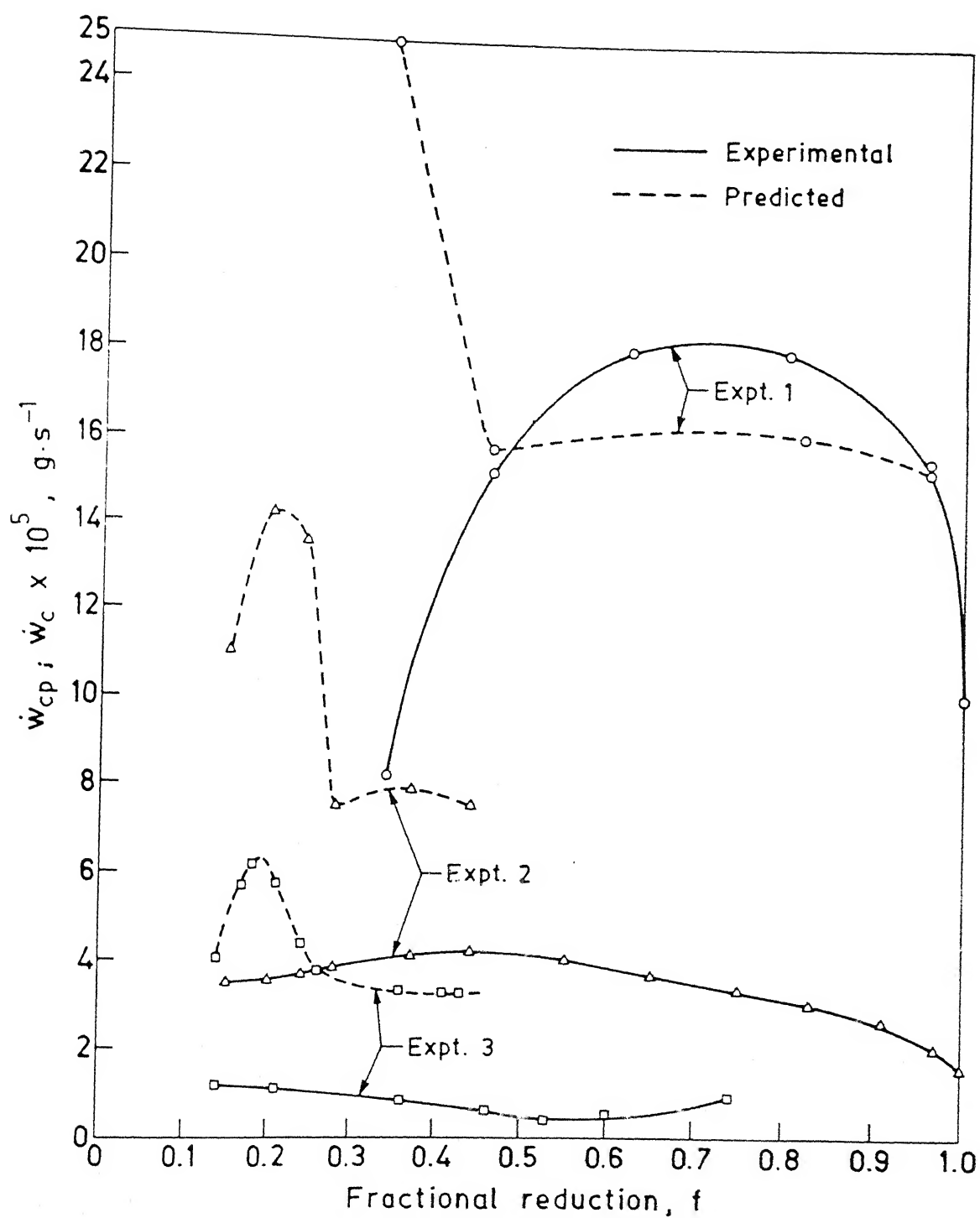


Fig. 7.11. Experimental (\dot{w}_c) and predicted (\dot{w}_{cp}) rate of carbon loss for iron oxide powder and coconut char powder mixture.

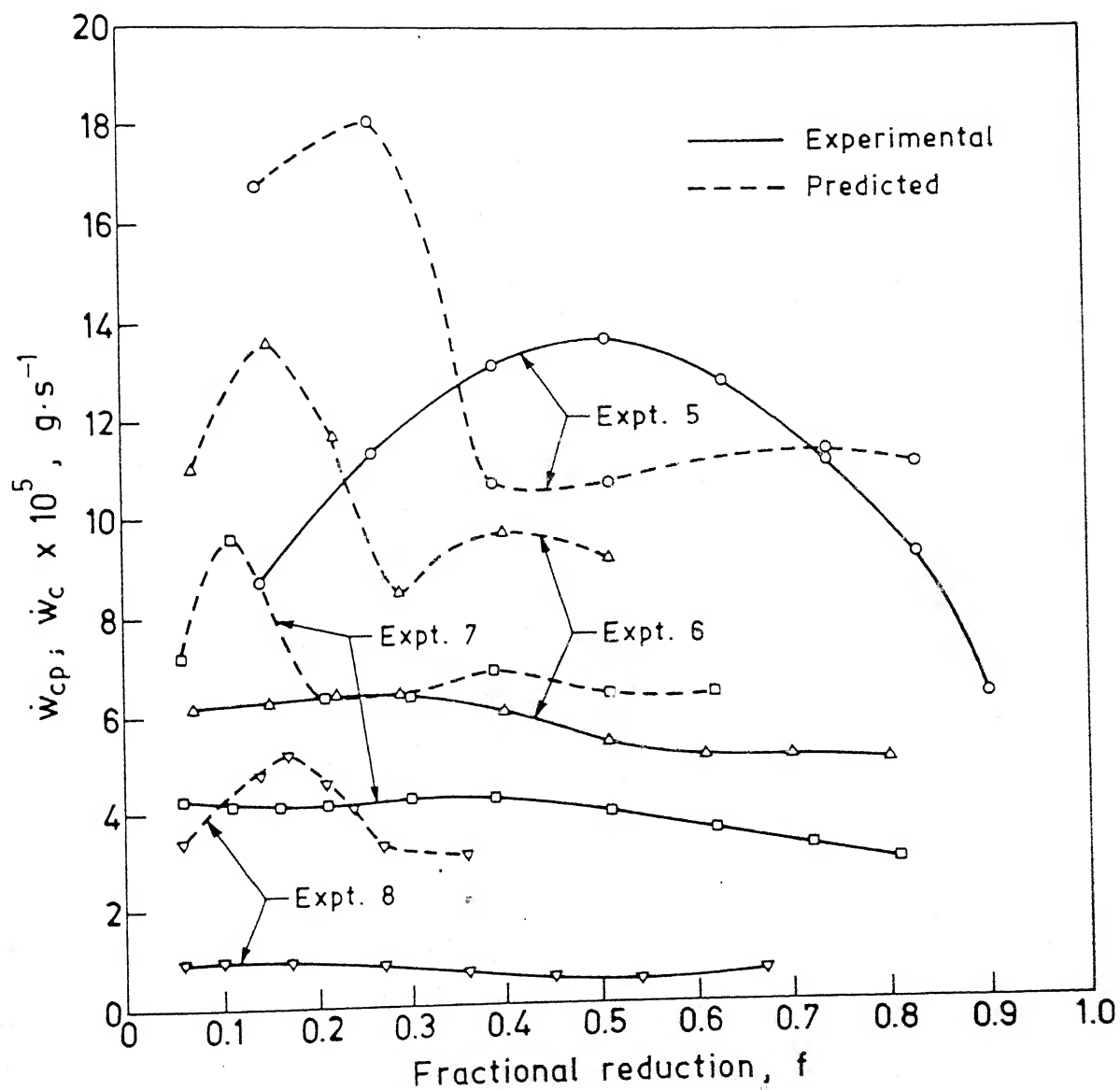


Fig. 7.12. Experimental (\dot{w}_c) and predicted (\dot{w}_{cp}) rate of carbon loss for iron oxide micropellet and coconut char powder mixture.

7.5 Discussion of Results

It may be noticed from Figs.7.3 - 7.10 that at all the temperatures, the experimental gas composition versus fractional reduction plots follow the equilibrium gas profiles for stagewise reduction and thus confirms that reduction of iron oxide by carbon took place in a stagewise manner. Again in case of iron oxide and coconut char powder mixture the experimental gas profiles closely follow the equilibrium gas composition line atleast at the third stage for all temperatures. It may also be noticed from Figs.7.3 and 7.4 that experimental gas composition lines fall below the equilibrium lines for stage 1 and stage 2. It may be due to the fact that reactions $\text{Fe}_2\text{O}_3 \rightarrow \text{Fe}_3\text{O}_4$ and $\text{Fe}_3\text{O}_4 \rightarrow \text{Fe}_x\text{O}$ took place quite fast and gas composition changed very rapidly. So slight error in injection time will cause appreciable drift of the line from left to right. So, though the lines are shown to be below the equilibrium gas composition profile, they may be considered to be close to the equilibrium gas composition.

If the rate of reduction is faster than that of gasification, then it is expected that as soon as CO will be generated, it will react with iron oxide and thus the product gas will be close to the equilibrium composition. From Figs.7.3 - 7.5 it is apparent that atleast for the third stage, gasification of carbon is exclusively the rate controlling step for the overall reduction reaction.

But the situation is somewhat different for iron oxide micropellet and coconut char powder mixture. From Figs.7.7 - 7.10 it may be seen that, at highest temperature, and for the third stage, the

actual gas composition line is well above the equilibrium line. But with decrease of temperature, the experimental gas composition gradually falls closer to the equilibrium gas composition.

This is in accordance with the expectation. In micropellets, iron oxide reduction is slower than in iron oxide powder due to mass transfer limitations. Hence reduction step is likely to be partially rate controlling. This is especially true at higher temperatures where gasification rate is considerably enhanced due to its high activation energy. On the other hand rates of mass transfer and oxide reduction would not increase so much due to lower activation energies. Comparing the values of \dot{W}_C for powder mixture and micropellet + powder mixture, it may also be noted that the carbon loss rate for powder mixture is marginally higher than that in micropellet + powder system at 1283K. At lower temperatures i.e. at 1204K and 1151K, rates for both the systems are comparable indicating that an increase in iron oxide particle size from -325 mesh to 0.2 mm di not affect the rate at lower temperature appreciably. The marginally higher rate for powder system at high temperature may be attributed to the mass transfer limitation with the micropellet.

Again, it may be noted that at highest temperature and both for iron oxide powder and micropellet systems, \dot{W}_C increases significantly with the progress of fractional reduction, reaches a peak value and finally decreases. This is a clear indication that there was significant catalytic effect from freshly produced iron on the rate of gasification. No prominent catalytic effect could be observed at lower temperatures. Fruehan(119) concluded that there was no catalytic effect from freshly produced iron on gasification rate of

coconut char in carbothermic reduction. He attributed it to high reactivity of coconut char. In the present investigation this was not found to be correct at higher temperature ranges. The probable explanation for catalytic effect at higher temperatures may be as follows.

It has been well established in Sec.1.2.6 that the extent of catalysis depends on intimacy of contact between carbon and iron particles. At higher temperature this is likely to increase due to:

- (a) more sintering of particles,
- (b) more mass transfer resistance tending to confine the reactions towards surface regions of particles.

Figs.7.11 and 7.12 present the comparison of the experimental rate of carbon loss (\dot{W}_C) and the rate predicted from gasification (\dot{W}_{Cp}) for carbothermic reduction. It may be noted that for both the systems (powders and micropellets) nature of variation of \dot{W}_C and \dot{W}_{Cp} are quite different. In case of \dot{W}_{Cp} , there appear sharp peaks in the range of 10-20 pct. reduction depending upon experimental conditions and then fall to an almost steady state value. But for experimental rate, there is a gradual variation of the values with progress of reduction.

So for comparison purposes, if the so-called steady state values of the predicted rates of carbon loss are considered, it may be noted that there exist almost a factor of 2 difference with those of the experimental carbon loss rates. The reason for the anomaly may be due to the fact that the gasification rate values used for \dot{W}_{Cp} calculation were at 5 pct. conversion whereas \dot{W}_C present the values of instantaneous carbon loss rate during carbothermic reduction. It has

already been shown that gasification rate changes quite significantly with progress of fractional conversion Sec.1.2.5. So comparison of instantaneous rate with the rate at a fixed conversion might have incorporated the abovesaid discrepancy.

7.6 Comparison with Carbothermic Rate Data of Abraham(3)

It has already been mentioned in Sec.1.3.3 that Abraham et al(123) carried out reduction study of iron oxide in presence of solid carbon for the following types of geometries

- (a) iron oxide and graphite powder mixture
- (b) oxide pellet and graphite powder mixture
- (c) oxide micropellet and graphite powder mixture
- (d) oxide pellet separated from graphite powder bed

They observed appreciable catalytic effect on the rate of gasification by iron for the first three types of geometries. However, when iron oxide pellet and graphite were separated from each other, there was no chance of any contact between carbon particles and iron produced by carbothermic reduction, and hence no catalytic effect.

Both porous and dense pellets of iron oxide had been employed by Abraham et al.(123) for experiments and were kept in varying distances from graphite powder. Analysis of the product gas by solid electrolyte cell constituted the basic data for rate measurement alongwith monitoring of the volumetric rate of gas generation. As the solid electrolyte cell is susceptible to cracking under rapid change in temperature, reaction zone was brought to the required temperature from room temperature by gradual heating, only after inserting the solid electrolyte cell inside the chamber. One sample result of their experiments has been presented in Fig.7.13.

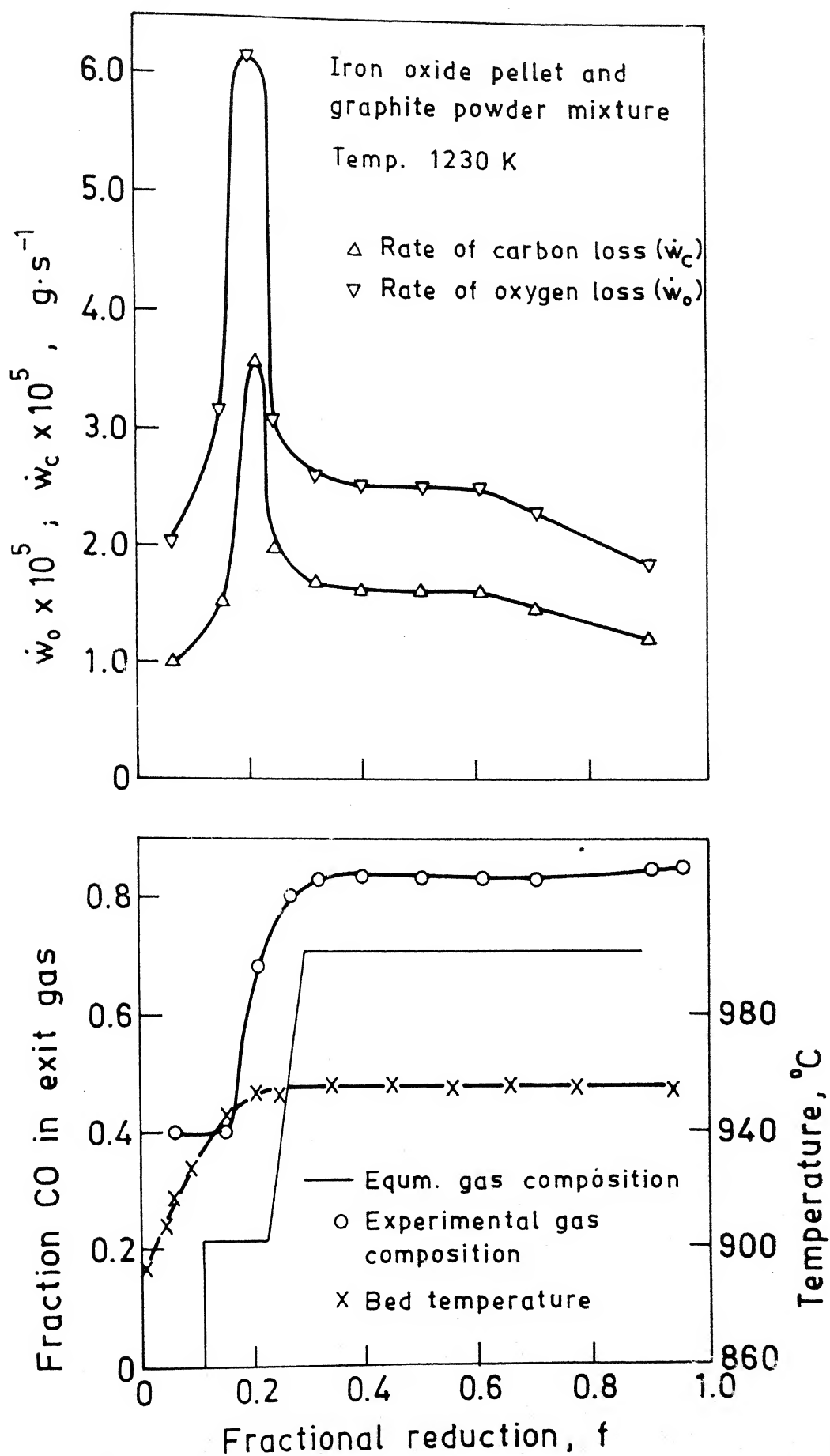


Fig. 7.13. Sample result of Abraham et al. (3) for iron oxide pellet and graphite powder mixture.

Abraham (3) also tried to predict the rate of carbon loss from the gasification data and compared them with the carbon loss rate calculated from carbothermic experiments. Fig.7.14 presents one such comparison, for the experimental set presented in Fig.(7.13). In predicting the rate of carbon loss from gasification data, Abraham used the experimental data on the variation of gas composition and temperature with progress of reduction as shown in Fig.(7.13). They then utilized their measurements of reactivity of graphite in pure CO_2 at various temperatures and extrapolated the rate of gasification in CO_2 to mixtures of CO-CO_2 by using Eq.1.22 and by employing the temperature dependence of I_2 and I_3 provided by Rao et al(32).

It may be observed from Fig.7.14 that the qualitative nature of both the experimental as well as the predicted r_g curves match quite well. However, there exist a quantitative disagreement. The experimental r_g values are about one order of magnitude higher than those of predicted values. The two following reasons were thought to be responsible for the disagreement.

- (a) the reactivity data of graphite determined by Abraham et al in CO_2 may be erroneous
- (b) extrapolation of rate in CO_2 to CO-CO_2 mixture based on I_2 and I_3 of Rao and Jalan (32) may not be valid.

As a result, the reactivity value of graphite in CO_2 was redetermined. But it may be seen from Fig.6.1 that reactivity value of graphite at higher temperature is not much different from that of Abraham et al.. On the other hand reactivity values of graphite at lower temperatures for the present set of studies are even less than those of Abraham et al.. So the probable reason for the disagreement

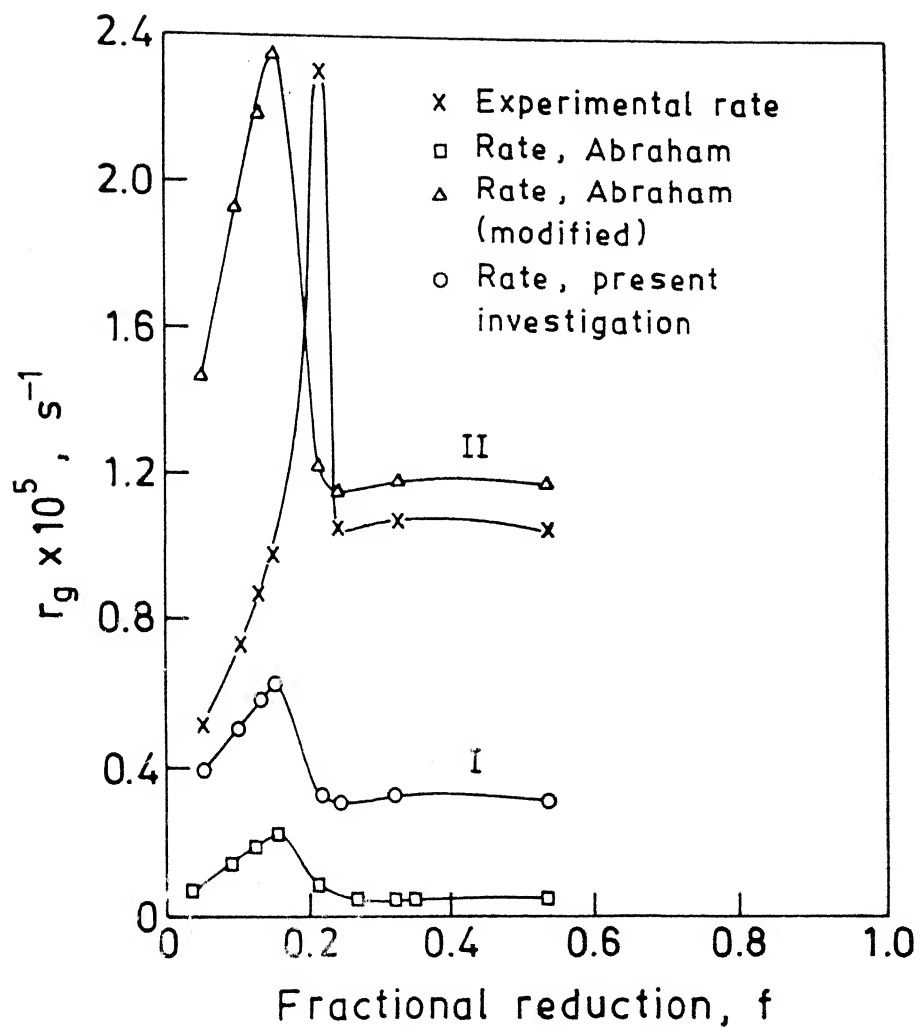


Fig. 7.14. Comparison of experimental reduction rate with rate predicted from gasification.

lies in incorrectness of the extrapolation formula used. In order to check this point it is necessary to carry out study on reactivity of graphite in CO-CO₂ mixtures. But due to insufficient sensitivity of the present set-up, as described in Sec.2.1.2 and Sec.2.3, it was not possible to do any experiment in this regard. Tiwari (141) performed a series of experiments with graphite in varying CO-CO₂ atmosphere, ranging upto 80 pct. CO in the temperature range of 1243K to 1373K using a Cahn 1000 electro balance. His data were utilised to check the extrapolation formula. Fig.7.15 presents the $(r_g)_{CO-CO_2} / (r_g)_{CO_2}$ curves, both for experimental observation of Tiwari and those calculated using extrapolation formula of Rao et al(32). It may be noted from Fig.7.15 that there exists a significant disagreement between measurement and prediction. It is worth mentioning here that though the extrapolation formula is basically valid for intrinsic rate but it can as well be used for r_g , atleast in case of graphite. This is because of the fact that graphite is an inherently slow reactive material and specially under CO rich gaseous environment the rate of reaction will almost be free from heat and mass transfer limitations.

Fig.7.14 shows two curves calculated on the basis of this new information. One curve (marked I) was calculated using the reactivity value in pure CO₂ of the present investigation. The other curve (curve II) was calculated using values of reactivity of graphite as determined by Abraham et al.(123) in pure CO₂. For extrapolation of rate in CO-CO₂ mixture, Tiwari's(141) findings [Fig.7.15] were utilized.

It may be noted that curve II gives quite a good match qualitatively as well as quantitatively with r_g obtained from

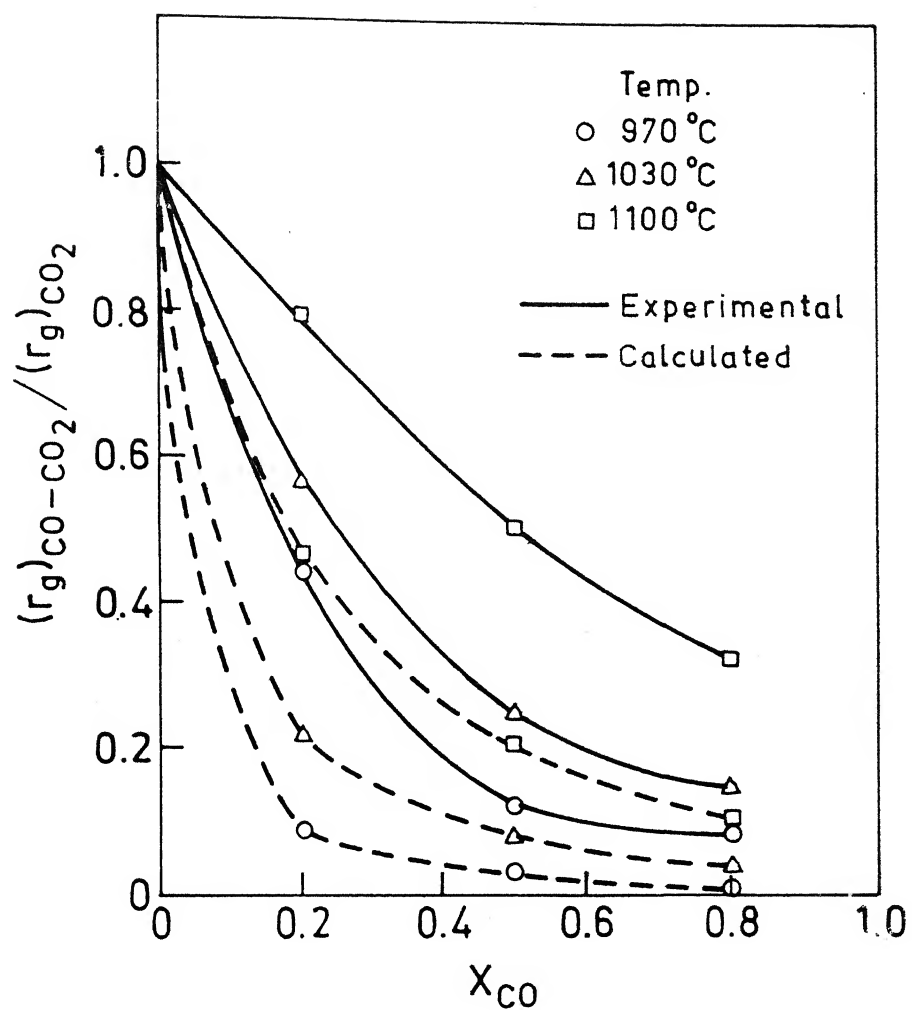


Fig. 7.15 Comparison of $(r_g)_{CO-CO_2} / (r_g)_{CO_2}$ observed by Tiwari (141) and calculated from extrapolation formula. (32)

experimental carbothermic data. Even if curve I is taken, difference is much less now. So it seems that the primary cause of mismatch between observed and predicted values in study of Abraham et al. lies in using erroneous formula for extrapolation of rate from pure CO_2 to CO-CO_2 mixture.

Again it may be recalled from Sec.1.2.3 [Table 1.3] that I_2 and I_3 values calculated for different investigators and for various forms of carbon vary widely. So the conclusion of universal nature of I_2 and I_3 as was reached by Rao et al(32) appeared incorrect. The conclusion arrived at here confirms the above.

CHAPTER 8

SUMMARY AND CONCLUSIONS

A critical review of literature on kinetic of gasification of carbon and carbothermic reduction of iron oxide revealed some gaps and anomalies in the fundamental aspects. The experimental scheme was planned in an effort to either eliminate or throw some light on the above.

Gasification rates of graphite were determined with CO_2 in the temperature range of 1222-1283K and with bed depths of powder samples varying from 0.2 to 0.5 cm. Its purpose was to try to throw light on quantitative disagreements between measured and predicted rates of carbothermic reduction observed by Abraham (3) in this laboratory earlier.

Prediction of rates of carbothermic reduction was attempted assuming it to be controlled by rate of gasification of carbon and using experimental values of the latter. Abraham avoided the complications arising out of catalytic action of reduced iron on rate of gasification during carbothermic reduction by employing a geometry where iron oxide and graphite were physically separated in an enclosure.

In powder mixtures of iron oxide and carbon, it appeared from literature that reactive form of carbon are not significantly subjected to this catalytic effect. To check the validity of this as well as to avoid complicating effect of catalysis, coconut char was selected for further investigations. The char was prepared in the laboratory from coconut shells. The measurements consisted of :

(a) rate of gasification of coconut char in CO_2 as well as in various CO-CO_2 and $\text{CO}_2\text{-Ar}$ gas mixtures in the temperature range of 1081-1283K by thermogravimetry.

(b) rate of carbon loss and rate of oxygen loss during carbothermic reduction by a combination of thermogravimetry and determination of product gas composition by gas chromatography. Pure Fe_2O_3 and coconut char mixture was employed. The char was in the form of powder. Iron oxide was either taken as powder or as sintered micropellets. Temperature range was 1073-1284K.

For the above experimental program, necessary apparatus were fabricated and/or assembled and tested for reliability and precision to the extent possible.

Computer programs were developed to process the raw data in order to determine :

(a) instantaneous fractional rate of carbon loss (r_i) as function of time as well as fractional conversion (F) in gasification experiments,

(b) instantaneous rates of carbon loss (\dot{w}_c) as function of time as well as fractional reduction of oxide (f) in carbothermic reduction,

(c) mass transfer analysis to determine isothermal effectiveness factor (η) to evaluate intrinsic chemical rate constant (K_c) for gasification data of graphite and coconut char.

(d) simultaneous heat and mass transfer analysis to determine non-isothermal effectiveness factor (η_T) to evaluate intrinsic chemical rate constant (K_{CT}). K_{CT} was employed for interpretation of gasification data of coconut char in preference to K_c , since

isothermal effects were significant. But it was not so with graphite. As the literature reported model for heat transfer analysis was found to have some limitations, a separate model was developed for this purpose. Tridiagonal matrix method was employed for solution of the governing differential equation. Required computer program was developed.

Since r_i was found to be function of F in gasification of graphite and coconut char, rates at 5% conversion were employed for all further interpretations. Rate means r_g .

Following conclusions may be drawn from the present investigation.

A. Gasification of carbon

1. Instantaneous rates of gasification for both graphite and coconut char vary with fractional conversion. No well defined pattern of variation, neither any steady-state region could be identified.

2. The experimentally measured gasification rates of both graphite and coconut char compared well with some values reported in literature.

3. Mass transfer limitations were found to be significant for both graphite and coconut char. This required theoretical analysis of mass transfer to calculate isothermal effectiveness factor in order to determine intrinsic chemical rate constant (K_c).

4. Mathematical techniques for mass transfer analysis as reported in literature are not rigorous but somewhat approximate due to simplifying assumptions which cannot be avoided.

5. Under the present experimental conditions, rate of gasification of coconut char was found to be also affected by

significant non-isothermal effect due to endothermic nature of gasification reaction. This effect is more significant at higher temperature as expected. This required evaluation of non-isothermal effectiveness factor for eliminating both heat and mass transfer limitations.

6. Experimentally determined r_g were plotted as function of bed depth. Value of r_g^0 obtained by extrapolation to zero bed depth (i.e. bed depth $\rightarrow 0$) matched well with K_c and K_{CT} for both graphite and coconut char. This is expected and confirms reliability of experimental data as well as heat and mass transfer analysis. Therefore, zero bed depth extrapolation may be an alternative route for calculation of intrinsic rate of gasification even without performing any heat and mass transfer analysis.

7. Carbon monoxide was found to have inhibiting effect on rate of gasification of coconut char. This is qualitatively in agreement with literature.

8. Gasification kinetics of coconut char did not obey a first order rate equation with respect to gas composition.

9. It was not possible to conclude with certainty whether Langmuir-Hinshelwood rate equation was valid or not for the present set of data on gasification of coconut char. It was noticed that there is confusion in literature as well.

10. Activation energies for intrinsic chemical rate constants of gasification were determined as 260 kJ/mol and 250 kJ/mol for graphite and coconut char respectively. These are in reasonable agreement with literature.

11. Gasification rate of graphite in the present investigation

were comparable to those obtained by Abraham(3) who had employed the same sample.

B. Carbothermic reduction of iron oxide

1. Product gas composition versus fractional reduction plots confirmed stagewise reduction for the oxide (viz. $\text{Fe}_2\text{O}_3 \rightarrow \text{Fe}_3\text{O}_4 \rightarrow \text{Fe}_x\text{O} \rightarrow \text{Fe}$).

2. Comparison of experimental gas composition with those for wustite-iron equilibria indicated that gasification reaction was primarily controlling carbothermic reduction rates for powder mixtures of oxide and char. However, for micropellet-char system at higher temperatures it appears to be a case of rate control by both gasification and oxide reduction reactions. This may be explained by large activation energy of gasification reaction and more mass transfer resistance within a micropellet as compared to that in oxide powder.

3. Instantaneous carbon loss rate versus fractional reduction data indicate catalytic enhancement of gasification rate at wustite \rightarrow iron stage at higher temperatures. However, it is much less at lower temperature. This is at variance with conclusions reported in literature on reduction of iron oxide by coconut char. At higher temperature, more sintering is expected. Also, gasification reaction would be restricted more to external surface of char particles due to more resistance to pore diffusion. Both the above effects are expected to enhance contact catalysis by metallic Fe and hence satisfactorily explain the behaviour pattern.

4. Comparison of measured carbon loss rates did not agree well with those predicted from gasification data of char. This may be

attributed, first of all, to the fact that gasification rates of 5% conversion were employed. Secondly, catalytic effect in some cases are present. Other causes also are not ruled out.

5. Rates of carbon loss were calculated for one set of experiment. of Abraham (3) on separated oxide and graphite system. For this graphite reactivity data from the present set of experiments in CO_2 along with Tiwari's data on gasification rates in CO-CO_2 mixtures were utilized. This exercise by an large removed the quantitative discrepancy with experimental data of Abraham. Similar conclusions are expected for other sets of experiments of Abraham on separated oxide and graphite system.

6. It may be concluded that the above discrepancy had primarily arisen in Abraham's study because he had employed Langmuir-Hinshelwood type rate expressions with I_2 and I_3 taken from literature on the basis of literature recommendations (32).

CHAPTER 9

SUGGESTIONS FOR FUTURE STUDIES

The present investigation has allowed the author to draw some conclusions on kinetics of gasification of carbon as well as carbothermic reduction of iron oxide. However, the following suggestions are being noted for further investigations.

1. It could not be clearly established whether rate equation Langmuir-Hinshelwood mechanism, as proposed by some in literature is valid or not for gasification reaction. This would call for further precise data collection on gasification rate in varying CO-CO₂ gas mixtures.

2. The approach employed in the present investigation for gasification reaction, viz. evaluation of chemical rate constant, after elimination of mass and heat transfer effects, is recommended. Cross-check by extrapolation to zero bed depth is also desirable. However determination of pore surface area by BET also should be done to find out chemical rate constant based on unit pore surface area, which is a more fundamental parameter.

3. It would be desirable to further examine the limitations and approximations of the techniques of heat and mass transfer analysis available in literature and see whether they can be improved upon.

4. From structural point of view the differences in rates of gasification of various forms of carbon may be attributed to the extent of imperfections present in the structure. Graphite being the most perfect form of carbon, graphitization of all types of pure carbon should exhibit the same rate per unit pore surface area. It

would be interesting to carry out investigations on this aspect.

5. The present investigation along with Tiwari's data has been able to predict the rate of carbothermic reduction for iron oxide and graphite in separation from rate of gasification of graphite. It has also tried to correlate the two for mixture of coconut char and oxide. However, for mixtures, it is perhaps necessary to do further work in this direction.

6. It would also be of interest to try to predict rate of carbothermic reduction from gas composition and supplementary data on reduction of iron oxides/ores by gases containing CO and CO₂.

REFERENCES

1. S.K. Gupta, Proc. of International Symposium on B.F. Iron Making, NML, Jamshedpur, 1985, Nov., p.197
2. A. Chatterjee et al., Trans. I.I.M., 1986, Vol.39, p.411
3. M.C. Abraham, Ph.D. Thesis, I.I.T., Kanpur, 1976
4. J.W. Hassler, 'Active Carbon', Chemical Publishing Co. N.Y., 1951
5. A.R. Ubbelohde and F.A. Lewis, 'Graphite and its Crystal Compounds', Clarendon Press, Oxford, 1960, p.5
6. H.T. Pinnick, J. Chem. Phys., 1952, Vol.20, p.756
7. A.F. Semechkova and D.A. Frank-Kamenetski, Acta Physicochim, 1940, Vol.12, p.899
8. J. Gadsby, C.N. Hinshelwood and K.W. Sykes, Proc. Roy. Soc., 1946, Vol.A187, p.129
9. A. Koy, Gas Research Board Communication, No.G.R.B.40, 1948
10. J. Gadsby, F.J. Long, P. Sleightholm and K.W. Sykes, Proc. Roy. Soc., 1948, Vol.A193, p.357
11. P.C. Wu, Sc.D. Thesis, M.I.T., Cambridge, Mass., 1949
12. W.K. Lewis, E.R. Gilliland and G.T. McBride, Ind. Eng.Chem., 1949, Vol.41, p.1213
13. F. Bonner and J. Turkevich, J. Amer. Chem. Soc. 1951, Vol.73, p.561
14. A.E. Reif, J. Phys. Chem., 1952, Vol.56, p.785
15. ibid, p.778
16. A.A. Orning and E. Sterling, J. Phys. Chem., 1954, Vol.58, p.1044
17. S. Ergun, Ind. Eng. Chem., 1955, Vol.47, p.2075
18. M. Rossberg and E. Wicke, Chem. Ing. Tech., 1956, Vol.28, p.181
19. S. Ergun, J. Phys. Chem., 1956, Vol.60, p.480
20. E. Wicke, Chemical Reaction Engineering, Ist. European Symposium, Pergamon Press Inc. N.Y., 1957, p.61
21. P.L. Walker Jr., F. Rusinko Jr. and L.G. Austin, 'Advan. Catal', Academic Press, INC, N.Y., 1959, Vol.11, p.134-221
22. A.F. Armington, Ph.D. Thesis, The Pennsylvania State Univ., 1960

23. H.J. Grabke, Ber. Bunsenges, Phys. Chem., 1966, Vol.70, p.664
24. M. Mentser and S. Ergun, Carbon, 1967, Vol.5, p.331
25. K. Hedden and A. Lowe, Carbon, 1967, Vol.5, p.339
26. E.T. Turkdogan, V. Koump, J.V. Vinters, and T.F. Perzak, Carbon, 1968, Vol.6, p.467
27. C. Wegner, 'Heterogeneous Kinetics at Elevated Temperature' Plenum Press, N.Y., 1970
28. E.T. Turkdogan and J.V. Vinters, Carbon, 1969, Vol.7, p.101
29. E.T. Turkdogan and J.V. Vinters, Carbon, 1970, Vol.8, p.39
30. E.T. Turkdogan, R.G. Olsson and J.V. Vinters, Carbon, 1970, Vol.8, p.545
31. A.S. Fedoseev, Tr. Mosk, Khim. Tekhnol. Inst., 1976, Vol.91, p.40
32. Y.K. Rao and B.P. Jalan, Met. Trans., 1972, Vol.3, p.2465
33. S. Kobayashi, Y. Omori, Tetsu To Hagana, 1977, Vol.63(7), p.1081
34. V.M. Sergeev, T.A. Bovina, Khim. Tverd. Topl., 1977, Vol.4, p.68
35. G.P. Khaustovich, A.E. Lebedev, Khim. Tverd. Topl., 1980, Vol.3, p.121
36. E.L. Gol'dberg, Khim. Tverd. Topl., 1980, Vol.3, p.127
37. W.J. Stephen, B. McEnaney, Ext. Abstr. Program-Bienn. Conf., Carbon, 1981, 15th., p.423
38. A.G. Simons, Carbon, 1982, Vol.20(2), p.117
39. N.J. Desai, R.T. Yang, AIChE J., 1982, Vol.28(2), p.237
40. A. Baranski, R. Dziembaj, C. Dunajewski, M. Lebiedziejewski, K. Pawlowski, Carbon, 1982, Vol.20(5), p.401
41. O. Sy, J.M. Calo, Pro-Int. Conf., Coal-Sci., 1983, p.445
42. S.P. Mehrotra and V.K. Sinha, Trans. ISIJ, 1983, Vol.23, p.723
43. R.T.S. Yang, R.Z. Duan, Carbon, 1985, Vol.23(3), p.325
44. H. Freund, Fuel, 1985, Vol.64(5), p.657
45. F. Scheidt, F. Jeannot, C. Gleitzer, J. Mater. Sci. Lett., 1985, Vol.4(10), p.1252

46. H. Fruend, Prepr. Pap.-Am. Chem. Soc., Div. Fuel Chem., 1985, Vol.30(1), p.311
47. H. Fruend, Fuel, 1986, Vol.65(1), p.63
48. A.J. Britten, L.J. Falconer and F.L. Brown, Carbon, 1985, Vol. 23(6), p.627
49. N. Standish and A.F.A. Tanjung, Fuel, 1988, Vol.67(5), p.666
50. P.C. Wu, W.E. Lower and H.C. Hottel, Fuel, 1988, Vol.67(2), p.205
51. K.J. Laidler, 'Chemical Kinetics', Tata Mcgraw-Hill Publishing Company Ltd., p.266
52. I. Langmuir, Trans. Faraday Soc., 1921, Vol.17, p.621
53. C.N. Hinshelwood, 'Kinetics of Chemical Changes', Clarendon Press, Oxford, 1926, p.145, 1940, p.187
54. E.K. Rideal, Proc. Cambridge Phil. Soc., 1989, Vol.35, p.130
55. S. Ergun, U.S. Bur. Mines Bull., 1962, Vol.598, p.38
56. J.L. Johnson, 'Chemistry of Coal Utilization', 2nd. Suppl. Vol., Wiley and Sons, N.Y., 1981
57. J.T. Sears, H. Muralidhare and C.Y. Wen, Ind. Eng. Chem. Proc. Des. Dev., 1980, Vol.19, p.358
58. E. Hippo and P.L. Walker, Fuel, 1975, Vol.54, p.245
59. J.L. Johnson, 'Kinetics of Coal Gasification', John Wiley and Sons, N.Y., 1979, p. 131
60. T. Adsehiri and T. Frusawa, Fuel, 1986, Vol.65, p.927
61. D.A. Aderibigbe and J. Szekely, Ironmaking and Steelmaking, 1981, Vol.8, p.11
62. M. Alam and T. DebRoy, ISS Trans., 1984, Vol.5, p.7
63. L.R. Radovic et al. Fuel, 1983, Vol.62, p.849
64. P.L. Walker Jr., M. Shelefand, R.A. Anderson, 'Chemistry and Physics of Carbon', Edited by P.L. Walker Jr., Vol.4, Marcel Dekker Inc. N.Y., 1968
65. F.J. Vastola and P.L. Walker Jr., J. Chim. Phys., 1961, Vol.58, p.20
66. F.J. Long and K.W. Sykes, J. Chim. Phys., 1950, Vol.47, p.361

67. F.J. Long and K.W. Sykes, Proc. Roy. Soc. (London), 1952, Vol.A215, p.100
68. M. Letort and G. Martin, Bull. Soc. Chim. (France), 1947, Vol.14, p.400
69. E.T. Turkdogan and J.V. Vinters, Carbon, 1972, Vol.10, p.97
70. K. Otto, C. Lehman, L. Bartosiewicz and M. Shelef, Carbon, 1982, Vol.20(3), p.243
71. S. Yokoyama, K. Miyahara, K. Tanaka and J. Tashiro, Sekiyu Gakkaishi, 1983, Vol.26(96), p.455
72. T. Wigmans, P. Tromp, J.A. Moulijn, Carbon, 1984, Vol.22(3), p.319
73. M.B. Cerfontain, R. Meijer, J.A. Moulijn, Proc-Int. Conf. Coal Sci., 1985, p.277
74. M. Alam and T. DeRoy, Met. Trans. B, 1986, Vol.17(3), p.565
75. J.M. Saber, J.L. Falconer and L.F. Brown, J. Chem. Soc., Chem. Commun., 1987, Vol.6, p.445
76. G.W. Roberts and C.N. Shatterfield, I&EC Fundamentals, 1965, Vol.4, No.3, p.288
77. R.H. Tien and E.T. Turkdogan, Carbon, 1970, Vol.8, p.607
78. R.H. Tien and E.T. Turkdogan, Carbon, 1972, Vol.10, p.35
79. A. Ghosh and S.K. Ajmani, 'On evaluation of chemical rate constants for reduction of iron oxides by carbon', proceedings of symposium on Kinetics of Metallurgical Processes, IIT, Kharagpur, 1989, p. 1-17
80. M.J. Groeneveld and W.P.M. Van Swaaij, Chem. Eng. Sci., 1980, Vol.35, p.307
81. W.F. De Groot and F. Shafizadeh, Fuel, 1984, Vol.63, p.210
82. I.W. Smith, 19th. International Symposium on Combustion, The Combustion Institute, 1982, p.1045
83. K.H. Van Heek, H. Juntger and W. Peter, J. Inst. Fuel, 1973, Vol.46, p.249
84. M.C. Abraham and A. Ghosh
85. J. Szekely and D.A. Aderibigbe

86. R.B. Anderson, J. Bayer, and L.J.E. Hafer, Fuel, 1965, Vol.(44), p.443
87. L.E.B.Soledade, Om P. Maharaj and P.L. Walker Jr. Fuel, 1978, Vol.57, p.56
88. R.J. Tyler, Fuel, 1986, Vol.65, p.236
89. A.K. Agarwal and J.T. Sears, Ind. Eng. Chem. Process Des.Dev., 1980, Vol.19, No.3, p.365
90. B. Neumann, C. Kroger and E. Fingas, Z. Anorg. Chem., 1931, Vol.197, p.321
91. G. Milner, E. Spivey and G.W. Cobb, J. Chem. Soc., 1943, p.578
92. V.W. Bavkloh and R. Durrer, Arch. Eisenhüttenw, 1931, Vol.4, p.455
93. W. Bankloh and G. Zimmerman, Stahl U. Eisen, 1933, Vol.53, p.172
94. D. Bandyopadhyay, N. Chakraborti and A. Ghosh, Steel Research, 1988, Vol.59(12), p.537
95. W. Schotie, A.I. Ch.E Journal, 1960, Vol.6, p.63
96. R.G. Oeissler and C.S. Eian, NACA, RM E52C05, 1952
97. Geiger and Pouirier 'Transport Phenomena', p.196
98. A.E. Reif, J. Phys. Chem., 1952, Vol.56, p.785
99. J.E.F. Salles, L.F.A. De Castro and R.P. Tavares, Metallurgia-ABM, 1985, Vol.41, p.15
100. G.T. Mcbridge Jr. 'Gasification of carbon dioxide in a fluidized bed', Sc.D Thesis, Chem. Eng., M.I.T., 1947
101. J.F. Stanger and P.L. Walker Jr., Carbon, 1976, Vol.14, p.345
102. M. Mentser and S. Ergun, 'A study of carbon dioxide-carbon reaction by oxygen exchange', Bull. US Bur. Mines No.664, 1973
103. D.L. Biederman, 'A study of the oxidation of graphite by carbon dioxide', Ph.D Thesis, Penn. State Univ., 1965
104. R.B. Bird, W.E. Stewart and E.N. Lightfoot, 'Transport Phenomena' John Wiley & Sons., 1960, p.511
105. J.M. Smith, 'Chemical Engineering Kinetics', McGraw Hill Book Co., N.Y., 2nd edition, 1970, Chap.11

106. P.B. Weisz and A.B. Schwartz, J. Catal., 1962, Vol.1, p.399
107. V. Arkharov, V.N. Bogoslovskii, M.G. Zhuravleva and Q.I. Chufarov, Zh. Fiz. Khim., 1955, Vol.29, no.2, p.272
108. T.S. Yun, Trans. ASM, 1961, Vol.54, p.129
109. A. Prasad and R. Tupkary, International Conference on the Science and Technology of Iron and Steel, Tokyo, 1970, p.249
110. Y.K. Rao, Met. Trans., 1971, Vol.2, p.1439
111. M.C. Abraham and A. Ghosh, Engineering World, Feb., 1973
112. B. Baldwin, J.I.S.I., 1955, Vol.179, p.30
113. E. Bicknese and R. Clark, Trans. IMS-AIME, 1966, Vol.236, p.2
114. Ken-Ichi Otsuka and Diazo Kunii, Journal of Chemical Engineering of Japan, 1969, Vol.2, No.1, p.46
115. E.T. Turkdogan and J.V. Vinters, Carbon, 1970, Vol.8, p.39
116. P.C. Ghosh and S.N. Tiwari, JISI, London, 1970, Vol.208, p.255
117. E.T. Turkdogan and J.V. Vinters, Carbon, 1969, Vol.7, p.101
118. R.S. Ghosh and N.G. De, J. Singh and A. Lahiri, Iron and Steel International, 1975, Dec., p.459
119. R.J. Fruehan, Met. Trans., 1977, Vol.8B, p.279
120. R.H. Tien and E.T. Turkdogan, Met. Trans., 1977, Vol.8B, p.305
121. N.S. Srinivasan and A.K. Lahiri, Met. Trans., 1977, Vol.8B, p.175
122. A.K. Gokhale, A.K. Sengupta and A. Ghosh, Steel India, 1979, Vol.2, No.1, p.36
123. M.C. Abraham and A. Ghosh, Ironmaking and Steelmaking, 1979, No.1, p.14
124. C.E. Seaton, J.S. Foster and J. Velasco, Trans. ISIJ, 1983, Vol.23, p.490
125. H.S. Ray and N. Kundu, Thermochimica Acta, 1986, Vol.101, p.107
126. F. Ajersch, Canadian Metallurgical Quarterly, 1987, Vol.26, No.2, p.137
127. A. Chatterjee and R. Singh, Iron Steel Inst., 1981, Vol.54(2), p.79

128. C.W. Zerbachev et al., Iron Steel Eng., 1982, Vol.59(10), p.23
129. R.L. Stephenson, Iron Steelmaker, 1982, Vol.9(2), p.40
130. L.L. Teoh, SEAI SI Q., 1985, Vol.14(1), p.15
131. A.K. Roy, K.K. Prasad and P.K. Chowdhury, Metal News, 1989, Vol.11, No.1, p.6
132. W.D. Jones, 'Fundamental Principles of Powder Metallurgy', Edward Arnolds Publ. Ltd., London, 1960, p.262-270
133. W. Jandar, Z. Anorg. Allgan. Chem., 1927, Vol.163, p.1, ibid, 1927, Vol.166, p.31
134. A.M. Ginstling and B.I. Brounshtein, J. Appl. Chem., U.S.S.R., 1950, Vol.23, No.12, p.1327
135. R.E. Carter, J. Chem. Phys., 1961, Vol.34, p.2010
136. H.Y. Sohn and J. Szekely, Chemical Engineering Science, 1973, Vol.28, p.1789
137. N.S. Srinivasan and A.K. Lahiri, Mett. Trans., 1975, Vol.6B, p.269
138. Y.K. Rao and Y.K. Chuang, Met. Trans., 1976, Vol.7B, p.495
139. W.M. McKewan, in 'Steelmaking - Chipman Conference', J.F. Elliot and T.R. Meadowcroft edited, The M.I.T. Press, Cambridge, 1965
140. Y.K. Rao, Chem. Eng. Sci., 1974, Vol.29, p.1435
141. P. Tiwari, Private Communication, 1989, IIT, Kanpur
142. N.S. Srinivasan and A.K. Lahiri, Met. Trans., 1975, Vol.6B, p.269
143. H.N. Dharwadkar, Ph.D Thesis, IIT, Kanpur, 1982
144. J.F. Elliot and M. Gleiser, 'Thermochemistry for Steelmaking', Vol.1, 1960

APPENDIX -1

 ΔH° and ΔG° values of CO

T , °K	ΔH° cal/mol	ΔG° cal/mol
298.15	-26,416 (± 10)	-32,808 (± 20)
400	-26,320	-35,010
500	-26,300	-37,180
600	-26,330	-39,360
700	-26,410	-41,530
800	-26,510	-43,680
900	-26,640	-45,820
1,000	-26,770	-47,940
1,100	-26,910	-50,050
1,200	-27,060	-52,150
1,300	-27,210	-54,240
1,400	-27,380	-56,310
1,500	-27,540	-58,370
1,600	-27,730	-60,430
1,700	-27,900	-62,460
1,800	-28,080	-64,480
1,900	-28,260	-66,500
2,000	-28,460	-68,510
2,100	-28,650	-70,520
2,200	-28,830	-72,490
2,300	-29,030	-74,480
2,400	-29,240	-76,440
2,500	-29,450	-78,410
2,600	-29,660	-80,360
2,700	-29,870	-82,310
2,800	-30,090	-84,250
2,900	-30,320	-86,180
3,000	-30,560	-88,100

APPENDIX -2

 ΔH° and ΔG° values of CO_2

T , °K	ΔH° cal/mol	ΔG° cal/mol
298.15	-94,052	-94,260
400	(± 10)	(± 30)
500	-94,070	-94,320
600	-94,090	-94,390
700	-94,120	-94,440
800	-94,170	-94,500
900	-94,220	-94,540
1,000	-94,270	-94,580
1,100	-94,320	-94,610
1,200	-94,360	-94,640
1,300	-94,410	-94,660
1,400	-94,460	-94,680
1,500	-94,510	-94,690
1,600	-94,560	-94,710
1,700	-94,620	-94,730
1,800	-94,670	-94,720
1,900	-94,710	-94,720
2,000	-94,770	-94,720
2,100	-94,830	-94,720
2,200	-94,880	-94,720
2,300	-94,930	-94,690
2,400	-95,000	-94,690
2,500	-95,070	-94,680
2,600	-95,140	-94,680
2,700	-95,210	-94,660
2,800	-95,290	-94,640
2,900	-95,370	-94,610
3,000	-95,470	-94,580
	-95,570	-94,540

APPENDIX -3

 ΔH° and ΔG° values of Fe_2O_3

T , °K	ΔH° cal/mol	ΔG° cal/mol	T , °K	ΔH° cal/mol	ΔG° cal/mol
298.15	-196,200 ($\pm 1,000$)	-176,800 ($\pm 1,500$)	1,665	-190,700	-95,300
400	-195,800	-170,200	1,665	-191,300	-95,300
500	-195,200	-163,900	1,700	-191,200	-93,300
600	-194,600	-157,700	1,800	-190,700	-87,500
700	-193,900	-151,600	1,809	-190,600	-87,000
800	-193,100	-145,600	1,809	-198,000	-87,000
900	-192,400	-138,900	1,900	-197,700	-81,400
950	-192,100	-136,800	2,000	-197,400	-75,300
950	-191,900	-136,800	2,100	-197,100	-69,200
1,000	-191,900	-133,900	2,200	-196,800	-63,200
1,100	-192,400	-128,100	2,300	-196,500	-57,100
1,184	-192,300	-123,200	2,400	-196,300	-51,000
1,184	-192,700	-123,200	2,500	-196,100	-45,000
1,200	-192,700	-122,200	2,600	-195,800	-38,900
1,300	-192,300	-116,400	2,700	-195,600	-32,900
1,400	-191,900	-110,600	2,800	-195,400	-26,900
1,500	-191,500	-104,800	2,900	-195,300	-20,900
1,600	-191,100	-99,000	3,000	-195,100	-14,900

APPENDIX -4

 ΔH° and ΔG° values of Fe_3O_4

T , °K	ΔH° cal/mol	ΔG° cal/mol	T , °K	ΔH° cal/mol	ΔG° cal/mol
298.15	-266,800 ($\pm 2,000$)	-242,200 ($\pm 2,200$)	1,700	-259,600	-139,000
400	-266,100	-233,900	1,800	-259,500	-131,900
500	-265,300	-225,900	1,809	-259,500	-131,300
600	-264,300	-218,100	1,809	-270,600	-131,300
700	-262,900	-210,500	1,870	-270,600	-126,600
800	-261,200	-203,100	1,870	-237,600	-126,600
900	-259,500	-196,000	1,900	-237,700	-124,800
1,000	-259,700	-188,900	2,000	-237,800	-118,900
1,100	-260,500	-181,800	2,100	-238,000	-112,900
1,184	-260,500	-175,700	2,200	-238,300	-107,000
1,184	-261,200	-175,700	2,300	-238,500	-101,000
1,200	-261,100	-174,600	2,400	-238,800	-95,000
1,300	-260,600	-167,400	2,500	-239,000	-89,000
1,400	-260,100	-160,300	2,600	-239,300	-83,000
1,500	-259,600	-153,200	2,700	-239,700	-77,000
1,600	-259,100	-146,100	2,800	-240,000	-71,000
1,665	-258,800	-141,500	2,900	-240,400	-64,900
1,665	-259,600	-141,500	3,000	-240,800	-58,900

APPENDIX -5

 ΔH° and ΔG° values of Fe_xO

T , °K	ΔH° cal/mol	ΔG° cal/mol	T , °K	ΔH° cal/mol	ΔG° cal/mol
298.15	-63,500 (± 200)	-58,150 (± 250)	1,665	-54,800	-37,400
400	-63,250	-56,800	1,665	-55,050	-37,400
500	-63,050	-55,300	1,700	-55,000	-37,100
600	-62,850	-53,600	1,800	-54,700	-36,000
700	-62,700	-52,100	1,809	-54,700	-35,900
800	-62,600	-50,600	1,809	-58,200	-35,900
900	-62,650	-49,100	1,900	-58,000	-34,800
1,000	-62,800	-47,550	2,000	-57,850	-33,600
1,100	-63,100	-46,050	2,100	-57,650	-32,400
1,184	-63,100	-44,700	2,200	-57,500	-31,200
1,184	-63,300	-44,700	2,300	-57,350	-30,000
1,200	-63,300	-44,450	2,400	-57,200	-28,800
1,300	-63,100	-42,900	2,500	-57,050	-27,650
1,400	-62,900	-41,400	2,600	-56,900	-26,500
1,500	-62,700	-39,850	2,700	-56,750	-25,300
1,600	-62,500	-38,300	2,800	-56,650	-24,150
1,650	-62,350	-37,550	2,900	-56,500	-23,000
1,650	-54,850	-37,550	3,000	-56,400	-21,800

APPENDIX -6

Examples of dimensional inconsistencies
of the model of Tien et al.(78)

A number of equations in reference (7) are dimensionally inaccurate. Two typical examples are given below:

(i) The relation between k_1 and k_2 is stated as:

$$\frac{k_1}{k_2} = \frac{\rho}{60M} e^{-b(T_b - T)} \quad (A.1)$$

where

$$b = 2.3 \times 10^{-2} \text{ K}^{-1} \text{ for graphite and coke}$$

and

$$T_b = 1660 \text{ K for graphite and } 1568 \text{ K for co}$$

The correct unit of k_1 $60 \text{ M}/\rho$ would be $\text{atm}^{-1} \text{ min}^{-1}$ (incorrectly stated in the text as min^{-1}). The unit of k_2 is atm^{-1} . The exponential is dimensionless. Therefore the dimension of the left hand and right hand sides of the Equation (A.1) are not matching.

(ii) The general differential equation for nonisothermal internal oxidation of carbon is given as

$$\frac{D_e P}{R T_s} \nabla \cdot \left(\frac{F}{1+y} \nabla y \right) = \theta e^{\psi y} \left(\frac{y}{a-y} \right) \quad (A.2)$$

where F is a dimensionless quantity, D_e is effective gas diffusivity and R is universal gas constant. The parameter ψ is related to k_1 and k_2 as

$$\frac{k_1}{k_2} = \theta e^{\psi y} \quad (A.3)$$

Since the term ψy is a dimensionless parameter, the right hand side of the equation (A.2) has the same unit as θ which is $\text{gm-atom c/cm}^3/\text{sec}$ as obtained from equation (A.3) (improperly stated in the text as sec^{-1}). A straight forward dimensional analysis shows that the left hand side of equation (A.2) has a unit of $\text{gm-atom(or mole)/cm sec}$.

APPENDIX 7

PROGRAM FOR NON-ISOTHERMAL RATE CALCULATION

```

C      T=TEMPERATURE
C      WL=WT.LOSS IN GRAM
C      TI=TIME IN MIN
C      ACO2=RATE OF FLOW OF CO2 IN GM-MOLE/MIN
C      R=RATE OF REACTION AT 5% CONVERSION IN SEC-1
C      DELG=DELGO/(RT)
C      RT=RECIPROCAL OF TEMPERATURE
C      ZP=VALUE OF U AT PREVIOUS ITERATION
C      AN=ELEMENTS OF SUB DIAGONAL OF TDM
C      BN=ELEMENTS OF DIAGONAL OF TDM
C      CN=ELEMENTS OF SUPER DIAGONAL OF TDM
C      D=LOAD MATRIX
C      V=SOLUTION MATRIX
C      RELAX=UNDER/OVER/NORMAL RELAXATION VALUE
C      L=NO. OF GRID POINTS
C      M=NO. OF ITERATION
C
      DIMENSION T(5),WL(3,12),TI(3,12),ACO2(3,12),R(3,12),DELG(5)
      DIMENSION PCO(3,12),PCO2(3,12),PCO2E(5),FAI1(5),FAICO(5)
      DIMENSION FCO2(3,12),RT(3,3),ALFAI1(3,3),ALFAICO(5)
      DIMENSION FAI1N(5),FAICON(5)
      DIMENSION ZP(300),V(300),AN(300),BN(300),CN(300)
      DIMENSION DN(300),BETA1(10,10,300),BETA(5,10),TS(10),C2(10)
      DIMENSION MN(15)
      REAL*8 X(20),Y(20)
      REAL*8 SUMX(10,15),SUMY(10,15),SUMSX(10,15),SUMCX(10,15)
      REAL*8 SUMFOX(10,15),SUMFX(10,15),SUMXY(10,15)
      REAL*8 SUMSXY(10,25),YFIT(25)
      REAL*8 A(3,3),B(3,3),C(3,1),D(3,1),A0(10),A1(10),A2(10)
      DIMENSION CA(10),CB(10),CC(10),AK1(10),AK2(5),RO(5,10),RCP(5,10)
      DIMENSION ETA(5,10),ROW(5,10),RATIO(10),YSTAR(5,10),ASTAR(5)
      DIMENSION DELH(5),ALC(5,10),EFFEK(5,10),SUMRATIO(5),RATIOAV(5)
      DIMENSION RATIONEW(5),SIGMA(10),RATIONAV(5),CO2P(5,10)

      OPEN (UNIT=20,FILE='B:NONISO.DAT')
      OPEN (UNIT=21,FILE='B:NONISO.OUT')
C
      P=1.0
      ZS=1.0
      NN1=3
      READ (20,*) INC1,INC2,INC3
      DO 10 I=1,NN1
      READ (20,*) T(I)
      READ (20,*) N
      READ (20,*) (WL(I,J),J=1,N)
      READ (20,*) (TI(I,J),J=1,N)
      READ (20,*) (FCO2(I,J),J=1,N)
      READ (20,*) (R(I,J),J=1,N)
      READ (20,*) DELG(I)
      READ (20,*) NN

```

```

READ (20,*) (ROW(I,J),J=1,NN)
READ (20,*) DELH(I)
READ (20,*) (EFFEK(I,J),J=1,NN)
READ (20,*) (ALC(I,J),J=1,NN)
C READ (20,*) (RO(I,J),J=1,NN)
C READ (20,*) (CO2P(I,J),J=1,NN)

DO 15 J=1,N
ACD2(I,J)=FCO2(I,J)/22.4
15 CONTINUE
C
CALL PRECAL (WL,TI,ACD2,R,DELG,N,I,PCO,PCO2,PCO2E,FAI1,FAICO)
WRITE (21,1001) (PCO(I,J),PCO2(I,J),J=1,N)
WRITE (21,1002) PCO2E(I),FAI1(I),FAICO(I)
10 CONTINUE
J=1
DO 20 I=1,NN1
RT(I,J)=1.0/T(I)
ALFAI1(I,J)=ALOG10(FAI1(I))
ALFAICO(I)=ALOG10(FAICO(I))
20 CONTINUE
CALL LIN2 (ALFAI1,RT,NN1,CF,AM1)
WRITE (21,1003)
WRITE (21,*) CF,AM1
DO 30 I=1,NN1
ALFAI1(I,J)=AM1/T(I)+CF
FAI1N(I)=EXP(2.303*ALFAI1(I,J))
30 CONTINUE
CALL LIN2 (ALFAICO,RT,NN1,CF,AM1)
WRITE (21,1005)
WRITE (21,*) CF,AM1
WRITE (5,('*WRITE IM VALUE'))
READ (5,*) IM
READ (5,*) L,RELAX,M
DO 40 I=1,NN1
ALFAICO(I)=AM1/T(I)+CF
FAICON(I)=EXP(2.303*ALFAICO(I))
GO TO (31,32,33),I
31 NNF=1+INC1
GO TO 34
32 NNF=1+INC2
GO TO 34
33 NNF=1+INC3
GO TO 34
34 AK2(I)=1.0/FAICON(I)
SUMRATIO(I)=0.0
DO 35 J=1,NNF
AK1(J)=ROW(I,J)*FAI1N(I)/12.0
RATIO(J)=AK1(J)/AK2(I)
SUMRATIO(I)=SUMRATIO(I)+RATIO(J)
35 CONTINUE
RATIOAV(I)=SUMRATIO(I)/NNF
NAV=0
RATIONEW(I)=0.0

```

```

DO 36 J=1,NNF
SIGMA(J)=SQRT(((RATIO(J)-RATIOAV(I)**2)/NNF))
IF ((RATIO(J).GT.(RATIOAV(I)+2.0*SIGMA(J))) .OR. (RATIO(J) .LT.
1 (RATIOAV(I)-2.0*SIGMA(J)))) GO TO 36
RATIONEW(I)=RATIONEW(I)+RATIO(J)
NAV=NAV+1
36 CONTINUE
RATIONAV(I)=RATIONEW(I)/NAV
40 CONTINUE
CALL LIN2 (RATIONAV,T,NN1,C1,B1)
WRITE (21,*) C1,B1
DO 50 I=1,NN1
C2(I)=B1*T(I)
WRITE (5,*) C2(I)
50 CONTINUE
DO 51 I=1,IM
GO TO (52,53,54),I
52 NNF=1+INC1
GO TO 55
53 NNF=1+INC2
GO TO 55
54 NNF=1+INC3
GO TO 55
55 DO 56 J=1,NNF
YSTAR(I,J)=CO2P(I,J)/P
ASTAR (I)=(1.0+AK2(I)*P)/(AK2(I)*P)
BETA(I,J)=(ALC(I,J)**2*DELH(I)*YSTAR(I,J)*ROW(I,J)/(12.0*T(I)*
1 EFFEK(I,J)*(ASTAR(I)-YSTAR(I,J))))
56 CONTINUE
51 CONTINUE
1001 FORMAT (10X,'CO PRESS.',20X,'CO2 PRESS.'/8X,E11.4,17X,E13.4/)
1002 FORMAT (5X,'CO2 EQ. PRESS.',20X,'FAI1',20X,'FAICO'/3X,E13.4,
1 19X,E11.4,16X,F6.4/)
1003 FORMAT (/20X,'SLOPE AND INTERCEPT FOR FAI1'/)
1004 FORMAT (10X,'INTERCEPT',25X,'SLOPE'/4X,F8.4,21X,F11.2/)
1005 FORMAT (20X,'SLOPE AND INTERCEPT FOR FAICO'/)
IC=1
AN(1)=0
BN(1)=-1.0
CN(1)=1.0
H=1.0/(L-1)
DO 60 I=1,L
ZP(I)=ZS
60 CONTINUE
AN(L)=0.0
BN(L)=1.0
CN(L)=0.0
DN(L)=ZS
N1=1
DO 130 K=1,IM
GO TO (121,122,123),I
121 NNF=1+INC1
GO TO 124
122 NNF=1+INC2

```

```

GO TO 124
123 NNF=1+INC3
GO TO 124
124 DO 120 II=1,NNF
BETA1(K,II,1)=BETA(K,II)
DO 70 J=2,L-1
BETA1(K,II,J)=BETA(K,II)
AN(J)=1.0
BN(J)=-2.0
CN(J)=1.0
DN(J)=H**2*BETA1(K,II,J)*(C1+C2(K)*ZP(J))
70 CONTINUE
DN(1)=0.5*H**2*BETA1(K,II,1)*(C1+C2(K)*ZP(1))
WRITE (5,*) IC
CALL TRIDAG (IF,L,AN,BN,CN,DN,V)
DO 80 N=1,L
ZP(N)=ZP(N)+RELAX*(V(N)-ZP(N))
80 CONTINUE
WRITE (21,1006) BETA(K,II),C1,C2(K),L,M,T(K)
WRITE (21,1007) (V(N),N=1,L)
1006 FORMAT (/3X,'BETA VALUE',4X,'INTERCEPT',7X,'SLOPE',5X,
1 'NO.OF GRID'5X,'NO.OF ITER',5X,'TEMP'/F11.2,4X,E11.4,3X,
2 E11.4,7X,I3,12X,I2,5X,F6.0/)
1007 FORMAT (5F13.5/)
MN(1)=0
X(1)=0.0
Y(1)=V(1)
DO 90 I=2,10
MN(I)=1+MN(I-1)
X(I)=H*20.0*MN(I)
MM=20*(I-1)
Y(I)=V(MM)
90 CONTINUE
X(11)=1.0
Y(11)=1.0

```

C
C
C
C

PROGRAMME FOR POLYNOMIAL CURVE FITTING

```

N1=11
SUMX(K,II)=0
SUMY(K,II)=0
SUMSX(K,II)=0
SUMCX(K,II)=0
SUMFOX(K,II)=0
SUMFX(K,II)=0
SUMXY(K,II)=0
SUMSXY(K,II)=0
DO 100 I=1,N1
SUMX(K,II)=SUMX(K,II)+X(I)
SUMY(K,II)=SUMY(K,II)+Y(I)
SUMSX(K,II)=SUMSX(K,II)+X(I)**2
SUMCX(K,II)=SUMCX(K,II)+X(I)**3
SUMFOX(K,II)=SUMFOX(K,II)+X(I)**4

```

```

SUMFX(K,II)=SUMFX(K,II)+X(I)**5
SUMXY(K,II)=SUMXY(K,II)+X(I)*Y(I)
SUMSXY(K,II)=SUMSXY(K,II)+X(I)**2*Y(I)
100  CONTINUE
    A(1,1)=N1
    A(1,2)=SUMX(K,II)
    A(1,3)=SUMSX(K,II)
    A(2,1)=SUMX(K,II)
    A(2,2)=SUMSX(K,II)
    A(2,3)=SUMCX(K,II)
    A(3,1)=SUMSX(K,II)
    A(3,2)=SUMCX(K,II)
    A(3,3)=SUMFOX(K,II)
    CALL GJORD(3,A)
    C(1,1)=SUMY(K,II)
    C(2,1)=SUMXY(K,II)
    C(3,1)=SUMSXY(K,II)
    CALL MATMUL (A,C,D,3,1)
    A0(II)=D(1,1)
    A1(II)=D(2,1)
    A2(II)=D(3,1)
    DO 110 J=1,N1
    YFIT(J)=A0(II)+A1(II)*X(J)+A2(II)*X(J)**2
110  CONTINUE
    WRITE (21,1008) A0(II),A1(II),A2(II)
    WRITE (21,1009) (X(J),YFIT(J),J=1,N1)
1008  FORMAT (/6X,'A0',10X,'A1',10X,'A2'/2X,3(F8.4,4X))
1009  FORMAT (/6X,'DISTANCE',30X,'TEMPERATURE'/(F15.4,32X,F8.4))
    CA(II)=C1+C2(K)*A0(II)
    CB(II)=C2(K)*A1(II)
    CC(II)=C2(K)*A2(II)
    RCP(K,II)=YSTAR(K,II)/(ASTAR(K)-YSTAR(K,II))*(CA(II)+
1  0.5*CB(II)+CC(II)/3.0)
    RO(K,II)=(FAI1N(K)*ROW(K,II)*(CO2P(K,II)-PCO2E(K))/(12.0*(1+
1  (PCO(K,II)/FAICON(K))))))
    ETA(K,II)=RCP(K,II)/RO(K,II)
    WRITE (21,1010)
    WRITE (21,1011) RCP(K,II),RO(K,II),ETA(K,II)
    IC=IC+1
120  CONTINUE
130  CONTINUE
1010  FORMAT (5X,'RCP VALUE',15X,'RO VALUE',15X,'ETA VALUE')
1011  FORMAT (3X,E11.4,13X,E11.4,13X,F6.4)
    STOP
    END

C -----
C SUBROUTINE FOR PARTIAL PRESSURE CALCULATION
C -----
SUBROUTINE PRECAL (WL,TI,ACO2,R,DELG,N,I,PCO,PCO2,PCO2E,
1 FAI1,FAICO)
    DIMENSION WL(3,12),TI(3,12),ACO2(3,12),R(3,12),DELG(5)
    DIMENSION WTLOSS(3,12),ACO(3,12),XCO(3,12),PCO(3,12)
    DIMENSION PCO2(3,12),PCO2E(5),A(3,12),FAI1(5),FAICO(5)

```

```

P=1.0
PCO2E(I)=(2.0+DELG(I))-SQRT((2.0+DELG(I))**2-4.0)/2.0
DO 20 J=1,N
WTLOSS(I,J)=WL(I,J)/12.0
ACD(I,J)=WTLOSS(I,J)*2.0/TI(I,J)
XCD(I,J)=ACD(I,J)/ACD2(I,J)
PCD(I,J)=XCD(I,J)*P
PCD2(I,J)=1.0-PCD(I,J)
A(I,J)=(PCD2(I,J)-PCO2E(I))/R(I,J)
WRITE (5,*) A(I,J)
20 CONTINUE
CALL LIN1 (A,PCD,N,I,C,M1)
FAI1(I)=1.0/C
FAICO(I)=1.0/(FAI1(I)*M1)
RETURN
END

```

```

C -----
C SUBROUTINE FOR LINEAR CURVE FIT
C -----
SUBROUTINE LIN1 (Y1,X1,N,I,C,M1)
DIMENSION X1(3,1),Y1(3,1)
DIMENSION SUMX(5),SUMSX(5),SUMY(5),SUMXY(5),DENOM(5)
C
SUMX(I)=0
SUMSX(I)=0
SUMY(I)=0
SUMXY(I)=0
DO 30 J=1,N
SUMX(I)=SUMX(I)+X1(I,J)
SUMSX(I)=SUMSX(I)+X1(I,J)**2
SUMY(I)=SUMY(I)+Y1(I,J)
SUMXY(I)=SUMXY(I)+X1(I,J)*Y1(I,J)
30 CONTINUE
DENOM(I)=N*SUMSX(I)-SUMX(I)*SUMX(I)
C=(SUMY(I)*SUMSX(I)-SUMX(I)*SUMXY(I))/DENOM(I)
M1=(N*SUMXY(I)-SUMX(I)*SUMY(I))/DENOM(I)
RETURN
END

```

```

C -----
C SUBROUTINE LIN2
C -----
SUBROUTINE LIN2 (Y1,X1,NN1,CF,AM1)
DIMENSION X1(5),Y1(5)
C
SUMX=0.0
SUMSX=0.0
SUMY=0.0
SUMXY=0.0
DO 40 I=1,NN1
SUMX=SUMX+X1(I)

```



```

SUMY=SUMY+Y1(I)
SUMSX=SUMSX+X1(I)**2
SUMXY=SUMXY+X1(I)*Y1(I)
40  CONTINUE
    DENOM=NN1*SUMSX-SUMX*SUMX
    CF=(SUMY*SUMSX-SUMX*SUMXY)/DENOM
    AM1=(NN1*SUMXY-SUMX*SUMY)/DENOM
    RETURN
    END
C*****
C  SUBROUTINE FOR MATRIX INVERSION BY GAUSS JORDON METHOD
C*****

SUBROUTINE GJORD (N4,A)
REAL*8 A(N4,N4)
DO 50 KK=1,N4
    DO 10 J=1,N4
        IF (J.EQ.KK) GO TO 10
        A(KK,J)=A(KK,J)/A(KK,KK)
10    CONTINUE
    A(KK,KK)=1/A(KK,KK)
    DO 30 I=1,N4
        IF (I.EQ.KK) GO TO 30
        DO 20 J=1,N4
            IF (J.EQ.KK) GO TO 20
            A(I,J)=A(I,J)-A(KK,J)*A(I,KK)
20    CONTINUE
30    CONTINUE
    DO 40 I=1,N4
        IF (I.EQ.KK) GO TO 40
        A(I,KK)=-A(I,KK)*A(KK,KK)
40    CONTINUE
50    CONTINUE
    RETURN
    END

C*****
C  SUBROUTINE FOR MATRIX MULTIPLICATION
C*****

SUBROUTINE MATMUL (B,C,D,ML,NL)
REAL*8 B(ML,ML),C(ML,NL),D(ML,NL)
DO I=1,ML
    DO J=1,NL
        D(I,J)=0.0
        DO K=1,ML
            D(I,J)=D(I,J)+B(I,K)*C(K,J)
        ENDDO
    ENDDO
ENDDO
RETURN
END

```

```
SUBROUTINE TRIDAG(IF,L,AN,BN,CN,DN,V)  
DIMENSION AN(300),BN(300),CN(300),DN(300),V(300)  
DIMENSION BETA(301),GAMMA(301)
```

C

```
IF=1  
BETA(IF)=BN(IF)  
GAMMA(IF)=DN(IF)/BETA(IF)  
IFP1=IF+1  
DO 10 I=IFP1,L  
BETA(I)=BN(I)-AN(I)*CN(I-1)/BETA(I-1)  
GAMMA(I)=(DN(I)-AN(I)*GAMMA(I-1))/BETA(I)  
CONTINUE
```

10

C

```
V(L)=GAMMA(L)  
LAST=L-IF  
DO 20 K=1, LAST  
I=L-K  
V(I)=GAMMA(I)-CN(I)*V(I+1)/BETA(I)  
CONTINUE  
RETURN  
END
```

20

APPENDIX 8

PROGRAM FOR INSTANTANEOUS RATE CALCULATION OF GASIFICATION

```

c*****
c      Reactivity calculation with polynomial curve fitting
c*****
c      wbs=Wt. of bucket + sample
c      wb= Wt. of bucket
c      wbi=Initial wt. of sample
c      wbss=Starting wt. of sample
c      wbsht=Wt.of bucket + sample + hanging assembly after 10 min. of
c            argon flow
c      wbsht=Instantaneous wt. of bucket + sample + hanging assembly
c      pcw=Percentage wt. loss in argon at 10 th. min.
c      delw=Wt. loss of the sample after 10 th. min. during reactivity study
c      fc=Fixed carbon
c      y=Instantaneous wt. loss
c      dely=Instantaneous wt. loss due to evaporation
c      pc=Percentage instantaneous wt. loss
c      ya=Actual instantaneous wt. loss
c      x=Time in minute
c      wbss1=Starting wt. of carbon without fixed carbon correction
      IMPLICIT REAL*8 (A-H, O-Z)
      REAL*8 WBS(50),WB(50),WBI(50),WBSS1(50),WBSS(50),WBSH1(50)
      REAL*8 WBSH1(2,20)
      REAL*8 PCW(50),DELW(20),Y(2,20),DELY(2,20),PC(2,20),X(20)
      REAL*8 SUMX(20),SUMYA(20),SUMSX(20),SUMCX(20)
      REAL*8 SUMFOX(20),SUMFX(20),SUMSIX(20),SUMXYA(20)
      REAL*8 SUMSXYA(20),SUMCXYA(20),NN1(20)
      REAL*8 YFIT(20),REACI(20),WC(2,20),RAV(20)
      REAL*8 AO(2,2),A1(2,2),A2(2,2)
      REAL*8 A3(2,2),FDIF(20)
      REAL*8 A(4,4),B(4,4),C(4,1),D(4,1),YA(2,20)
      N=2
      NSET=0
      FC=0.974
      N1=12
      OPEN (UNIT=20, FILE='B:REACTIVE.DAT')
      OPEN (UNIT=23, FILE='B:TIMEETC.DAT')
      OPEN (UNIT=36, FILE='B:REACTIVE.OUT')
      READ (23,*) (X(I),I=1,N1)
      READ (23,*) (PCW(I),I=1,N)
      READ (23,*) ((PC(I,J),J=1,N1),I=1,N)
10      READ (20,*,END=999) (WBS(I),I=1,N)
      READ (20,*,END=998) (WB(I),I=1,N)
      READ (20,*,END=998) (WBSH1(I),I=1,N)
      READ (20,*,END=998) ((WBSH1(I,J),J=1,N1),I=1,N)
      NSET=NSET+1
      WRITE(5,('( ' DATA SET : ',I2)')NSET
      WRITE(36,1001)NSET
1001  FORMAT(/25X,'D A T A      S E T   = ',I2/)
      DO 20 I=1,N

```

```

    WBI(I)=(WBS(I)-WB(I))
    DELW(I)=(WBI(I)*PCW(I)/100)
    WBSS1(I)=(WBI(I)-DELW(I))
    WBSS(I)=WBSS1(I)*FC
20  CONTINUE
    DO 40 I=1,N
        DO 30 J=1,N1
            Y(I,J)=WBSH1(I)-WBSH1(I,J)
            DELY(I,J)=WBSS1(I)*PC(I,J)/100
            YA(I,J)=Y(I,J)-DELY(I,J)
            WC(I,J)=WBSS(I)-YA(I,J)
30      CONTINUE
40      CONTINUE
C
    IFLAG=1
50      DO 60 I=1,N
        SUMX(I)=0
        SUMYA(I)=0
        SUMSX(I)=0
        SUMCX(I)=0
        SUMFOX(I)=0
        SUMFX(I)=0
        SUMSIX(I)=0
        SUMXYA(I)=0
        SUMSXIA(I)=0
        SUMCXIA(I)=0
60      CONTINUE
        DO 90 I=1,N
            DO 70 J=1,N1
                SUMX(I)=SUMX(I)+X(J)
                SUMYA(I)=SUMYA(I)+YA(I,J)
                SUMSX(I)=SUMSX(I)+X(J)**2
                SUMCX(I)=SUMCX(I)+X(J)**3
                SUMFOX(I)=SUMFOX(I)+X(J)**4
                SUMFX(I)=SUMFX(I)+X(J)**5
                SUMSIX(I)=SUMSIX(I)+X(J)**6
                SUMXYA(I)=SUMXYA(I)+X(J)*YA(I,J)
                SUMSXIA(I)=SUMSXIA(I)+X(J)**2*YA(I,J)
                SUMCXIA(I)=SUMCXIA(I)+X(J)**3*YA(I,J)
70      CONTINUE
        A(1,1)=12.0/SUMYA(I)
        A(1,2)=SUMX(I)/SUMYA(I)
        A(1,3)=SUMSX(I)/SUMYA(I)
        A(1,4)=SUMCX(I)/SUMYA(I)
        A(2,1)=SUMX(I)/SUMXYA(I)
        A(2,2)=SUMSX(I)/SUMXYA(I)
        A(2,3)=SUMCX(I)/SUMXYA(I)
        A(2,4)=SUMFOX(I)/SUMXYA(I)
        A(3,1)=SUMSX(I)/SUMSXIA(I)
        A(3,2)=SUMCX(I)/SUMSXIA(I)
        A(3,3)=SUMFOX(I)/SUMSXIA(I)
        A(3,4)=SUMFX(I)/SUMSXIA(I)
        A(4,1)=SUMCX(I)/SUMCXIA(I)
        A(4,2)=SUMFOX(I)/SUMCXIA(I)

```

```

A(4,3)=SUMFX(I)/SUMCX YA(I)
A(4,4)=SUMSIX(I)/SUMCX YA(I)
CALL GJORD(4,A)
C(1,1)=1
C(2,1)=1
C(3,1)=1
C(4,1)=1
CALL MATMUL (A,4, C,4, 4,4,1, D,4)
AO(IFLAG,I)=D(1,1)
A1(IFLAG,I)=D(2,1)
A2(IFLAG,I)=D(3,1)
A3(IFLAG,I)=D(4,1)
DO 80 J=1,N1
    YFIT(J)=AO(IFLAG,I)+A1(IFLAG,I)*X(J)
1      +A2(IFLAG,I)*X(J)**2+A3(IFLAG,I)*X(J)**3
80     CONTINUE
    WRITE (36,1002) AO(IFLAG,I),A1(IFLAG,I),A2(IFLAG,I),
1      A3(IFLAG,I)
1002    FORMAT (/6X,'AO',10X,'A1',10X,'A2',10X,'A3'/2X,4(F8.4,4X))
    IF (IFLAG .EQ. 2) THEN
        IF (I .EQ. 1) THEN
            DO J = 1, N1
                RAV (J) = YFIT (J)
            END DO
            WRITE (36, 1003) (X(J),YA(I,J),YFIT(J),J =1,N1)
        ELSE
            DO J = 1, N1
                RAV (J) = 0.5 * (RAV(J) + YFIT (J))
            END DO
            WRITE(36,1005) (X(J),YA(I,J),YFIT(J),RAV(J),J=1,N1)
        ENDIF
    ELSE
        WRITE (36,1004) (X(J), YA(I, J), YFIT(J), J = 1, N1)
    ENDIF
C1003    FORMAT (/6X,'TIME(s)',6X,'INS. REAC',9X,'FIT. REAC'/
C      1    (F13.2,6X,2(F8.4,10X)))
1004    FORMAT (/6X,'TIME(Min)/10',4X,'WT.LOSS(gm)',15X,'YFIT'/
      1    (F13.2,9X, 2(F8.4, 10X)))
C1005    FORMAT (/6X,'TIME(s)',6X,'INS. REAC',9X,'FIT. REAC',
C      1    10X,'REAC AV'/(F13.2,6X, 2(F8.4, 10X),F8.5))
90     CONTINUE
    IF (IFLAG .EQ. 2) GO TO 10
    DO 110 I=1,N
        DO 100 J=1,N1
            FDIF(J)=A1(IFLAG,I)+A2(IFLAG,I)*2*X(J)
1      +A3(IFLAG,I)*3*X(J)**2
            REACI(J)=FDIF(J)/WC(I,J)
            YA(I,J)=REACI(J)
100     CONTINUE
110     CONTINUE
        IFLAG=IFLAG+1
        GO TO 50
998     WRITE (5, *) ' INSUFFICIENT DATA !!'
999     CLOSE (UNIT = 20)

```

```

      STOP
      END
C*****
C      SUBROUTINE FOR MATRIX INVERSION BY GAUSS JORDON METHOD
C*****
      SUBROUTINE GJORD (N4,A)
      REAL*8 A(N4,N4)
      DO 50 K=1,N4
        DO 10 J=1,N4
          IF (J.EQ.K) GO TO 10
          A(K,J)=A(K,J)/A(K,K)
10       CONTINUE
          A(K,K)=1/A(K,K)
          DO 30 I=1,N4
            IF (I.EQ.K) GO TO 30
            DO 20 J=1,N4
              IF (J.EQ.K) GO TO 20
              A(I,J)=A(I,J)-A(K,J)*A(I,K)
20          CONTINUE
30       CONTINUE
          DO 40 I=1,N4
            IF (I.EQ.K) GO TO 40
            A(I,K)=-A(I,K)*A(K,K)
40          CONTINUE
50       CONTINUE
      RETURN
      END
C*****
C      SUBROUTINE FOR MATRIX MULTIPLICATION
C      matD (L X N) = matC(L X M) X matB(M X N)
C*****
      SUBROUTINE MATMUL (B,IB,C,IC,L,M,N,D,ID)
      REAL*8 B(IB,M),C(IC,N),D(ID,N)
      DO I=1,L
        DO J=1,N
          D(I,J)=0.0
          DO K=1,M
            D(I,J)=D(I,J)+B(I,K)*C(K,J)
          ENDDO
        ENDDO
      RETURN
      END

```

APPENDIX 9

PROGRAM FOR THE CALCULATION OF A AND E FACTORS OF ISOTHERMAL
MASS TRANSFER ANALYSIS

```

C      Y= MOLECULAR WEIGHT OF ARGON OR CARBON MONOXIDE
C      ROW= BULK DENSITY
C      ALC= BED DEPTH
C      POR= POROSITY OF BED
C      RD= RATE OF GASIFICATION IN SEC-1)
C
      DIMENSION T(5),OHM(5,9),SIG(5,9),B(5,9),Y(5,9)
      DIMENSION ANUM(5,9),DIN(5,9)
      DIMENSION DB(5,9),DK(5,9),C(5,9),D(5,9),DE(5,9)
      DIMENSION ROW(5,9),ALC(5,9),POR(5,9),RD(5,9)
      DIMENSION FAICO(5),AK2(5),A(5),E(5,9)
C
      OPEN (UNIT=20,FILE='B:REPCHAR.DAT')
      OPEN (UNIT=22,FILE='B:REPCHAR.OUT')
C
      R=82.05
      P=1.0
      X=44.0
      PS=0.0029
      S=PS/3.0
      N=4
      DO 5 I=1,N
      READ (20,*) N1
      READ (20,*) (Y(I,J),J=1,N1)
      READ (20,*) T(I)
      READ (20,*) (OHM(I,J),J=1,N1)
      READ (20,*) (SIG(I,J),J=1,N1)
      READ (20,*) (ROW(I,J),J=1,N1)
      READ (20,*) (ALC(I,J),J=1,N1)
      READ (20,*) (POR(I,J),J=1,N1)
      READ (20,*) (RD(I,J),J=1,N1)
      DO 10 J=1,N1
        B(I,J)=(X+Y(I,J))/(X*Y(I,J))
        ANUM(I,J)=SQRT(T(I)**3*B(I,J))
        DIN(I,J)=P*SIG(I,J)**2*OHM(I,J)
        DB(I,J)=0.0018583*ANUM(I,J)/DIN(I,J)
        DK(I,J)=9.73E3*S*(T(I)/X)**0.5
        C(I,J)=1/DK(I,J)+1/DB(I,J)
        D(I,J)=1/C(I,J)
        DE(I,J)=POR(I,J)**2*D(I,J)/SQRT(3.0)
        FAICO(I)=EXP(2.303*(-5940/T(I)+3.46))
        AK2(I)=1/FAICO(I)
        A(I)=(1+AK2(I))/AK2(I)
        E(I,J)=R*T(I)*ALC(I,J)**2*ROW(I,J)*RD(I,J)/
1      (DE(I,J)*AK2(I)*12)
10     CONTINUE
      WRITE (22,1001) (T(I),ALC(I,J),DE(I,J),J=1,N1)
      WRITE (22,1002) (A(I),E(I,J),J=1,N1)
5     CONTINUE

```

287
1001 FORMAT (5X, 'TEMPERATURE', 10X, 'BED DEPTH', 10X, 'DIFFUSIVITY' / 8X,
 2 F6.1, 14X, F6.3, 14X, F6.4 /)
1002 FORMAT (10X, 'A-FACTOR', 24X, 'E-FACTOR' / (F17.4, 15X, F17.4))
 STOP
 END

APPENDIX 10

PROGRAM FOR CARBOTHERMIC RATE CALCULATION

```

C      N=ORDER OF POLYNOMIAL FIT
C      IN= NO. OF GAS ANALYSIS EXPERIMENTS
C      K= NO. OF POINTS IN EACH GAS ANALYSIS EXPERIMENT
C      MM= NO. OF POINTS IN EACH CARBOTHERMIC EXPERIMENT
C      Y= PCT. CO IN GAS ANALYSIS EXPT.
C      X= TIME INSTANT FOR GAS ANALYSIS
C      T= TIME INSTANT FOR WT. LOSS MEASUREMENT IN CARBOTHERMIC
C      REDUCTION
C      REAC= RATE OF TOTAL WT. LOSS IN CARBOTHERMIC REDUCTION
C      REACC=RATE OF CARBON LOSS
C      REACO=RATE OF OXYGEN LOSS
C      WCI=WEIGHT OF INITIAL CARBON
C      WCIN=WEIGHT OF INSTANTANEOUS CARBON
C      REACCI=TOTAL CARBON LOSS IN TIME T=T
C      REACOI=TOTAL OXYGEN LOSS IN TIME T=T
C      TO=TOTAL REMOVABLE OXYGEN FROM IRON OXIDE
C
C      REAL*8 A(20),E(20),D(10,1),C(8,8),B(10,5)
C      DIMENSION X(10,50),Y(10,50),T(10,50),REAC(10,50),REACO(10,50)
C      DIMENSION COFF(10),YFIT(50),REACC(10,50),WTLOSS(10,50),YFITI(50)
C      DIMENSION REACCI(10,50),REACOI(10,50),PCT(10,50),TO(10,2)
C      DIMENSION WCI(10,2),WCIN(50)
C
C      OPEN (UNIT=20,FILE='B:RED.DAT')
C      OPEN (UNIT=21,FILE='B:RED.OUT')
C      OPEN (UNIT=22,FILE='B:R.OUT')
C
C      NSET=1
C      NSET1=1
C      READ (20,*) IN
C      DO 10 I=1,IN
C      READ (20,*) N
C      READ (20,*) IK
C      READ (20,*) (X(I,J),J=1,IK)
C      READ (20,*) (Y(I,J),J=1,IK)
C      READ (20,*) MM
C      READ (20,*) (T(I,J),J=1,MM)
C      READ (20,*) (REAC(I,J),J=1,MM)
C      READ (20,*) (WTLOSS(I,J),J=1,MM)
C      READ (20,*) (TO(I,J),J=1,2)
C      READ (20,*) (WCI(I,J),J=1,2)
C
C      IA=0.5*MM
C      IIA=IA+1
C      IFLAG=1
C      WRITE (5,*) NSET
C      WRITE (21,1000) NSET
5      DO 20 J=1,N+N
C          A(J)=0.0

```

```

20      CONTINUE
C
C.....ASSIGNING PARAMETERS TO THE COEFFICIENT MATRIX
C
      DO 30 M=1,N+N
        DO 40 J=1,IK
          A(M)=A(M)+X(I,J)**M
40      CONTINUE
30      CONTINUE
C      WRITE (5, '(F4.2)') (X(I,J),J=1,IK)
      DO 50 J=1,N+1
        E(J)=0.0
50      CONTINUE
      KK=0.0
      DO 60 J=1,N+1
        DO 70 IM=1,IK
          E(J)=E(J)+Y(I,IM)*X(I,IM)**KK
70      CONTINUE
      KK=KK+1
60      CONTINUE
      DO 80 J=1,N+1
        D(J,1)=E(J)/E(N+1)
80      CONTINUE
      C(1,1)=IK/E(N+1)
      J=1
      DO 90 II=2,N+1
        C(1,II)=A(J)/E(N+1)
        J=J+1
90      CONTINUE
      J=1
      DO 100 M=2,N+1
        DO 110 II=1,N+1
          C(M,II)=A(J)/E(N+1)
          J=J+1
110     CONTINUE
      J=J-N
100     CONTINUE
C
C      SOLUTION OF THE SIMULTANEOUS EQUATIONS
C
      CALL GJORD (N+1,C)
      CALL MATMUL (C,D,B,N+1,1)
C
C      REPRODUCTION OF THE Y VALUES
C
      DO 120 J=1,N+1
        COFF(J)=B(J,1)
120     CONTINUE
      DO 115 IM=1,IK
        YFIT(IM)=0.0
115     CONTINUE
      DO 130 IM=1,IK
        DO 140 J=2,N+1
          YFIT(IM)=YFIT(IM)+COFF(J)*X(I,IM)**(J-1)

```

```

140      CONTINUE
      YFIT(IM)=YFIT(IM)+COFF(1)
130    CONTINUE
      IF (IK.EQ.IA) GO TO 180
      WRITE (21,1001)
      WRITE (21,1002)
      WRITE (21,1003) (X(I,IM),Y(I,IM),YFIT(IM),IM=1,IK)
      DO 150 IM=1,MM
        YFIT(IM)=0.0
150    CONTINUE
      DO 155 IM=1,IA
        DO 160 J=2,N+1
          YFIT(IM)=YFIT(IM)+COFF(J)*T(I,IM)**(J-1)
160    CONTINUE
      YFIT(IM)=YFIT(IM)+COFF(1)
      IF ((YFIT(IM)-Y(I,IK)).GE.0.03) GO TO 157
      C    WRITE (5,*) IM
155    CONTINUE
157    DO 158 J=IM,IA
      YFIT(J)=Y(I,IK)
      C    WRITE (5,*) J
158    CONTINUE
      DO 159 IM=IIA,MM
        DO 161 J=2,N+1
          YFIT(IM)=YFIT(IM)+COFF(J)*T(I,IM)**(J-1)
161    CONTINUE
      YFIT(IM)=YFIT(IM)+COFF(1)
      IF ((YFIT(IM)-Y(I,IK)).GE.0.02) GO TO 162
      C    WRITE (5,*) IM
159    CONTINUE
162    DO 163 J=IM,MM
      YFIT(J)=Y(I,IK)
      C    WRITE (5,*) J
163    CONTINUE
      WRITE (21,1004) (T(I,IM),YFIT(IM),IM=1,MM)
      C    CALCULATION OF THE RATE OF CARBON LOSS
      DO 165 J=1,MM
        REACC(I,J)=3.0*REAC(I,J)/(7*YFIT(J)+11.0*(1-YFIT(J)))
        REACO(I,J)=REAC(I,J)*((8.0-4.0*YFIT(J))/(11.0-4.0*YFIT(J)))
165    CONTINUE
      N=7
      INC=1
      DO 170 IJ=1,IA
        X(I,IJ)=T(I,IJ)
        Y(I,IJ)=REACC(I,IJ)
        INC=INC+1
170    CONTINUE
      GO TO 176
172    IL=1
      DO 175 IJ=IA+1,MM
        L=IL
        X(I,L)=T(I,IJ)
        Y(I,L)=REACC(I,IJ)
        IL=IL+1

```

```

        INC=INC+1
175  CONTINUE
        NSET1=NSET1+1
        WRITE (5, '(F4.2)') (X(I,L), L=1, IA)
176  WRITE (21, 1009) NSET1
        WRITE (21, 1005)
        WRITE (21, 1006)
        IK=IA
        GO TO 5
180  WRITE (21, 1007) (X(I,IM), Y(I,IM), YFIT(IM), IM=1, IK)
        DO 190 L=1, IA
            YFITI(L)=0.0
190  CONTINUE
        DO 191 L=1, IA
            DO 200 K=1, N+1
                YFITI(L)=YFITI(L)+COFF(K)*(X(I,L)**K)/K
                WCIN(L)=WCI(I, IFLAG)-YFITI(L)
200  CONTINUE
C      CALCULATION OF THE TOTAL WEIGHT LOSS OF CARBON AT TIME
C      INSTANT T=T
        REACCI(I,L)=YFITI(L)
191  CONTINUE
C      CALCULATION OF THE TOTAL WEIGHT LOSS OF OXYGEN AT TIME
C      INSTANT T=T AND PERCENTAGE REDUCTION
        IL=1
        IF (IJ.GT.L) GO TO 220
        DO 210 L=1, IA
            REACOI(I,L)=WTLOSS(I,L)-REACCI(I,L)
            PCT(I,L)=REACOI(I,L)/TO(I,1)
210  CONTINUE
        WRITE (21, 1008) (REACCI(I,L), REACOI(I,L), PCT(I,L), L=1, IA)
        WRITE (22, 1010) (REACOI(I,L), PCT(I,L), WCIN(L), L=1, IA)
        IFLAG=IFLAG+1
        IF (INC.EQ.IIA) GO TO 172
220  DO 230 J=IIA, MM
            L=IL
            REACOI(I,L)=WTLOSS(I,J)-REACCI(I,L)
            PCT(I,L)=REACOI(I,L)/TO(I,2)
            IL=IL+1
230  CONTINUE
        WRITE (21, 1008) (REACCI(I,L), REACOI(I,L), PCT(I,L), L=1, IA)
        WRITE (22, 1010) (REACOI(I,L), PCT(I,L), WCIN(L), L=1, IA)
        NSET=NSET+1
        NSET1=1
        IFLAG=1
10  CONTINUE
1000  FORMAT (25X, 'DATA SET : ', I2//)
1001  FORMAT (5X, 'ORIGINAL AND REPRODUCED DATA OF PCT.CO'//)
1002  FORMAT (8X, 'TIME', 15X, '% CO', 15X, '% CO REPRODUCED'//)
1003  FORMAT (6X, F6.2, 15X, F4.2, 21X, F4.2//)
1004  FORMAT (//5X, '% CO REPRODUCED AT THE TIME INSTANTS OF
1  CARBOTHERMIC REDUCTION'//10X, 'TIME', 20X, '% CO'/(8X, F6.2,
2  20X, F4.2//))
1005  FORMAT (//5X, 'RATE OF CARBON AND OXYGEN LOSS IN CARBOTHERMIC

```

```

1 REDUCTION'//)
1006 FORMAT (8X,'TIME',17X,'RATE',15X,'RATE REPRODUCED'//)
1007 FORMAT (6X,F6.2,16X,F6.4,18X,F6.4//)
1008 FORMAT (/5X,'INT.C LOSS',10X,'INT. O2 LOSS',10X,'PCT. REDUN'//
1 (7X,F6.3,14X,F6.3,15X,F6.2//))
1009 FORMAT (/25X,'SET NO. :',12//)
1010 FORMAT (/10X,'RATE OF OXYGEN LOSS AND WEIGHT OF CARBON AT TIME
1 T=T'//5X,'RATE OF O LOSS',10X,'PCT. REDUN',10X,'INS. C WT.'/(9X,
1 F6.4,17X,F4.2,15X,F6.4))
STOP
END

C *****
C SUBROUTINE FOR MATRIX INVERSION BY GAUSS JORDON METHOD
C *****
SUBROUTINE GJORD (N4,C)
REAL*8 C(N4,N4)
DO 50 K=1,N4
DO 10 J=1,N4
IF (J.EQ.K) GO TO 10
C(K,J)=C(K,J)/C(K,K)
10 CONTINUE
C(K,K)=1/C(K,K)
DO 30 I=1,N4
IF(I.EQ.K) GO TO 30
DO 20 J=1,N4
IF (J.EQ.K) GO TO 20
C(I,J)=C(I,J)-C(K,J)*C(I,K)
20 CONTINUE
30 CONTINUE
DO 40 I=1,N4
IF (I.EQ.K) GO TO 40
C(I,K)=-C(I,K)*C(K,K)
40 CONTINUE
50 CONTINUE
RETURN
END

C *****
C SUBROUTINE FOR MATRIX MULTIPLICATION
C MAT D(LxM) =MAT C(LxM) X MAT B(MxN)
C *****
SUBROUTINE MATMUL (B,C,D,L,M)
REAL*8 B(L,L),C(L,M),D(L,M)
J=M
DO I=1,L
D(I,J)=0.0
DO K=1,L
D(I,J)=D(I,J)+B(I,K)*C(K,J)
ENDDO
ENDDO
RETURN
END

```

Temp.=1246K

Expt.No. : 20

Gas composition : CO₂=100%, Ar = 0%

SET 1

Initial wt. of sample =0.0462 gm.

SET 2

Initial wt. of sample =0.0559gm

TIME(Min)/10	WT.LOSS(gm)
0.05	0.0006
0.10	0.0015
0.15	0.0033
0.20	0.0053
0.25	0.0073
0.30	0.0095
0.35	0.0121
0.40	0.0148
0.50	0.0208

TIME(Min)/10	WT.LOSS(gm)
0.05	0.0008
0.10	0.0021
0.15	0.0043
0.20	0.0065
0.25	0.0088
0.30	0.0113
0.35	0.0140
0.40	0.0171
0.50	0.0238

Expt.No. : 34

Gas composition : CO₂ = 80%, Ar = 20%

Initial wt. of sample =0.0550 gm.

Initial wt. of sample =0.0573gm

TIME(Min)/10	WT.LOSS(gm)
0.05	0.0014
0.10	0.0031
0.15	0.0052
0.20	0.0072
0.25	0.0088
0.30	0.0118
0.35	0.0147
0.40	0.0170
0.50	0.0227
0.60	0.0288
0.70	0.0346

TIME(Min)/10	WT.LOSS(gm)
0.05	0.0018
0.10	0.0036
0.15	0.0061
0.20	0.0082
0.25	0.0111
0.30	0.0136
0.35	0.0158
0.40	0.0191
0.50	0.0251
0.60	0.0316
0.70	0.0376

Expt.No. : 35

Gas composition : CO₂ = 50%, Ar = 50%

Initial wt. of sample =0.0631 gm.

Initial wt. of sample =0.0706gm

TIME(Min)/10	WT.LOSS(gm)
0.05	0.0021
0.10	0.0037
0.15	0.0061
0.20	0.0086
0.25	0.0105
0.30	0.0132
0.35	0.0161
0.40	0.0191
0.50	0.0250
0.60	0.0310
0.70	0.0371

TIME(Min)/10	WT.LOSS(gm)
0.05	0.0019
0.10	0.0038
0.15	0.0060
0.20	0.0080
0.25	0.0103
0.30	0.0129
0.35	0.0157
0.40	0.0180
0.50	0.0242
0.60	0.0303
0.70	0.0370

Expt.No. : 36

Gas composition : CO₂ = 20%, Ar = 80%

Initial wt. of sample =0.0559 gm.

Initial wt. of sample =0.0521gm

TIME(Min)/10	WT.LOSS(gm)
0.05	0.0018
0.10	0.0025
0.15	0.0035
0.20	0.0045
0.25	0.0055
0.30	0.0065
0.35	0.0077
0.40	0.0090
0.50	0.0116
0.60	0.0147
0.70	0.0183
0.80	0.0215

TIME(Min)/10	WT.LOSS(gm)
0.05	0.0007
0.10	0.0009
0.15	0.0016
0.20	0.0024
0.25	0.0035
0.30	0.0049
0.35	0.0060
0.40	0.0071
0.50	0.0094
0.60	0.0120
0.70	0.0150
0.80	0.0175

Temp.= 1204 K

Expt.No. : 24
 Gas composition : CO₂ = 100%, Ar = 0%

SET 1

Initial wt. of sample = 0.0445 gm.

TIME(Min)/10	WT.LOSS(gm)
0.10	0.0026
0.20	0.0067
0.30	0.0123
0.40	0.0183
0.50	0.0243
0.60	0.0291
0.70	0.0342

SET 2

Initial wt. of sample = 0.0511 gm.

TIME(Min)/10	WT.LOSS(gm)
0.10	0.0029
0.20	0.0076
0.30	0.0136
0.40	0.0208
0.50	0.0276
0.60	0.0332
0.70	0.0386

Expt.No. : 37
 Gas composition : CO₂ = 80%, Ar = 20%

Initial wt. of sample = 0.0543 gm. Initial wt. of sample = 0.0503 gm.

TIME(Min)/10	WT.LOSS(gm)
0.05	0.0029
0.10	0.0061
0.15	0.0092
0.20	0.0132
0.25	0.0166
0.30	0.0210
0.40	0.0261
0.50	0.0311
0.60	0.0348
0.70	0.0384

TIME(Min)/10	WT.LOSS(gm)
0.05	0.0027
0.10	0.0056
0.15	0.0091
0.20	0.0121
0.25	0.0150
0.30	0.0202
0.40	0.0244
0.50	0.0290
0.60	0.0332
0.70	0.0372

Expt.No. : 38
 Gas composition : CO₂ = 50%, Ar = 50%

Initial wt. of sample = 0.0487 gm. Initial wt. of sample = 0.0619 gm.

TIME(Min)/10	WT.LOSS(gm)
0.05	0.0014
0.10	0.0022
0.15	0.0032
0.20	0.0041
0.25	0.0049
0.30	0.0060
0.40	0.0080
0.50	0.0103
0.60	0.0129
0.70	0.0158
0.80	0.0185
1.00	0.0250

TIME(Min)/10	WT.LOSS(gm)
0.05	0.0016
0.10	0.0020
0.15	0.0031
0.20	0.0038
0.25	0.0049
0.30	0.0058
0.40	0.0082
0.50	0.0103
0.60	0.0126
0.70	0.0155
0.80	0.0187
1.00	0.0255

Expt.No. : 39
 Gas composition : CO₂ = 20%, Ar = 80%

Initial wt. of sample = 0.0558 gm. Initial wt. of sample = 0.0659 gm.

TIME(Min)/10	WT.LOSS(gm)
0.05	0.0006
0.10	0.0010
0.15	0.0015
0.20	0.0020
0.25	0.0025
0.30	0.0031
0.40	0.0047
0.60	0.0069
0.80	0.0095
1.00	0.0127
1.20	0.0163
1.40	0.0202

TIME(Min)/10	WT.LOSS(gm)
0.05	0.0006
0.10	0.0011
0.15	0.0013
0.20	0.0019
0.25	0.0023
0.30	0.0028
0.40	0.0040
0.60	0.0064
0.80	0.0091
1.00	0.0119
1.20	0.0150
1.40	0.0171

Expt.No. : 40

Temp. = 1151 K

Gas composition: CO₂ = 80%, Ar = 20%

SET 1

Initial wt. of sample = 0.0526 gm.

SET 2

Initial wt. of sample = 0.0529 gm.

TIME(Min)/10	WT.LOSS(gm)
0.10	0.0025
0.20	0.0033
0.30	0.0050
0.50	0.0068
0.70	0.0090
0.90	0.0119
1.20	0.0161
1.50	0.0225
1.80	0.0290
2.10	0.0359

TIME(Min)/10	WT.LOSS(gm)
0.10	0.0017
0.20	0.0028
0.30	0.0039
0.50	0.0067
0.70	0.0096
0.90	0.0121
1.20	0.0175
1.50	0.0237
1.80	0.0311
2.10	0.0375

Expt.No. : 41

Gas composition : CO₂ = 50%, Ar = 50%

Initial wt. of sample = 0.0529 gm.

Initial wt. of sample = 0.0573 gm.

TIME(Min)/10	WT.LOSS(gm)
0.10	0.0010
0.20	0.0020
0.30	0.0029
0.40	0.0041
0.50	0.0052
0.70	0.0071
0.90	0.0099
1.20	0.0140
1.50	0.0184
1.80	0.0235
2.10	0.0297

TIME(Min)/10	WT.LOSS(gm)
0.10	0.0017
0.20	0.0027
0.30	0.0041
0.40	0.0049
0.50	0.0062
0.70	0.0085
0.90	0.0119
1.20	0.0160
1.50	0.0207
1.80	0.0260
2.10	0.0322

Expt.No. : 42

Gas composition : CO₂ = 20%, Ar = 80%

Initial wt. of sample = 0.0492 gm.

Initial wt. of sample = 0.0589 gm.

TIME(Min)/10	WT.LOSS(gm)
0.10	0.0020
0.20	0.0026
0.30	0.0032
0.40	0.0042
0.50	0.0049
0.70	0.0061
0.90	0.0078
1.20	0.0100
1.50	0.0133
1.80	0.0160

TIME(Min)/10	WT.LOSS(gm)
0.10	0.0011
0.20	0.0018
0.30	0.0023
0.40	0.0033
0.50	0.0038
0.70	0.0050
0.90	0.0068
1.20	0.0091
1.50	0.0120
1.80	0.0149

APPENDIX -12

Weight loss versus time data for coconut char in
CO - CO₂ mixtures

Expt.No. : 43 Temp.= 1285 K
Gas composition: CO = 20%, CO₂ = 80%

SET 1

Initial wt. of sample=0.0628 gm.

SET 2

Initial wt. of sample= 0.0572 gm.

TIME(Min)/10	WT.LOSS(gm)	TIME(Min)/10	WT.LOSS(gm)
0.10	0.0024	0.10	0.0023
0.20	0.0109	0.20	0.0117
0.30	0.0196	0.30	0.0208
0.40	0.0300	0.40	0.0312
0.50	0.0390	0.50	0.0392
0.60	0.0468	0.60	0.0415

Expt.No. : 44
Gas composition : CO = 50%, CO₂ = 50%

Initial wt. of sample=0.0527 gm. Initial wt. of sample= 0.0559 gm.

TIME(Min)/10	WT.LOSS(gm)	TIME(Min)/10	WT.LOSS(gm)
0.10	0.0017	0.10	0.0016
0.20	0.0067	0.20	0.0069
0.30	0.0113	0.30	0.0124
0.40	0.0172	0.40	0.0191
0.50	0.0235	0.50	0.0261
0.60	0.0276	0.60	0.0328
0.70	0.0332	0.70	0.0389
0.80	0.0382	0.80	0.0417

Expt.No. : 45
Gas composition : CO = 80%, CO₂ = 20%

Initial wt. of sample=0.0679 gm. Initial wt. of sample= 0.0601 gm.

TIME(Min)/10	WT.LOSS(gm)	TIME(Min)/10	WT.LOSS(gm)
0.10	0.0018	0.10	0.0006
0.20	0.0045	0.20	0.0033
0.30	0.0075	0.30	0.0066
0.40	0.0106	0.40	0.0099
0.50	0.0140	0.50	0.0135
0.60	0.0176	0.60	0.0166
0.70	0.0212	0.70	0.0194

APPENDIX -12 (Contd.)

Temp. = 1246 K

Expt.No. : 46
 Gas composition : CO = 20%, CO₂ = 80%

SET 1

Initial wt. of sample = 0.0527 gm.

TIME(Min)/10	WT.LOSS(gm)
0.10	0.0017
0.30	0.0147
0.50	0.0317
0.70	0.0387

SET 2

Initial wt. of sample = 0.0593 gm.

TIME(Min)/10	WT.LOSS(gm)
0.10	0.0016
0.30	0.0183
0.50	0.0339
0.70	0.0446

Expt.No. : 47
 Gas composition : CO = 50%, CO₂ = 50%

Initial wt. of sample = 0.0549 gm.

Initial wt. of sample = 0.0593 gm.

TIME(Min)/10	WT.LOSS(gm)
0.10	0.0019
0.30	0.0120
0.50	0.0245
0.70	0.0360
0.90	0.0402

TIME(Min)/10	WT.LOSS(gm)
0.10	0.0015
0.30	0.0122
0.50	0.0238
0.70	0.0365
0.90	0.0446

Expt.No. : 48
 Gas composition : CO = 80%, CO₂ = 20%

Initial wt. of sample = 0.0655 gm.

Initial wt. of sample = 0.0577 gm.

TIME(Min)/10	WT.LOSS(gm)
0.10	0.0011
0.30	0.0056
0.50	0.0102
0.70	0.0166
0.90	0.0223
1.10	0.0282
1.30	0.0347
1.50	0.0411
1.70	0.0463

TIME(Min)/10	WT.LOSS(gm)
0.10	0.0010
0.30	0.0050
0.50	0.0095
0.70	0.0140
0.90	0.0192
1.10	0.0250
1.30	0.0315
1.50	0.0380
1.70	0.0419

APPENDIX -12 (Contd.)

Temp.= 1204 K

Expt.No. : 49
 Gas composition : CO = 20%, CO₂ = 80%

SET 1

Initial wt. of sample = 0.0579 gm.

SET 2

Initial wt. of sample = 0.0768 gm.

TIME(Min)/10	WT.LOSS(gm)	TIME(Min)/10	WT.LOSS(gm)
0.10	0.0015	0.10	0.0005
0.30	0.0049	0.30	0.0052
0.50	0.0079	0.50	0.0112
0.70	0.0124	0.70	0.0187
0.90	0.0191	0.90	0.0258
1.20	0.0279	1.20	0.0396
1.50	0.0389	1.50	0.0529
1.80	0.0421	1.80	0.0587

Expt.No. : 50
 Gas composition : CO = 50%, CO₂ = 50%

Initial wt. of sample = 0.0620 gm. Initial wt. of sample = 0.0616 gm.

TIME(Min)/10	WT.LOSS(gm)	TIME(Min)/10	WT.LOSS(gm)
0.10	0.0010	0.10	0.0007
0.30	0.0057	0.30	0.0053
0.50	0.0117	0.50	0.0115
0.70	0.0176	0.70	0.0175
0.90	0.0248	0.90	0.0245
1.20	0.0353	1.20	0.0355
1.50	0.0437	1.50	0.0442

Expt.No. : 51
 Gas composition : CO = 80%, CO₂ = 20%

Initial wt. of sample = 0.0543 gm. Initial wt. of sample = 0.0607 gm.

TIME(Min)/10	WT.LOSS(gm)	TIME(Min)/10	WT.LOSS(gm)
0.10	0.0000	0.10	0.0007
0.30	0.0026	0.30	0.0027
0.50	0.0054	0.50	0.0051
0.70	0.0076	0.70	0.0074
0.90	0.0092	0.90	0.0108
1.20	0.0134	1.20	0.0154
1.50	0.0180	1.50	0.0193
2.00	0.0270	2.00	0.0282
2.50	0.0358	2.50	0.0353
3.00	0.0400	3.00	0.0432

APPENDIX -12 (Contd.)

Temp.= 1145 K
 Expt.No. : 52
 Gas composition : CO = 20%, CO₂ = 80%

SET 1

Initial wt. of sample = 0.0553 gm.

SET 2

Initial wt. of sample = 0.0544 gm.

TIME(Min)/10	WT.LOSS(gm)
0.10	0.0008
0.30	0.0026
0.50	0.0047
1.00	0.0099
1.50	0.0146

TIME(Min)/10	WT.LOSS(gm)
0.10	0.0009
0.30	0.0021
0.50	0.0047
1.00	0.0114
1.50	0.0172

Expt.No. : 53
 Gas composition : CO = 50%, CO₂ = 50%

Initial wt. of sample = 0.0519 gm.

Initial wt. of sample = 0.0588 gm.

TIME(Min)/10	WT.LOSS(gm)
0.10	0.0000
0.30	0.0008
0.50	0.0013
1.00	0.0031
1.50	0.0058
2.00	0.0082
2.50	0.0134

TIME(Min)/10	WT.LOSS(gm)
0.10	0.0000
0.30	0.0010
0.50	0.0017
1.00	0.0043
1.50	0.0068
2.00	0.0097

APPENDIX -13

Weight loss versus time data for carbothermic
reduction

Temp.=1284 K
Expt.No.=1*
C/Fe₂O₃=2
SET 1
Initial wt.of sample
= 0.5070 gm.

TIME(Min)/10	WT.LOSS(gm)
0.20	0.0155
0.30	0.0310
0.40	0.0415
0.50	0.0475
0.70	0.0594
0.90	0.0711
1.20	0.0896
1.50	0.1084
1.80	0.1276
2.10	0.1461
2.40	0.1586
2.70	0.1721
3.00	0.1764

SET 2
Initial wt.of sample
= 0.5902 gm.

TIME(Min)/10	WT.LOSS(gm)
0.20	0.0141
0.30	0.0274
0.40	0.0393
0.50	0.0456
0.70	0.0572
0.90	0.0682
1.20	0.0852
1.50	0.1021
1.80	0.1236
2.10	0.1400
2.40	0.1536
2.70	0.1630
3.00	0.1673

Temp.=1208 K
Expt.No.=2*
C/Fe₂O₃ =2

SET 1
Initial wt.of sample
= 0.5633 gm.

TIME(Min)/10	WT.LOSS(gm)
0.20	0.0087
0.30	0.0151
0.40	0.0192
0.50	0.0234
0.70	0.0320
0.90	0.0372
1.10	0.0397
1.50	0.0441
1.80	0.0469
2.10	0.0497
2.40	0.0526
2.70	0.0553
3.00	0.0602
3.50	0.0643
4.00	0.0686
4.50	0.0730
5.00	0.0775
5.50	0.0824
6.00	0.0866
6.50	0.0910
7.50	0.1007
8.50	0.1103

SET 2
Initial wt.of sample
= 0.5336 gm.

TIME(Min)/10	WT.LOSS(gm)
0.20	0.0103
0.30	0.0161
0.40	0.0203
0.50	0.0251
0.70	0.0338
0.90	0.0391
1.20	0.0430
1.50	0.0461
1.80	0.0493
2.10	0.0525
2.40	0.0549
2.70	0.0577
3.00	0.0606
3.50	0.0654
4.00	0.0700
4.50	0.0747
5.00	0.0792
5.50	0.0839
6.00	0.0887
6.50	0.0936
7.50	0.1032
8.50	0.1129

NOTE: * means powder mixture

APPENDIX- 13 (Contd.)

SET 1
Initial wt.of sample
= 0.5032 gm.

Temp.=1145 K
Expt.No.=3*
C/Fe₂O₃ =2

TIME(Min)/10	WT.LOSS(gm)
0.20	0.0036
0.30	0.0117
0.40	0.0160
0.50	0.0169
0.70	0.0187
0.90	0.0202
1.20	0.0223
1.50	0.0246
1.80	0.0267
2.10	0.0287
2.40	0.0308
2.70	0.0327
3.00	0.0347
3.50	0.0378
4.00	0.0406
4.50	0.0422
5.00	0.0433
5.50	0.0443
6.00	0.0451
6.50	0.0458
7.50	0.0468
8.50	0.0477
9.00	0.0482

SET 2
Initial wt.of sample
= 0.4973 gm.

TIME(Min)/10	WT.LOSS(gm)
0.20	0.0042
0.30	0.0137
0.40	0.0197
0.50	0.0210
0.70	0.0230
0.90	0.0247
1.20	0.0270
1.50	0.0294
1.80	0.0318
2.10	0.0340
2.40	0.0363
2.70	0.0384
3.00	0.0407
3.50	0.0443
4.00	0.0468
4.50	0.0489
5.00	0.0504
5.50	0.0517
6.00	0.0527
6.50	0.0534
7.50	0.0546
8.50	0.0556
9.00	0.0561

Temp.=1078 K
Expt.No.=4*
C/Fe₂O₃ =2

SET 1
Initial wt.of sample
= 0.5290 gm.

SET 2
Initial wt.of sample
= 0.5943 gm.

TIME(Min)/10	WT.LOSS(gm)
0.20	0.0280
0.30	0.0506
0.40	0.0756
0.50	0.1031
0.60	0.1306
0.70	0.1556
0.80	0.1616

TIME(Min)/10	WT.LOSS(gm)
0.20	0.0310
0.30	0.0550
0.40	0.0820
0.50	0.1116
0.60	0.1426
0.70	0.1676
0.80	0.1786

NOTE: * means powder mixture

APPENDIX -13 (Contd.)

Temp.=1284 K
Expt.No.=5**

SET 1

Initial C = 0.3447 gm.
Initial Fe₂O₃ = 0.1567 gm.

TIME(Min)/10	WT.LOSS(gm)
0.20	0.0120
0.30	0.0300
0.40	0.0425
0.50	0.0505
0.70	0.0675
0.90	0.0864
1.10	0.1046
1.30	0.1216
1.50	0.1396
1.80	0.1611

SET 2

Initial C = 0.3324 gm.
Initial Fe₂O₃ = 0.1813 gm.

TIME(Min)/10	WT.LOSS(gm)
0.20	0.0083
0.30	0.0253
0.40	0.0399
0.50	0.0483
0.70	0.0654
0.90	0.0829
1.10	0.1014
1.30	0.1185
1.50	0.1404
1.80	0.1581

Temp.=1235 K
Expt.No.=6**

SET 1

Initial C = 0.3571 gm.
Initial Fe₂O₃ = 0.1649 gm.

TIME(Min)/10	WT.LOSS(gm)
0.20	0.0195
0.30	0.0415
0.40	0.0595
0.50	0.0806
0.60	0.0991
0.70	0.1191
0.80	0.1361
0.90	0.1479
1.00	0.1536

SET 2

Initial C = 0.3425 gm.
Initial Fe₂O₃ = 0.1703 gm.

TIME(Min)/10	WT.LOSS(gm)
0.20	0.0190
0.30	0.0430
0.40	0.0591
0.50	0.0806
0.60	0.1041
0.70	0.1246
0.80	0.1431
0.90	0.1569

NOTE: ** means micropellet of oxide + powder of coconut char

APPENDIX -13 (Contd.)

Temp.=1210 K
Expt.No.=7**

SET 1

Initial C = 0.3483 gm.
Initial Fe₂O₃ = 0.1688 gm.

TIME(Min)/10	WT.LOSS(gm)
0.20	0.0020
0.30	0.0054
0.40	0.0096
0.50	0.0123
0.70	0.0187
0.90	0.0250
1.20	0.0294
1.50	0.0320
1.80	0.0348
2.10	0.0376
2.40	0.0399
2.70	0.0428
3.00	0.0460
3.50	0.0509
4.00	0.0565
4.50	0.0604
5.00	0.0651
5.50	0.0703
6.00	0.0748
6.50	0.0801
7.50	0.0902
8.50	0.0994
9.00	0.1036

Temp.=1145 K
Expt.No.=8**

SET 1

Initial C = 0.2885 gm.
Initial Fe₂O₃ = 0.1487 gm.

TIME(Min)/10	WT.LOSS(gm)
0.20	0.0065
0.30	0.0200
0.40	0.0320
0.50	0.0390
0.70	0.0510
0.90	0.0622
1.20	0.0814
1.50	0.0996
1.80	0.1175
2.10	0.1342
2.40	0.1530
2.70	0.1542

SET 2

Initial C = 0.3426 gm.
Initial Fe₂O₃ = 0.1699 gm.

TIME(Min)/10	WT.LOSS(gm)
0.20	0.0038
0.30	0.0084
0.40	0.0153
0.50	0.0209
0.70	0.0327
0.90	0.0383
1.20	0.0403
1.50	0.0421
1.80	0.0458
2.10	0.0495
2.40	0.0535
2.70	0.0569
3.00	0.0608
3.50	0.0673
4.00	0.0735
4.50	0.0794
5.00	0.0853
5.50	0.0914
6.00	0.0974
6.50	0.1030
7.50	0.1142
8.50	0.1241
9.00	0.1284

SET 2

Initial C = 0.3429 gm.
Initial Fe₂O₃ = 0.1586 gm.

TIME(Min)/10	WT.LOSS(gm)
0.20	0.0020
0.30	0.0161
0.40	0.0286
0.50	0.0374
0.70	0.0484
0.90	0.0595
1.20	0.0766
1.50	0.0929
1.80	0.1143
2.10	0.1295
2.40	0.1446
2.70	0.1544

NOTE: ** means micropellet of oxide + powder of coconut char

Th
669.1
B223 k

This book is to be returned on the date last stamped.

This image shows a blank sheet of white paper with horizontal blue ruling lines. A single vertical red margin line runs down the center of the page, creating two equal-width columns. The paper has a slightly aged appearance with some minor discoloration and faint smudges. There are no markings or text on the page.

1